

A SIMULINK MODEL FOR CALCULATION OF FUEL CELL STACK PERFORMANCE

Jeremy A. Schaeffer¹, Lea-Der Chen¹ and James P. Seaba²

¹Department of Mechanical and Industrial Engineering
National Advanced Driving Simulator
The University of Iowa
Iowa City, IA 52242

²Emerging Technology
420 S. Keeler Avenue
ConocoPhillips
Bartlesville, OK 74004

Introduction

A fuel cell is an electrochemical device that converts the chemical energy stored in the fuel into electrical work. To generate the necessary cell voltage, fuel cells are often connected in series to form a fuel cell stack. If the electrolyte used in the fuel cell is liquid, for example, as that in phosphoric acid [1] and alkaline fuel cells, the electrolyte of different cells is shared through a common manifold, which might result in the presence of shunt current. Similarly, shunt current may also be present when water is used as the coolant in polymer electrolyte fuel cell stacks. An electrical circuit model is used to simulate the electrical processes of liquid electrolyte fuel cell stacks. The calculation is compared with experimental data of an electrolyzer stack [2].

Electrical Circuit

The shunt current can be modeled using the electrical circuit shown in Fig. 1 [2], in which 20 represents the manifold, 24, 26, 28, 30, 32, and 34 represent the channels, and 4, 6, 8, 10, 12, and 14 represent the individual cells; R_e represents the cell (or electrolyte) resistance, R_c the channel resistance, and R_m the manifold resistance, and V_0 is the cell potential, I the current flowing through the stack. The i 's represent the current that flows through the cell after the shunt current (j 's) has been accounted for. The k 's represent the current that flows through the manifold segments [2]. Most of the current will flow through the cell (R_c) because this resistance is generally the smallest as compared to R_m and R_e . A small amount of current, or shunt current, will flow through the channel and manifold. To reduce the shunt current, a protective current, k_0 (shown on the far left of the manifold), is applied in [2].

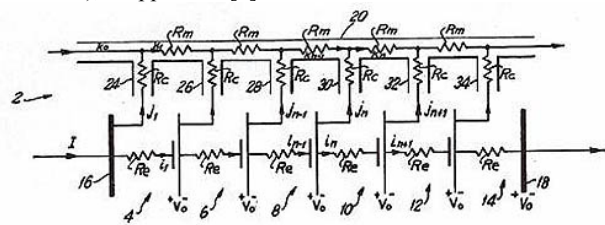


Figure 1. Electrical circuit used to model fuel cell stack [2].

An electrical circuit is created in Simulink[®] environment to model the electrical current and voltage of the circuit given in Fig. 1. The Simulink[®] model is given in Fig. 2, which calculates the current flowing through the cells (EC), channels (CC), and manifold (MC) by using a Matlab[®] function.

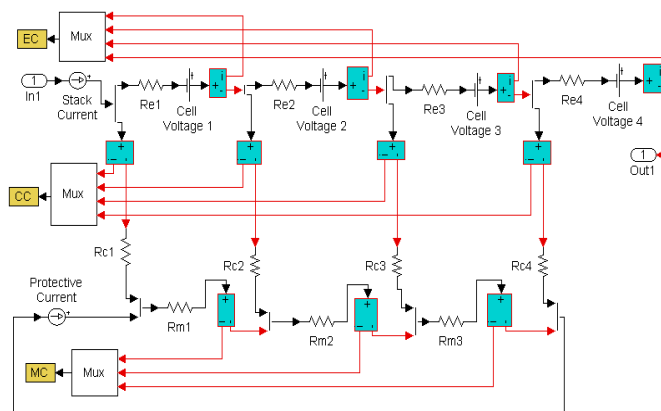


Figure 2. Illustration of a Simulink[®] model for 4-cell stack, protective current applied to the manifold.

Results and Discussion

Due to limited availability of fuel cell stack data, results of the Simulink[®] stack model were compared with experimental data of a 10-cell electrolyzer stack [3]. The applied current (420 mA), protective current (17.5 mA) and electrode area (968 mm² or 1.5 in²) were given in [3]. The distance between the electrodes was estimated to be 31.75 mm (1.25 in) [3]. The resistance of the channel, manifold segment, and electrolyte (based on an estimated electrolyte conductance of 0.15 Ω⁻¹ cm⁻¹) is estimated to be 1000 Ω, 150 Ω, and 2.187 Ω, respectively. The cell voltage is set to 2.54 V. The experimental results had a precision error of either ± 0.39 mA or ± 1 mA, depending on whether the range selector for the current meter was set to 10 mA or 30 mA full scale [3]. The Simulink[®] results, along with experimental data of no protective current, are shown in Fig. 3 in which error bars denote experimental precision error of ± 1 mA. The Simulink[®] results are in reasonable agreement with experimental data. The calculation underestimates the shunt currents in channels 1 and 10 by 31% and overestimates the shunt currents in 3 through 9. The maximum difference in channels 3 through 9 is 1.4209 mA. It is noted that the calculation results in a positive current for channel 5, while the experiment registered a small negative current was within the experimental uncertainty of 10 and 30 mA.

Experimental Results vs. Simulation Results - Shunt Current w/o Current Protection

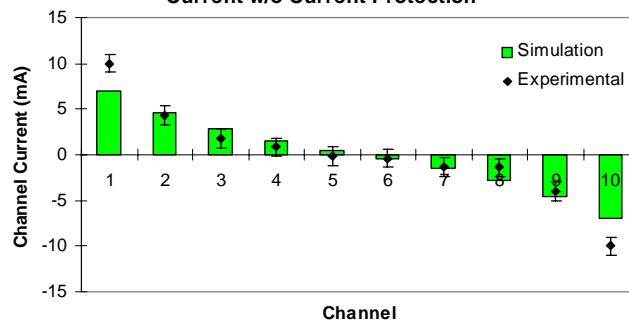


Figure 3. Comparison of simulation and experimental shunt current without protective current: $R_e = 2.187 \Omega$, $R_m = 150 \Omega$, $R_c = 1000 \Omega$, $V = 2.54 \text{ V}$, $I = 0.42 \text{ A}$; Error bars ± 1 mA.

A protective current of 17.5 mA was applied to the manifold in the Simulink[®] model, similar to the condition given in [2]. The channel current results are summarized in Fig. 4. The calculation shows a symmetric decreasing trend, with current leaving the stack through the first 5 channels and entering the stack through the last 5 channels and maximum magnitudes at the end channels. The experimental results, however, do not show a clear trend in channel currents. The experimental data show that current was leaving channels 6, 8, and 9 while the calculation shows that current was entering the stack at these channels. It is noted that the measured channel currents are within the precision error; cf., Fig. 4; thus, it is difficult to make a definitive assessment on the results with protective current.

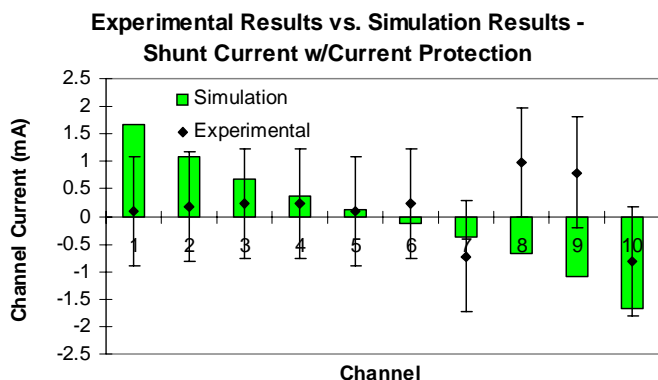


Figure 4. Comparison of simulation and experimental shunt current with protective current; $R_c = 2.187 \Omega$, $R_m = 150 \Omega$, $R_c = 1000 \Omega$, $V = 2.54 \text{ V}$, $I = 0.42 \text{ A}$, $I_p = 0.0175 \text{ A}$.

To estimate the uncertainty in stack parameters, a Monte Carlo simulation was performed with a sample size of 15,000, which was shown to be sufficient for present study [4]. A standard deviation of 5% of the mean value is applied to channel and manifold resistance and cell voltage, with and without protective currents. Detailed results are reported in [4]. This variation in the manifold resistance causes the resulting channel currents to vary approximately $\pm 0.2 \text{ mA}$. It can also be seen that this variation results in zero probability of the channel current flow reversing directions (it does not result in any probability of current that normally leaves the stack to enter the stack, or vice versa).

The results of varying the manifold resistance with standard deviation of 5% of the mean value are shown in Fig. 5. This variation in the manifold resistance causes the channel currents to vary approximately ± 0.3 to $\pm 0.4 \text{ mA}$. The variation of 5% standard deviation results in a non-zero finite probability of channel current flow reversing directions in channels 5 and 6. There is also a small non-zero finite probability of channel current flow reversing directions in channels 4 and 7. Similar results are obtained when varying channel resistance, cell resistance, and voltage with a standard deviation of 5% of the mean value with protective current applied. The Monte Carlo simulation shows a maximum difference of 0.391% of the shunt current magnitude when the channel resistance values are varied and a maximum power loss of 0.184% when the manifold resistance is varied.

A Simulink[®] model is built for a 100-cell stack with a common manifold. The Simulink model calculation of a four-node circuit was validated by the calculation using second software, PSpice[®]. Agreement to the seventh decimal point or better was obtained [4]. The resistance in each manifold segment is 75Ω , the resistance in

each channel is 500Ω , and the resistance in each cell is 0.25Ω . The cell voltage is set at 0.65 V and the current flowing through the stack is 1 A . The calculated shunt currents are shown in Fig. 6 when protective current is not applied. The overall amount of current flowing in the channels is 23.9 mA and the power lost due to shunt current is 1.13%. When a protective current of 12.0 mA is applied, the shunt currents are reduced to 10^{-15} A , shown by the insert in Fig. 6. Calculation of the protective current is given in [4].

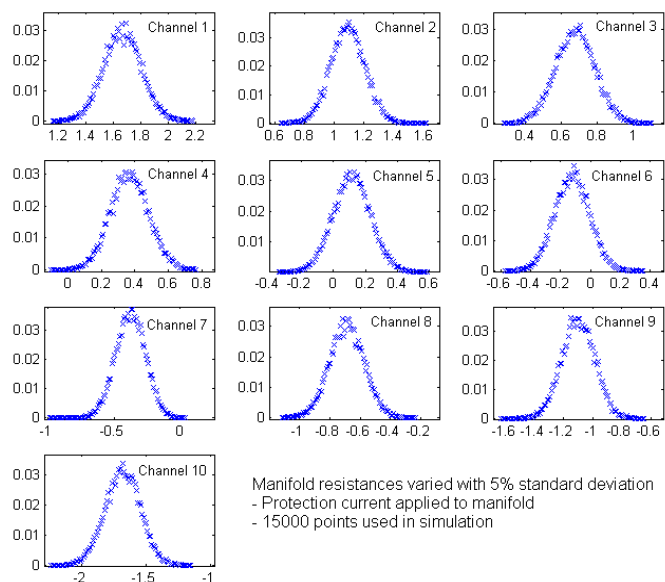


Figure 5. Histogram of Monte Carlo simulation of channel currents with standard deviation of the manifold resistance set by 5% and with protective current applied.

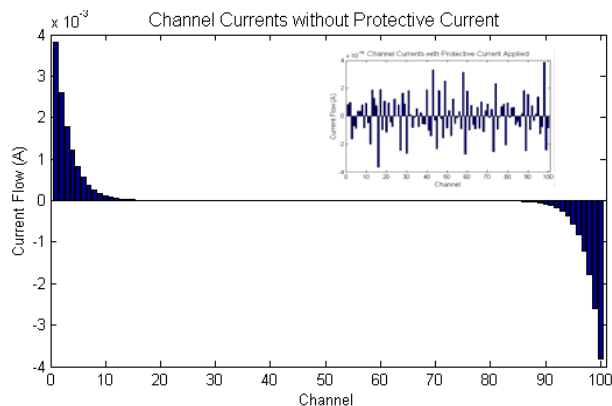


Figure 6. Channel currents of 100-cell fuel cell stack..

Acknowledgment

This work was supported, in part, by ConocoPhillips..

References

1. Katz, M., *J. Electrochemical Soc.*, **1978**, 125 (4): 515-520.
2. Zahn, M.; Grimes, P.G.; Bellows, R.J., U.S. Pat. No. 4,197,169, **1980**.
3. Bellows, R.J, Private Communication, **2004**.
4. Schaeffer, J., *Electrical Circuit Modeling of Fuel Cells*, MS Thesis, Dept. Mech. and Ind. Eng., The University of Iowa, Iowa City, IA, **2004**.

A UNIQUE SUB 5KW SOLID OXIDE FUEL CELL/HEAT ENGINE HYBRID GENERATOR

Andy C. Foley

School Of Mechanical Engineering
Ohio University
Athens , OH.

Nomenclature

E : Ideal Voltage (V)
 ΔG : Change in Gibbs free energy (kJ/kmol)
 n : Number of electrons released per molecule fuel.
 T : Temperature (K)
 F : Faraday's constant (96485 C)
 i : Current density. (mA/cm²) i_l : leakage current
 i_0 : Exchange current
 ΔV : Change in voltage.
 r : Area specific resistance (Ωcm^2)

Introduction

With ever increasing demands for more efficient power generation and distribution the goal of providing an efficient 5 kW generator suitable for domestic use is the focus of this research. This paper therefore describes an analytical model of a hybrid fuel cell/heat engine generator. The model generator quantifies the benefits of the significant symbiosis to be had from two existing and well established technologies. The first technology utilized is that of the Stirling engine. These have been around since 1826 and as external combustion engines probably represent one of the most robust and simple types of heat engine available. Despite these obvious advantages Stirling engines have not achieved widespread use as they have been unable to compete successfully with internal combustion engines. Primarily because of their low specific power ratings and the significant cost reductions brought about by the existing mass manufacture of the internal combustion engine.

The second technology is that of Solid oxide fuel cells (SOFC). As with most fuel cell technologies these are currently experiencing a fervor of interest and after the low temperature Polymer Electrolyte Membrane (PEM) these cells appear to be the most promising for short term commercialization. Indeed it is already possible to purchase a 200 KW hybrid SOFC gas turbine generator from Siemens Westinghouse. Initial capital costs however still mean that these generators are catering for the fairly small niche market that can afford to bear the high initial expense.

Primary benefits of using the SOFC relate to its relatively inexpensive solid electrolyte compared to other cell electrolytes consisting of molten salts, caustic alkaloids or expensive fragile membrane. This offers a simple and potentially robust fuel cell that also has the benefit of not requiring expensive catalysts at its operating temperature of 900 °C + . This high operating temperature also brings the added advantage that waste product gases are of a temperature compatible with a downstream heat engine. Finally the nature of this particular electrolyte is such that oxygen ions (O⁻) carry charge from the cathode to the fuel anode, unlike most other types of fuel cell that rely on Hydrogen ions (H⁺) to carry charge from the anode to the cathode. This subtle difference means that the SOFC is able to use various hydrocarbon fuels apart from pure Hydrogen. Indeed fuels such as Carbon monoxide would actually poison other types of fuel cell.

Finally the reforming required to make this multi fuel capability possible is also conveniently possible within the fuel cell itself. The quantity and temperature of heat required being provided by the

SOFC's own 'losses' and the reformer design therefore being the relatively straightforward process of heat exchange and re-cycling of the anode's waste water product.

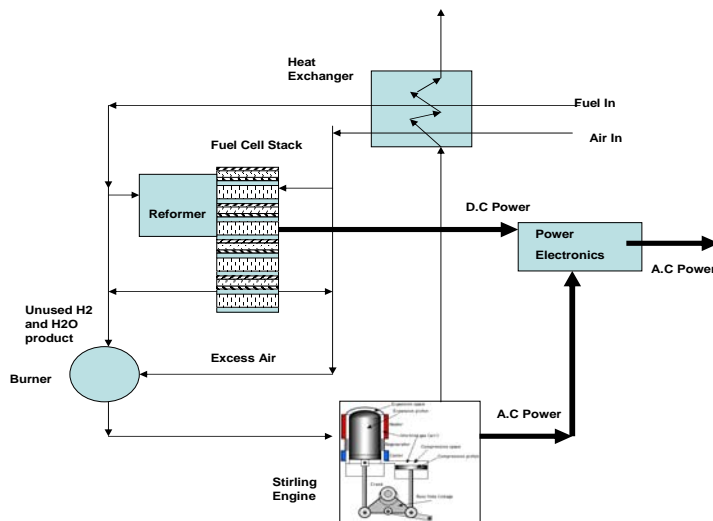


Figure 1. Schematic of SOFC / Stirling Hybrid

Numerical Modeling

Once design of a fuel cell system commences it is not long before one realizes that there are a myriad of parameters that need to be considered. Fortunately once the application has been decided a number of these are easily fixed. For our application we were interested in a domestic power generation system that will produce D.C power that can be relatively easily inverted to 110V A.C. As such a Voltage setting of 48 V D.C was selected to allow efficient Voltage conversion and reduced D.C currents but also low enough so as to not pose a significant human safety risk.

To undertake the detailed and somewhat iterative modeling of this hybrid system, Microsoft Excel with its application Visual Basic was found convenient for the Fuel Cell stack modeling. For the Stirling Engine analysis the use of the 'Simple Analysis' code (ref. Israeli (1984)) for the modeling of the Stirling cycle was found more than comprehensive.

Figure 1 shows a schematic of the system.

Method Of Solution

Modified Nernst Equation. Based on a desired operating temperature and pressure decided by the user (1000°C and 1.1 bar) the Fuel Cell spreadsheet and associated visual basic code calculates the ideal operating voltage of the fuel cell can be calculated from the Nernst equation :-

$$E = \frac{\Delta G}{nF} + \frac{RT}{nF} \log_e \left[\frac{a_{H_2} (a_{O_2})^{\frac{1}{2}}}{a_{H_2O}} \right] \dots \dots \dots (1)$$

where a_x is the activity of the reactant/product.

For SOFC's at high temperature this is the ratio of the partial pressure of the species to atmospheric pressure.

Once operating voltage, pressure and temperature have been set the user has a number of parameters to input. The primary parameter is a fuel flow rate (liters/hour). For the model presented in this paper the

fuel used is Hydrogen, however Methane or other suitable Hydrocarbons could easily be used.

After the fuel flow rate has been fixed the user has the option of deciding on a fuel utilization rate. Typically this is about 90% as some flow rate of Hydrogen is required to take the water product away from the anode and also keep concentration losses to a minimum at the cell exit.

With a fuel flow rate input the current passing through an individual cell is calculated based on the number of electrons freed in the oxidation of the fuel. (i.e. 2 electrons for each Diatomic hydrogen molecule.)

Losses. Knowing the current available for a given flow rate it is now possible to calculate the voltage losses within the fuel cell itself. These comprise activation losses, leakage losses, ohmic losses and concentration losses.

Activation losses are calculated using the Tafel equation with constants taken from Davies (1967).

Data for leakage losses are calculated measuring fuel use during open circuit operation or alternately can be derived from published Voltage/ Current performance graphs if the electrolyte thickness is known. (Pham (2001)). For the relatively thick electrolyte used in the current design, leakage is significantly reduced to just under 1% of total fuel flow. Calculation of the resulting voltage loss is achieved by including the leakage with the useful current flow in the Tafel equation: i.e.

$$\Delta V_{act+leak} = \frac{RT}{2\alpha F} \log_e \left(\frac{i + i_l}{i_0} \right)$$

The next loss considered is the Ohmic loss. The area specific resistance is a function of the electrolyte thickness and conductivity which are in turn functions of temperature. Correlations for this parameter were taken from Laramie & Dicks (2003). And the voltage loss computed simply from :-

$$\Delta V_{ohm} = i \times r$$

Finally concentration losses were computed by applying the Nernst equation at the exit to the fuel cell where Hydrogen and Oxygen concentrations were at their lowest and computing the resulting Nernst voltage. The difference between the voltage so computed at inlet and that at the outlet was halved and to a first, and reasonable approximation, this equated to documented empirical concentration losses.

Once all the losses were accounted for the operational fuel cell voltage was computed and hence the number of cells required in the stack could be found.

The final part of the design involved optimizing the individual fuel cell size such that the current density was high enough to provide a useful specific power and hence a compact stack whilst at the same time producing only moderate ohmic and concentration losses. By examination of figure 2. it can be seen that useful operational range was achieved between 550mA/cm² and 800 mA/cm². The efficiency is kept above 45% and specific power has not dropped significantly from its peak.

Stack Geometry. Once the actual cell operating voltage and optimum current density have been determined it is relatively straightforward to dimension an appropriate stack. For the design arrived at in this study 80 cells each of 7cm diameter were required. Each cell had a standard yttrium stabilized zirconia electrolyte (ZrO₂)_{0.92}(Y₂O₃)_{0.08}, Nickel zirconia anode and strontium doped

lanthanum manganite (La_{0.84} Sr_{0.16}) MnO₃ cathode. The electrolyte was a relatively robust 200µm thick which makes fabrication easier and prolongs fuel cell life. Between each cell a bipolar plate is inserted to allow gas distribution and enhance stack structural stability. Material for these plates is an inconel alloy although work is being undertaken with the possible use of stainless steel and various thermal barrier coatings.

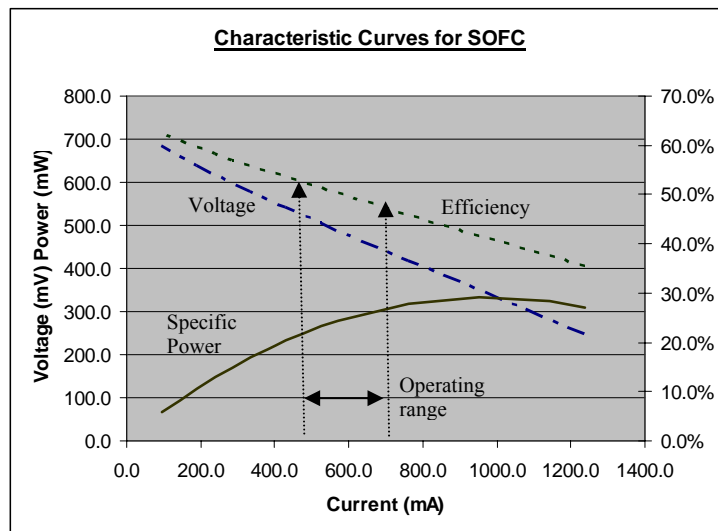


Figure 2. Model Performance Characteristics for SOFC design.

Stirling Engine. For the initial product design initial capital costs were a key factor and hence a simple Alpha type Stirling engine was selected as the downstream heat engine.(Figure 3.) This engine would take the hot excess air (Stoichiometry of cell was set at 5) and the unused Hydrogen/Water products and use these to heat the engines hot space. (Combustion of the excess hydrogen further enhances the heating capability of the waste products). Using appropriate heat transfer coefficients for a scaled Stirling engine available to the author a very conservative 20% efficiency of this engine was predicted. With some refinement to the design it is conceivable that this value will ultimately be improved to around 30%.

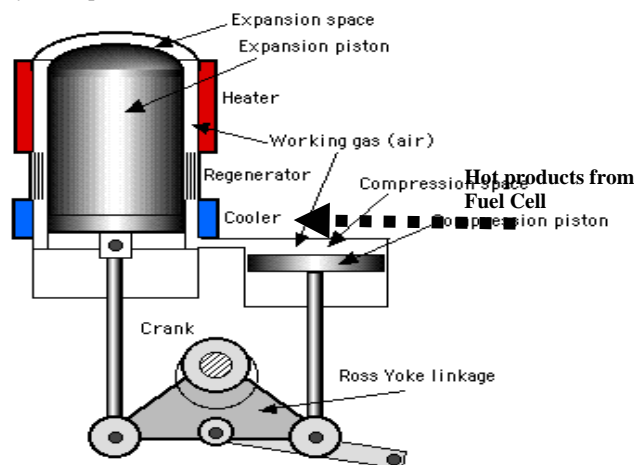


Figure 3. Alpha Type Stirling Engine with Ross Yoke Linkage.

Table 1. Model performance for three operating points around nominal 5KW output.

Fuel Flow liters/hour	Cell current density (mA)	Cell Operating Voltage (mV)	Stack Power (W)	Stirling Power (W)	Total Hybrid Power Output (W)	System Efficiency based on LHV of Hydrogen
30.0	421.6	550.1	2855.7	768.4	3624.2	54.1%
40.0	562.2	497.2	3807.7	1214.7	5022.3	50.8%
50.0	702.7	445.7	4759.6	1803.9	6563.5	47.6%

← Operating point.

Overall Performance Of Hybrid Generator. The cell operating point consumed 40 liters per hour of hydrogen or reformed equivalent. At this point just over 5KW combined power was produced at an efficiency of almost 51%. 25% of this total power was produced by the Stirling Engine. It is also interesting to note that by increasing the fuel flow 25% a predicted increase in power of 30% can be achieved with only a 3.2% reduction in efficiency.

Conclusions

The preliminary analytical design of a simple Stirling/ Solid Oxide fuel cell generator has been undertaken. Using 'off the shelf' materials and well established technologies it has been conservatively predicted that a 5KW generator with an efficiency of 51% can be fabricated. For a system of this size, this is almost double what a comparable internal combustion distributed power generator is capable of. As none of the materials are unique and the envisaged fabrication techniques are standard it is hoped that final bulk manufacturing costs can reach the prized \$400 / KW mark although a detailed cost analysis has yet to be completed.

Currently fabrication of an initial 500W prototype is underway and trials are planned in the coming months. Analytical investigations into moderate pressurization of the system using the Stirling engine are also commencing as are investigations into bi-polar plate design and materials.

References

- (1) Urieli, I. (1984);. *Stirling Cycle Engine Analysis*. : A.Hilger , ASIN 0852744358.
- (2) Davies C.W (1967); *Electrochemistry*, Newnes, London. p.188
- (3) Pham A, Brandon W et al (2001) pap *Demonstration of High Power Density Planar Solid Oxide Fuel Cell Stacks*, Proceedings of Electrochemical Society Vol 2001-16 p.148-154.
- (4) Laraminie, J. Dicks, A (2003) ; *Fuel Cell Systems Explained 2nd Ed*, p 211; Wiley 2003 ISBN 0-470-84857-X

PERFORMANCE OF PBI-BASED MEAs AND STACKS IN ELEVATED TEMPERATURE FUEL CELLS FOR PORTABLE ELECTRONIC APPLICATIONS

Allison M. Fisher, Stephen R. Samms, Jerry Hallmark, Ramesh Koripella, Stephen Roger, and Billy Mylan

Energy Technologies-Motorola Labs
2100 E. Elliot Rd.
Tempe, AZ 8584

Introduction

Low temperature polymer electrolyte membrane fuel cells (PEMFCs) are of three main types: direct liquid methanol, direct hydrogen, and reformate, although reforming of hydrocarbons or chemical hydrides is also being considered.¹ Direct methanol fuel cells currently require high loadings of precious metal catalyst, and tend to be limited in power density. Low temperature direct hydrogen fuel cells have relatively high power densities and require a minimum of precious metal catalyst, but require very pure H₂ fuel in order to operate properly. Carrying the fuel for these cells as pure H₂ gas is not practical because of the low energy densities of current H₂ storage technologies. Methanol reformate fuel cells are based on the generation of H₂ on-board by reformation of methanol fuel. Methanol is a convenient fuel for portable applications because it has a relatively high energy density (4780 W_h/l or 6090 W_h/kg at 100% theoretical electrochemical efficiency) while being able to be steam-reformed at temperatures as low as 200°C. However, at lower temperatures methanol reformate PEMFCs will lower a system's energy density dramatically because it requires either an additional series of bulky and often inefficient reactors, or an expensive and higher pressure palladium-based membrane separator in order to clean the H₂ product sufficiently to avoid CO poisoning of the catalyst (<<100ppm CO at 80°C).

Interest in elevated temperature (>100°C) PEMFCs has been growing steadily since the demonstration in the mid 1990s that polybenzimidazole doped with strong oxo-acids are capable of good proton conductivity, low gas permeability, and do not require humidification, among other benefits.² These benefits, along with the relatively high power densities possible using them, provide a solution to the issues associated with low-temperature PEMFCs. Operation at temperatures near 200°C significantly increases carbon monoxide tolerance of the electrocatalysts, allowing operation with H₂ fuel containing up to ~100-300x the CO limits for low temperature direct hydrogen cells.³ The benefit of high CO tolerance is that the production of the H₂ feed by reformation of a liquid hydrocarbon, such as methanol, can be done in a single, relatively small reactor and with no Pd membrane separator, significantly reducing the penalty paid for on-board fuel processing. Additional benefits include: enhanced kinetics for both electrode reactions, and simplified water management, as only gas-phase water is present.

While other materials are actively under investigation as candidates for elevated temperature PEMFC applications,^{1,4,5} PBI-based MEAs are currently the only commercially available materials for elevated temperature PEMFCs. We have built linear compact elevated-temperature stacks using Celtec® MEAs for integration with our methanol-steam reformation based miniature fuel processor. This paper describes the performance of these stacks under H₂-Air and simulated reformate at temperatures of 160°C.

Experimental

Materials. Celtec® MEAs were obtained from PEMEA, Inc, our development partner for micro applications. Simulated

reformed gases (75% H₂-24% CO₂-1% CO; 74% H₂-24% CO₂-2% CO) were purchased from Scott Specialty Gases. A variety of cell hardware material candidates were investigated, as the fuel cell environment is extremely corrosive. An accelerated corrosion test for stack plate materials was developed as a way to estimate the effect of the PBI MEA and operating conditions on cell hardware. Briefly, in this test two plate materials and controls were heated in phosphoric acid (200C) with a potential of 0.65V between plates for 100hr as illustrated in Figure 1. The weight of the sample was measured before and after exposure in order to determine mass loss.

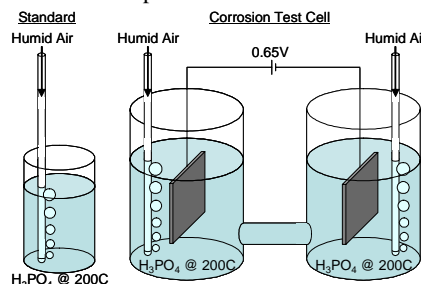


Figure 1. The accelerated corrosion test of material candidates for cell hardware..

Cell/Stack Assembly and Testing. Single cells and stacks were assembled by sandwiching the MEAs between graphite endplates, bipolar plates, gaskets, and backing plates. The assembly was tightened until leak-tight at 5psi. Cells and stacks were tested using test stations purchased from Fuel Cell Technologies, Inc. Breakin was carried out using H₂-Air at a constant current of approximately 200mA/cm² at 160°C for 72hr.

Results and Discussion

One critical issue when building elevated temperature stacks is finding chemically and thermally robust cell hardware and sealing materials. The hot phosphoric acid environment of an elevated-temperature PEMFC so harsh that few materials may be capable of holding up over thousands of hours of operation. Like the MEAs used for low-temperature fuel cells, PBI MEAs are susceptible to poisoning by metals, resulting in permanent performance degradation. Our initial work building PBI-based elevated temperature stacks focused on planar 4-cell stacks housed in low-temperature cofired ceramic substrates.⁶ Not surprisingly, some performance degradation was observed during long-term testing in these materials. As a result, we developed a corrosion testing procedure as a way to evaluate the potential long-term stability of cell hardware materials. A variety of ceramic and graphite materials were subjected to this test, and a lightweight graphite composite was found to be stable to this corrosion test. Endplates and bipolar plates were fabricated using this material based on a simple flow field design for benchmarking elevated temperature stacks capable of generating up to 30W for powering a net 20W-25W fuel cell system prototype.

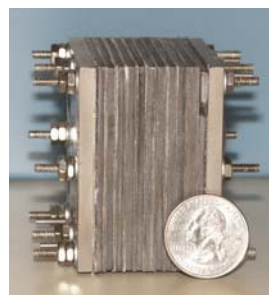


Figure 2. A 10-cell elevated temperature stack..

Figure 2 shows a 10-cell stack made recently using these graphite materials and Celtec® MEAs. Overall dimensions are 2.32in X 2.32in X 1.60in. Fuel cell testing using the graphite hardware was begun recently using single cells. For thermal and efficiency reasons, the stacks incorporated into portable fuel cell systems will be operated at current densities near 200mA/cm². Cell polarization and power density curves in this region are shown in Figure 3. Performance is observed to be somewhat lower than obtained in poco graphite cell hardware, probably because of the higher resistance using this form of graphite (~0.25Ωcm² vs. ~0.10Ωcm²).

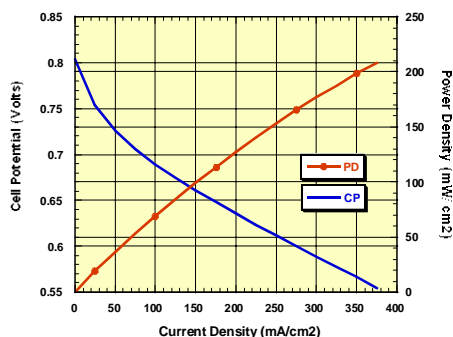


Figure 3. Single cell performance of Celtec® MEA in stack hardware under H₂-Air at 160°C.

The lifetime of PBI-based MEAs like Celtec® under fuel cell conditions have been demonstrated to be more than 6000hr at 160°C with minimal performance degradation.¹ Figure 4 shows the performance of a single cell under H₂-Air over 200hrs at constant current of 200mA/cm².

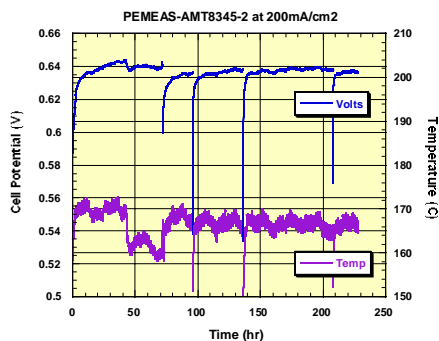


Figure 4. Constant current performance of Celtec® MEA in stack hardware under H₂-Air at ~165°C.

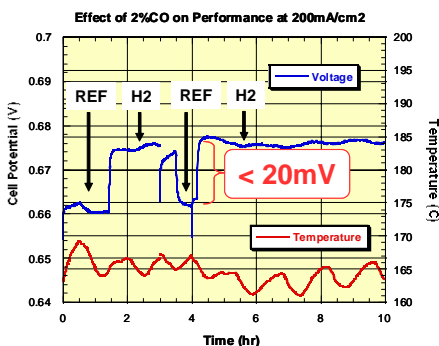


Figure 5. Effect of CO on cell voltage at 200mA/cm² and 165°C.

Using simulated reformat instead of H₂, a performance loss of <20mV at ~165°C was observed. Figure 5 shows the effect of 2%CO on the performance of a Celtec® MEA in poco graphite hardware. As cell temperature is increased up to 200°C, the effect of CO diminishes.

Our initial stack results are shown in Figure 6 under H₂-Air. Subcells were within 30mV and stable at 198mA/cm² and 160°C. Total stack voltage was 3.29V, corresponding to a power output of 8W. Assuming a voltage loss of 15mV/cell when running under simulated reformat, this stack would produce in excess of 7.5W.

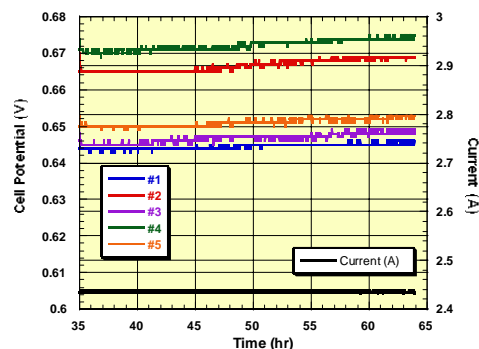


Figure 6. Constant current performance of 5-cell Celtec® stack at 160°C.

Conclusions

Portable energy is one of the key arenas for PEM fuel cells to enter into the power source market. It is expected that miniature fuel cells will one day provide power for a wide range of consumer/portable products such as cellular phones, 2-way radios, laptop computers, PDAs, portable cameras and electronic games. We have successfully built elevated-temperature stacks using Celtec® MEAs and lightweight, compact graphite cell hardware. The performance of a 5-cell stack using a simple flow field design was shown to be capable of generating an average of 0.658V/cell, for a total output of 8W under H₂-Air, and estimated to produce 7.8W under simulated reformat-Air.

Acknowledgement. This work was supported through collaborative participation in the Power and Energy Consortium sponsored by the U.S. Army Research Laboratory under the Collaborative Technology Alliance Program, Cooperative Agreement DAAD19-01-2-0010.

References

- (1) Li, Q.; He, R.; Jensen, J.O.; Bjerrum, N.J. *Chem. Mater.*, **2003**, *15* (26), 4896.
- (2) Ma, Y.-L.; Wainright, J.S.; Litt, M.H.; Savinell, R.F. *J. Electrochem. Soc.*, **2004**, *151*(1), A8.
- (3) Li, Q.; He, R.; Gao, J.-A.; Jensen, J.O.; Bjerrum, N.J. *J. Electrochem. Soc.*, **2003**, *150*(12), A1608.
- (4) Jannasch, P. *Curr. Opin. Coll. Interface Sci.*, **2003**, *8*, 96.
- (5) Savadogo, O. *J. Power Sources*, **2004**, *127*(1-2), 135.
- (6) Rogers, S.; Gervasio, D.; Koripella, R.; Samms, S.; Tasic, S. *Proceedings of the Power Sources Conference*, **2002**, *40*, 269.

REACTION ENGINEERING PERSPECTIVE OF PEM FUEL CELLS: THE STIRRED TANK REACTOR AS A BUILDING BLOCK

Ee-Sunn J. Chia, Jay B. Benziger, and Ioannis G. Kevrekidis

Department of Chemical Engineering
Princeton University
Princeton, NJ 08544

Introduction

There has been widespread research on polymer electrolyte membrane (PEM) fuel cells since they have been touted as the next alternative power source. The PEM fuel cell consists of two reactors separated by an ion-conducting barrier (membrane). Protons produced at the anode are transported across the membrane to the cathode where water is produced. The two sequential chemical reactions in a PEM fuel cell are thus coupled to the transport of the intermediate products between the reactors. Before PEM fuel cells become commercially viable for mobile applications, predictive models of fuel cell performance that correctly incorporate the transient interplay of reaction and transport processes are critical.

PEM fuel cells are often constructed and modeled as two- and three- dimensional integral reactors.¹⁻⁴ These integral reactors may be modeled as differential (stirred tank) reactors in series. A differential fuel cell reactor has uniform compositions at the anode and cathode; the only spatial gradients are transverse through the membrane. This circumvents the complexities of the existing integral reactors since there are no spatial variations involved in the stirred tank reactor. From a differential PEM fuel cell, we are able to extract valuable information pertaining to the kinetics and the convective transport. We have shown that a stirred tank PEM fuel cell reactor exhibits ignition/extinction phenomena and have reproducibly demonstrated steady state multiplicity.⁵⁻⁷

We present here a summary of the stirred tank PEM fuel cell reactor findings, the remarkable analogy to the autocatalytic in an exothermic stirred tank reactor, and an extension of the stirred tank PEM fuel cell to approximate the conventional integral reactor.

PEM Fuel Cell Reactor

Differential Reactor. The differential PEM fuel cell shown in **Figure 1** consists of two stirred tank reactors separated by the membrane electrode assembly (MEA) with a membrane area of 1 cm². The current collecting graphite plates contained gas plenums with volumes of 0.2 cm³. Pillars were machined onto the graphite plates to ensure a uniform sealing pressure on the MEA. The fuel cell was designed to ensure uniform gas compositions above the membrane.

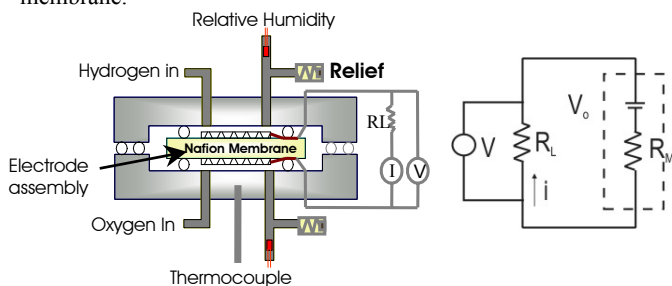


Figure 1. Schematic depiction of the stirred tank PEM fuel cell reactor and its equivalent circuit. The membrane electrode assembly separates the anode and cathode chambers.

The fuel cell is connected in series to an external load resistance R_L . The voltage and current are measured across R_L . The fuel cell was constructed such that the residence times of the reactant gases ($Volume/Flow\ rate$) are larger than the characteristic diffusion time ($Volume^{2/3}/D$). Flow rates of the reactant gases (1-10 mL/min) were controlled with mass flow controllers. As the reaction progresses, the amount of water in the membrane changes and this alters the membrane resistance, R_M (a dryer membrane indicates a higher value of R_M). We study the fuel cell behavior under the influence of four operating parameters: temperature (T), external load resistance (R_L), flow rates of reactants into the anode and cathode, and relative humidity of the inlet reactant streams.

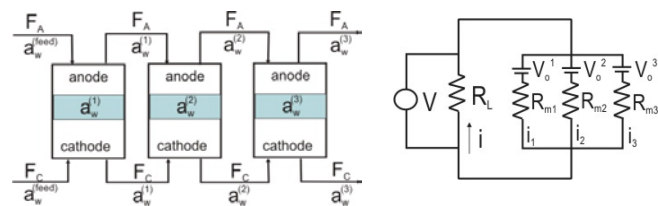


Figure 2. Stirred tank reactors in series approximate an integral reactor. The reactors are parallel electrically.

Integral Reactor. The other extreme of a well-mixed reactor is the plug flow (integral) reactor where the reactants flow downstream without dispersion. The stirred tank PEM fuel cell can be thought of as a differential element in an integral reactor. Therefore, we may approximate the standard serpentine flow PEM fuel cell integral reactor by placing many stirred tank PEM fuel cells in series as shown in **Figure 2**. The membrane hydration in each tank will vary downstream. Thus each tank is associated with a different R_M . Although several reactors are placed in series, they are electrically in parallel as depicted in **Figure 2**.

Results and Discussion

Multiple steady states. Water plays an important role in the fuel cell because it eases proton transport from the anode to the cathode. In fact, Yang et al. has shown that the membrane conductivity is exponentially dependent on the water activity in the membrane but only weakly dependent on temperature.⁸ It is the water balance in the fuel cell that leads to the multiple steady states shown in **Figure 3**. The steady state current achieved in a stirred tank reactor fuel cell depends on the initial water content in the membrane.⁵ Moreover, the water balance in the stirred tank reactor fuel cell is analogous to the energy balance in the classical chemical engineering exothermic stirred tank reactor.

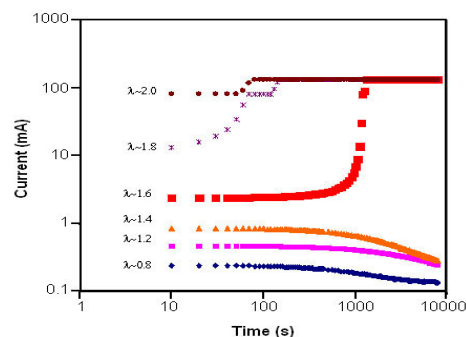


Figure 3. Start-up of the PEM fuel cell ($T=50^{\circ}\text{C}$) with different initial membrane water contents ($\lambda = \text{H}_2\text{O}/\text{SO}_3$) and dry feeds.

The product water in the PEM fuel cell hydrates the membrane, enhances proton transport, and thereby autocatalytically accelerates the reaction rate. In an exothermic reaction, the produced heat accelerates the reaction via an Arrhenius temperature dependence in the reaction rate constant. Based on this analogy, we have shown that the classical analysis of heat autocatalycity can be implemented to our stirred tank PEM fuel cell as well.⁷

Dynamics. We have also observed the fuel cell response to changes in the operating parameters. As depicted in **Figure 4** a decrease in R_L is followed by a sharp jump in current before a relatively slower equilibration to the new steady state current. We have observed similar types of responses to changes in other parameters. We believe that the membrane acts as a *reservoir* for water and any change in operating conditions will alter the water balance inside the membrane. The membrane requires about 10^2 s to equilibrate to the new operating conditions.

In addition to these responses, we have recorded the occurrence of autonomous oscillations in the stirred tank reactor PEM fuel cell. Despite maintaining fixed operating conditions, the fuel cell oscillates regularly between two currents as shown in **Figure 5**. We believe that the oscillations are attributed to a coupling between the transport processes and the mechanical relaxation of the membrane.⁹

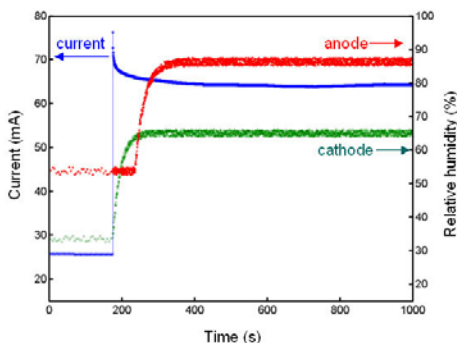


Figure 4. Response to a decrease in R_L from 20Ω to 7Ω . The fuel cell current increases sharply but eventually equilibrates at a lower current.

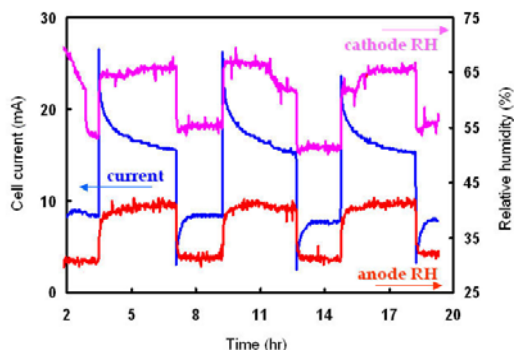


Figure 5. Autonomous oscillations observed under fixed conditions of $T=80^\circ\text{C}$, $R_L=20\Omega$, $F_{\text{anode}}=5$ mL/min, $F_{\text{cathode}}=10$ mL/min.

Tanks in series. We have placed several stirred tanks in series to approximate the behavior of an integral PEM fuel cell. The product water or unused reactant exiting an earlier tank will be fed directly into the subsequent tank. Tracking how the current evolves in each tank over time is equivalent to tracking the current down an integral reactor over time. This method allows us to observe regions where the fuel cell will ignite. Hydrogen may flow co-current or counter-current to the oxygen flow. **Figure 6** shows that in counter-current flow, a large current is attainable in the middle tanks but only

the last tank in a co-current flow scheme will generate a large current at long times. When the flows are co-current, the initial tanks remain dryer while more water is brought into the last tank, creating suitable ignition conditions in the final tank. However, in a counter-current scheme, water from the first and last tanks are flowing in opposite directions, making it easier for ignition in the middle. The flow rate of hydrogen is twice that of oxygen in **Figure 6**.

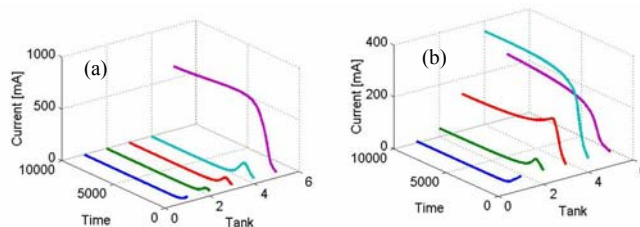


Figure 6. Current profiles for 5 tanks in series with flow of reactants in (a) co-current and (b) counter-current.

Conclusions

Our results have indicated that the interplay of proton transport with water activity in the PEM membrane underpins the observed dynamical phenomena. Water ionizes and shields stationary anions in the membrane, enhancing proton transport by orders of magnitude. Existing fuel cell literature contains extensive reports that PEM fuel cells only operate when sufficient water is present in the membrane. We have demonstrated that it is possible to operate the PEM fuel cell with dry feeds of hydrogen and oxygen. We have elucidated the role of a *critical initial* membrane water content for ignition.

We have established that the product water catalyzes the reaction in an autocatalytic manner analogous to the autocatalytic rate acceleration in the exothermic stirred tank reactor. The water balance in the membrane leads to multiple steady states in the fuel cell. In addition, the membrane functions like a reservoir for water and needs time to equilibrate to changes in the operating conditions. Although the model reactors are not optimal for reactant conversion, they are specifically designed to measure system parameters, including effective kinetic and transport properties.

Acknowledgement. This work is supported under NSF grant CT50354279.

References

- (1) Springer, T. E.; Zawodzinski, T. A.; Gottesfeld, G., *J. Electrochem. Soc.* **1991**, *138*, 2334.
- (2) Bernardi, D. M.; Verbrugge M. W., *J. Electrochem. Soc.* **1992**, *139*, 2477.
- (3) Fuller, T. F.; Newman, J., *J. Electrochem. Soc.* **1993**, *140*, 1218.
- (4) Janssen, G. J. M., *J. Electrochem. Soc.* **2001**, *148*, A1313.
- (5) Moxley, J. M.; Tulyani, S.; Benziger, J. B., *Chem. Eng. Sci.* **2003**, *58*, 4705.
- (6) Benziger, J. B.; Chia, E.; Karnas, E.; Moxley, J.; Teuscher, C.; Kevrekidis, I. G., *AIChE J* (in press).
- (7) Chia, E.; Benziger, J. B.; Kevrekidis, I.G., *AIChE J* (in press).
- (8) Yang, C. R.; Srinivasan, S.; Bocarsly, A. B.; Tulyani, S.; Benziger, J. B., *J. Membrane Science* (in press).
- (9) Benziger, J. B.; Chia, E.; Moxley, J.; Kevrekidis, I. G. *Chem. Eng. Sci* (submitted).

DYNAMIC SIMULATION OF FUEL CELL SYSTEMS

Rory A. Roberts, Jack Brouwer, and Scott Samuelsen

National Fuel Cell Research Center
University of California, Irvine

Abstract

The development of dynamic simulation tools for fuel cell systems and fuel cell/gas turbine (FC/GT) systems is required to understand the response of fuel cell systems to both scheduled and unscheduled perturbations. These tools supply the foundation on which control strategies can be developed and tested before they are actually implemented in a physical system. For high temperature fuel cell systems that generally incorporate reformation of hydrocarbon fuels externally and/or internally, knowing how the system can potentially respond to a load perturbation or a fuel flow composition perturbation is extremely important to system performance and reliability.

In addition, when developing control strategies for high temperature fuel cell systems, it is important to identify of the hazardous conditions that may lead to degradation in performance or the destruction of the fuel cell and other components of the system. Being able to identify these conditions with a detailed and robust dynamic model can lead to safer and more responsive operation for fuel cell systems. This work provides a dynamic simulation of a load perturbation that could produce undesirable conditions if proper control strategies are not designed for the fuel cell system. In addition, the dynamic simulations provide insights into both component and system dynamic performance parameters that illuminate some less than obvious dynamic responses within representative integrated high temperature FC/GT hybrid systems.

Approach

Dynamic models for molten carbonate fuel cells (MCFC), heat exchangers, gas turbines (GT) and catalytic oxidizers have been developed in a Simulink™ platform. The dynamic models are based on first principles. Descriptions of the models are found in previous papers^{1,2}. All the models incorporate the conservation equations for energy, mass, and momentum. The MCFC model incorporates the electrochemistry and internal reformation chemistry reactions as well. The catalytic oxidizer model assumes complete combustion. The gas turbine uses general performance maps. These components are integrated to simulate a complete molten carbonate fuel cell/gas turbine (MCFC/GT) system.

In each of the significant component models (e.g., fuel cell, heat exchanger) some degree of geometric resolution is captured, albeit in a simplified (usually one-dimensional) manner. The dynamic equations that govern the concurrent processes of heat, mass, and momentum transfer, chemical reaction and electrochemical reaction are solved, for example along one dimension of the component representing that which varies most significantly and including geometrical features such as actual fuel cell size and shape. This approach to dynamic simulation is significantly more computationally intensive than the traditional bulk component model approach, but it provides significant added value. First, insights into the performance parameters of each component are provided (e.g., temperature profiles) so that one can determine whether or not significant component stress or other conditions of concern may be reached during responses to perturbations. Only if this insight is provided can one determine what needs to be controlled and how to control it. Secondly, accurate predictions of component performance cannot be achieved without this dimensional and geometric resolution. This is certainly the case for reactors such as catalytic

oxidizers or fuel cells which rates of chemical reaction are exponentially dependent upon local temperature. This is also true for systems as simple as heat exchangers whose dynamic performance cannot be captured through a bulk effectiveness heat transfer model. As a result, these more complex and computationally intensive, yet simply resolved component models both contribute to increased insight and more accurate predictions of fuel cell system performance.

Results

A complete dynamic MCFC/GT system model was constructed to simulate a 1MW MCFC/GT system similar to the sub-MW Direct Fuel Cell/Gas Turbine (DFC/GT) hybrid system developed by FuelCell Energy. A diagram of the system configuration is presented in Figure 1. The model was developed by integrating individual robust simulation modules of the type described above, each simulating the dynamic performance of a component shown in Figure 1. The integration is accomplished using the graphical user interface and toolbox utilities of Simulink™.

To demonstrate the dynamics of this type of hybrid fuel cell system, a load perturbation was simulated on an open loop system of the type presented in Figure 1. For the load perturbation investigated, the MCFC underwent a 3% load drop. The power drop was achieved by changing the external load resistance applied to the MCFC. Figure 2 presents the results for the MCFC, GT and total plant power as the integrated system responds to the load perturbation. The MCFC power initially drops, undershooting by approximately 12% (90 kW) of the final steady state power. This effect is due to the temporary deficit of fuel in the anode gas (at the end of the anode compartment of the fuel cell). The MCFC power quickly recovers to a lower steady state value of power output. The total plant power reflects the dynamics of the MCFC power response. The GT power begins to rise after 5 seconds due to a rise in the turbine inlet temperature (TIT). It takes approximately two minutes for the GT to reach steady state. There is a slight recovery in total power because of the rise in GT power.

When the MCFC drops to a lower power level, there is more unspent fuel in the anode stream. This increase in unspent fuel causes the catalytic oxidizer temperature to rise. The rise in catalytic oxidizer temperature is illustrated in Figure 3. The rise in catalytic oxidizer temperature increases the GT TIT, which results in higher GT power. The increase in catalytic oxidizer temperature also increases the cathode inlet temperature, which is presented in Figure 3 as well.

Decreasing the MCFC power by 3% caused an 11% increase in GT power and an overall 2% decrease in total plant power. The cathode inlet temperature experienced a 14°C temperature rise, which could potentially overheat the MCFC.

Conclusions

Open loop results were presented to demonstrate the dynamics of the MCFC/GT system. From the dynamic results it can be seen that great care must be taken to control the MCFC/GT hybrid system. Safe operating temperatures need to be maintained throughout the system to improve the performance and life cycle of the system. To design FC/GT systems with load following capabilities one must include intelligent control strategies that can meet changing load demands while maintaining high performance and safe operation. The integration of various component technologies (e.g., fuel cell, GT, heat exchangers) results in a complex system with dynamic response characteristics that are not easy to elucidate without robust and geometrically resolved models.

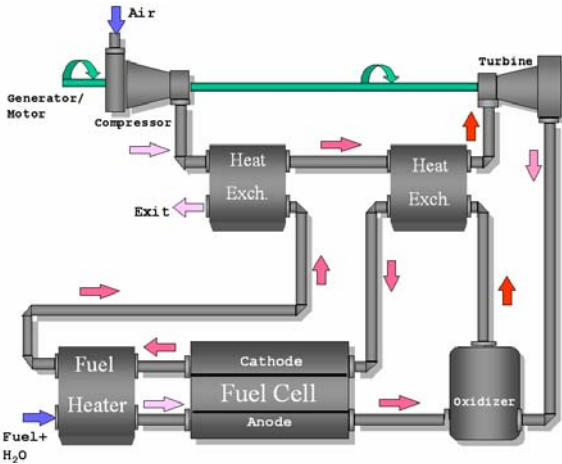


Figure 1. DFC/GT hybrid system diagram

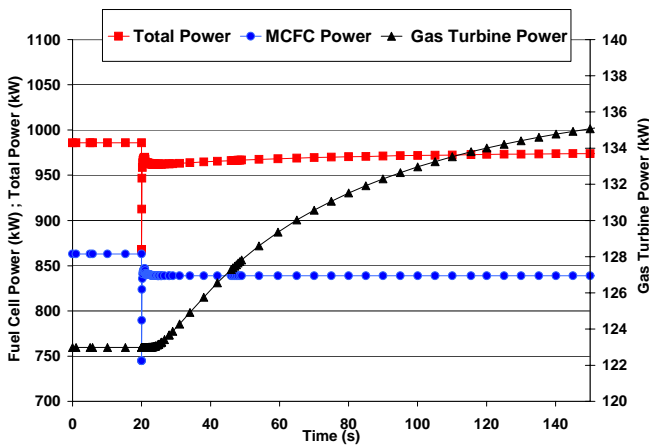


Figure 2. Total plant power, MCFC, and gas turbine power due to a load drop on the MCFC

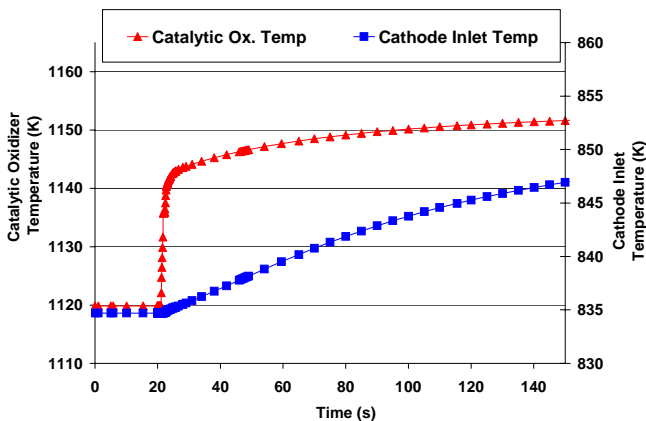


Figure 3. Catalytic oxidizer temperature and cathode inlet temperature

Acknowledgements. This project was made possible by support received from the California Energy Commission, and the U.S. Department of Defense Fuel Cell Program.

Legal Notice

This paper was prepared in part as a result of work sponsored by the California Energy Commission (Commission). It does not necessarily represent the views of the Commission, its employees, or the State of California. The Commission, The State of California, its employees, Contractors and Subcontractors make no warranty, expressed or implied, and assume no legal liability for the information in this paper; nor does any party represent that the use of this information will not infringe upon privately owned rights. This paper has not been approved or disapproved by the Commission nor has the Commission passed upon the accuracy or adequacy of the information in this paper.

References

1. Roberts, R.A., Brouwer, Jack, Gemmen, Randall, Liese, Eric, *Dynamic Simulation of Carbonate Fuel Cell-Gas Turbine Hybrid Systems*. ASME Turbo Expo, Vienna, Austria, 2004. **GT2004-53653**.
2. Roberts, R.A., Brouwer, Jack, Gemmen, Randall, Liese, Eric, *Inter-Laboratory Dynamic Modeling of a Carbonate Fuel Cell for Hybrid Application*. 2003 ASME Turbo Expo, Atlanta, Georgia, 2003. **GT2003-38774**.

PEM FUEL CELLS: HOW THINGS WORK

Thomas A. Zawodzinski

Department of Chemical Engineering, Case Western Reserve
University, 10900 Euclid Ave.,
Cleveland, OH 44106

Proton exchange membrane (PEM) fuel cells operating on hydrogen are a particularly appealing technology with a wide range of potential applications. This talk will introduce the technology by describing the components of a typical PEM fuel cell system and how they function. After an initial birds-eye overview, the current state of the art of individual materials and the structure and function of central components such as polymer membranes and electrodes will be described. Key aspects of function that have impact at the system level, such as water management and its implications for materials function and properties, will also be discussed. Finally, a few illustrations of the speaker's research group's current efforts on new membranes and electrodes will be presented. Emerging research opportunities at the fundamental level will be touched on, with an emphasis on needed understanding.

CAN AVAILABLE MEMBRANES AND CATALYSTS MEET AUTOMOTIVE POLYMER ELECTROLYTE FUEL CELL REQUIREMENTS?

Mark Mathias, Hubert Gasteiger, Rohit Makharia, Shyam Kocha, Tim Fuller, Tao Xie, and Jason Pisco

General Motors
Fuel Cell Activities
10 Carriage Street
Honeoye Falls, NY

Introduction

Over the past few years, significant R&D efforts have been aimed at meeting the challenging cost and performance targets required for the use of polymer electrolyte fuel cells (PEFCs) in automotive applications. Besides engineering advances in bipolar plate materials and design, the optimization of membrane-electrode assemblies (MEAs) was an important enabler in reducing the cost and performance gaps towards commercial viability for the automotive market. On the one hand, platinum loadings were reduced from several $\text{mg}_{\text{Pt}}/\text{cm}^2_{\text{MEA}}$ to values of 0.5-0.6 $\text{mg}_{\text{Pt}}/\text{cm}^2_{\text{MEA}}$ in current applications and loadings as low as 0.25 $\text{mg}_{\text{Pt}}/\text{cm}^2_{\text{MEA}}$ have been demonstrated on the research level.² On the other hand, implementation of thin membranes (20-30 μm)^{3,4} as well as improvements in diffusion medium materials, essentially doubled the achievable power density of MEAs to ca. 0.9 $\text{W}/\text{cm}^2_{\text{MEA}}$ (at 0.65 V),⁵ thereby not only reducing the size of a PEFC fuel cell system, but also reducing its overall materials cost (controlled to a large extent by membrane and Pt-catalyst cost). In this paper, we evaluate current cost, performance, and durability issues associated with PEFC membranes and catalysts, and we suggest areas where a renewed focus of R&D effort will accelerate the commercialization of PEFCs in automotive applications.

Membrane Requirements

Membrane Cost. The current polymer electrolyte fuel cell membranes of choice are based on poly[perfluorosulfonic acid] (PFSA), and are produced by DuPont, Asahi Glass, Asahi Kasai, and Solvay. PFSA membrane has been commercialized for the chlor-alkali industry, but the market volume is small (<65 metric tons (MT)/year)⁶ and the price is high (~\$5000/kg), characteristic of a specialty material. This compares with the commodity poly[tetrafluoro-ethylene] which is produced at a volume of 80,000

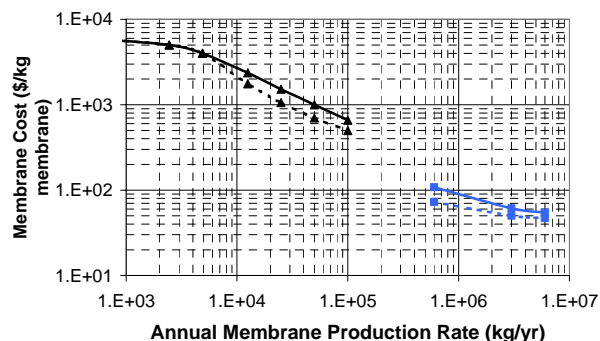


Figure 1. Price projection of PFSA membrane (25 micron thick, 0.05 kg/m^2 , 1100 EW) at high volume. Low volume projections provided by DuPont.⁷ High volume numbers from GM cost study. Two lines in each case roughly indicate uncertainty on projections.

MT/year and sells in the neighborhood of \$10/kg. To assess the high-volume automotive price potential of PFSA membrane, we conducted a study in which we designed for cost estimation purposes, vinyl ether monomer, PFSA polymer, and membrane production plants. The price projections are shown in **Figure 1** and indicate that at 1 million vehicles/yr (100 kW/vehicle at ca. $1\text{kg}_{\text{membrane}}/100\text{kW}$), which would require approximately 1,000 MT/yr of PFSA, the membrane cost would drop to less than \$100/kg. This translates to approximately \$1/kW, an affordable price against the \$50/kW total power system target, and demonstrates that PFSA price should not be prohibitive for automotive application. Whereas there are reasons why alternatives to PFSA membranes are of interest, the high price of PFSA membrane is at best a secondary one.

Membrane Performance. Current PEFCs systems run at a maximum of 80°C because operation above that temperature requires too much system support of the membrane (e.g. pressure, humidification) to maintain close to 100% relative humidity (RH) required for good proton conduction. Also, current membranes have glass transition temperatures in the range of 80-120°C and are thus subject to creep and hole-formation at temperatures in that range. **Figure 2** shows the conductivity vs. RH for a Nafion® 1100 EW ($\text{EW} = \text{g}_{\text{polymer}}/\text{mol}_{\text{H}^+}$) membrane at 80°C, although the conductivity vs. RH response is not very sensitive to temperature up to 120°C.⁸ At the fully humidified condition, the conductivity of ~0.1 S/cm translates to a tolerable 25 mV loss for a 25 μm membrane at a current density of 1A/cm². The figure also shows that the conductivity drops off very quickly with RH, thereby requiring the fuel cell system to provide for humidification of the reactant streams. There would be great value in reducing system complexity (and thus cost) from a membrane that maintains good conductivity to low-RH such as shown in the “desired” curve in Figure 2 (0.1 S/cm at 50% RH), even if limited to a maximum of 80-100°C operation. Indeed developments by manufacturers have shown promising progress in this direction for PFSA membranes. An example is shown on Figure 2, a low (<800) EW PFSA that has conductivity of 0.06-0.07 S/cm at 50% RH and 80°C.

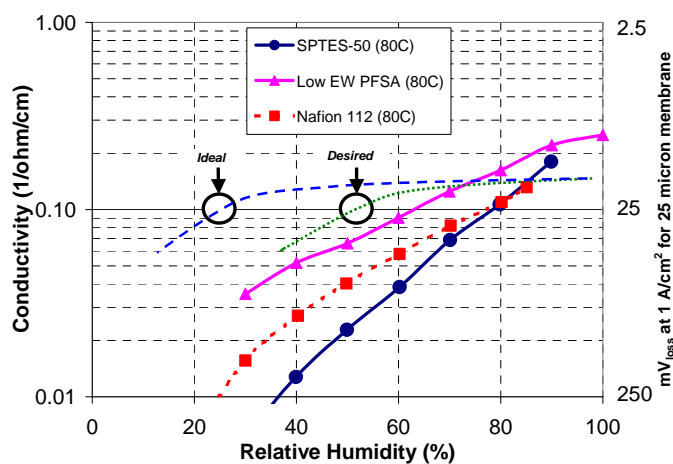


Figure 2. Conductivity vs. RH at 80°C for Nafion® 112, sulfonated polyaryleneethioethersulfone (SPTES),⁹ and low-EW (<800) PFSA. Also indicated are desired (50% RH inlet, 150 kPa_{abs} , 80-100°C) and ideal (0% RH inlet, 120 kPa_{abs} , 100°C) conductivity characteristics to enable system simplification and vehicle heat rejection.

Also shown in Figure 2 are data from a sulfonated polyarylenethioethersulfone (SPTES-50, 1.6 mEq/gm) from Dang and coworkers.⁹ This conductivity vs. RH performance is the characteristic of many hydrocarbon membranes -- it surpasses Nafion® 112 at high RH (>80%) but drops off more sharply than Nafion® 112 as the RH is decreased. Available hydrocarbon membranes do not yet appear competitive with materials in the PFSA family with regards to their low-RH (<75%RH) conductivity.

Unfortunately, it turns out that the heat rejection rate of current automotive radiators is insufficient to reject continuous full power waste heat loads with the 80°C fuel cell stack temperature. Operation at 80°C results in significant adjustment in thermal system complexity/cost, vehicle design, and/or negative impact on the high-power vehicle capability (e.g. length of time at full load). Vehicle system analysis indicates that 120°C high-power operation would enable the use of radiators similar to those available today,¹⁰ and this has driven the need for development of a high-temperature membrane that could operate at temperature of up to 120°C. We earlier argued that such a membrane would need to have a characteristic conductivity curve like that shown as the "ideal" curve in Figure 2 in order not to increase system-support demands over those of state-of-the-art membranes.⁵ This has led to development projects focused on high-temperature (120°C), low-RH (25%) membranes.

Our latest estimates, encompassing the impact of higher temperature on Pt catalyst dissolution rates (discussed below) suggest that extended operation above 80°C may result in unacceptable Pt cathode catalyst dissolution rates. Operation limited to 80°C will result in heat rejection systems for fuel cell vehicles that are more complex than in current automotive applications. This in turn drives for a more aggressive simplification of the fuel cell system, achievable for example by the development of low-RH membranes which would enable stack operation at 80°C without external humidification. Very short excursions of up to 100°C may be tolerable, but fuel cell stack temperatures above 80°C risk unacceptably high cathode catalyst degradation rates. In light of these arguments, low-RH (0.1S/cm at 25-50%RH) membranes with a main operating temperature of 60-80°C and short-time temperature excursions up to ca. 100°C now appear to be the desired development goal to enable simpler fuel cell systems that could compensate for the increased complexity of the thermal system. The "ideal" curve shown in Figure 2 (0.1S/cm at 25%RH) is an appropriate membrane development target for 100°C operation -- such a membrane would enable a system pressure of 120 kPa_{abs} and no external humidification, a significant simplification over current state-of-the-art requirements.

Phosphoric acid doped polybenzimidazole (PBI), first identified by Case Western Reserve University and now under development by PEMEAS GmbH, is a high-temperature membrane that allows operation up to approximately 200°C with very low humidification requirement.¹¹ However, issues that prohibit its use for automotive are instability in the presence of liquid water and inefficient cathode structures resulting in low areal power density.

Whereas much work is ongoing to develop alternative membranes to PFSA, the vast majority of approaches rely on the sulfonic acid based conduction mechanisms. Fundamental work such as morphological investigations¹² and molecular modeling are needed to determine the physical limits of these materials in terms of conductivity vs. RH characteristic shown in Figure 2. Also, the data in Figure 2 suggest that PFSA's may have an intrinsic morphological advantage at low-RH over the hydrocarbon materials, and this requires investigation at the fundamental level.

Membrane Durability. To be successful in automotive application, membranes must survive 10 years in a vehicle and 5,500 hours of operation including transient operation with start-stop and freeze-thaw cycles. Even though thin polymer electrolyte membranes (20-30 μm) enable high power density operation, the requirements on their chemical and mechanical stability are significantly more demanding compared to the thick membranes (100-200 μm) used in the past. While PFSA membranes are chemically very stable, they are known to degrade in the fuel cell environment⁴ via peroxy-radical attack, strongly enhanced in the presence of trace iron contamination.¹³ While the exact degradation mechanism is being actively investigated, its understanding is clearly required to improve the chemical stability of PFSA's.

Less is understood about the mechanical property requirements of polymer electrolyte membranes, but it is clear that dimensional stability as a function water uptake and removal is a critical consideration. For example, membranes expand when wet but sometimes shrink to less than their pre-wet size when dried again due to relief of residual processing stresses in the material. More work is needed to understand the connection between these *ex-situ* properties and *in-situ* failure. Clearly though, dimensional stability and limited water uptake when wet (<100 wt% maximum, <50 wt% preferred) are desired for suitable membranes. To support these efforts, deepened fundamental understanding of the morphology of these materials both through experiments (e.g. SAXS, SANS) and molecular modeling is needed.

Electrocatalyst Requirements

Cost and Performance. In current H₂/air applications, MEA (membrane-electrode assembly) Pt-loadings are on the order of 0.2-0.4 mg_{Pt}/cm² on the anode and typically 0.4 mg_{Pt}/cm² on the cathode.³ Owing to the fast H₂ oxidation kinetics on carbon supported platinum catalysts (Pt/C), anode Pt-loadings can be lowered to 0.05 mg_{Pt}/cm² without performance loss.² At nominal operating conditions with H₂/air (s=2/2) at 150kPa_{abs} and 80°C, state-of-the-art MEAs with a total Pt-loading of 0.45 mg_{Pt}/cm² achieve power densities of P_{MEA}≈0.7 W/cm² at a single cell voltage of 0.65 V.^{2,14} As shown in the first row of Table 1, this demonstrated performance equates to Pt-specific power densities, P_{Pt}, of 0.63 g_{Pt}/kW. While being a significant improvement over MEA performance achieved in the 90's,¹ these Pt-loadings still result in noble metal costs of approximately 22 \$/kW (assuming ≈35 \$/g_{Pt} for a Pt/C catalyst) and do not meet the stringent cost requirements for automotive applications.

Table 1. MEA power densities, P_{MEA} [W/cm²], and Pt-specific power densities, P_{Pt} [g_{Pt}/kW], in state-of-the-art MEAs and mass-transport optimized MEAs with anode Pt-loadings of 0.05 mg_{Pt}/cm².

assumptions	catalyst activity	cathode loading [mg _{Pt} /cm ²]	P _{MEA} at 0.65V [W/cm ²]	P _{Pt} at 0.65V [g _{Pt} /kW]
current MEA	Pt/C	0.4	0.71	0.63
opt. MEA	Pt/C	0.4	0.91	0.48
opt. MEA	2x Pt/C	0.1	0.78	0.19
opt. MEA	4x Pt/C	0.1	0.91	0.17

One approach to reduce the cost per kW is based on improving the mass-transport losses observed at high current densities, resulting from the non-optimized performance of currently used diffusion

media and bipolar plate flow fields. The feasibility of this approach has been demonstrated on the research level, and optimized MEAs can be achieved by improved diffusion media treatments and coatings. This enables the achievement of improved power densities of $\approx 0.9 \text{ W/cm}^2$, thereby lowering the Pt-specific power density to $0.48 \text{ g}_{\text{Pt}}/\text{kW}$ (see 2nd row in table 1) or $\approx 17 \text{ \$/kW}$ of catalyst cost. While being a noticeable improvement, MEA Pt-loadings must be reduced to approximately $0.15 \text{ mg}_{\text{Pt}}/\text{cm}^2/\text{MEA}$ without significant performance loss in order to meet the stringent automotive cost requirements.

Contrary to the fast kinetics for H_2 oxidation on the anode catalyst, the oxygen reduction kinetics are very sluggish and a lowering of the cathode Pt-loading by a factor of 2 results in a cell voltage loss of 20 mV ,² while the required lowering by a factor of 4 which is needed to achieve $0.15 \text{ mg}_{\text{Pt}}/\text{cm}^2/\text{MEA}$ would result in a loss of at least 40 mV . For efficiency reasons, a loss of 40 mV is not acceptable and novel cathode catalysts with improved activity are required. Platinum-cobalt alloys (PtCo/C) and other Pt-alloys have been demonstrated to yield an activity improvement by a factor of 2 compared to a conventional Pt/C catalysts¹⁴ and implementation of these catalysts enables a lowering of the cathode Pt-loading to $0.1 \text{ mg}_{\text{Pt}}/\text{cm}^2$ at an overall performance loss of 20 mV . In this case (see 3rd row of table 1), the Pt-specific power density reduces to $0.19 \text{ g}_{\text{Pt}}/\text{kW}$, yielding a catalyst cost of $\approx 7 \text{ \$/kW}$. While this is acceptable from a catalyst cost point of view, Pt-alloy catalysts with a 4-fold activity enhancement would be desirable in order to improve the overall MEA power density to $\approx 0.9 \text{ W/cm}^2$, thereby reducing the cost of the other stack components (membranes, bipolar plates, diffusion media) via reduction of the overall plate area of a fuel cell stack.

In summary, the catalyst and MEA technology demonstrated on the research level is capable to meet automotive costs. Implementation in fuel cell applications, however, requires a renewed focus on the performance optimization of Pt-alloy catalysts and detailed studies on the durability of Pt-based fuel cell catalysts at the targeted anode and cathode loadings of 0.05 and $0.1 \text{ mg}_{\text{Pt}}/\text{cm}^2$, respectively.

Catalyst Durability. While Pt catalysts are very stable at the low electrode potentials occurring at the anode electrode (0 to 0.05 V vs. the reversible hydrogen electrode potential (RHE)), Pt sintering and dissolution as well as carbon corrosion pose significant concerns at the high electrode potentials occurring in the cathode electrode ($\approx 0.9 \text{ V}$ vs. RHE at idle conditions where minimal currents are drawn from the fuel cell stack). This has been observed in the past in the development of phosphoric acid fuel cells (PAFC) for stationary power applications, leading to operating strategies which circumvent idle conditions and limit high cell voltages to significantly below 0.9 V .^{15,16} In automotive applications, a large fraction of a vehicle's operating time will be spent at idle (i.e., cathode potentials of $\approx 0.9 \text{ V}$ vs. RHE), and the question arises whether Pt-dissolution at the lower operating temperature of $60\text{-}80^\circ\text{C}$ (in contrast to the 200°C for a PAFC) still has deleterious effects on cathode catalyst durability in a PEFC. Although very few data on the occurrence of Pt-dissolution in PEFCs are published, a recent report by Patterson¹⁷ shows that Pt can be found in the membrane after MEA aging in a fuel cell, indicating that Pt-dissolution is indeed an issue even at the low operating temperatures of a PEFC. A subsequent publication by Darling and Meyers¹⁸ models the Pt-dissolution process as the formation of Pt^{+2} and either its diffusion away from the electrode or its redeposition on the catalyst, both effects leading to a loss of Pt surface area concomitant with a loss in fuel cell performance.

In order to estimate the temperature dependence of Pt-dissolution at idle conditions, one might refer to the data by Bindra et al.¹⁹ who measured the Pt-solubility in phosphoric acid at 196°C . As shown in Figure 3 (solid line), the Pt-solubility reported at 196°C is consistent with Pt being oxidized to soluble Pt^{2+} ions, with the solubility increasing by a decade for every increase in voltage by $\approx 45 \text{ mV}$ (i.e., $RT/2F$). Based on this Nernstian behavior of the Pt-dissolution process, the Pt-solubility at 25°C may be estimated from the Pt/Pt^{+2} equilibrium published by Pourbaix²⁰ (Figure 3, dashed line). As a rough estimate, one may now calculate approximate activation energies for Pt-dissolution at $0.85\text{-}0.95 \text{ V}$ of $\approx 85\text{-}65 \text{ kJ/mol}$, and use these values to estimate the Pt^{+2} equilibrium concentrations at both 80 and 120°C that are shown in Figure 3 (short-dashed lines). As evident from figure 3, the Pt^{+2} equilibrium concentration at 0.9 V increases by two orders of magnitude from 25 to 80°C and an additional order of magnitude from 80 to 120°C .

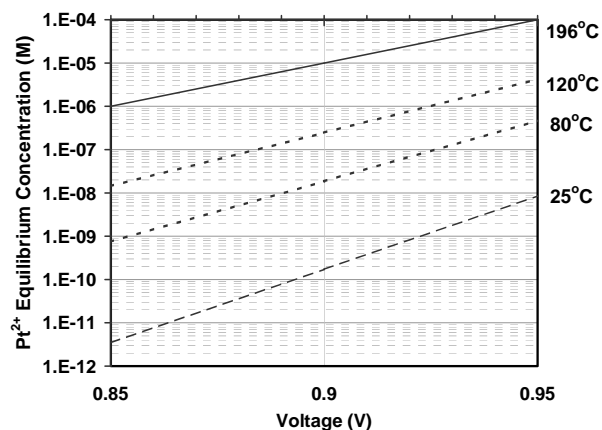


Figure 3. Equilibrium Pt^{2+} concentration in electrolyte as a function of temperature and voltage.

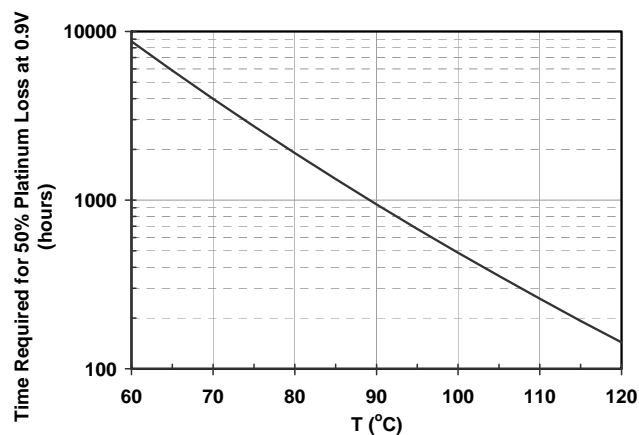


Figure 4. Estimated time required for 50% Pt loss from a Pt cathode catalyst at a loading of $0.1 \text{ mg}_{\text{Pt}}/\text{cm}^2$ during continuous operation at 0.9 V as a function of temperature.

Having estimated the Pt^{+2} equilibrium concentration, $c_{\text{Pt}^{+2}}$, at 0.9 V vs. temperature, one can now conduct a back-on-the-envelope calculation of the overall Pt loss as was used previously by Ross²¹

who estimated the Pt-loss from PAFC electrodes by means of a simple Fickian semi-infinite 1D diffusion equation:

$$N_{\text{Pt}} \approx D_{\text{eff}} \cdot C_{\text{Pt}^{+2}}/t$$

where N_{Pt} is the Pt-flux away from the electrode, t is the thickness of the electrode, and D_{eff} is the effective diffusion coefficient of Pt^{+2} in the ionomer phase of the electrode. Assuming that Pt^{+2} diffusion occurs in the aqueous phase of the ionomer, its diffusion coefficient is expected to be on the order of $1 \cdot 10^5 \text{ cm}^2/\text{s}$ as was used by Ross²¹, while the effective diffusion coefficient can be estimated as:

$$D_{\text{eff}} \approx D \cdot \varepsilon$$

where ε is the volume fraction of the ionomer in the electrode, with a value of ≈ 0.2 ,^{Ref 3} resulting in a value of $D_{\text{eff}} \approx 2 \cdot 10^6 \text{ cm}^2/\text{s}$. If we now assume an average electrode thickness, t , of $10 \mu\text{m}$ ^{Ref 3} and a Pt cathode loading of $0.1 \text{ mg}_{\text{Pt}}/\text{cm}^2$, we can estimate the total time required to lose 50% of the Pt from the cathode, assuming that Pt^{+2} diffuses into either the membrane or the gas diffusion medium where it becomes essentially inactive for the oxygen reduction reaction. This estimated Pt-loss at 0.9V versus temperature is shown in **Figure 4**. Figure 4 suggests that PEFC operation at idle conditions (i.e., at $\approx 0.9\text{V}$) at the currently typical operating temperature of 80°C would lead to a loss of 50% of the active Pt surface area over an operating time (at idle!) of 2000 hours. While significant time at idle conditions are expected in a vehicle driving cycle, a total of $\approx 40\%$ idling time over the entire service life of a PEFC vehicle is certainly a worst case scenario and unlikely to occur. Therefore, based on the presented back-on-the-envelope calculation, PEFC-vehicle operation at 80°C seems to be quite feasible. On the other hand, if a PEFC vehicle were to be operated at 120°C by means of a previously proposed high-temperature membrane,⁵ not more than 150 hours (see Figure 4) at idle conditions would be allowable, a requirement which does not appear feasible for vehicle operation.

In summary, our analysis suggests that fundamental Pt instability may limit the operation of PEFCs in realistic automotive applications to 80°C , with a few allowable excursions to higher temperatures in the vicinity of 100°C . This limit on the upper operating temperature of PEFC vehicles may be even more stringent as previous literature data indicate that voltage cycling (i.e., idle/load cycles) of Pt electrodes may lead to even enhanced Pt-dissolution rates.^{17,18,22}

Summary

The currently known material set for PEFCs, i.e., PFSA membranes and Pt-based catalysts, are in principle able to meet the cost requirements for automotive applications. It should be stressed that alternative, non-PFSA based membranes are desirable if they enable low-RH operation, but that they are not required in terms of cost reduction, contrary to frequently made statements in this respect by the scientific community. Nevertheless, significant advances in materials optimization as well as in understanding and mitigating the currently observed degradation mechanisms are needed. Therefore, future R&D efforts should address the following issues:

- Understanding of the physical limits of materials based on the sulfonic acid conduction mechanism in order to enable the development of low-RH membranes operating at $60\text{-}100^\circ\text{C}$.
- Understanding of the fundamental chemical degradation mechanisms of ionomers used both in the electrode and in the membrane.
- Fundamental understanding of the morphology of membranes and its impact on their mechanical properties, particularly in terms of long-term creep and structural changes under cyclic conditions (i.e., cyclic variations of temperature and RH).

- Development of Pt-alloy cathode catalysts with improved activity and durability.
- Catalyst degradation considerations clearly demonstrate that PEFC operating temperatures need to be limited to $60\text{-}80^\circ\text{C}$, only allowing for short-term temperature excursions up to a maximum of 100°C . This is in strong contrast to previously communicated high-temperature requirements for 120°C operation.

Acknowledgment. We would like to thank Cortney Mittelsteadt of Giner Electrochemical Systems, LLC, for providing the conductivity data in Fig. 2.

References

1. Strasser, K.; In *Handbook of Fuel Cells – Fundamentals, Technology and Applications*; Vielstich, W.; Lamm, A.; Gasteiger, H. A. Eds.; John Wiley & Sons: Chichester, UK: **2003**; Vol. 4, Ch. 88, pp 1201-1214.
2. Gasteiger, H. A.; Panels, J. E.; Yan, S. G.; *J. Power Sources*, **127** (2004) 162.
3. Gasteiger, H. A.; Gu, W.; Makharia, R.; Mathias, M. F.; Sompalli, S.; In *Handbook of Fuel Cells* (ibid.): **2003**; Vol. 3, Ch. 46, pp 593-610.
4. Cleghorn, S.; Kolde, J.; Liu, W.; In *Handbook of Fuel Cells* (ibid.): **2003**; Vol. 3, Ch. 44, pp 566-575.
5. Mathias, M. F.; Gasteiger, H. A. In *Proceedings of the Proton Conducting Membrane Fuel Cells III Symposium*; The Electrochemical Society: **2002**, in press.
6. Doyle, M.; Rajendran, G.; In *Handbook of Fuel Cells* (ibid.): **2003**; Vol. 3, Ch. 30, pp 351-395.
7. DuPont Nafion® Fuel Cell Division, Fayetteville, NC.
8. Alberti, G.; Casciola, M.; Massinelli, L.; Bauer, B.; *J. Membrane Science*, **2001**, *185*, 73.
9. Bai, Z.; Williams, L. D.; Durstock, M. F.; Dang, T. D.; *Polym. Prepr.*, **2004**, *45(1)*, 60.
10. Masten, D. A.; Bosco, A. D.; In *Handbook of Fuel Cells* (ibid.): **2003**; Vol. 4, Ch. 53, pp 714-724.
11. Wainright, J. S.; Litt, M. H.; Savinell, R. F.; In *Handbook of Fuel Cells* (ibid.): **2003**; Vol. 3, Ch. 34, pp 436-446.
12. Rubatat, L.; Rollet, A. L.; Gebel, G.; Diat, O.; *Macromolecules*, **2002**, *35*, 4050.
13. LaConti, A. B.; Hamdan, M.; McDonald, R. C.; In *Handbook of Fuel Cells* (ibid.): **2003**; Vol. 3, Ch. 49, pp 647-662.
14. Gasteiger, H. A.; Kocha, S. S.; Sompalli, S.; Wagner, F. T.; submitted to *J. Appl. Catal. B*.
15. Breault, R. D.; In *Handbook of Fuel Cells* (ibid.): **2003**; Vol. 4, Ch. 59, pp 797-810.
16. Landsman, D. A.; Luczak, F. J.; In *Handbook of Fuel Cells* (ibid.): **2003**; Vol. 4, Ch. 60, pp 811-831.
17. Patterson, T.; In *Fuel Cell Technology Topical Conference Proceedings*, 2002 AIChE Spring National Meeting, March 10-14, **2002**.
18. Darling, R. M.; Meyers, J. P.; *J. Electrochem. Soc.*, **2003**, *150*, A1523.
19. Bindra, P.; Clouser, S.; Yeager, E.; *J. Electrochem. Soc.*, **1979**, *126*, 1631.
20. Pourbaix, M.; *Atlas of Electrochemical Equilibria in Aqueous Solutions*, Pergamon Press: Oxford, **1966**.
21. Ross, P.N.; In *Catalyst Deactivation*, Petersen, E.E.; Bell, A.T. Eds.; Marcel Dekker, Inc: New York, **1987**.
22. Kinoshita, K.; Lindquist, J. T.; Stonehart, P.; *J. Electroanal. Chem. Interfacial Electrochem.*, **1973**, *48*, 157.

DIRECT METHANOL FUEL CELLS FOR PORTABLE POWER APPLICATIONS

Shimshon Gottesfeld

MTI MicroFuel Cells
Albany, NY

When it comes to portable power applications, the key merit characteristics of fuel cells are somewhat different than in potential transportation, or stationary power applications. In the latter applications, it is the higher conversion efficiency of a fuel (basically hydrogen) derivable from a variety of potential sources and the low tail pipe emissions associated with such fuel, as well as the lower emission of CO₂ per unit energy consumed. In the case of portable power applications, the central merit characteristic is the high energy density of fuels vs. that of advanced batteries. The need for longer use time of hand held, or laptop devices of increasing functionality, creates market pull for portable power sources of higher energy density. Direct methanol fuel cells emerge as an interesting option, thanks to the high energy density and benign nature of a liquid fuel (100% methanol) stored in a small cartridge. At presently demonstrated conversion efficiencies near ambient conditions (methanol fuel – to – Wh to the load), a volume/weight of 5cc /4g of methanol fuel would provide the same energy as that of a fully charged, Li ion battery of 1300 mAh, typically associated with volume/weight of 20cc/24g.

The challenge of translating such an intrinsically strong advantage in energy density, fuel vs. battery, into a viable power source technology, is, however, non-trivial. Obviously, what replaces the battery in a complete “power-pack” based on a fuel cell, is not the fuel alone, rather the sum total of volumes and weights of: fuel + fuel cell + “balance of plant” (BOP) + hybridizing battery. So, while the advantages of fuel of high energy density look highly attractive for portable power applications, the complete implementation of the power pack requires to both maximize the conversion efficiency fuel-to-electric power and to minimize, at the same time, the weights and volumes of the fuel cell and BOP components to maintain an energy density advantage for the complete power pack.

Minimizing the volume/weight of the fuel cell, requires to achieve high power density and that requirement is made more severe when operating near ambient conditions, i.e., when advantages of enhanced internal cell temperature and/or pressure, cannot be utilized. How high a power density is required for some application, is obviously a function of the power demand in that application, as well as the power demand duty cycle. Applications of relatively low average power demand (average over a full day) with peak power demands limited to short durations, can be accommodated more easily with portable fuel cell technology recently developed. In such cases, the fuel cell would provide the average power over the day and a hybridizing battery would provide the peak power demands, thereby packaging most effectively energy (fuel) and power (battery). In a way, the approach can be then described as replacing a large part of the present battery in a given device, by fuel, of much higher energy content per unit weight/volume, while maintaining a small part of the present battery for purposes of peak power.

As to the BOP component of the fuel cell-based power pack, it has presented significant challenges in terms of both volume/weight and, more importantly perhaps, complexity. Therefore, the new,

direct methanol fuel cell (DMFC) –based technology platform developed at MTI Microfuel Cells has very unique combined properties of liquid fuel of high energy density, consumed directly in the fuel cell (no fuel processing upstream the fuel cell), with the BOP reduced to the bare minimum. The latter element required to come up with a rather revolutionary approach to operation of DMFCs, which allows to use direct feed of 100% methanol fuel into the cell anode, eliminating completely the need to dilute the fuel with water on entry to the cell and/or to collect for that purpose water at the air cathode and pump it back to the anode recirculation loop. The result is a highly simple, basically passive system using no liquid pumps and no air blowing. Further discussion of the potential of such a DMFC–based power pack to enter the market of hand held portable power devices, will be provided in this talk

ENZYMATIC BIOFUEL CELLS FOR IMPLANTABLE AND MICRO-SCALE DEVICES

Scott Calabrese Barton^a and Plamen Atanassov^b

^aDept. of Chemical Engineering, Columbia University, New York, NY 10027; ^bDept. of Chemical and Nuclear Engineering, University of New Mexico, Albuquerque, NM 87131

Introduction

Technology for electrical power generation using enzyme catalysts, established four decades ago, has recently received increased attention associated with demand for micro-scale and implantable power supplies. The main challenges, namely the fragility of enzyme molecules, characteristic low current density, and poor fundamental understanding of redox biocatalysis, are currently being addressed from a variety of research perspectives, to take advantage of enzyme selectivity, low temperature and moderate pH activity, and manufacturability in small-scale devices. Such an effort benefits from four decades of multidisciplinary research in biosensors and related bioelectrochemical fields. This review paper summarizes the current state of enzymatic biofuel cell research in the context of foreseeable applications and assesses the future prospects of the technology. Emphasis is placed on device performance and engineering aspects, with a view toward practical portable power devices based on enzymatic biofuel cells.

Research in biocatalytically modified electrodes, particularly for sensor applications, has provided a significant technological underpinning for current biofuel cell development. There exists significant overlap in technical requirements between sensors and biofuel cells, including chemical and mechanical stability, selectivity, and cost of materials. However, these two technologies diverge in the areas of current density, cell potential and stability.

There exists extensive review literature in the area of biological fuel cells. Notably, Palmore and Whitesides summarized biological fuel cell concepts and performance up until about 1992.¹ More recently, Katz and Willner discussed recent progress in novel electrode chemistries for both microbial and enzymatic fuel cells.² We do not duplicate these valuable contributions, but instead focus on the strengths and weaknesses of state-of-art materials in the context of specific classes of applications, and point to areas where additional knowledge is currently needed to exploit biological fuel cells. With some exceptions, we focus on contributions made after 1992.

Biofuel cells have traditionally been classified according to whether the catalytic enzymes were located inside or outside of living cells. If living cells are involved the system is considered to be microbial, and if not it is considered enzymatic. Although microbial fuel cells possess unique features unmatched by enzymatic cells, such as long-term stability and fuel efficiency, the power densities associated with such devices are typically much lower owing to resistance to mass transfer across cell membranes. Thus, microbial fuel cells are expected to find limited application in small-scale electronic devices. This review will focus on enzymatic biofuel cells. While such cells typically demonstrate reduced stability due to the limited lifetime of extracellular enzymes, and are typically unable to fully oxidize fuels, they allow for substantial concentration of catalysts and removal of mass transfer barriers and provide higher current and power densities, approaching the range of applicability to micro- and mini-scale electronics applications.

Applications and Requirements

The range of possible applications for biofuel cells may be broken down into three main subclasses:

1. Implantable power, such as micro-scale cells implanted in human or animal tissue, or larger cells implanted in blood vessels.
2. Power derived from ambient fuels or oxidants, mainly plant saps and juices, but extending to sewage and other waste streams.
3. Power derived from conventional fuels including hydrogen, methanol or higher alcohols.

Classes 1 and 2 are closely related. The fuels available for implantable power, such as blood borne glucose or lactate, are ambient in the sense that they are present in a physiological environment in the absence of a fuel cell device. One major distinction between these two classes is that the ambient-fueled cell need not be implanted, and focuses on plant- or waste-derived fuels, whereas the implantable cell focuses on animal-derived fuels and is present within the physiological system. Class 3 is unique in that this class competes with well-established conventional fuel cell technology. To a greater or lesser extent, all three classes share the fundamental technical requirements of high power density and high activity.

Enzyme Catalyzed Direct Electron Transfer

There are two ways of coupling an electrode process to an enzyme reaction (see Figure 2).³⁻⁵ The first approach is based on the utilization of low-molecular weight redox mediators.⁴ The second is to pursue direct (mediatorless) electron transfer.⁵ In this case, the electron is transferred directly from the electrode to the substrate molecule (or vice versa) via the active site of the enzyme. Direct (mediatorless) electron exchange between a redox group of protein and the electrode surface has been studied for a number of proteins such as cytochrome c, peroxidase, ferredoxin, plastocyanin, azurin, azotoflavin, glucose oxidase, etc.⁶⁻⁸ These studies developed an electrochemical basis for the investigation of protein structure, mechanisms of redox transformations of protein molecules, and metabolic processes involving redox transformations. Recently, the ability of oxidoreductase enzymes to catalyze mediatorless electron transfer from the electrode surface to the substrate molecule (or vice versa) has been demonstrated for laccase, lactate dehydrogenase, peroxidase, hydrogenase, p-cresolmethylhydroxylase, methylamine dehydrogenase, succinate dehydrogenase, fumarate reductase, D-fructose dehydrogenase, alcohol dehydrogenase, and D-gluconate dehydrogenase.³

Mediated electron transfer

The main purpose of redox mediation is to increase the rate of electron transfer between the active site of enzyme biocatalysts and an electrode by eliminating the need for the enzyme to interact directly with the electrode surface. Depending on the enzyme and reaction conditions, mediated electron transfer rates may exceed by orders of magnitude that of the direct mechanism. However, by introducing an additional transfer step, enzyme-mediator electron transfer is isolated from direct electrode potential control. For typically fast (Nernstian) kinetics between the mediator and electrode surface, the electrode potential merely controls the relative concentration of oxidized and reduced mediator at the surface. The electrode thus provides a boundary condition for electron flux to and from solution via the mediator.

The practical impact of such considerations is that the working potential of a mediated biocatalytic electrode is dominated by the

redox potential of the mediator couple, and the operating potential of a biofuel cell comprising two such electrodes will be primarily determined by the difference in redox potential of the two mediator couples. The differences in redox potential between the mediator and enzyme, and enzyme and substrate, represent driving forces for electron transfer, and therefore must be nonzero. As shown in Figure 2 for a glucose-oxygen biofuel cell,⁹ this difference represents an activation overpotential that reduces the observed open circuit potential from a theoretical maximum, given by the potential difference between the substrates. Some examples of diffusional mediators to be discussed are NADH cofactors, ABTS, and redox hydrogels.

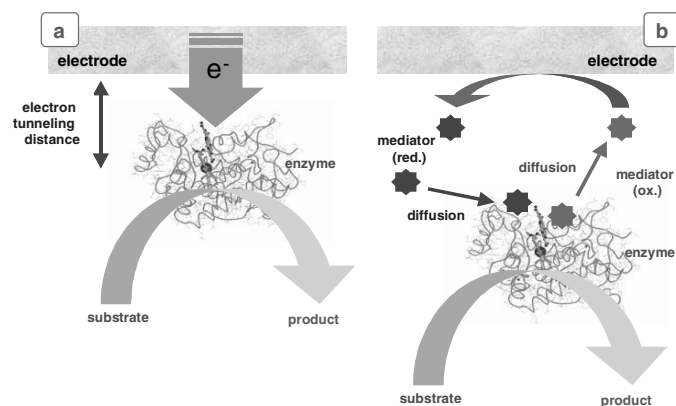


Figure 1. Alternative electron transfer mechanisms. (a) Direct electron transfer (tunneling mechanism) from electrode surface to the active site of an enzyme; (b) Electron transfer via redox mediator.

Engineering of enzymatic biofuel cell Systems

The recent literature in bioelectrochemical technology, covering primarily the electrochemical aspects of enzyme immobilization and mediation, includes few reports describing engineering aspects of enzymatic biofuel cells or related devices. Current engineering efforts address issues of catalytic rate and stability by seeking improved kinetic and thermodynamic properties in modified enzymes or synthesized enzyme mimics. Equally important is the development of materials and electrode structures that fully maximize the reaction rates of known biocatalysts within a stable environment. Ultimately, the performance of biocatalysts can only be assessed by their implementation in practical devices.

Future Outlook

The development of successful power sources has always been driven by specific applications. So it must also be for successful biofuel cells. Therefore, technological paths will be determined by application specifics: Implanted biofuel cells must exhibit biocompatibility, and cathodes for *ex vivo* electronics must take advantage of gas-phase oxygen. That being said, a general statement can be made that for the advantages of biofuel cells to compel adoption, the weaknesses relative to conventional technology must be minimized. It is clear that the advantages of biocatalysts are reactant selectivity, activity in physiological conditions, and manufacturability. The weaknesses are equally clear- modest absolute activity, and low stability, issues of significance, to a greater or lesser extent, in every conceivable application of this technology.

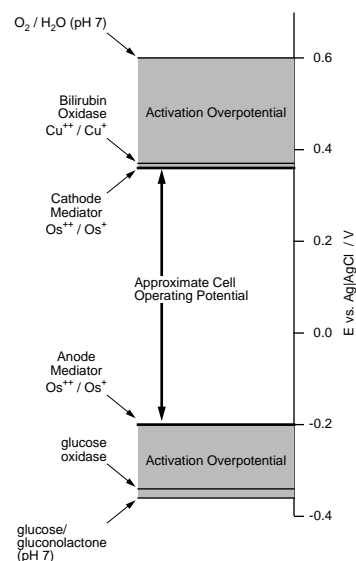


Figure 2. Potential Schematic for a mediated biofuel cell.

References

1. Palmore, G. T. R.; Whitesides, G. M., Microbial and enzymic biofuel cells. *ACS Symp. Ser.* **1994**, 566, (Enzymatic Conversion of Biomass for Fuels Production), 271-90.
2. Katz, E.; Shipway, A. N.; Willner, I., Biochemical fuel cells. In *Handbook of Fuel Cells – Fundamentals, Technology and Applications*, ed.; Vielstich, W.; Gasteiger, H. A.; Lamm, A., Eds., John Wiley and Sons, Ltd.: London, 2003; Vol. 1, pp. 355-381.
3. Ghindilis, A. L.; Atanasov, P.; Wilkins, E., Enzyme-catalyzed direct electron transfer. Fundamentals and analytical applications. *Electroanalysis* **1997**, 9, (9), 661-674.
4. Bartlett, P. N.; Tebbutt, P.; Whitaker, R. G., Kinetic aspects of the use of modified electrodes and mediators in bioelectrochemistry. *Progress in Reaction Kinetics* **1991**, 16, (2), 55-155.
5. Tarasevich, M. R., Bioelectrocatalysis. In *Comprehensive Treatise of Electrochemistry*, Plenum Press: New York, 1985; Vol. 10, pp. 231-295.
6. Hill, H. A. O., Bio-Electrochemistry. *Pure and Applied Chemistry* **1987**, 59, (6), 743-748.
7. Nakamura, K.; Aizawa, M.; Miyawaki, O., *Electro-enzymology, coenzyme regeneration*. Springer-Verlag: Berlin ; New York, 1988; p viii, 166.
8. Guo, L. H.; Hill, H. A. O., Direct Electrochemistry of Proteins and Enzymes. *Advances in Inorganic Chemistry* **1991**, 36, 341-375.
9. Kim, H. H.; Mano, N.; Zhang, X. C.; Heller, A., A miniature membrane-less biofuel cell operating under physiological conditions at 0.5 V. *Journal of the Electrochemical Society* **2003**, 150, (2), A209-A213.

SOLID OXIDE FUEL CELLS: AN OVERVIEW

S. C. Singhal

Pacific Northwest National Laboratory
902 Battelle Boulevard
P. O. Box 999
Richland, WA 99352, USA

Introduction

Solid oxide fuel cells (SOFCs),¹ based on an oxide ion conducting electrolyte, offer a clean, low-pollution technology to electrochemically generate electricity at high efficiencies. These fuel cells provide many advantages including high efficiency, reliability, modularity, fuel adaptability, and very low levels of SO_x and NO_x emissions. Quiet, vibration-free operation of SOFCs also eliminates noise usually associated with conventional power generation systems. Furthermore, because of their high operation temperature (700-1000°C), some hydrocarbon fuels such as natural gas can be reformed within the cell stack eliminating the need for an expensive, external reformer. This paper reviews the current status of the SOFC technology for use in stationary power systems and transportation auxiliary power units.

SOFCs essentially consist of two porous electrodes separated by a dense, oxide ion conducting electrolyte. Oxygen supplied at the cathode (air electrode) reacts with incoming electrons from the external circuit to form oxide ions, which migrate to the anode (fuel electrode) through the oxide ion conducting electrolyte. At the anode, oxide ions combine with H₂ and/or CO in the fuel to form H₂O (and/or CO₂), liberating electrons. Electrons flow from the anode through the external circuit to the cathode. The overall cell reaction is simply the oxidation of fuel (H₂ and/or CO).

Cell Materials

Oxides such as yttria-stabilized zirconia (YSZ), rare earth doped ceria, rare earth doped bismuth oxide, and doped lanthanum gallates have been widely investigated as electrolytes.¹ Of these, YSZ has been most successfully employed in SOFCs. The yttria dopant serves dual roles: it stabilizes the high temperature cubic phase in zirconia and also generates oxygen vacancies; the high oxide ion conductivity in YSZ is attributed to these oxygen vacancies. Zirconia doped with about 10 mole percent yttria is generally used as the electrolyte. The thermal expansion of 10 mole percent YSZ is about 10×10⁻⁶/°C; materials for all other cell components are chosen to have thermal expansion near this value.

Lanthanum manganite suitably doped with alkaline and rare earth elements is generally used as cathode. Lanthanum manganite is a p-type perovskite and shows reversible oxidation-reduction behavior. The material can have oxygen excess or deficiency depending upon the ambient oxygen partial pressure and temperature. The electronic conductivity of lanthanum manganite is due to hopping of an electron hole between the +3 and +4 valence states of Mn. This conductivity is enhanced by doping with a divalent ion such as calcium or strontium. Furthermore, any interactions between doped lanthanum manganite and yttria-stabilized zirconia electrolyte up to 1000°C are minimal. In addition to lanthanum manganite, other perovskites such as doped lanthanum cobaltite, ferrite and nickelite have also been used as cathode materials. These oxides have generally higher activity for oxygen reduction than lanthanum manganite. However, the thermal expansion coefficient of cobaltites is much higher than that of the YSZ electrolyte, and the electrical conductivities of ferrites and nickelites are low.

The reducing conditions present on the fuel side of an SOFC permit the use of a metal such as nickel (alternately cobalt or

ruthenium) as the anode (fuel electrode). However, the thermal expansion of nickel is considerably larger than that of YSZ. Nickel can also sinter at the cell operating temperature resulting in a decrease in the fuel electrode porosity. These problems are minimized by using a Ni/YSZ cermet for the anode. The YSZ prevents sintering of the nickel particles, decreases the thermal expansion coefficient bringing it closer to that of the electrolyte, and provides better adhesion of the fuel electrode with the electrolyte. Even though Ni-YSZ cermet remains the most commonly utilized anode material for SOFCs, recently copper-based anodes have also been proposed for intermediate-temperature (< 800°C) SOFCs intended to operate directly on hydrocarbon fuels.

The interconnection should have nearly 100 percent electronic conductivity; stability in both oxidizing and reducing atmospheres at the cell operating temperature; low permeability for oxygen and hydrogen to minimize direct combination of oxidant and fuel during cell operation; a thermal expansion coefficient close to that of the air electrode and the electrolyte; and non-reactivity with other cell materials. To satisfy these requirements, doped lanthanum chromite is used as the interconnection material for cells intended for operation at about 1000°C. Lanthanum chromite is a p-type conductor; its conductivity is due to small polaron hopping from room temperature to 1400°C at oxygen pressures as low as 10⁻¹⁸ atm. The conductivity is enhanced as lower valence ions (e.g., Ca, Mg, Sr, etc.) are substituted on either the La³⁺ or the Cr³⁺ sites. In cells intended for operation at lower temperatures (< 800°C), it is possible to use oxidation-resistant metallic materials for the interconnection. Many stainless steels and high temperature chromia-forming alloys are being developed for this application and their successful use will result in substantial reduction in the cost of SOFC stacks.

Cell Designs

The two most common designs of SOFCs are the tubular and the planar. In the tubular cells, as illustrated by the Siemens Westinghouse design shown in **Figure 1**, the cell components are deposited in the form of thin layers on a doped lanthanum manganite cathode tube¹⁻³ which is fabricated by extrusion and sintering. YSZ electrolyte is deposited in the form of about 40 μm thick dense layer by electrochemical vapor deposition⁴ or by plasma spraying; and the Ni/YSZ anode is deposited either by nickel slurry application followed by electrochemical vapor deposition of YSZ, by sintering of a Ni+YSZ slurry, or by plasma spraying. The doped lanthanum chromite interconnection strip along the length of the cell is deposited by plasma spraying.⁵

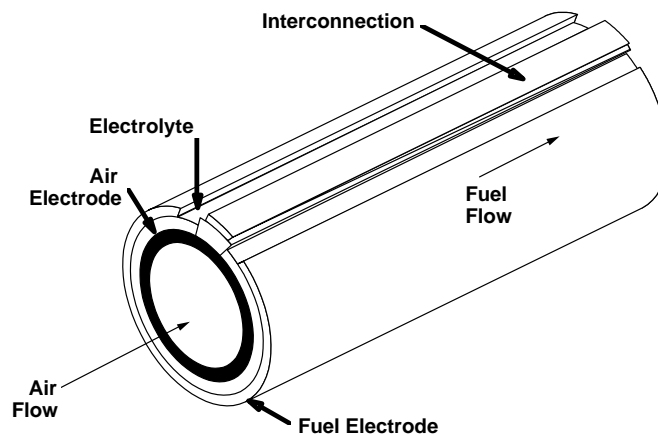


Figure 1. Tubular design solid oxide fuel cell.

Tubular cells perform satisfactorily for extended periods of time under a variety of operating conditions with less than 0.1% per 1000 hours performance degradation and have a power density at 1000°C of about 0.20-0.25 W/cm². To date, the tubular design has progressed the most and power generation systems of up to 250 kW size have been produced and operated using such cells. To construct an electric generator, individual cells are connected in both electrical parallel and series to form a semi-rigid bundle that becomes the basic building block of a generator. The cell bundles are arrayed in series to build voltage and form generator modules. These modules are further combined in either series or parallel to form SOFC generators. Using this scheme, Siemens Westinghouse fabricated a 100 kW size and a 250 kW size atmospheric power generation system. The 100 kW system was successfully operated for over two years in the Netherlands and Germany on desulfurized natural gas without any significant performance degradation.

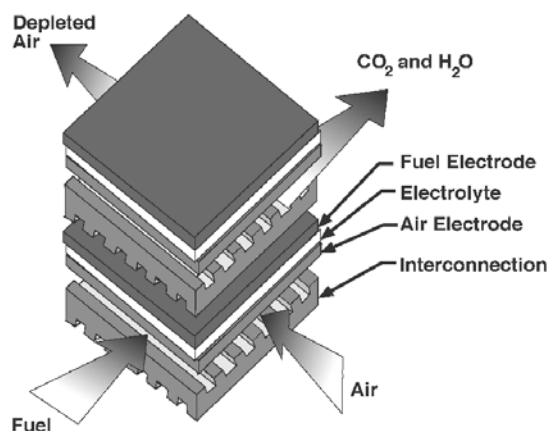


Figure 2. Planar design solid oxide fuel cell.

Even though the tubular SOFCs have progressed the most, their electrical resistance is high, power densities (W/cm² and W/cm³) low, and manufacturing costs high. The low power density (0.20 to 0.25 W/cm²) makes tubular SOFCs suitable only for stationary power generation and not very attractive for transportation applications. Planar SOFCs, in contrast, are capable of achieving very high power densities of up to about 2 W/cm². In the planar design, illustrated in **Figure 2** in its most generic version, the cell components are configured as thin, flat plates. The interconnection, which is ribbed on both sides, forms gas flow channels and serves as a bipolar gas separator contacting the anode and the cathode of adjoining cells. The cells are fabricated by low-cost conventional ceramic processing techniques such as tape casting, slurry sintering, screen printing, or by plasma spraying. Different organizations have developed several different variations of the planar design and use different manufacturing processes. In electrolyte-supported cells, the thickness of the electrolyte, typically yttria-stabilized zirconia (YSZ), is 50 to 150 μm, making their ohmic resistance high, and such cells are suitable for operation at ~1000°C. In electrode-supported designs, the electrolyte thickness can be much lower, typically 5 to 20 μm, which decreases their ohmic resistance and makes them better suited for operation at lower temperatures (~800°C). Lower temperature operation results in less degradation of cell and stack components, makes feasible use of inexpensive metallic interconnects, is less demanding on seals, and aids in faster heat up and cool down. The anode (Ni/YSZ cermet) is selected as the supporting electrode, because it provides superior thermal and electrical conductivity,

superior mechanical strength, and minimal chemical interaction with the electrolyte. Kim et al⁶ have reported power densities as high as 1.8 W/cm² at 800°C for such anode-supported SOFCs.

Sizeable cost reductions are possible with the planar design cells through a concept called “mass customization” that is being pursued in the U.S. Department of Energy’s Solid State Energy Conversion Alliance (SECA).⁷ This concept involves the development of a 3 to 10 kW size core SOFC module, that can be mass produced and then combined for different size applications in stationary power generation, transportation, and military market sectors, thus eliminating the need to produce custom-designed and inherently more expensive fuel cell stacks to meet a specific power rating. Very high power densities of anode-supported planar SOFCs make them very attractive for use in the core SOFC module.

Using planar cells, stationary power systems of up to 25 kW size have been fabricated by various organizations and tested for up to a few thousand hours with only limited success because of the problems with the glass seals that are employed to isolate air from fuel in cell stacks. Another application of the high power density planar SOFCs is in on-board auxiliary power units (APUs) in vehicles. Such APUs, operating on existing fuel base, can supply the ever-increasing electrical power demands of luxury automobiles, recreational vehicles, and heavy-duty trucks. Delphi/Battelle has developed a 5 kW APU using anode-supported SOFCs.³ Such units operate on gasoline, which is reformed through partial oxidation. APUs require fast heatup and ability to be thermally cycled. Thermomechanical, thermal-fluids, and stress modeling is being conducted to aid in achieving stack designs with such attributes.

Summary

SOFCs provide a highly efficient, low-pollution power generation technology. Performance of tubular SOFCs has been confirmed by successful operation in several power generation systems of up to 250 kW size, though their cost still remains to be reduced. Planar SOFCs, particularly anode-supported, provide much higher power densities and potentially much lower cost than the tubular cells. The challenge in commercializing planar SOFCs offering high power densities requires successful development of seals for isolating oxidant from fuel, development of low-cost oxidation-resistant metallic alloys for use as interconnection, and lower cost. Additionally, for transportation applications, ability for rapid start up and thermal cycling needs to be developed. When fully developed, planar SOFCs will have widespread application in the stationary distributed power generation, transportation and military market sectors. Systems based on both the tubular and the planar SOFCs are ideal power generation systems – reliable, clean, quiet, environmental friendly, and fuel conserving.

References

1. Singhal, S. C. and Kendall, K., *Solid Oxide Fuel Cells: Fundamentals, Design and Applications*, Elsevier, Oxford, UK, **2003**.
2. Singhal, S. C., *Materials Research Bulletin*, **2000**, 25(3), 16-21.
3. Singhal, S. C., *Solid State Ionics*, **2002**, 152-153, 405-410.
4. Pal, U. B. and Singhal, S. C., *J. Electrochem. Soc.*, **1990**, 137, 2937-41.
5. Kuo, L. J. H., Vora, S. D., and Singhal, S. C., *J. Am. Ceram. Soc.*, **1997**, 80, 589-93.
6. Kim, J-W, Virkar, A. Fung, K-Z., Mehta, K., and Singhal, S. C., *J. Electrochem. Soc.*, **1999**, 46, 69-78.
7. Surdoval, W. A., Singhal, S. C., and McVay, G. L., in *Solid Oxide Fuel Cells VII*, Yokokawa, H., and Singhal, S. C., eds., The Electrochemical Society, Inc., Pennington, NJ, **2001**, PV 2001-16, 53-62.

CHEMICAL SYSTEMS FOR HYDROGEN STORAGE

George J. Thomas

Consultant,
Sandia National Laboratories
Livermore, CA 94551

Hydrogen storage systems for use in hydrogen-fueled vehicles will require high energy density and high specific energy in order to achieve comparable performance to conventional gasoline-fueled vehicles. It is believed that this issue remains as one of the critical barriers to the development of fuel cell powered vehicles. With the president's initiative and increased funding levels in hydrogen and fuel cell development, there are a number of new and exciting areas of research which have emerged aimed at developing high density hydrogen storage media.

At the present time, essentially all hydrogen-fueled vehicles use either compressed gas or liquid hydrogen tanks for onboard storage. Both of these technologies are straightforward, relatively mature and are commercially available. Compressed gas systems have progressed rapidly over the last few years. These cylindrical tanks, constructed with high strength carbon fiber composite materials, are robust, lightweight and have been demonstrated at hydrogen pressures up to 700 bar. However, even at this pressure at ambient temperature, the volumetric density of the hydrogen is insufficient for long-term use. Liquid hydrogen storage has been advocated mainly by BMW and a number of their demonstration vehicles have employed tanks which were developed by Linde. The high energy cost of liquefying hydrogen has been stated as a key issue in its utilization as a fuel.

This presentation will focus on chemistry-based hydrogen storage methods, that is, hydrogen storage materials. Storage materials can be broadly classified as having reversible or non-reversible hydrogen behavior. Reversible materials absorb and desorb hydrogen from the gas phase based on the hydrogen gas overpressure and temperature. These materials can therefore be recharged in-situ onboard the vehicle by supplying hydrogen at the appropriate pressure. On the other hand, non-reversible systems require chemical processing, perhaps including intermediate phases and additional materials, to be recharged. In this case, the spent material (depleted of hydrogen) which could be in liquid or solid form, must be removed from the vehicle and reprocessed elsewhere. These materials are generally referred to as chemical hydrides. Although reversible systems would be the preferred method, both options are currently under consideration.

There are many materials which have reversible hydrogen properties. These include materials where the hydrogen is adsorbed to the surface and those where the material is absorbed into the bulk. Single wall carbon nanotubes and other nanostructured materials, such as metal organic frameworks (MOFs), are examples of adsorbed hydrogen systems being studied. Critical issues which must be answered with adsorbed systems are hydrogen capacity, volumetric density and hydrogen binding energies.

Materials where hydrogen is absorbed and chemically bound in the bulk offer the potential of having the highest volumetric density of hydrogen, surpassing even that of liquid hydrogen. Metal hydrides are the best known class of materials with this property and these have been extensively studied for more than 30 years. Although they exhibit good capacities and good kinetic properties,

they are generally too heavy. Lighter weight hydrides typically have stronger covalent or ionic hydrogen bonds and hence require high temperatures for hydrogen release. Emphasis in this area of research has shifted in recent years to other materials. Complex hydrides, particularly those formed with Al-H or B-H complexes, offer higher hydrogen capacities, lighter weight over intermetallic hydrides and reduced hydrogen binding energies over covalent or ionic hydrides. However, only NaAlH_4 , doped with Ti, has been demonstrated to be reversible at this time. Work on this and other complex hydrides, as well as effective dopant materials and processes to achieve reversible behavior and the desired kinetic and thermodynamic properties, is currently being pursued. A number of other alternative materials have also shown promising early results and are being proposed for further study, including imide-amides and amine borane systems.

In this overview presentation we will discuss inherent limitations of hydrogen storage concepts and briefly describe some of the specific chemical systems mentioned above. Emphasis will be on material performance relative to that required in storage applications.

OVERVIEW OF HYDROGEN PRODUCTION

Carolyn C. Elam and Robert J. Evans

National Renewable Energy Laboratory,
1617 Cole Blvd, Golden, CO 80401

Introduction

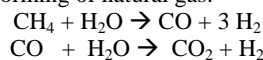
Hydrogen, like electricity, can be produced from many sources, including fossil fuels, renewable resources, and nuclear energy. Today, hydrogen is produced primarily from natural gas using well-known commercial thermal processes. In the future, it could be produced directly from renewable resources. In the meantime, we can adapt current technologies to produce hydrogen with significantly reduced CO₂ emissions, through carbon capture and sequestration processes, and by using renewable and nuclear electricity to produce hydrogen with no production-side CO₂ emissions.

The transition to a Hydrogen Economy will progress through the development and commercialization of a range of advanced technologies to produce, store, and use hydrogen. Hydrogen would first be produced by distributed thermochemical and electrolytic means and then eventually via photolytic processes. In the near- to mid-term, on-site production from natural gas or electricity will provide hydrogen for the moderate but growing needs of various energy sectors. Eventually, larger networks of pipelines will permit distribution of hydrogen, produced throughout the country by a variety of means from domestic resources, to urban centers, airports, and seaports.

There are technical and economic hurdles to the implementation of hydrogen energy systems. The cost of hydrogen production from renewable resources (with low or no CO₂ emissions) is not currently competitive with that of production from fossil feedstocks (with high CO₂ emissions). Hydrogen can provide storage options for intermittent renewable technologies such as solar and wind. It can transform base-load technologies such as nuclear, geothermal, biomass, and hydro into load-following systems. When combined with emerging decarbonization technologies, hydrogen could reduce the climate impacts of continued fossil fuel use.

Current Hydrogen Production Processes

Nearly half of the worldwide production of hydrogen is via large-scale steam reforming of natural gas:



By 2030-2050, world-wide oil production and U.S. production of natural gas are expected to have reached or passed their peak, thereby increasing their costs. In addition, their *value* as feedstocks for chemical production would far exceed their value as fuels. Coupled with carbon constraints, this would require a paradigm shift in the fuels used to produce hydrogen.

There is a need to build on the established steam reforming technology base, which primarily uses natural gas and is accomplished in large, central facilities, to provide low-cost hydrogen for nearer-term hydrogen demonstration projects, while research continues on cleaner fossil- and renewable-based hydrogen production systems.

With continued improvements in renewable power systems (wind, solar, biomass, geothermal, etc), hydrogen would be produced without significant (or any) carbon emissions. Eventually, through continued support of long-term RD&D, direct water-splitting technologies would be available, realizing the ultimate Hydrogen Vision (sunlight + water = hydrogen = electricity + water + usable heat). This feedstock flexibility is an essential and unique feature of

hydrogen - with (in some cases, only minor) modification to existing and developing technologies, hydrogen can be produced efficiently and cleanly from nearly any resource, including natural gas, coal, nuclear power, renewable energy and wastes.

It is anticipated that coal gasification combined with sequestration strategies would compete with natural gas, renewables and nuclear to produce hydrogen. Renewable, nuclear and fossil fuel/sequestration systems would lead to the centralized production of hydrogen, transporting it to cities for use in distributed generation systems and as fuels for fuel cell vehicles.

Nearly half of the worldwide production of hydrogen is via steam methane reforming; a catalytic process that involves reacting natural gas or other light hydrocarbons with steam. The primary by-product from this process is carbon dioxide, the majority of which is exhausted to the atmosphere. At the large scale, this is the most energy-efficient and cost-competitive commercial technology available. In order to reduce carbon emissions to the atmosphere, these plants could be engineered to allow the capture and sequestration of the carbon dioxide emissions from the process.

High purity hydrogen is also produced by electrolysis - the use of electricity to split water into its elements, hydrogen and oxygen. Electrolysers are commercially available around the world and any source of electricity can be used. The cost of electricity directly impacts the cost for hydrogen production; however, electrolysis is the nearer-term option for small-scale distributed hydrogen production. The emissions from this production technology are solely from electricity production. Use of renewables, such as wind or solar, can make this a clean and sustainable option for hydrogen production.

Research, Development and Demonstration Status and Needs

Fossil Production Systems

Current RD&D efforts are focused on developing improved processes for smaller-scale hydrogen production systems, based on established industrial production processes or innovative reactor designs. These include industry-led cost-shared development and deployment of small-scale autothermal reformers (ATR) and steam methane reformers (SMR). Process improvements may have limited impact on greenhouse gas (GHG) emissions due to the focus on using conventional fossil fuels to keep costs low. However, well-to-wheels efficiency improvements relative to conventional systems can directly reduce GHG and other emissions.

Fundamental and applied research and development of high-temperature, high-pressure separation and purification processes need to proceed at a rate sufficient to allow significant impact on process efficiency and cost. Such efforts would enable demonstration of large integrated coal gasification plants, such as integrated gasification combined cycle (IGCC) coal plants combined with sequestration. The facilities would co-produce electricity and hydrogen (via water-gas shift of the syngas), depending on power and fuel demands. Support is also needed for accelerated materials research and system development for ceramic/membrane reactors and microchannel reformers to meet the growth in demand for distributed and centralized hydrogen generation at lower capital costs and increased efficiency.

Renewable Production Systems

Current RD&D efforts are focused on a broad range of options to produce hydrogen from biomass (fermentative processes, integrated biomass pyrolysis systems, and supercritical water processes), intermittent renewables (wind and solar), and base-load renewables (geothermal and hydro).

Intermittent Renewables

For intermittent renewables, hydrogen-production efforts are focused on integrating wind-electrolysis systems, reducing the costs of electrolyzers, and on developing small-scale units for home refueling applications. These efforts include industry-led cost-shared development of small-scale electrolyzers, industry-university partnerships to integrate renewable systems, and national lab efforts to develop high-temperature steam electrolyzers. Cost reductions in wind and photovoltaic technologies will have direct impacts on the economic competitiveness of renewable electrolysis.

Nuclear-Based Production Systems

Nuclear power-to-hydrogen is receiving increasing attention as we address the mounting evidence of the greenhouse gas impacts of continued and increased use of fossil fuels. Conventional electrolyzers can be used to produce hydrogen from nuclear power. Waste heat from high-temperature nuclear reactors (Gen IV) or from concentrated solar power could be used for hydrogen production via chemical cycles.

Current R&D efforts are primarily focused on the development of high-temperature steam electrolyzers. Parallel development of next-generation nuclear power facilities are expected to result in systems that can be used to produce hydrogen with no production-side CO₂ emissions.

Additional research areas include development efforts on improved materials, higher temperature and pressure operation of conventional alkaline electrolyzers, polymer membrane electrolyzer development, and optimization of control strategies. Acceleration of the development of high-temperature steam electrolyzers, with their reduced electrical demands and higher efficiencies is also needed.

Direct Hydrogen Production Systems

Current RD&D efforts are focused on fundamental approaches to producing hydrogen using sunlight and water through photobiological, photoelectrochemical, and photochemical means. These long-term processes are "the Holy Grail" of the Hydrogen Economy - they are the ultimate clean, sustainable hydrogen production method. However, the R&D investment these technologies receive is limited. Resources will need to be invested in these technologies over a significant period of time before the required fundamental understanding is achieved and industry invests resources in commercialization.

Accelerated understanding of the fundamental aspects of microbial production systems, including thermophilic, algal, and fermentative approaches, is needed to pursue the applied process development efforts to develop and implement microbial hydrogen systems. Improved fundamental understanding is required to permit development of better semiconductor-based photoelectrochemical systems. Accelerated scale-up and validation of promising photoelectrochemical and photochemical systems, and the development of new photolytic processes is also needed.

Biomass

Biomass has the potential to accelerate the realization of hydrogen as a major fuel of the future. Since biomass is renewable and consumes atmospheric CO₂ during growth, it can have a small net CO₂ impact compared to fossil fuels. However, hydrogen from biomass has major challenges. There are no completed technology demonstrations. The yield of hydrogen is low from biomass since the hydrogen content in biomass is low to begin with (approximately 6% versus 25% for methane) and the energy content is low due to the 40% oxygen content of biomass.

Biomass conversion technologies can be divided into two categories: 1) direct production routes and 2) conversion of storable

intermediates. Direct routes have the advantage of simplicity. Indirect routes have additional production steps, but have an advantage in that there can be distributed production of the intermediates, minimizing the transportation costs of the biomass. The intermediates can then be shipped to a central, larger-scale hydrogen production facility. Both classes have thermochemical and biological routes. Of these options, gasification coupled with water-gas shift is the most widely practiced process route for biomass to hydrogen. Thermal, steam and partial oxidation gasification technologies are under development around the world. Feedstocks include both dedicated crops and agricultural and forest product residues of hardwood, softwood and herbaceous species.

Conclusions

Abundant, reliable, and affordable energy is an essential component in a healthy economy. Because hydrogen can be produced from a wide variety of domestically available resources and can be used in heat, power and fuel applications, it is uniquely positioned to contribute to our growing energy demands, particularly in the environmentally- and traditional resource- constrained scenarios facing many communities. By diversifying our energy supply, we will not only reduce our dependence on imported fuels, but will also benefit from cleaner technologies and investment in our communities.

POLYBENZIMIDAZOLE BASED SEGMENTED BLOCK COPOLYMERS FOR HIGH TEMPERATURE FUEL CELL MEMBRANES

Eugene Scanlon and Brian C. Benicewicz*

NYS Center for Polymer Synthesis
Department of Chemistry and Chemical Biology
Rensselaer Polytechnic Institute
Troy, NY 12180
*benice@rpi.edu

Introduction

Polymer electrolyte membrane fuel cells (PEMFC) are the ongoing focus of current research for potential applications ranging from mobile devices such as cell phones and laptop computers utilizing micro fuel cells to automotive applications and stationary devices generating power on the kW scale.

PEMFC's employing polybenzimidazole (PBI) membranes with a phosphoric acid electrolyte have been recognized for their outstanding high temperature performance ($>160^{\circ}\text{C}$).^{1,2} High temperature operation provides favorable electrode kinetics and an increased tolerance to fuel impurities such as carbon monoxide which can poison the Pt catalyst. Conventional perfluorinated ionomers such as Nafion® are limited to temperatures of 100°C or less due to their reliance on water to conduct protons. This reliance on water imposes additional hardware requirements to maintain high membrane hydration levels. In general, hydrated perfluorinated ionomers exhibit low tolerance to CO due to their low operating temperatures.

Recently, we have reported the synthesis of different isomers of PBI and their copolymers. A novel technique for film fabrication, called the PPA process, was developed which greatly simplified the PEM preparation and produced membranes with much improved properties as compared to membranes produced from imbibing processes.³

In this contribution, we report the synthesis of segmented block copolymers based on PBI and its isomers using the PPA process. The resulting membranes have excellent thermal resistance, high acid content, high conductivity and good mechanical properties. These membranes are promising candidates for high temperature fuel cell applications in mobile and stationary devices.

Experimental

Oligomer Block Synthesis. 4,4'-Sulfonylbis[1,2-benzenediamine] (TAS) and isophthalic acid (IA) were added to a resin flask in equimolar amounts. To this flask polyphosphoric acid (PPA) was added until the weight percent of monomer was between 2 and 7%. In a second resin flask 3,3',4,4'-tetraaminobiphenyl (TAB) and terephthalic acid (TA) were added in equimolar amounts to which PPA was also added until the weight percent of monomer was between 2 and 7%. These two flasks were submerged in an oil bath and outfitted with a nitrogen inlet and outlet and an overhead mechanical stirrer. They were then polymerized under appropriate conditions to control the degree of polymerization of each block (Scheme 1).

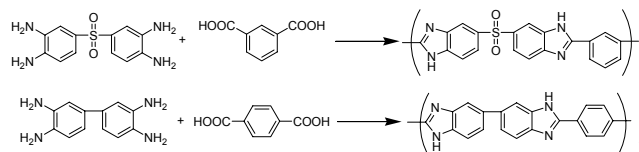
Segmented Copolymer Synthesis and Membrane Fabrication. After prepolymerization of the starting blocks, the two reactions were combined in a separate resin flask and heated further to complete the polymerization to high molecular weights. After completion of the polymerization, the solution was cast directly on a glass substrate by use of a casting blade with a gap thickness of between 15 and 25mils. The substrate was allowed to stand in a humidity box with a controlled relative humidity of between 25-65%

for three to four days. Absorption of water from the atmosphere within the humidity chamber hydrolyzed the PPA to phosphoric acid (PA) and subsequently induced a sol-gel transition that produced membranes with high acid loading.

Blend and Random Copolymer Synthesis. Blends of the two homopolymers were prepared by fully polymerizing each of the "blocks" prior to mixing. Random copolymers were prepared by charging all four monomers at the beginning of the reaction prior to the polymerization procedure.

Polymer and Membrane Characterization. Acid content was determined using a Metrohm 716 DMS Titrino autotitrator with 0.1M standardized NaOH and reported as the average of three samples. After titration, the samples were washed and dried at vacuum at 100°C to obtain the polymer and water content. The inherent viscosity (I.V.) was measured by dissolving the polymer in 96% sulfuric acid at a concentration of 0.2g/dL and measuring the flow times using an Ubbelohde suspended volume viscometer at 30°C . Conductivity was measured with a four point probe impedance method using a Zahner IM6e electrochemical workstation in the frequency range of 1Hz to 100KHz. The experimental data was fitted to a model of a resistor and capacitor in parallel. The conductivity was measured as a function of temperature through use of a programmable oven. Mechanical properties were measured by cutting ASTM type V specimens and tested using a United Testing tensile tester with a 5lb. load cell. All samples were preloaded to 0.1N and the testing speed was 5mm/min.

Fuel Cell Testing. Cells were built with an active area of 44cm^2 using commercially available electrodes. The catalyst was 30 wt% Pt/C with a $1\text{mg}/\text{cm}^2$ loading on both anode and cathode. Fuel cell tests were carried out using a test station purchased from Fuel Cell Technologies, Inc.



Scheme 1. Synthesis of segmented PBI copolymers using the PPA process.

Results and Discussion.

Previous work in our laboratory had characterized the TAS+IA homopolymer as having high solubility in both PPA as well as PA. The TAB+TA homopolymer was characterized as having lower solubility in both PPA and PA. Films produced from the TAB+TA homopolymer using the PPA process exhibited good mechanical strength. In this work, integration of these characteristics was investigated by preparing and analyzing the properties of the random copolymer, polymer blend and segmented block copolymer containing equimolar amounts of each repeat unit structure.

Table 1 shows the I.V. and titration results comparing a random copolymer, segmented block copolymer and a polymer blend, each containing 50 mole percent of each repeat unit. The I.V.'s listed are for the two separate oligomers or polymers before mixing and the final polymer. For the random copolymer, initial oligomers were not generated. For the homopolymer blend, the two components were fully polymerized and subsequently mixed. The segmented block-copolymer had the highest I.V. and the highest acid content with the lowest polymer content.

Table 1. Initial Polymerization and Titration Results for the Random, Blend and Segmented Block Copolymer Systems

	I.V. (dL/g)			Content (wt%)		
	TAS+IA	TAB+TA	Final	Polymer	Water	Acid
Random	-	-	1.54	17.7	30.4	51.9
Blend	.65	2.24	1.32	5.3	17.2	77.6
Segmented	.49	.24	1.78	3.7	15.7	80.6

Table 2 shows the conductivity and mechanical properties of the three systems. Conductivity measurements were performed twice on each sample. The first heating run showed variable results due to the water contained in each sample and its removal at temperatures above 100°C. The second heating run was reproducible and is reported in the table. The segmented system had a conductivity of 0.38 S/cm, which is very high compared to the previously reported data for PBI and Nafion®. These high values were due in part to the very high acid content of the membrane. Surprisingly, the segmented membrane also had the highest mechanical properties of the three systems even though the polymer content was the lowest. This combination of properties was attributed to the segmented nature of the block copolymer that combined the excellent mechanical properties of the TAB+TA system with the high acid loading of the TAS+IA system.

Table 2. Conductivity and Mechanical Properties of the Random, Blend and Segmented Copolymer Systems

	Conductivity at 160°C (S/cm)	Stress (Mpa)	Strain (%)
Random	0.24	0.2-0.3	20-55
Blend	0.06	1-1.4	75-175
Segmented	0.38	1.2-1.8	400-525

Fuel cell performance curves at atmospheric pressure are shown in Figure 1. Of interest is the very modest loss when using a reformat containing 40% hydrogen as a fuel compared to pure hydrogen. This is particularly impressive considering the reformat contained 2000 ppm CO. When using hydrogen as a fuel an oxygen gain of 70mV at 0.2A/cm² was measured.

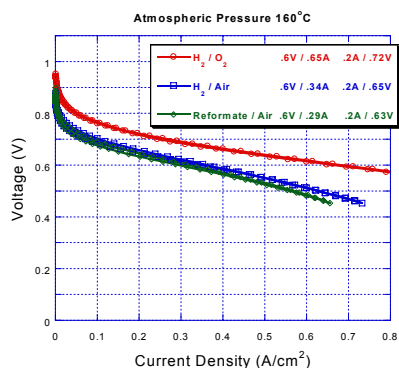


Figure 1. Performance curve for segmented block copolymer membrane at 160°C and atmospheric pressure. Flow rates were 241 sccm H₂, 602 sccm reformat, 1003 sccm air, and 201 sccm O₂. The reformat composition was 40.0% H₂, 0.2% CO, 19.0% CO₂ and 40.8% N₂.

Fuel cell performance curves at 15psi or approximately 1 atmosphere over pressure are shown in Figure 2. A similar effect with regards to the minimal losses associated with reformat are noticed, as well as a similar oxygen gain. Operating at 15psi with hydrogen and air showed the same approximate performance as operating at atmospheric pressure with hydrogen and oxygen.

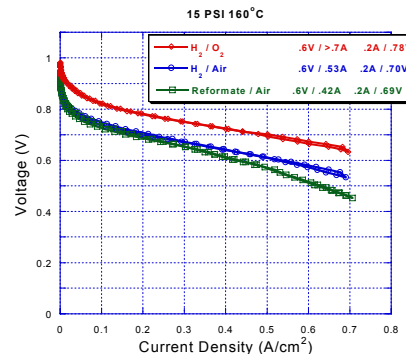


Figure 2. Performance curve for segmented block copolymer membrane at 160°C and 15 psi. Flow rates were 241 sccm H₂, 602 sccm reformat, 1003 sccm air, and 201 sccm O₂. The reformat composition was 40.0% H₂, 0.2% CO, 19.0% CO₂ and 40.8% N₂.

Conclusions

A novel high temperature electrolyte membrane based on a segmented block copolymer of PBI was synthesized. The membrane displayed a very high acid loading and high conductivity. The membrane also exhibited excellent mechanical properties and fuel cell performance.

Acknowledgements

The authors wish to thank Celanese Ventures, GmbH, Plug Power and NYSTAR for their financial and technical support.

References

- (1) Wainright, J.S.; Wang, J.T.; Weng, D.; Savinell, R.F.; Litt, M. *Journal of the Electrochem. Soc.* **1995**, *142*, L121-L123.
- (2) Ma, Y.L.; Wainright, J.S.; Litt, M.H.; Savinell, R.F. *Journal of the Electrochem. Soc.* **2004**, *151*, A8-A16.
- (3) Xiao, L.; Zhang, H.; Choe, E.-W.; Scanlon, E.; Ramanathan, L.S.; Benicewicz, B.C. *Preprints of Symposia - American Chemical Society, Division of Fuel Chemistry* **2003**, *48*, 447-448.

PROTON CONDUCTING POLYANILINE MOLECULAR SIEVES COMPOSITES

Decio Coutinho, Zhiwei Yang, Fangxia Feng, John P. Ferraris, and Kenneth J. Balkus Jr.

Department of Chemistry and the UTD NanoTech Institute, University of Texas at Dallas, Richardson TX 75083-0688

Introduction

Proton-conducting solid materials have grown in interest due to their potential applications in electrochemical devices, such as batteries, chemical sensors, fuel cells, and supercapacitors. Mesoporous molecular sieves offer many advantages such as thermal, chemical, and mechanical stability as well as significant water uptake at elevated temperatures.¹ The mesoporous molecular sieves pore walls may be easily functionalized with proton conducting groups, which combines the thermal and mechanical stability of the metal oxide framework with proton conducting properties of the organic moieties incorporated into the pores. These materials possess a uniform pore architecture that can be tuned by changing the organic template used or by swelling with the appropriate additives. Another attractive property of mesoporous materials is the compositional variance that can be achieved. In addition to silica, alumina and various transition metals, mesoporous molecular sieves may also be prepared with hybrid organic bridged silys.^{2,3}

The uniform pore architecture of mesoporous materials make them very attractive as hosts for the encapsulation of polymers. In fact, several reports describe the encapsulation of conducting polymers such as polypyrrole, polythiophene, and polyaniline into molecular sieves.⁴⁻⁶ Polyaniline (PANI) is a widely studied conducting polymer.⁷ However, when PANI is placed inside the pores of an insulator, such as MCM-41, several studies have shown that the DC conductivity is close to insulating.⁴ The current study describes the preparation, proton and DC conductivity measurements of PANI-SBA-15 composites. In this study, an aniline functionalized mesoporous molecular sieve in which the pore walls are decorated with aminophenylsilane was synthesized (AP-SBA-15) and used for the encapsulation of PANI. All-silica SBA-15 was also used in this study. The aniline monomer tethered to the AP-SBA-15 pore walls functions as the anchor for PANI which then becomes tethered to the walls, while the polymer encapsulated into all-silica SBA-15 could theoretically be extracted from the pores.

Experimental

Aniline containing SBA-15 (AP-SBA-15) was prepared as follows: tetramethylorthosilicate (TMOS) was combined with aminophenyltrimethoxysilane (APTMS) and added to a solution containing 1.2 g of Pluronic 123 (P123) and 40 ml of 2M HCl and heated to 40°C with stirring for 24 hours followed by heating at 90°C for 2 days. The amounts of TMOS and APTMS varied (APTMS/Si = 0.05-0.20) while keeping the number of moles of Si at 0.0145 moles. The surfactant was removed by refluxing the as-synthesized material in ethanol for ~24 hours. All silica SBA-15 was prepared as reported in reference 2. Polyaniline containing SBA-15 (PANI-SBA-15) was prepared as follows: Template free AP-SBA-15 (0.2 g) and all-silica SBA-15 (0.2 g) were dried under vacuum at ~100°C for 24 hours and then placed in a solution containing 0.2 grams of aniline hydrochloride (AHC) and 10 mL of methanol. The dispersion was stirred for ~5 minutes and then allowed to dry at room temperature. The aniline/SBA-15 powder was dispersed in ~20 mL of 1M HCl. To this dispersion, a solution of 0.35 g of ammonium persulfate (APS) in 10 mL of 1 M HCl was added and the mixture was stirred at room temperature

for ~12 hours. The dark green solids were filtered, washed thoroughly with water and dried at 50°C. To remove the excess bulk PANI formed outside the mesopores, PANI-SBA-15 composites were first stirred in 0.05 M NH₄OH to convert the green emeraldine salt to the emeraldine base and then Soxhlet extracted in 1-methyl-2-pyrrolidone (NMP) for ~12 hours. After extraction the dark blue powder was stirred in 2 M HCl to produce the emeraldine salt again.

Polyaniline was also polymerized in-situ during the synthesis of SBA-15. In this synthesis, TMOS was combined with APTMS (APTMS/Si = 0.05 and 0.1, total moles of silicon = 0.0145) and added to a solution containing 1.2 g of P123, 0.6 g of AHC, and 40 ml of 2M HCl and stirred at room temperature for 1 hour. Then 0.7 g of APS was added to the mixture, which was stirred at room temperature for ~20 minutes. The dark green gel was aged at 45°C for 24 hours followed by heating at 90°C for 48 hours. The as-synthesized samples were Soxhlet extracted with NMP as detailed above. The PANI-SBA-15 materials were also calcined at 550°C for 24 hours.

The samples were characterized by powder X-ray diffraction (XRD), infrared spectroscopy (FTIR), scanning electron microscopy (SEM), and nitrogen adsorption. The conductivity measurements were made following a published procedure reported previously [10]. Measured amounts of the powder and water added were mixed completely. The resulting wet mixtures were placed into a glass tube with the surface area of 1 cm², which was clamped between two stainless-steel pistons as the electrodes. The impedance spectroscopy measurements were conducted on a Voltalab PGZ301 analyzer, using Potential Dynamic EIS method over the frequency range 1–105 Hz at room temperature.

Results and Discussion

Mesoporous SBA-15 containing the conducting polymer, polyaniline, was prepared both in-situ and in a post treatment of the mesoporous aminophenyl functionalized SBA-15. Unlike the aminopropyl functionalized materials prepared with aminopropyltrimethoxysilane, the functionalization of SBA-15 with p-aminophenyltrimethoxysilane by co-condensation under acidic conditions produces very well ordered mesoporous SBA-15 with high APTMS content. As shown in Figure 1, the XRD patterns for the as-synthesized AP-SBA-15 materials display three well resolved reflections typical for hexagonally arranged mesoporous silica, which corresponds to the (100), (200), and (211) reflections. The Surface area for AP-SBA-15 prepared with an APTMS/Si of 0.05 is ~735 m²/g which is very similar to the surface area of the all-silica SBA-15 (Table 1). However, the pore size for this AP-SBA-15 is substantially larger than that for all-silica SBA-15 (7.8 and 6.5 nm respectively). As the APTMS/Si was increased to 0.2, the surface area decreased to 535 m²/g and the pore size decreased to 6.5 nm.

SEM images of AP-SBA-15 (not shown) reveal small disks ~1 μm in diameter and 100-200 nm thick. As the APTMS/Si ratio is increased, the morphology changes to less defined shapes. Most of the AP-SBA-15 powder composed of plates, but there are large amounts of small particles.

The post synthesis polymerization of polyaniline in the SBA-15 mesochannels was accomplished by the aniline monomer into the mesopores and then adding the oxidant to complete the polymerization. This process also produced excess bulk PANI on the outside of the SBA-15 particles as seen in Figure 2. The SBA-15 particles are completely covered with fibrous PANI. To remove the excess PANI, the composite powder was stirred in 0.05 M NH₄OH overnight to yield the emeraldine base form of PANI, which is soluble in NMP, and the excess polymer was Soxhlet extracted in NMP. The resulting powder was dark blue. These processes were performed

using template free AP-SBA-15 and all-silica SBA-15 calcined at 550°C. In the functionalized AP-SBA-15, the polymer should become tethered to walls, because the aniline monomer attached to the pore walls can provide an anchor for the polymer. In this scenario, the polymer would not be extractable. In the calcined all-silica SBA-15, the polymer would be formed in the pores, but it would not be tethered to the walls, and it could be extracted leaving the pores empty again. After extraction, scanning electron microscopy did not show any evidence of bulk PANI among the mesoporous particles (Figure 2). However, it is possible that the outside surface of the SBA-15 particles is coated with PANI. PANI SBA-15 samples prepared with AP-SBA-15 retained its dark blue color, but the sample prepared with all-silica SBA-15 became pale blue.

Polyaniline was also polymerized in-situ during the synthesis of SBA-15. Again, the as-synthesized mesoporous PANI-SBA-15 was dark green, indicating that the emeraldine salt was formed. This synthesis also yielded dark green solids and the XRD patterns (Figure 1) show a well ordered material similar to all-silica SBA-15. The as-synthesized material was also immersed in dilute NH₄OH followed by extraction in NMP. It is clear from the SEM images (Figure 2) that the as-synthesized composites contain a substantial amount of excess PANI as small diameter fibers around the bigger SBA-15 particles. However after extraction there is no evidence of excess bulk polymer.

Nitrogen adsorption studies for the PANI-SBA-15 composites are summarized in (Table 1). The samples prepared by post synthesis encapsulation (samples 4 and 5) using AP-SBA-15 showed a significant decrease in the pore size and surface area, while the samples prepared with all-silica SBA-15 showed a decrease in surface area, but not a significant change in pore size or volume. The composites prepared by in-situ polymerization of PANI (samples 6 and 7) after extraction display a substantially different isotherm from the calcined materials. These materials have a much smaller surface area and pore size (Table 1) than the calcined materials which indicates that the pores are partially filled with polymer.

When a conducting polymer is encapsulated in a zeolite, the electrical conductivity decreases significantly.⁸ One of the reasons is that the polymer confined in the zeolite pores cannot create good contact with the electrodes. In this case, this was an advantage, because the main interest of this study was to determine the proton conductivity of PANI encapsulated in the SBA-15 mesopores. Electrical conductivity measurements conducted using the dry emeraldine salt form of aniline doped with hydrochloric acid. The proton conductivities were measured using the same powder at room temperature. During the proton conductivities measurement, water was added to the powder to determine the effect of water content on the conductivity of the composite. PANI-SBA-15 samples exhibited very low electrical conductivities. The as made PANI-SBA-15 samples, which contained a large amount of excess bulk PANI exhibited electrical conductivities in the 10⁻⁴-10⁻⁵ S/cm range. These results compare well with literature reported values for PANI-zeolite composites.⁴ After extraction of the excess bulk PANI, the conductivities were not detectable and the material was insulating. The proton conductivity after extraction was in the 10⁻³ S/cm range and it varied significantly depending on the water content. It is worth noting that the PANI in the PANI-SBA-15 composite was doped with HCl. In most cases, stronger acids such as phosphoric acid or triflic acid are used to dope proton conducting membranes such as polybenzimidazole.

Table 1. Physiochemical properties of AP- and PANI-SBA-15

Sample	APTMS/Si	BET SA (m ² /g)	Pore size (nm)	Pore Vol (cc/g)
1	0	719	6.53	1.09
2	0.05	739	7.78	1.22
3	0.20	575	6.59	1.29
4	0.05	552	3.78	0.81
5	0	461	6.25	1.02
6	0.05	595	3.81	0.68
7	0.10	536	3.79	0.40

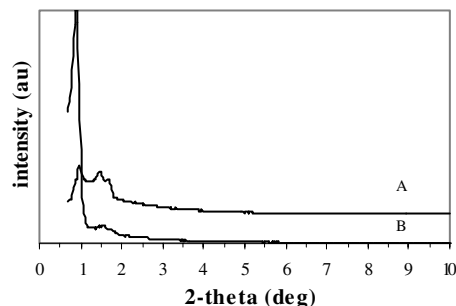


Figure 1. XRD patterns of (A) template free AP-SBA-15 (Sample 2) and (B) PANI-SBA-15 (sample 6) after extraction.

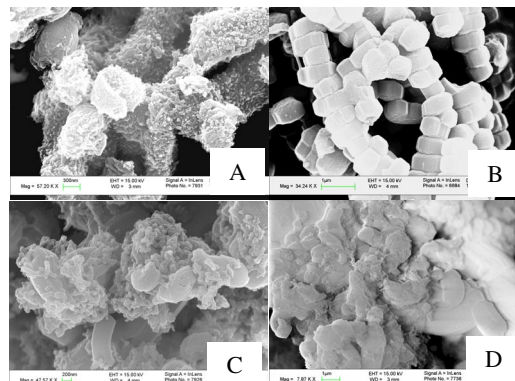


Figure 2. SEM of (A) as prepared PANI-SBA-15 (sample 4), (B) sample 4 after extraction in NMP, (C) as-synthesized PANI-SBA-15 (sample 6) and (D) sample 6 after extraction in NMP.

References

- (1) Kresge, C.T.; Lenowicz, M.E.; Roth, W.J.; Vartuli, J.C.; Beck, J.S.; *Nature* **1992**, 359, 710.
- (2) Yang, P.; Zhao, D.; Margolese, D.I.; Chmelka, B.F.; Stucky, G.D.; *Chem. Mater.* **1999**, 11, 2813.
- (3) Inagaki, S.; Guan, S.; Ohsuna, T.; Terasaki, O.; *Nature*, **2002**, 416, 304.
- (4) Wu, C-G.; Bein, T.; *Science*, **1994**, 264, 1757.S
- (5) Cardin, D.J.; *Adv. Mater.* **2002**, 14, 553.
- (6) Choi, H.J.; Cho, M.S.; Ahn, W.S.; *Synth. Met.* **2003**, 135-136, 711.
- (7) MacDiarmid, A.G.; *Synth. Met.* **1997**, 84, 27.
- (8) Mikhailenko, S.; Desplandier-Giscard, D.; Danumah, C.; Kaliaguine, S.; *Micropor. Mesopor. Mater.* **2002**, 52, 29.

PROTON EXCHANGE MEMBRANE FUEL CELLS: I. SYNTHESIS AND CHARACTERIZATION OF DISULFONATED POLY (ARYLENE ETHER BENZONITRILE) COPOLYMERS

Mehmet Sankir, William L. Harrison, Kent B. Wiles, Yanxiang Li and
James E. McGrath*

Macromolecular Science and Engineering and Materials Research Institute,
Virginia Polytechnic Institute and State University,
Blacksburg, VA 24061, USA
jmcgrath@vt.edu

Abstract

A series of benzonitrile containing sulfonated poly(arylene ether sulfone) copolymers were synthesized by direct nucleophilic substitution copolymerization. The 4,4'-biphenol, 2,6-dichlorobenzonitrile and 3,3'-disulfonated 4,4'-dichlorodiphenyl sulfone (SDCDPS) were used to produce novel sulfonated copolymers with various degrees of disulfonation (0-45 mol% SDCDPS), yielding ion exchange capacities (IEC's) up to 2.02 mmol/g. NMR analysis coupled with titration of sulfonated moieties confirmed both chemical structure and copolymer composition. GPC and intrinsic viscosity analyses indicated high molecular weight copolymers were synthesized. The copolymers produced ductile films with thin film conductivities reaching 0.12 S/cm, suggesting they are good candidates for proton exchange membranes in fuel cells. Characterizations such as TGA, water uptake, proton conductivity and morphology will be presented

Introduction

Our research group, and others, has been investigating novel, commercially viable proton conducting membranes for polymer electrolyte fuel cells. Polymer electrolyte fuel cell membranes require several qualities, such as good mechanical properties/stabilities, good proton conductivities, and have low permeabilities of the reactant fuels. Currently, expensive perfluorinated sulfonic acid polymers are employed despite their reported limitations. Alternative PEMs are primarily based on aromatic engineering polymers, such as poly ether sulfones and poly ether ketones that have been chemically modified to contain sulfonic acid groups along the main chain. In contrast, our approach has been to control the degree of sulfonation by copolymerizing sulfonated monomers. It has also been demonstrated that exact control (distribution) of sulfonation over the entire sequence is better via direct copolymerization versus post-sulfonation by titration and NMR studies [1-3]. The synthesis and characterization of high molecular weight, nitrile-functional copolymers using SDCDPS, 2,6-dichlorobenzonitrile and hexafluoroisopropylidene diphenol (hexafluorobisphenol A) have recently been reported by our group [4]. In this contribution, we report the systematic study of the synthesis of benzonitrile containing wholly aromatic disulfonated poly (arylene ether) copolymers (PAEB) by directly copolymerizing SDCDPS, 2,6-dichlorobenzonitrile and 4,4'-biphenol. The influence of the pendant nitrile group on this copolymer system is being explored as it may affect properties such as water uptake and proton conductivity by possible hydrogen bonding.

Experimental

Reagents. 4,4'-biphenol was kindly provided by Eastman Chemical, 2,6-dichlorobenzonitrile was purchased from Aldrich and both were used without any purification. The disodium salt of 3,3'-disulfonated 4,4'-dichlorodiphenyl sulfone (SDCDPS) was synthesized through the reaction of 4,4'-dichlorodiphenyl sulfone (Solvay Advanced Polymers) and fuming sulfuric acid, as described previously [5]. All other reagents were obtained from commercial sources and purified, as needed, via common procedures.

Synthesis of Sulfonated Poly (arylene ether benzonitrile). Sulfonated poly (arylene ether benzonitrile) (PAEB) copolymers were achieved with various degrees of disulfonation (0-45 mol% SDCDPS) via direct copolymerization of sulfonated dichlorodiphenyl sulfone (SDCDPS), 2,6-dichlorobenzonitrile and biphenol (BP). 2.2609 g (0.0131 mol) 2,6-dichlorobenzonitrile, 3.4767 g (0.0071 mol) SDCDPS and 3.7654 g (0.0202 mol) 4,4'-biphenol and 3.2139 g potassium carbonate (15% mol excess) were transferred to 3-neck flask equipped with a mechanical stirrer, a nitrogen inlet and a Dean Stark trap in order to synthesize 35 mol percent SDCDPS

containing copolymer, named as PAEB 35. Dry NMP (20 mL) was used as the polymerization solvent while toluene (10ml) was the azeotrope. The reaction mixture was refluxed for 4 hours at 150 °C to complete the dehydration process. The reaction temperature slowly increased to 190 °C for 16 hours just after the removing of the toluene gradually. The viscous reaction product was cooled and diluted with NMP and precipitated in deionized water as swollen fibers. After washing several times with deionized water, the precipitated copolymers were boiled in deionized water for 4 hours to remove the salts. Copolymers were isolated by filtration then dried in vacuum oven at 120 °C for 24 hours.

Film Casting and Membrane Acidification. Membranes in the potassium sulfonate form were prepared by first redissolving the copolymer in 5-10% (w/v) DMAc, filtered to afford, then cast onto clean glass substrates. The transparent solutions were carefully dried with infrared heat at gradually increasing temperatures (up to ~ 60 °C) under a nitrogen flow, until the film was dry. The sulfonated poly(arylene ether sulfone) copolymer films were converted to their acid- form by boiling the cast membranes in 0.5 M sulfuric acid for 1.5 hours, followed by 1.5 hour extraction in boiling deionized water, which has been referred to as Method 2 [6].

Characterization

A Nicolet Impact 400 FT-IR spectrometer was utilized on thin films to confirm the functional groups within the copolymers. Proton (¹H) NMR analysis were conducted on a Varian UNITY 400 spectrometer. All spectra were obtained from a 10% solution (w/v) in dimethylsulfoxide-d6 solution at room temperature. Gel permeation chromatography (GPC) with polystyrene standards was used to calculate the number average molecular weights (Mn). Intrinsic viscosities were determined in NMP at 25 °C using an Ubbelohde viscometer. The thermo-oxidative behavior of both the salt-form (sulfonate) and the acid-form copolymers was performed on a TA Instruments TGA Q 500. Dried, thin films (5 to 10 mg in salt form) were evaluated over the range of 30 to 800 °C at a heating rate of 10 °C/min in air. Titration of the sulfonic acid groups were performed on acidified membrane samples of known mass by exchanging with sodium sulfate then back titrating with 0.01M NaOH. Thin film conductivity measurements were conducted on acidified membranes while submerged in deionized water using a Hewlett Packard 4129A Impedance/Gain-Phase Analyzer recorded from 10 MHz to 10 Hz.

Results and Discussion

Disulfonated 4,4'- dichlorodiphenyl sulfone (SDCDPS) monomer with a near quantitative conversion was synthesized using a procedure reported by our group [4]. Direct nucleophilic polycondensation was used to synthesize several series of high molecular weight disulfonated poly(arylene ether sulfone) copolymers. The reaction includes two steps; four hours dehydration step, achieved by toluene refluxing at 155 °C and copolymerization step at 190 °C for 16 h. Synthetic route was depicted in Figure 1.

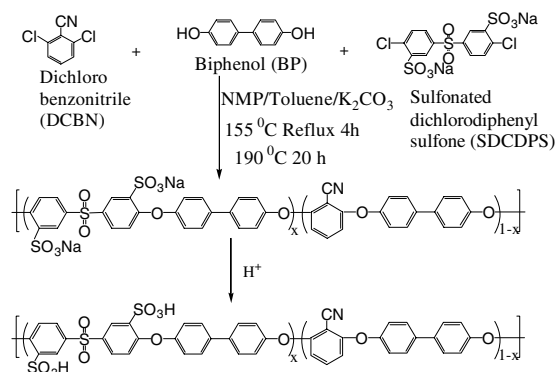
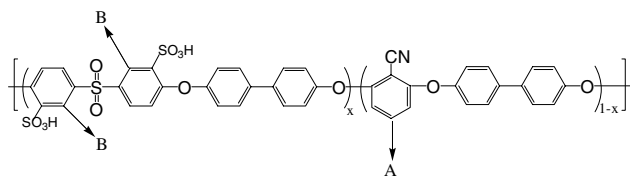


Figure 1. Copolymerization reaction mechanism includes two successive steps: Dehydration and copolymerization

¹H NMR was used for compositional and structural determinations (Figure 2). The observed degree of disulfonations from proton NMR was in close agreement with target disulfonations. High molecular weight PAEB

copolymers were synthesized as suggested by intrinsic viscosity, GPC, and film ductility.



$$\text{Mole percent disulfonation} = (100/(B/2+A/1)) * (B/2)$$

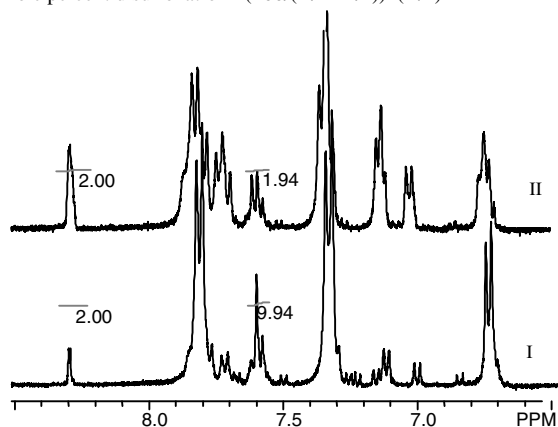


Figure 2. Calculation of mole percent sulfonation based on ^1H NMR. I: 9.5 % disulfonation, II: 34 % disulfonation where targets were 10 and 35, respectively.

Copolymers at various percent disulfonation and control copolymer with zero percent disulfonation were compared using FTIR spectra. The two new peaks resulting from sulfonic acid moieties were observed at 1070 cm^{-1} and 1095 cm^{-1} , respectively (Figure 3).

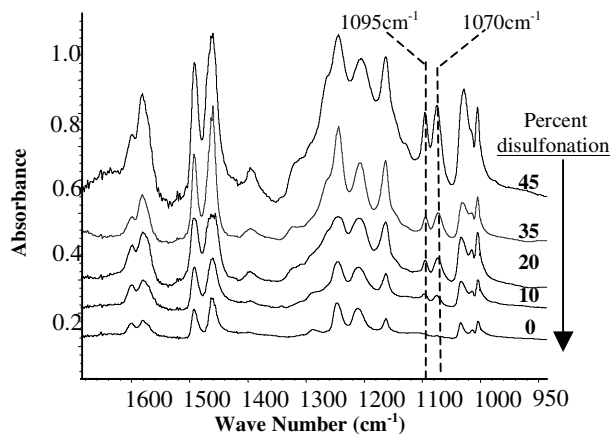


Figure 3. FTIR bands showing incorporation of sulfonic acid moieties into copolymer structure

The control polymer and salt forms of disulfonated copolymers showed very high thermooxidative stabilities ($\sim 500\text{ }^\circ\text{C}$), while the acidified membranes showed good thermooxidative stabilities ($>250\text{ }^\circ\text{C}$), which is sufficient for $120\text{ }^\circ\text{C}$ fuel cell operation (Figure 4). The increase in degree of disulfonation caused decrease in thermooxidative stabilities. The 5% weight loss temperatures for acid form of disulfonated copolymers varied in between 330 and $430\text{ }^\circ\text{C}$.

The target and actual degree of sulfonation, and intrinsic viscosities and the number average molecular weights of copolymers were shown in Table 1. Table 1 also shows the membrane properties such as water uptake values, proton conductivities at two different temperatures in liquid water, and IEC values as a function of degree of disulfonation.

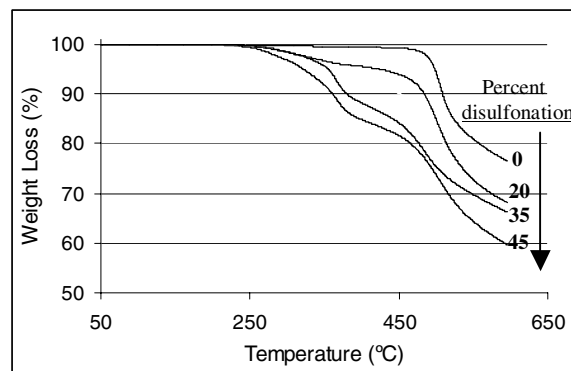


Figure 4. Influence of percent disulfonation on thermooxidative stability of acid form of PAEB copolymers ($10\text{ }^\circ\text{C}/\text{min}$ in air).

Since the controllable degree of disulfonation strongly influences the membrane properties, it was used as a design parameter for proton exchange membranes in fuel cell applications.

Table 1. Influence of the Percent Disulfonation on Several Features

PAEB XX target	PAEB XX actual	$[\eta]_{25^\circ\text{C}}^{\text{NMP}}$ dL/g	M_n	Water Uptake (%)	IEC mequiv/g		Proton Conductivity (mS/cm)	
					Cal	Exp	24°C	80°C
10	9.5	1.6	50K	6	0.6	0.5	10	14
20	19.7	1.9	80K	10	1.2	1.0	30	50
35	34	1.6	55K	40	1.8	1.8	60	130
45	44	1.2	65K	72	2.2	2.0	120	150

Conclusions

The benzonitrile containing thermally stable, ductile high molecular weight disulfonated copolymers were successfully synthesized. Structural and compositional characterizations showed that all the starting monomers were well incorporated into the copolymer. The spectrum of the physical properties as a function of degree of disulfonation was obtained to provide an input data while fabricating the proton exchange membrane for the desired fuel cell applications. Additional results will be discussed.

Acknowledgement. The authors would like to thank the National Science Foundation "Partnership for Innovation" Program (HER-0090556) and the Department of Energy (DE-FC36-01G01086) for support of this research effort.

References

- Wang, F.; Hickner, M.; Kim, Y. S.; Zawodzinski, T. A.; McGrath, J. E. *J. Membr. Sci.* **2002**, 197, 231.
- Wang, F.; Hickner, M.; Ji, Q.; Harrison, W.; Mecham, J.; Zawodzinski, T.; McGrath, J. E. *Macromol. Symp.* **2001**, 175(1), 387.
- Harrison, William L.; Wang, Feng; Mecham, Jeffery B.; Bhanu, Vinayak A.; Hill, Melinda; Kim, Seung Yu; McGrath, J.E. *J. Polym. Sci.: Part A: Polym. Chem.* **2003**, 42, 2264.
- Sumner, M.J.; Harrison, W.L.; Weyers, R.M.; Kim, Y.S.; McGrath, J.E.; Riffle, J.S.; Brink, A.; Brink, M.H. *J. Membrane Science* **2004**, accepted.
- Sankir M.; Bhanu, V.A.; Ghassemi, H.; Wiles, K.B.; Hill, M.H.; Harrison, W.; Sumner, M.; Glass, T.E.; Riffle, J.S.; McGrath, J.E. *Polymer Preprints* **2003**, 44, 1.
- Kim, Y.S.; Wang, F.; McCartney, S.; Hong, Y.T.; Harrison, W.; Zawodzinski, T. and McGrath, J.E. *J. Polym. Sci.: Part B: Poly. Phys.* **2003**, 41, 2816.

A NEW CLASS OF POLYELECTROLYTES, POLYPHENYLENE SULFONIC ACID AND ITS COPOLYMERS, AS PROTON EXCHANGE MEMBRANES FOR PEMFC'S

Sergio Granados-Focil, Morton H. Litt*

Department of Macromolecular Science and Engineering, Case Western Reserve University, 10900 Euclid Ave. Cleveland OH, 44106.

Introduction

Polymer membrane electrolyte fuel cells (PEMFC's) have become one of the most attractive alternative power sources for vehicles and portable electronic devices. PEMFC's are the best choice for these applications due to their high power densities and relatively low operating temperatures. The most widely used materials for polymer electrolyte membranes are the perfluorosulfonic acid polymers, like Nafion®. However, these materials present several disadvantages, such as very low conductivities at low relative humidity or temperatures above 80°C. A considerable amount of effort has been directed towards finding alternative materials that would overcome the disadvantages of Nafion®.^{1,2} Among these developments are sulfonated rigid rod liquid crystalline polyimides, where bulky or angled comonomers have been used to generate nanoscale pores lined with sulfonic acid groups. These nanopores increase the water absorption and thus the proton conductivity of the polyimide membranes at low relative humidities and high temperatures.²

We have previously reported the application of the structural approach used for the rigid rod polyimides to hydrolytically stable Poly(phenylene sulfonic acid)s.³ This study extends the same approach to grafted copolymers containing bulky and crosslinkable groups. Their conductivity as a function of temperature and relative humidity surpasses the values reported for Nafion®, the rigid rod sulfonated polyimides and the post-sulfonated PEEK's and poly(4-phenoxybenzoyl-1,4-phenylene)s.^{4,5}

Experimental

Materials. All reagents were purchased from the Aldrich Chemical Co. N-methylpyrrolidone (99%), was stirred overnight with calcium hydride, vacuum distilled and degassed prior to use. All the remaining solvents and reagents were used without further purification. Copper bronze was activated according to a previously reported procedure⁶ and was used immediately after preparation

Instrumentation. ¹H and ¹³C NMR spectra of the polymers and the monomers were obtained on a Varian Gemini 300 spectrometer using D₂O and DMSO *d*-6. FTIR spectra were recorded on a BOMEM Arid Zone FTIR spectrometer. Intrinsic viscosity of DMSO polymer solutions was measured using a Cannon Ubbelohde viscometer. Proton conductivity was measured using a 4-point probe configuration⁷ Solartron apparatus in the AC mode.

Synthesis. The synthetic procedures to obtain 4,4'-dibromo-2,2'-biphenyldisulfonic acid (I), Benzyltrimethylammonium(4,4'-dibromo-2,2'-biphenyl) disulfonate (II) and Poly(phenylene sulfonic acid) (III) have been reported previously.³ Optimization of the experimental conditions yields now intrinsic viscosities of 0.85dl/g for III.

Synthesis of Poly(phenylene sulfonic acid) grafted copolymers. 5g of polyphenylene sulfonic acid, III, and 15 ml of H₃PO₄ were added to a 50 ml 3-necked round bottom flask under nitrogen flow and stirred at 300 rpm. Once a homogeneous solution was formed, 30g of P₂O₅ were added in batches of 500 mg at a time

in order to keep the temperature of the reaction mixture below 100°C. After addition of the P₂O₅ was complete, a condenser was fitted to the flask, the temperature was raised to 130°C, and 65meq of the compound to be grafted into the backbone were added to the reaction mixture. The reaction was then allowed to continue for a period of time ranging from 30 to 120 minutes depending on the desired yield for the grafting process. Grafted copolymers containing 5% to 50% of grafted aromatic sulfone can be obtained using this method. The yield of the grafting process was confirmed by ¹H NMR and acid base titration of the resulting products.

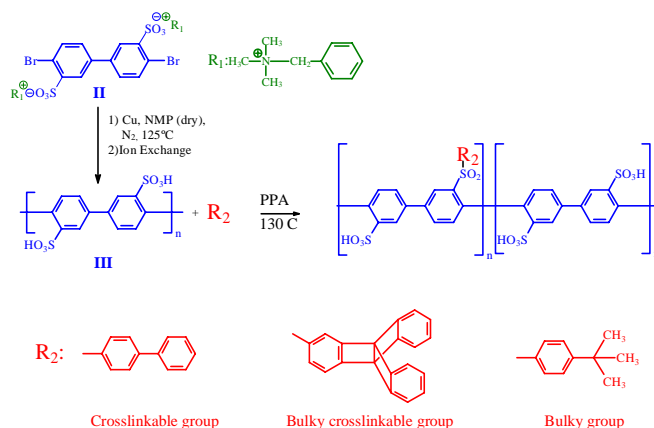


Figure 1. Synthesis scheme for the grafted copolymers.

Thermal Crosslinking of the Poly(phenylene sulfonic acid) copolymers containing grafted biphenyl or triptycene.

Copolymer films were placed between Teflon sheets and the assembly was put inside an aluminum box equipped to provide a preheated nitrogen flow. The box was then placed inside a convection oven preheated at the desired crosslinking temperature and kept at a constant temperature for a period of time ranging from 20 to 60 minutes.

Results and Discussion

Synthesis of grafted Poly(phenylene sulfonic acid) copolymers. The grafting of different aromatic compounds had different structural goals. Biphenyl was used as a thermal crosslinker group, while tert-butylbenzene was used to increase the distance between the polymer chains creating more space available for water molecules to be stored within the polymer membrane. The use of triptycene had a dual purpose, to generate crosslinkable films and to increase the intermolecular distance hopefully increasing the water retention capabilities of these crosslinked membranes. The grafting reactions were found to proceed heterogeneously requiring relatively severe conditions, namely the use of high temperature and an excess of the compound to be grafted into the backbone. Table 1 illustrates the conditions used to obtain different copolymer compositions.

Table 1. Experimental Conditions for the Grafting of Aromatic Rings to the Poly(Phenylene sulfonic acid).

Grafted compound	Reaction time (min)	Amount of grafted material (% total sulfonic acids converted to sulfone)
Biphenyl	30	10
Biphenyl	60	20
Biphenyl	120	55
Triptycene	30	6.5
Tert-butylbenzene	60	5
Tert-butylbenzene	120	25

According to the sulfonic acid titration analysis, the amount of sulfone groups present in the grafted copolymer was always found to be approximately 10%-15% lower than the amount expected when calculated based on the amount of aromatic sulfone found by ¹H NMR, analysis. This suggests the presence of undesired side reactions most likely due to the vigorous grafting conditions. The use of alternative solvents where the grafting process occurs homogeneously is currently being explored.

Thermal Crosslinking of the Poly(phenylene sulfonic acid) copolymers. The temperature and time required to produce insoluble films depended on the nature of the group being grafted into the polymer backbone but not on the amount present in the polymer. This indicates that a relatively small amount of crosslinker is enough to render the films insoluble, however the amount of swelling upon immersion in water was found to depend on the relative amount of crosslinker present. The conditions required to render the copolymer films water insoluble are summarized in table 2.

Table 2. Experimental Conditions for the Crosslinking of the copolymers containing biphenyl or triptycene.

Grafted compound	Crosslinking time (min)	Crosslinking temperature (°C)
Biphenyl	25	210
Triptycene	60	250

Proton conductivity of the Poly(phenylene sulfonic acid) grafted copolymers. The proton conductivity of the different copolymers was measured as a function of temperature and relative humidity, see figures 2 and 3. The data show that a small amount of grafted t-butylbenzene or biphenyl (5-10%) decreases the conductivity by a factor of 3, but it is still comparable to or higher than Nafion®'s.

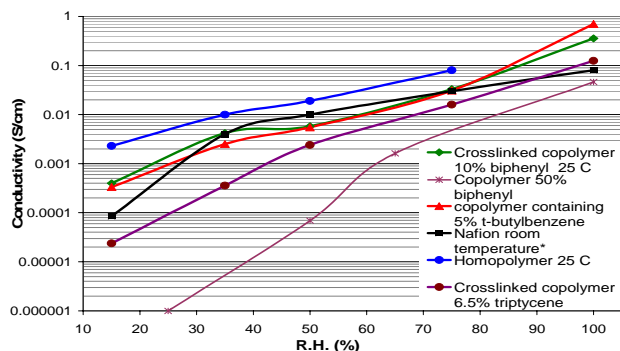


Figure 2. Conductivity vs. relative humidity at room temperature *(the conductivity of Nafion® does not change significantly over this temperature range⁸).

Figure 2 also shows that a large amount of biphenyl grafted into the polymer decreases the conductivity significantly, most likely due to an intrinsic change in the solid state structure of the membrane. In the case of the triptycene inserted membranes, the conductivity is much lower than that of the other copolymers with comparable amounts of grafted aromatic groups. ¹H-NMR analysis shows that 6.5% of the sulfonic acids have reacted with the triptycene after the grafting process. However, the amount of sulfone calculated from the titration of the sulfonic acids in the copolymer is approximately 10% mol. This suggests that a second aromatic ring had also reacted. Crosslinking of this copolymer required higher temperatures and longer times than those required by the grafted biphenyl copolymers. This treatment resulted in loss of sulfonic acid due to formation of

intermolecular sulfones and possibly thermal degradation of the polymer.

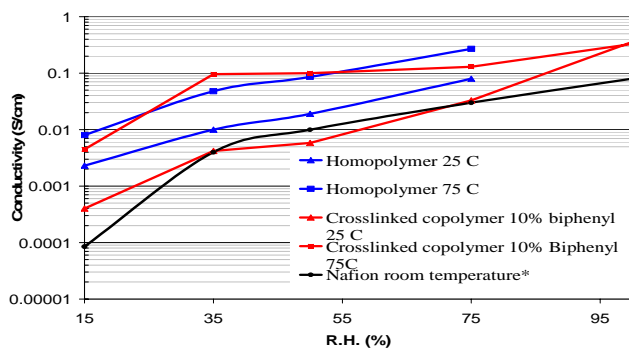


Figure 3. Conductivity as a function of relative humidity and temperature for the crosslinked films.

Dimensional stability and solubility of the copolymer membranes. Grafting of 5% mol tert-butylbenzene into the polymer backbone renders the copolymer insoluble while the grafting of up to 20% of biphenyl or 6.5% of triptycene gave water soluble copolymers. The difference in solubility among these materials may be due to hydrophobic bonding of the bulky non-polar tert-butyl groups, preventing the chains from dissolving in water. Dimensional changes of the copolymers films upon immersion in water occur almost exclusively in the thickness of the films, table 3.

Table 3. Dimensional Change upon immersion in water of films equilibrated at 20%R.H.

Grafted group	Grafted amount (% total sulfonic acids)	Δx (%)	Δy (%)	Δz (%)
Biphenyl	10	2	2	45
Biphenyl	20	1	1	35
Biphenyl	55	~0	1	15
Tert-butylbenzene	5	1	2	85
Tert-butylbenzene	25	1	1	50

Conclusions

Grafted copolymers of poly(phenylene sulfonic acid)s were made by reaction of the backbone's sulfonic acid groups with aromatic compounds in polyphosphoric acid. The grafting of biphenyl produces thermally crosslinkable films that have proton conductivities comparable to or higher than that of Nafion®. Grafting of small amounts of bulky monofunctional groups like tert-butylbenzene produces water insoluble films with proton conductivities similar to those of the thermally crosslinked films. Further work remains to be done in order to obtain dimensionally stable membranes.

References

- (1) Rikukawa R. M., Sanui K., *Prog. Polym. Sci.* **2000** 25 1463
- (2) Zhang Y., Litt M.H., *ACS Polym. Prepr. Aug.* **1999**, 40(2), 480
- (3) Granados-Focil, S., Litt, M.H., *Polym. Mat. Sci. and Eng.* **2003**, 89 438-439.
- (4) Bae J.-M. et. al. *Solid State Ionics* **2002** 147 189
- (5) Kobayashi H., et. al., *Solid State Ionics* **1998** 106 219
- (6) Vogel A.I., *Vogel's Textbook of practical chemistry*, **1989**, Longman, London, p. 426.
- (7) Cahan, B. D.; Wainright, J. S. *J Electrochem Soc* **1993** 140 L185
- (8) Sone Y., et. al., *Electrochem. Soc.* **1996**, 143 (4) 1254.

FULLERENE-BASED PEM FOR DRY OPERATION OF POLYMER ELECTROLYTE FUEL CELL

Ken Tasaki^{a†}, Arun Venkatesan^a,
Perumal Pugazhendhi^b, and Raouf, O. Loutfy^b

^aMC Research and Innovation Center,
7127 Hollister Ave. Suite 110, Goleta, CA 93117
^bMER Corporation, 7960 S. Kolb Rd. Tucson, AZ 85706

Introduction

Water management in polymer electrolyte fuel cells (PEFC) is one of the most difficult issues that require careful attention in designing a reliable fuel cell. A breakdown in water balance at the cathode side results in either drying out or water flood, while the anode side tends to get dry due to the water diffusion across the membrane. Currently dominant water-based proton-exchange membranes (PEM) require not only a humidifier which takes extra space, but also favor an even distribution of water throughout the membrane.

To eliminate the problems associated with water management, a number of efforts have been underway in the development of anhydride PEM.¹⁻³ Recently, Sony has developed proton-exchange membranes based on functionalized (mainly the OSO₃H and the OH groups) fullerenes for polymer electrolyte fuel cell (PEFC).⁴ Fullerenes are very unique in that they have a very low electron affinity and are easy to chemically functionalize; thus their performance (the conductivity, the thermal/chemical/mechanical stability...) can be fine tuned chemically. Also, fullerenes with multiple acid groups have a high volumetric density of proton conductive groups. The Sony group suggested that the ion conduction in the functionalized fullerene was due to the proton hopping between the functional groups on the fullerene, therefore requiring no humidification, though no detailed examination of the proton transport mechanism was reported.⁴ Still, chemical functionalization of fullerenes is well-established; thus their performance (the conductivity, the thermal, the chemical, and the mechanical stabilities) can be controlled and even fine-tuned chemically. Thus, they could be promising materials for a new type of tailored ionic conductors. Yet, so far, it is not clear whether the conductivity of Sony's fullerene membrane is due to the functional groups or C₆₀ itself is conductive. Theoretical calculations may provide an insight into the nature of C₆₀ as a proton conducting material. In this report, we examine C₆₀'s basic characteristics as a proton conductor primarily through theoretical calculations and report some experimental results on its application in PEFC.

Calculations

The activation energy barriers for proton hopping in fullerene were calculated at the PM3 method since higher levels of calculations are computationally prohibiting due to the size of the molecules. No activation energy barrier of proton transfer has been reported for C₆₀. The activation barrier was obtained by determining the transition state for the proton transfer pathway and then taking the energy difference between the transition state and the equilibrium structure. The transition state and the equilibrium structure were each separately optimized, while the former was further verified by frequency calculations where only one negative frequency was found. Additionally, the internal reaction coordinate calculations were

followed to validate the transfer path. All calculations were performed in the gas phase.

Experimental

Preparation of Membranes. A pellet of C₆₀ was made for electrochemical performance measurements by mixing the C₆₀ powder with 5 wt% of polytetrafluoroethylene as a binder and then pressing the mixed power to yield a pellet with 175 μm thickness. Separately, a Nafion 117 membrane soaked in MeOH was mixed with C₆₀-toluene solution to make a C₆₀-doped Nafion membrane. The loading of C₆₀ dopant in the Nafion membrane was approximately 1 wt%.

AC Impedance Measurements. AC impedance measurements were performed for the films at 30 °C in the frequency range of 1 to 105 Hz without any humidification after operating in a fuel cell under dry gas at 105 °C for several hours. The resistance associated with the membrane at zero phase angle was used to estimate the proton conductivity of the membrane using the equation, $\sigma = (1/R) (L/A)$, where R is the bulk resistance of the membrane, L represents the membrane thickness, and A the membrane area.

Cell Performance Measurements. A membrane-electrode-assembly (MEA) was constructed using each membrane prepared above: the C₆₀ pellet, Nafion 117, and Nafion 117 doped with 1 wt% C₆₀. 0.4 mg cm⁻² of platinum coated on the gas diffusion electrode was applied on each side of the membrane. The cell included highly conducting non-porous graphite plates with grooves to circulate hydrogen gas at the anode and the cathode compartments. The power of the cell was measured at 0.3 A cm⁻² with dry hydrogen and dry oxygen as fuel under atmospheric pressure at 30 °C after operating for 33 hrs with dry fuel gases.

Results and Discussion

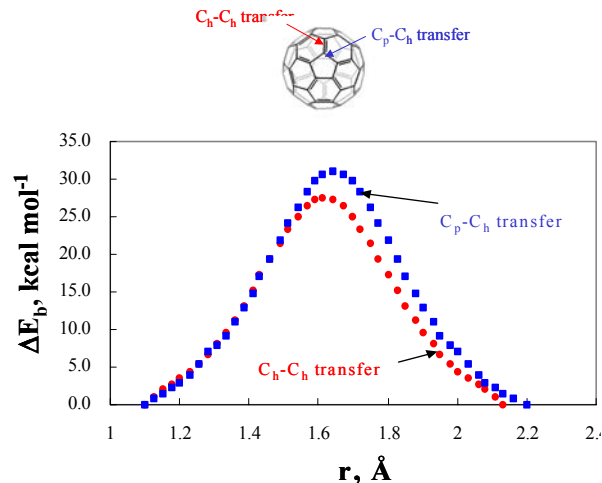
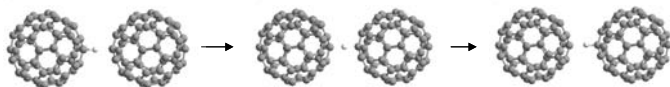


Figure 1. The intramolecular proton hopping potential energies for two possible path ways in C₆₀. r is the distance between the proton and the carbon to which the proton was originally attached.

Figure 1 shows the potential energy profiles for proton hopping on the surface of C₆₀ with the activation energy barriers of H⁺ transportation along the two paths: 27.8 kcal mol⁻¹ along the C-C bond dividing two hexagons (C_h-C_h) and 31.3 kcal mol⁻¹ along the bond dividing a hexagon and a pentagon (C_h-C_p) of C₆₀. The distance r refers to the distance between the proton and the carbon to which the proton was originally attached in C₆₀H⁺. At the distance ~ 2.2 Å, the proton is attached to the adjacent carbon. These values imply a

fast movement of a proton around the C₆₀ surface, which is qualitatively consistent with the experimental observation that only a single ¹³C-NMR spectrum was observed for the C₆₀H⁺ system at ambient temperature.⁵

Next, the activation barrier of H⁺ transportation between two C₆₀ molecules was computed for the process illustrated below (the proton shown by a white dot between two C₆₀ molecules):



The calculated activation barrier was only 3.29 kcal mol⁻¹. Our calculations suggest that C₆₀ itself is highly conductive.

In order to verify the above theoretical results, we assembled an MEA with a C₆₀ pellet as the membrane for polarization measurements under dry condition. **Figure 2** presents the polarization curve for the cell measured at 30 °C with dry hydrogen and oxygen as the fuels under atmospheric pressure. Though the current density is small since there is no acidic proton in the pellet, this is a direct evidence of C₆₀'s proton conductivity. Despite Sony's claim that the proton conductivity is due to the functional groups of fullerene, our finding opens up a possibility of C₆₀ as proton conductive material.

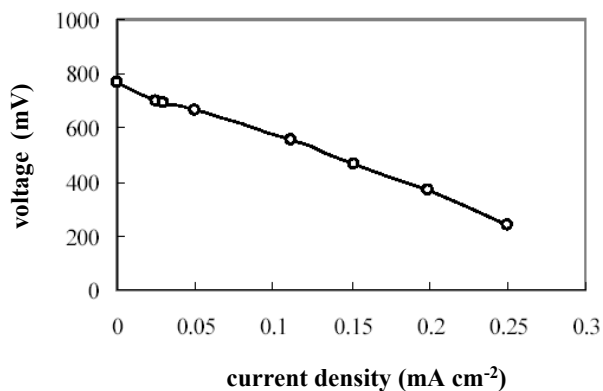


Figure 2. The polarization curve for a fuel cell with a C₆₀ pellet.

To examine the effect of C₆₀ as an additive to PEM, a Nafion 117 membrane was doped with 1 wt% of C₆₀, and the AC impedance was measured under dry condition. Table 1 lists the proton conductivity of the doped and undoped Nafion.

Table 1. The proton conductivity of doped Nafion films

	σ , mS cm ⁻¹
Nafion 117	1.7
Nafion 117 + C ₆₀	15

The proton conductivity of C₆₀-doped Nafion shows roughly an order of magnitude improvement over Nafion only under dry condition.

MEA's were also assembled for power measurements using dry H₂ and O₂ gases. Table 2 lists the maximum power density which was normalized by the thickness of the film, thus the unit in mW/cc.

Table 2. Maximum power density of fuel cell with dry Nafion 117 and dry Nafion 117 doped with C₆₀.^a

	mW/cc
Nafion 117	16
Nafion 117 + C ₆₀	200

Nafion doped with C₆₀ exhibits the power which is more than an order of magnitude higher than Nafion 117 alone.

Figure 3 shows the transient voltage of a fuel cell with the C₆₀-doped Nafion, a sharp contrast in stability from Nafion alone under dry condition. Our results suggest a promising potential of C₆₀ as an additive for Nafion under dry condition.

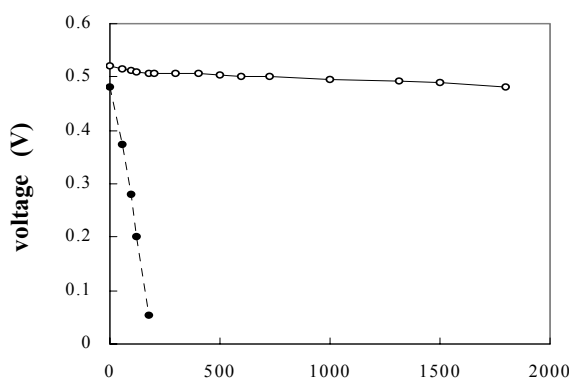


Figure 3. The voltages as a function of time at 30 °C with dry gases under 0.3 A cm⁻² of constant current: the Nafion doped with C₆₀ (solid line) and Nafion (broken line).

Acknowledgment

This work was supported by the High Temperature Polymer Membrane Program at U.S. Department of Energy.

References

- Haile, S. M.; Boysen, D. A.; Chisholm, C. R. I.; Merle, R. B.; *Nature*, **2001**, *410*, 910.
- Wainright, J. S.; Wang, J.-T.; Weng, D.; Savinell, R.F.; Litt, M. H. *J. Electrochem. Soc.* **1995**, *142*, L121.
- Schuster, M.F.H.; Meyer, W. H.; Schuster, M.; Kreuer, K. D. *Chem. Mater.* **2004**, *16*, 329.
- K. Hinokuma, *J. Electrochem. Soc.* **2003**, *150*, A112.
- C. Reed, K.-C. Kim, R. D. Bolskar, L. J. Mueller, *Science*, **289**, 101 (2000).

DESIGN OF POLYMER BLENDS FOR PROTON-EXCHANGE MEMBRANES IN FUEL CELLS

S. Swier, M. T. Shaw and R. A. Weiss

Dept. of Chemical Engineering and Polymer Program
Institute of Materials Science, University of Connecticut
Storrs, CT 06269

Introduction

Proton-exchange membranes (PEM) must have high proton conductivity and sufficient mechanical and chemical stability to withstand the conditions in the fuel cell. Perfluorinated polymer electrolyte membranes such as Nafion™ have been the principal choice in the past for this purpose. However, these materials are expensive, have relatively poor resistance to methanol transport (which is important in direct methanol fuel cells) and have poor mechanical properties when highly swollen by water. Contemporary PEM research involves the development of new polymer electrolytes based on hydrocarbon polymers [1].

Further flexibility in PEM materials design can be achieved by using polymer blends in which each component fulfills a different membrane requirement [2]. One strategy consists of combining a sulfonated aromatic hydrocarbon polymer with an engineering thermoplastic where intermolecular interactions assure a high level of compatibilization. PEKK is a commercial high temperature thermoplastic that has high temperature stability, excellent chemical and solvent resistance and excellent mechanical properties. Because of a higher ketone content, PEKK has a higher glass transition temperature (T_g), melting point (T_m), stiffness and strength than poly(ether ether ketone), PEEK, which has also been used to prepare PEMs.

This paper describes PEMs based on blends of sulfonated PEKK (SPEKK) and poly(etherimide), PEI. The idea of using SPEKK/SPEKK blends for PEMs is also discussed.

Experimental

PEKK (terephthaloyl/isophthaloyl ratio = 8/2) was obtained from Oxford Performance Materials. PEI Ultem 1000 was provided by General Electric. PEKK was sulfonated with a 53/47 (v/v) mixture of concentrated and fuming sulfuric acids. The ion-exchange capacity (IEC) in [meq/g], was determined by titration. Membranes of SPEKK, SPEKK/PEI and SPEKK/SPEKK blends were prepared by solution casting 5% (w/v) solutions in N-methyl-2-pyrrolidone (NMP) or dimethylacetamide (DMAc). Typically, the solvent was allowed to evaporate for about 1 day at 60°C, after which the films were dried at 120°C under vacuum for 3 days.

The blend membranes were characterized using transmission electron microscopy (TEM), atomic force microscopy (AFM), differential scanning calorimeter (DSC) and thermogravimetric analysis (TGA). A frequency response analyzer (Solartron SI 1260) combined with a potentiostat (Solartron SI 1287) was used to measure the proton conductivity of hydrated membranes. Single cell performance curves of the membranes were determined using a membrane-electrode-assembly (MEA) at 80°C and 1 atm. Gasses for the anode and cathode side were hydrogen and oxygen, respectively.

Results and Discussion

Thermal properties of SPEKK and PEI. TGA indicated that PEI was thermally stable up to 460°C, but desulfonation of SPEKK occurred at ca. 260°C. The T_g of dry SPEKK increased linearly from 150°C for PEKK to 215°C for SPEKK-IEC = 2.6 meq/g. The increase was due to hydrogen bonding between sulfonic acid groups

that reduces chain mobility. Water, however, plasticizes the SPEKK; e.g., when equilibrated in a 98% R.H. environment, the T_g of SPEKK with IEC = 2 meq/g decreased from 200°C to 60°C. PEI had a glass transition of 220°C.

Conductivity and swelling of SPEKK. The room temperature proton conductivities of hydrated SPEKK membranes increased exponentially with sulfonation level (Figure 1). This is due to the increase in the concentration of sulfonic acid sites, which form the locus for proton transport, and the increase in water uptake which plays an important role in increasing the mobility of protons through the membrane. SPEKK with an IEC of 1.9 meq/g. had a conductivity comparable to Nafion™ 112 (IEC = 0.9 meq/g, σ = 60 mS/cm), and its hydration number, $n(\text{H}_2\text{O})/n(\text{SO}_3\text{H})$ at 98% R.H. was 10, which was also comparable to that for Nafion™ [3].

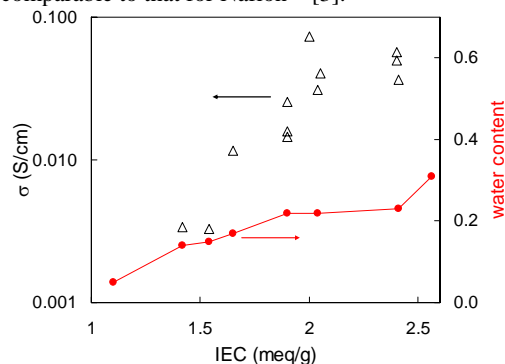


Figure 1. Proton-conductivity, σ in S/cm, and water uptake, $(w_{\text{wet}} - w_{\text{dry}})/w_{\text{wet}}$, of SPEKK in a 98% R.H. environment at 25°C

MEA performance comparable to Nafion™ was obtained (Figure 2) for SPEKK with IEC < 2 meq/g. However, the durability of highly water swollen membranes was poor. The use of SPEKK with a high IEC and corresponding conductivity in a polymer blend with either PEI or a low IEC SPEKK were investigated to remedy this problem.

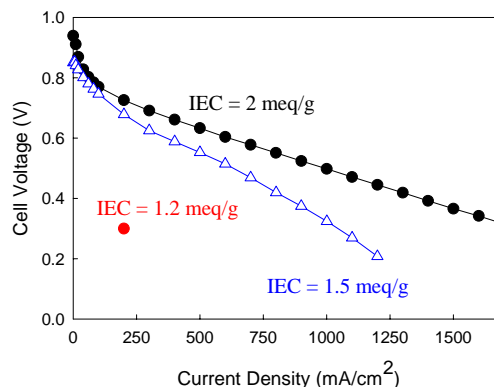


Figure 2. Membrane-electrode assembly (MEA) performance curves of SPEKK membranes at 80°C in H_2/O_2 (1 atm, 75 % R.H.); Nafion™ 112 under these conditions: 0.8 V at 200 mA/cm^2

Ternary phase diagram. The blends were cast from NMP. Unfortunately, the solubility of the SPEKK/PEI mixtures decreased with increasing IEC (Table 1), which is probably due to strong ion-dipole interactions.

Table 1. Cloud points as a function of IEC for SPEKK/PEI in NMP; *DMAc used as casting solvent.

IEC, meq/g	wt% SPEKK/PEI 50/50 in NMP at cloud point
1.1	24
1.5	22
1.7	23
2	17
2	16*
2.6	15

Binary blend morphology and conductivity. The SPEKK/PEI and SPEKK/SPEKK blends cast at 60°C exhibited a two-phase morphology, see Figure 3. DSC analysis indicated that the two phases in the SPEKK/PEI were essentially the pure components, but that some intermixing occurred in the SPEKK/SPEKK blend. This may be due to a combination of a postponed cloud point and the stronger intercomponent interactions in this blend.

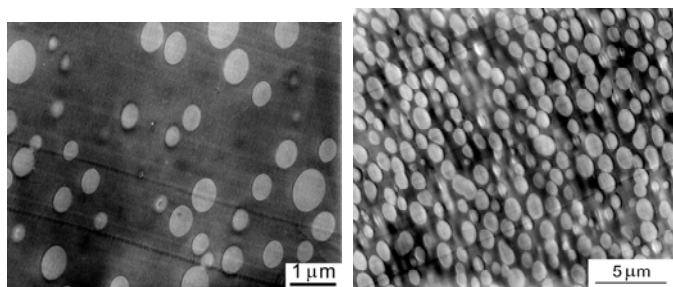


Figure 3. TEM micrographs of blends of SPEKK (IEC = 2 meq/g) with 15 wt% PEI (*left*) and with 50 wt% of SPEKK (IEC = 1.2 meq/g) (*right*); both blends were cast from NMP solutions at 60°C and stained with lead nitrate.

The effect of PEI content on particle size, conductivity and water uptake is summarized in Figure 4 (*left*). Adding the non-conductive polymer reduced the water swelling of these PEMs, but at the expense of a significant drop in conductivity of the SPEKK/PEI blends. The SPEKK/SPEKK blends, however, retained high conductivity, even in a 50/50 blends (see Table 2, *cfr.*: σ is 8 mS/cm for a 50/50 SPEKK IEC 2 / PEI blend). In that case, the low IEC component, which has relatively low water sorption and conductivity by itself, provided mechanical strength and durability to the membrane. Further investigation of the SPEKK/SPEKK system is currently in progress.

Table 2. Conductivity of 50/50 blends of SPEKK (IEC = 2 meq/g) with SPEKK's of different IEC's at 25°C and 98% R.H.

IEC, meq/g	σ , mS/cm
0.8	24
1.2	32
1.5	34

Effect of casting parameters. High-temperature annealing of the films after casting had no noticeable effect on the morphology, which may be due to low molecular mobility in the blend. A second strategy for controlling the morphology was to vary the temperature during casting. The effect of casting temperature is shown in Figure 4 (*right*). Smaller particle sizes were obtained by increasing the casting temperature. This is probably the combined result of postponed phase separation due to the UCST behavior of the ternary blend and faster

solvent evaporation resulting in a frozen-in morphology. Note that the particle size does not significantly affect the conductivity or swelling.

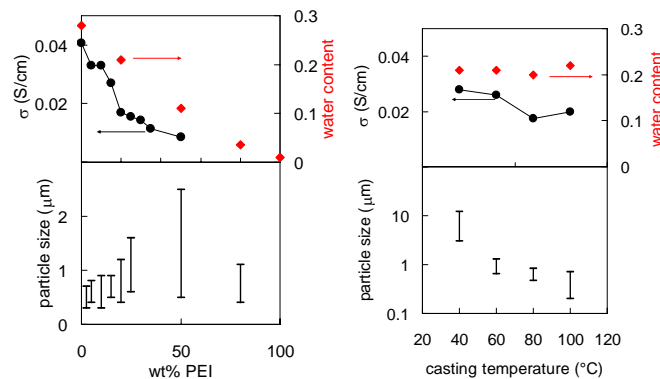


Figure 4. Properties of SPEKK (IEC = 2 meq/g) / PEI blends; cast at 60°C (*left*) and for 15 wt% PEI (*right*); water content and conductivities were determined at 25°C and 98% R.H.; brackets: range of smallest to largest particles

Preliminary results on the use of DMAc instead of NMP as the casting solvent indicate that significant improvements in membrane fuel cell durability can be achieved using this solvent. The reason for this effect might be different SPEKK-solvent interaction and/or a specific chemical reaction involving the DMAc.

Conclusions

Sulfonated poly(ether ketone ketone) (SPEKK) is a potential proton-exchange membrane material for fuel cell applications. Proton conductivities and MEA performance data are competitive with Nafion™ under similar conditions. A large depression in glass transition and significant swelling, however, limits the long term durability of SPEKK membranes. That limitation can be resolved by forming PEMs from blends of SPEKK with poly(ether imide) (PEI), wherein the SPEKK provides conductivity and the PEI improves the mechanical stability of the membrane. A promising alternative approach is the use of blends of SPEKK's with different sulfonation levels.

A specific objective of our work is to achieve a spinodal-like morphology in the membrane, where the interconnected SPEKK phase optimizes proton conductivity and a lower conductivity matrix consisting of PEI or SPEKK with low sulfonation level will provide mechanical stability of the hydrated membranes.

Acknowledgement. The authors wish to thank the Department of Energy (Grant 69797-001-03 3D) and Connecticut Innovations, Inc (Yankee Ingenuity Grant 01Y09) for support of this research, Vijay Ramani and Prof. J. E. Fenton for their help with the MEA tests and Oxford Performance Materials for supplying PEKK.

References

- [1] Rikukawa, M.; Sanui, K. *Prog. Polym. Sci.* **2000**, *25*, 1463.
- [2] Cui, W.; Kerres, J.; Eigenberger, G. *Sep. Purif. Technol.* **1998**, *14*, 145.
- [3] Zawodzinski, T.A.; Neeman, M.; Sillerud, L.O.; Gottesfeld, S. *J. Phys. Chem.* **1991**, *95*, 6040.

DEVELOPMENT OF NON-PERFLUORINATED POLYMER ELECTROLYTE MEMBRANES

L. Hedhli, K. Adjemian, S. Gaboury, P. Piccione, A. Lemacon

Atofina Chemicals, Inc. 900 First Av.
King of Prussia, PA 19406

Introduction

Intensive work in the area of polymer electrolyte membrane fuel cells (PEMFC) in recent years has led to enhancements in many aspects of this technology [1,2]. Despite these improvements, the perfluorinated sulfonated ionomer membrane, PFSI, still does not meet several of the major requirements needed to make fuel cell technology commercially viable including: low cost, mechanical strength, dimensional stability at elevated temperatures and low fuel crossover [3]. Atofina has been working on developing a new class of non-perfluorinated polymer electrolyte membranes.

Results and Discussion

As it is increasingly reported, it is possible to control the phase morphology of polymer composites thin films to achieve a unique set of properties [4,5]. Thus, our approach based on a composite polymer structure between a fluoropolymer -Kynar® polyvinylidene fluoride, PVDF - and a proprietary non-perfluorinated polyelectrolyte, enabled us to markedly improve the mechanical properties, fuel crossover resistance and thermal stability compared to PFSI, while meeting the low cost target required by the industry. In this work, Nafion® 112 membrane was used as the commercial PFSI membrane control in all experiments. Mechanical and swelling properties of these membranes - ranging from 17 to 50µm - match or exceed those of the control. At 25 µm thick, the PVDF-based membrane shows superior tear resistance compared to the 50µm control. The inherent strength of the PVDF-based membranes is further demonstrated by comparing axial creep resistance. Figure 1 depicts the gradual linear elongation at 80°C and 120 °C. While the control exhibits relatively large continual deformation with time, the developmental membrane exhibits almost no creep under the same conditions, even at 120°C.

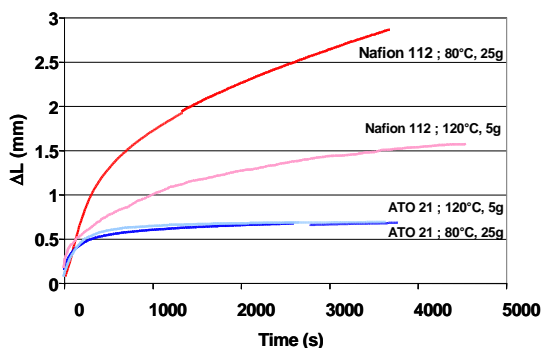


Figure 1. Axial creep data of ATO21 and PFSI membranes at 80°C/25g load and 120°C/5 g load.

A comparison of the electrochemical properties for the PVDF-based membranes and a commercial membrane is shown in Figure 2, where all membrane electrode assemblies (MEAs) were prepared by hot pressing ELAT® electrodes

with a Pt loading of 0.4 mg/cm² onto the membrane. Resistance values were measured using the current interrupt method. As one can see, the polarization curve of the MEA based on ATO 31C (in blue) is essentially superimposable to the control.

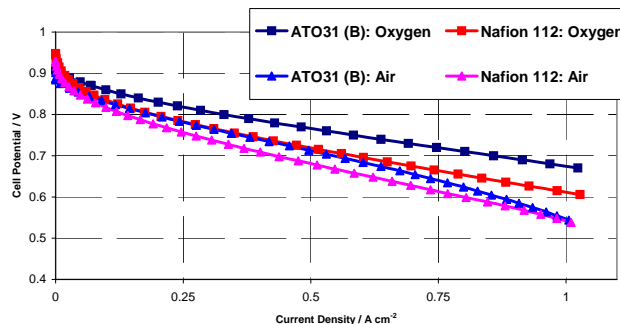


Figure 2. Polarization curve. T= 60°C, 100% RH, 1 atm.

Furthermore, Figure 3 shows two single-cell runs using ATO27 and ATO31 developmental membranes. Over the 1000 h period showed in this figure, the voltage loss was similar in magnitude to the 20% loss reported by Roelofs *et al.* for a commercial PFSI membrane after 600 hours [6]. Increased stability and overall fuel cell performance during long-term usage may be enhanced with the development of MEAs specifically tailored for our PVDF-based membranes, in particular through optimization of the electrode-membrane interface.

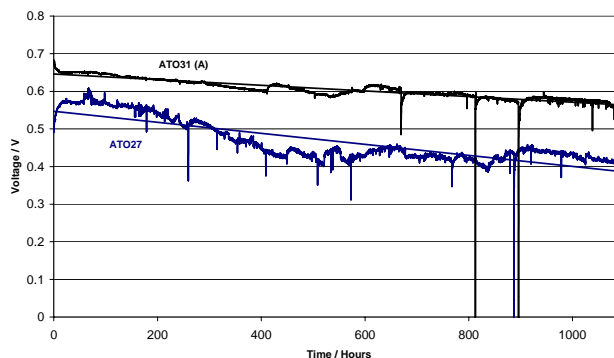


Figure 3. Endurance test. T= 60°C, 100% RH, 1 atm, H₂/O₂

Conclusions

A unique polymer electrolyte membrane technology has been developed based on alloys of Kynar® PVDF with a proprietary polyelectrolyte. Polarization curves for the 25 µm PVDF-based membranes show similar electrical performance than Nafion® 112 membranes. While optimization of the electrode-membrane interface is expected to yield further improved fuel cell performance, long-term durability testing for these PVDF-based membranes has been demonstrated well over 1500 hours. This new technology has already demonstrated the ability to produce membranes with good physical properties, good electrical properties, and a process that is flexible and easily scaled up.

References

- (1) Wheeler, D. J. *J. New Mat. Electrochem. Systems* **2001**, 4, 233
- (2) Ralph, T.; Hogarth, M. P. *Platinum Metals Rev.* **2002**, 46 (1), 3
- (3) Kerres, J. A. *J. Membrane Science* **2001**, 185, 3-27
- (4) Wang, H. ; Composto, R.J. *Europhys. Lett.* **2000**, 50, 622
- (5) Newby Z.; Composto R. J. *Macromolecules* **2000**, 33, 3274
- (6) Roelofs, M.; Reichert, D.; Kourtakis, K. *Fuel Cell Seminar* **2002**.

DIRECT SYNTHESIS OF DISULFONATED POLY(ARYLENE ETHER KETONE)S AND INVESTIGATION OF THEIR BEHAVIOR AS PROTON EXCHANGE MEMBRANE (PEM)

Yanxiang Li, Thekkekara Mukundan, William Harrison, Melinda Hill, Mehmet Sankir, Juan Yang, and James E. McGrath

Department of Chemistry and Materials Research Institute, Virginia Tech, Blacksburg, VA 24061

Introduction

Sulfonated poly(arylene ether ketone)s are promising candidates for proton exchange membranes in fuel cells. These materials have excellent physical properties, including high modulus, toughness, and good thermal and chemical resistance [1]. The method of direct polymerization of sulfonated comonomers has been proven to be better than the post sulfonation method, in that it can control the degree of sulfonation and avoid several side reactions [2, 3]. In this research, two sulfonated ketone type comonomers were synthesized. These comonomers were subjected to nucleophilic aromatic substitution step copolymerization with the unsulfonated monomers and 4, 4'-hexafluoroisopropylidenediphenol (6F-BPA) to obtain two kinds of copolymers containing sodium sulfonated groups. The copolymers were characterized by various methods, and their typical properties as PEM, such as IEC and water uptake, were investigated.

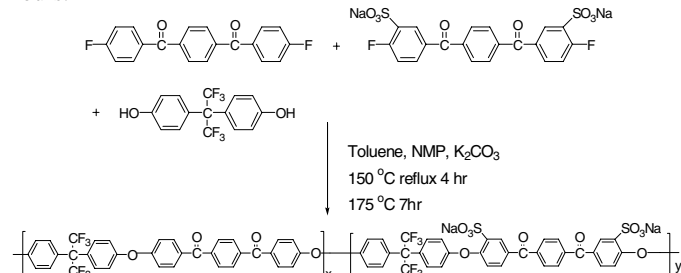
Experimental

Materials. 4, 4'-hexafluoroisopropylidenediphenol (6F-BPA), received from Ciba, was purified by sublimation and dried in vacuo. The ketone type monomers: 4, 4'-difluorobenzophenone (DFBP), and 1, 4-Bis (p-fluorobenzoyl) benzene (PBFB) were purchased from Aldrich and used as received, but all monomers were dried under vacuum prior to use. N- Methyl-2-pyrrolidinone (NMP; Fisher) was vacuum-distilled from calcium hydride onto molecular sieves in vacuo and then stored under nitrogen. N, N-dimethylacetamide (DMAC; Fisher) was used as received. Toluene, sodium chloride, and 30% fuming sulfuric acid were obtained from Aldrich and used as received. Potassium carbonate was vacuum dried before polymerization.

Synthesis of the disodium salt of comonomers. Sulfonated derivatized comonomers (SDFBP, SPBFB) were synthesized according to a modified literature method [2, 4]. A typical procedure was as follows: PBFB (30g) was dissolved in 60 mL of 30% fuming sulfuric acid in a 100mL, three necked flask equipped with a mechanical stirrer and a nitrogen inlet/outlet. The solution was heated to 150 °C for 6 hours to produce a homogeneous solution. Then it was cooled to room temperature, and poured into 450mL of ice-water. Next, 110.0g of NaCl was added which produced a white solid. The latter was filtered and re-dissolved in 300mL of deionized water. The solution was treated with 2N NaOH aqueous solution to a pH of 6~7 and diluted with deionized water to 500mL. Then, 110.0g NaCl was added to salt out the sodium form sulfonated monomer. The crude product was recrystallized twice from a mixture of isopropyl alcohol and deionized water (3/1 in volume). The anticipated structure was obtained at around 85% yields.

Polymerization. The copolymerization procedures for all ketone monomers were similar. A typical polymerization for PBFB-30 is described as follows: 3.3623 (10 mmol) 6F BPA, 2.2562 (7 mmol) PBFB, and 1.5792 (3 mmol) SPBFB were added to a 3-neck flask equipped with mechanical stirrer, nitrogen inlet and a Dean Stark trap. Next, 1.15 equivalent of potassium carbonate and NMP were introduced to afford a 33% solids concentration. Toluene (NMP/Toluene=3/4, v/v) was used as an azeotropic agent. The

reaction mixture was heated under reflux at 150 °C for 4 hours to remove most of the toluene and dehydrate the system. Next, the temperature was raised slowly to 175 °C. The solution became viscous after about 7 hours and was subsequently cooled to room temperature and diluted with NMP. The solution product was then isolated by addition to stirred deionized water. The precipitated fibrous copolymer was heated around 50 °C in deionized water overnight. Then it was filtered and vacuum dried at 120 °C for 24 hours.



Scheme 1. Synthesis of PBFB copolymer

Membrane preparation. Copolymer 1.0g was dissolved in 20mL of DMAC. The solutions were first filtered with 0.45 μm syringe filters, and then cast onto clean glass substrates. The film was carefully dried with infrared heat at gradually increasing temperature (up to ~ 60 °C) under a nitrogen atmosphere. The sodium form membranes then were converted into the acid form by boiling in 2N H₂SO₄ for 2 hours, followed by boiling in deionized water for 2 hours. The acid form films were stored in fresh deionized water.

Characterization

FTIR spectra were measured with a Nicolet Impact 400 FT-IR spectrometer with thin homogenous cast films. ¹H NMR spectra were obtained with a Varian 400 MHz spectrometer using DMSO-d₆ as a solvent. Intrinsic viscosity (IV) measurements were obtained in NMP at 25 °C using a Cannon Ubbelohde viscometer. Number average molecular weights (M_n) of obtained copolymers were determined by gel permeation chromatography based on polystyrene standards. Membrane water uptake was determined by a simple weight difference approach: Films were vacuum dried at 85 °C for 40 hours, weighed and then immersed in deionized water at room temperature for 24 hours. The wet membranes were wiped dry and quickly weighed again. The ratio of weighed gain to initial film weight was expressed as % water uptake. IEC was measured by titration with 0.01 N NaOH standard solution.

Results and Discussion

SDFBP and SPBFB comonomers were synthesized successfully and characterized by ¹H NMR. Figure 1 is the representative ¹H NMR spectrum for SPBFB comonomer.

Two series of poly(arylene ether ketone) copolymers with high molecular weights were synthesized via step-condensation process as show in Table 1 and Table 2. Copolymers with 0-50 mole % sulfonated comonomer contents were prepared. M_n and Intrinsic viscosity values correlated well. Calculated ion exchange capacity (IEC) and experimental results were shown. FTIR and ¹H NMR spectra were used to identify and characterize the two series of sulfonated copolymers. The degree of sulfonation determined by NMR is using the method in reference [3]. Figure 3 shows that in FTIR spectra with increasing of the sulfonation degree, the peak intensity at 1030 cm⁻¹ and 1087 cm⁻¹ will increase accordingly. Peaks

at 1030 cm^{-1} and 1087 cm^{-1} correspond to symmetric and asymmetric stretching of the sodium sulfonate groups. The IR spectra can thus qualitatively determine the functional groups of the synthesized copolymers.

The influence of sulfonated comonomer content on water uptake of copolymer membranes in the acid form is depicted in Figure 2. The copolymers synthesized using the SPBFB comonomer showed lower uptakes of water relative to the copolymers made with SDFBP comonomer at the same degree of sulfonation. This may be because the structure of PBFB copolymer is more rigid than the structure of DFBP copolymer and the space between sulfonic acid groups in PBFB copolymer is larger than that in DFBP copolymer.

Table 1. Copolymer Characterization at Different Degree of Sulfonation for DFBP/SDFBP Series

Polymer	Degree of Sulfonation by NMR	$[\eta]_{25}^{\circ\text{C}}$ (dl/g)	M_n	IEC(meq/g)	
				Cal.	Exp.
DFBP-00	0	1.48	148,459	0	0
DFBP-10	9	1.03	76,275	0.36	0.13
DFBP-20	18	0.92	46,901	0.72	0.55
DFBP-30	29	1.00	47,306	1.05	0.94
DFBP-40	40	1.44	59,620	1.38	1.12
DFBP-50	47	0.69	32,580	1.70	1.35

Table 2. Copolymer Characterization at Different Degree of Sulfonation for PBFB/SPBFB Series

Polymer	Degree of Sulfonation by NMR	$[\eta]_{25}^{\circ\text{C}}$ (dl/g)	M_n	IEC(meq/g)	
				Cal.	Exp.
PBFB-00	0	0.41	39,687	0	0
PBFB-20	22	2.15	89,784	0.62	0.43
PBFB-30	29	1.00	55,630	0.90	0.74
PBFB-40	40	1.00	51,077	1.17	0.87
PBFB-50	48	3.30	134,777	1.43	1.15

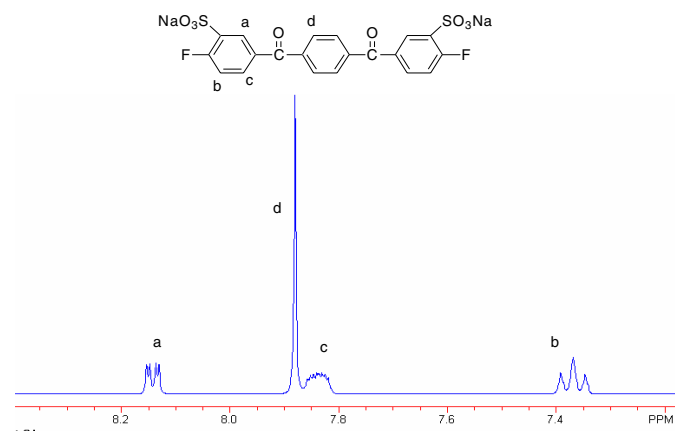


Figure 1. ^1H NMR spectrum of SPBFB monomer

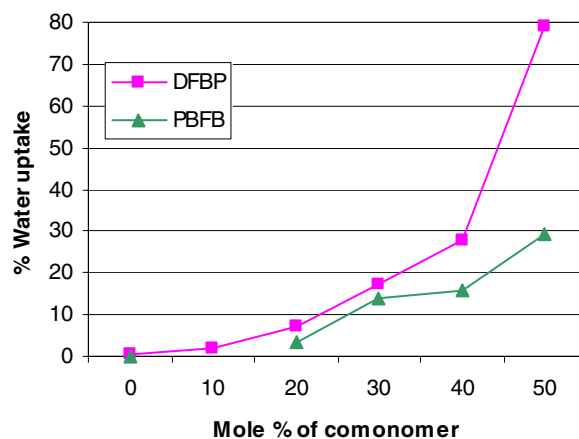


Figure 2. Water uptakes of copolymer membranes

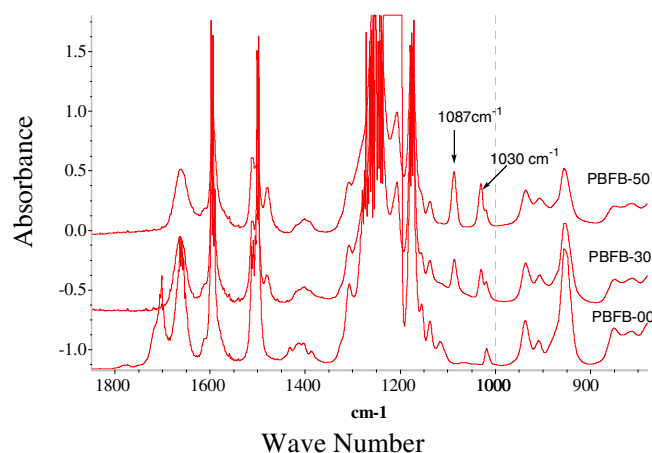


Figure 3. Influence of the degree of sulfonation on the FTIR spectra of PBFB/SPBFB series copolymers

Conclusions

Two sulfonated ketone type comonomers were successfully synthesized, and copolymerized to synthesize poly(arylene ether ketone) copolymers with sulfonation degree from 0 to 50%. PBFB series copolymers showed lower water uptakes relative to DFBP series at the same degree of sulfonation because of the more rigid structure of PBFB copolymer. Further discussion of their properties will be described at the meeting.

Acknowledgement. The authors would like to thank the Department of Energy (contract # DE-FC36-01G011086)

References

- (1) J. I. Kroschwitz, Ed; *Encyclopedia of Polymer Science and Engineering*, **1988**, Vol. 12, 313
- (2) Shengzhou Liu, Feng Wang, Tianlu Chen; *Macromol. Rapid Commun.* **2001**, 22, No.8, 579
- (3) William L. Harrison, Feng Wang, Jeffery B. Mecham, Vinayak A. Bhanu, Melinda Hill, Yu Seung Kim, James E. McGrath; *Journal of Polymer science: Part a: Polymer Chemistry*, **2003**, Vol. 41, 2264
- (4) Feng Wang, Jianke Li, Tianlu Chen, Jiping Xu; *Polymer*, **1999**, 40, 795

DISULFONATED POLY(ARYLENE ETHER PHENYL PHOSPHINE OXIDE SULFONE) TERPOLYMERS FOR PEM FUEL CELL SYSTEMS

Kenton B. Wiles, Cesar Munoz de Diego, James E. McGrath

Department of Chemistry and Materials Research Institute,
Macromolecular Science and Engineering Program
Virginia Polytechnic Institute and State University
Blacksburg, VA 24061

Introduction

Novel engineering systems based on proton exchange membrane (PEM) fuel cells as an alternate energy source is considered very attractive due to diminishing natural resources, global warming, acid rain and smog producing precursors associated with combustion energy processes. PEM fuel cells produce electrical energy from electrochemical reactions by delivering fuel (H_2) to the anode and an oxidizer (O_2) to the cathode. Limitations of the fuel cell include usable temperature ranges, hydrogen storage, fuel efficiency and cost. Polymer electrolyte membrane fuel cells are limited by the liquid water temperature range. The hydrogen ions are transported across the membranes in an aqueous environment and thus above the boiling point of water, the mechanism becomes severely limited. Temperatures above 100 °C would decrease platinum poisoning by carbon monoxide and would increase reaction kinetics.

PEMs based on Nafion[®] are limited to membrane performance below 80 °C presumably due to a thermal transition of the hydrated form and loss of water, dehydration. A novel approach¹ could involve the use of heteropolyacids (HPA) as an additive for compatible sulfonated hydrocarbon polymers. Many HPAs have high protonic conductivities but are also water-soluble. HPA composite membranes based on polymers that have a high affinity for the HPA additive can, in principle, make the HPA complex insoluble in water while still retaining high protonic conductivity at elevated temperatures.

Phosphine oxide containing polymers based on poly(arylene ether)s and poly(arylene thioether)s have been reported to be stable at high temperatures while being flame retardant and plasma resistant.² Generally these high performance polymers are used as flame retardant materials that also complex with certain metals to help in dispersion and retention of inorganic/organic additives.³ Furthermore, reports on phosphine oxide containing poly(arylene ether)s that have good interactions with a wide variety of thermoplastics and thermosets like phenoxy, epoxy and vinylester resins has recently been described.⁴ It has been proposed that these phosphine oxide containing materials could have an increased interaction with functionalized carbon fibers, glass fibers or inorganic additives due to the very polar phosphine oxide moieties. Synthetic procedures to produce phosphine oxide containing polymers have mainly incorporated 4,4'-bis(fluorophenyl) phenyl phosphine oxide (BFPPO), as the electrophile and bisphenols or thiobisphenols as the nucleophilic containing monomers.

By dissolving inorganic heteropolyacids in a dipolar solvent and blending the solution with dissolved ionic polymeric materials, composite membranes that aid in protonic conductivity at high temperatures can be solution cast. The HPAs, in the crystalline form, used in this type of research are protonically conductive inorganic fillers that may have a strong interaction with specific functional groups in the polymeric material. It has been hypothesized that the HPA in PEMs give alternative mechanisms to proton transport at temperatures above 100°C where very little water is

present. Composite membranes based on phosphotungstic acid have recently been shown to have higher conductivities and lower water swelling at elevated temperatures as compared to the pure copolymer membranes. Therefore, the present research employs phosphotungstic acid hydrate as an inorganic filler incorporated into 45 mol% disulfonated poly(arylene phenyl phosphine oxide ether sulfone) terpolymers synthesized using nucleophilic aromatic substitution reactions (Figure 1) for use in PEM fuel cells at temperatures above 100°C. Figure 2 indicates the possible interactions present in the 45mol% disulfonated PPO/HPA composite films that retain the water-soluble HPA molecules in the organic soluble PEM. These interactions aid in decreasing extraction of the HPA in aqueous environments, thereby allowing very little, if any, leaching of the ionically conducting HPA.

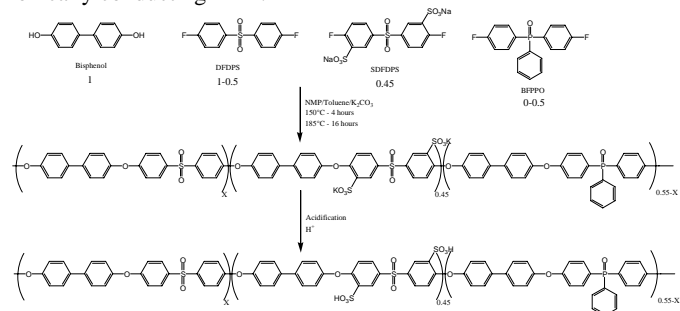


Figure 1. Synthesis of disulfonated poly(arylene phenyl phosphineoxide ether sulfone) terpolymers

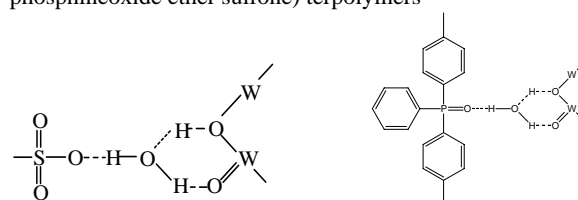


Figure 2. Possible interactions of HPA with sulfonates and phosphine oxide moieties

Experimental

Materials. 4,4'- bis(fluorophenyl) phenyl phosphine oxide (BFPPO) was synthesized using a reported procedure.⁵ Anhydrous potassium carbonate and 4, 4' - difluorodiphenylsulfone (DFDPS) were obtained from Aldrich. NMP and toluene (both from Burdick and Jackson) were dried as follows: NMP was dried overnight over calcium hydride with a nitrogen purge and distilled at reduced pressure; toluene was dried over molecular sieves. Disulfonation of DFDPS was performed in a similar fashion as previously described.⁶ Phosphotungstic acid hydrate was obtained from Fluka Chemika and dried at 80°C for 24 hours before use.

Films and Composite Membranes. Neat films of the copolymers were cast from 5 weight% solution in DMAc in a glass casting tray and carefully dried in a vacuum oven. The salt form films were then transformed into the acid form by boiling the films in 0.5M H_2SO_4 for 2 hours to convert the pendant sulfonic salt groups into free acid groups. The residual sulfuric acid was removed by boiling the films in deionized water for 2 hours. The composite membranes were obtained by dissolving both the acid form membranes and 30 weight percent HPA in DMAc in separate containers. The solutions were combined and allowed to mix by stirring for 24 hours. The solution was then cast onto glass casting trays and dried in a vacuum oven. Reacidification was performed by either a room temperature method (M1) or a high temperature boiling

method (M2).⁷ HPA extraction was measured by the difference in weight before and after reacidification of the composite membranes. The room temperature method (M1 = method 1) acidified the films using 1.5 M H₂SO₄ in water for 24 hours. The residual H₂SO₄ was removed by immersing the films in D. I. water for an additional 24 hours. The boiling method (M2 = method 2) acidified the films using 0.5 M H₂SO₄ in water at boiling conditions and then removing the residual acid by boiling in water for an additional 2 hours.

Characterization. Membrane water uptake was determined by a weight difference approach as described previously. Proton conductivity of the membranes under fully and partially hydrated conditions was determined at 120°C using a Solatron 1260 Impedance/Gain-Phase Analyzer over the frequency range of 10Hz-1 MHz following the reported procedure.⁸ The resistance of the films was taken at the frequency that produced the minimum imaginary response. The conductivity of the membranes was calculated from the measured resistance and the geometry of the cell.

Results and Discussion

Terpolymerizations produced terpolymers with high intrinsic viscosity values ranging from 1.0 to 1.2 dL/g in NMP at 30°C. Successful incorporation of various mole percents of phenyl phosphine oxide (PPO) moieties into the 45mol% disulfonated control poly(arylene ether sulfone) copolymer (BPSH 45) was monitored by FTIR of thin films and ¹H NMR of 5wt% solutions in DMSO-d₆. Water uptake measurements of the neat terpolymers are plotted in **Figure 3**.

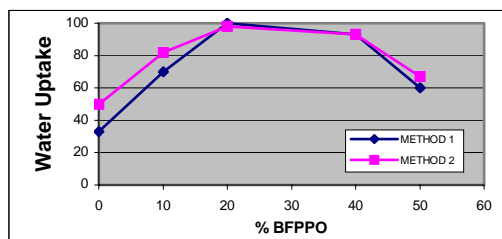


Figure 3. Water uptake measurements of neat terpolymers

Successful incorporation and complex formation of the HPA additive with phosphine oxide moieties were monitored by FTIR and ³¹P NMR. FTIR indicated significant band shifting for both the sulfonate and phosphine oxide groups when HPA was incorporated. ³¹P NMR showed a considerable shift of the phosphorous peak when HPA was incorporated into the entire series of terpolymers. Both of these sets of data suggest strong interactions of the HPA additive with the phosphine oxide moieties. Water uptake and extraction of the composite membranes are shown in **Figure 4** and **Figure 5**.

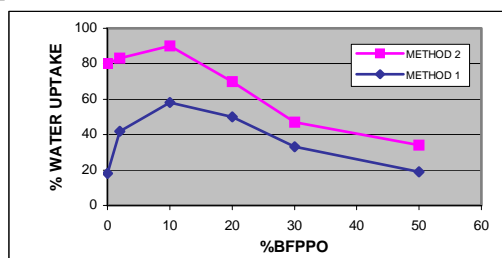


Figure 4. Water uptake of 30wt% HPA composite membranes for Method 1 and Method 2 reacidification techniques

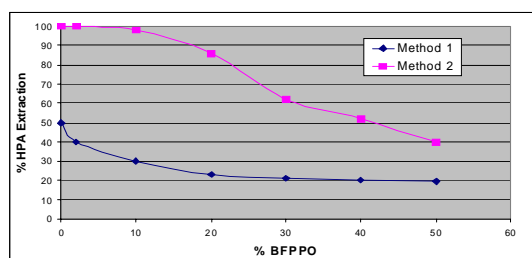


Figure 5. Extraction of HPA additive in 30wt% HPA composite membranes

Table 1 indicates the protonic conductivity and water sorption of both the neat polymers and the composite polymers with reference to the control BPSH 45 copolymer containing no PPO moieties. The selected PPO containing terpolymers indicate that with increasing phenyl phosphine oxide moieties, the conductivity decreases. This is presumably due to the strong interactions of the PPO with the sulfonate moieties. However, when HPA was incorporated, the conductivity increased at high temperatures and water sorption decreased. One might suggest that the strongly interacting nature of the terpolymer functional groups with the surface functionality of the HPA promotes this observation.

Table 1. Conductivity at 120°C and 45% R.H. and water uptake of neat and composite membranes as compared to 45mol% copolymer control containing no PPO moieties

Membrane	Conductivity M2 (mS/cm) Neat Polymer	% H ₂ O Uptake of Neat Polymer	Conductivity M1 (mS/cm) With 30wt%HPA	%H ₂ O Uptake of Composite M1
BPSH 45	11	50	14	35
10% PPO	9	80	21	58
20%PPO	3.3	95	20	50
30%PPO	3.1	90	15	35
40%PPO	3	88	10	28
50%PPO	2.9	65	7	20

Conclusions

Water sorption measurements indicated lower water sorption was possible in the terpolymer composite films relative to the neat film. Extraction of the HPA filler was found to be minimal for the acidification at room temperature while the acidification at boiling temperatures increased the extraction up to a factor of four. The high temperature/low humidity conductivity measurements indicated increased performance by incorporating HPA into the disulfonated terpolymer membranes using the room temperature reacidification technique.

Acknowledgments. The authors would like to thank Department of Energy for funding under contract sub-56844-FMIJOBDOE-99241.

References

- Kim, Y.S., Wang, F., Hickner, M., Zawodzinski, T. A. and McGrath, J. E. *J. Membrane Sci.*, 2003, 212, 263-282.
- Riley, D.J.; Gungor, A.; Srinivasan, S.A.; Sankarapandian, M.; Tchatchoua, C.; Muggli, M.W.; Ward, T.C. and McGrath, J.E., *Polym Eng. Sci.*, 1997, 37(9), 1501.
- Smith, C.D.; Grubbs, H.J.; Webster, H.F.; Gungor, A.; Wightman, J.P. and McGrath, J.E., *High Perform. Polym.*, 1991, 4, 211.
- Kosmala, B.; Schauer, J. *J. Appl. Polym. Sci.*, 2002, 85, 1118.
- Riley, D. J., *PhD. Dissertation*, VPI & SU, 1997.
- Wiles, K. B.; Munoz, C. M. and McGrath, J. E. *Polymer Preprints*, 2004, 45(1), 724.

⁷ Kim, Y. S.; Wang, F.; McCartney, S.; Hong, Y. T.; Harrison, W.; Zawodzinski, T. and McGrath, J. E. *J. Polym. Sci.; Part B: Poly. Phys.* **2003**, 41, 2816.

⁸ Zawodzinski, T.; Neeman, M.; Sillerud, L. O. and Gottesfeld, S. *J. Phys. Chem.* **1991**, 95, 6040.

MORPHOLOGY CONTROL OF POLY(PHENYLENE OXIDE) BY IONOMERIC POLY(STYRENESULFONIC ACID SODIUM SALT) COPOLYMERS FOR FUEL CELL MEMBRANE

Sung-Guk An, Jung-Kyu Woo, and Chang Gi Cho

Dept. of Fiber & Polymer Engineering
Hanyang University
Seoul 133-791, Korea

Abstract : Well-defined block copolymers of poly(styrene-*b*-styrenesulfonic acid sodium salt) were synthesized via living radical polymerization. Blends of various compositions of block copolymer/polyphenylene oxide were prepared, and their properties for proton exchange membrane were studied. Blend film showed well-defined two phase morphology. The molecular architecture of the block copolymer and the content of the block copolymer in the blend were important factors in controlling the properties of the film for proton exchange membrane. Also graft copolymers of poly(phenylene oxide-*g*-styrenesulfonic acid sodium salt) were prepared and their properties for proton exchange membrane were studied.

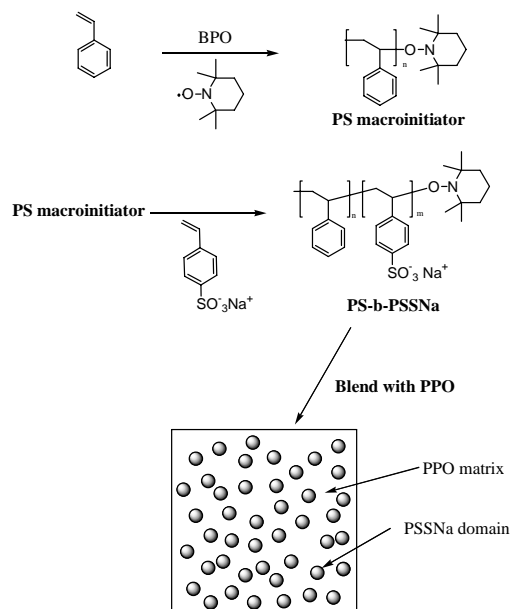
Introduction

Proton exchange membrane (PEM) is a key component in solid polymer electrolyte fuel cells [1]. Generally, proton exchange membrane (PEM) contains cationic exchange groups such as SO_3^- group. For PEM materials, poly(styrene sulfonic acid) (PSSA) and its copolymers have been widely studied because of their synthetic easiness and higher conductivities [2], and many studies utilized PSSA in the forms of random copolymers, block or graft copolymers. But poor physical properties of PSSA such as brittleness and relatively low T_g , discouraged many researcher from studying PSSA compared to engineering plastics (EP) such as polyimide, polysulfone, polyketone, and poly(2,6-dimethyl-1,4-phenylene oxide) (MPPO), etc. as possible PEM materials. Blends of these EP polymers with PSSA look desirable but they have been rarely studied because of poor miscibility of the ionomer in hydrophobic EP. In this work, poly(styrenesulfonic acid sodium salt) (PSSNa) was converted to PS-*b*-PSSNa block copolymers and MPPO-*g*-PSSNa graft copolymers. The block copolymers were blended with MPPO because of its good mechanical, chemical, and thermal properties. PEM performance of the blends and graft copolymers were studied.

Experimental

Synthesis of polystyrene-*b*-poly(styrene sulfonic acid) sodium salt (PS-*b*-PSSNa). Preparation of block copolymer and polymer blending are shown as in the Scheme 1. TEMPO terminated polystyrene macroinitiators were synthesized by reported method. For the block copolymerization, a 100 mL round bottom flask equipped with a reflux condenser was charge with styrenesulfonic acid (SSNa) and macroinitiator in DMAc. The flask was purged with high purity N_2 gas for 30 minute, and polymerization was conducted for 6 h at 125°C. The polymerization solution was cooled to room temperature and precipitated into 60/40 ether/methanol mixture. Precipitate was collected by filtration and dried in air. The product was washed with hot water in order to remove any possible homopolymerized SSNa, then PS-*b*-PSSNa was obtained by drying under vacuum. For the preparation of a blend membrane, MPPO and

PS-*b*-PSSNa were dissolved in NMP. The polymer solution was casted on glass plate and solvent was evaporated slowly in vacuum at 100°C. Acid treatment of the membrane was followed for proton conductivity measurement.



Scheme 1. Synthesis of PS-*b*-PSSNa and membrane preparation from polymer blend

Results and Discussion

The PS macroinitiator and block copolymers were characterized by GPC and $^1\text{H-NMR}$. Figure 1 shows the NMR spectra of the PS macroinitiator and block copolymer. TEMPO terminated macromer shows NMR spectrum of a typical polystyrene, and the block copolymer shows a new peak at 7.5 ppm originated from aromatic resonance absorption of PSSNa. The absorption peak at ca. 3 ppm of PS-*b*-PSSNa is originated from NMR solvent. The molecular weight of PS-*b*-PSSNa was characterized by FT-IR spectra as reported by other workers [2] (Figure 2) as well as by titration. Molecular weight determined by titration agreed well with that of theoretical, and agreed reasonably well with that by IR.

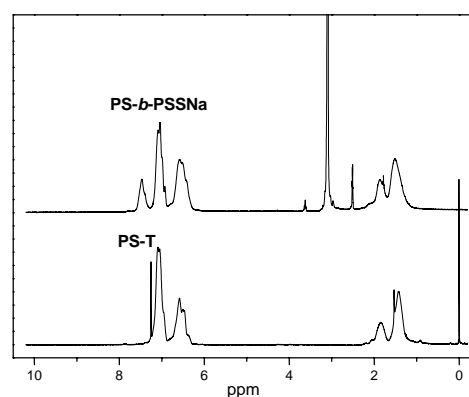


Figure 1. $^1\text{H-NMR}$ spectra of macroinitiator and block copolymer

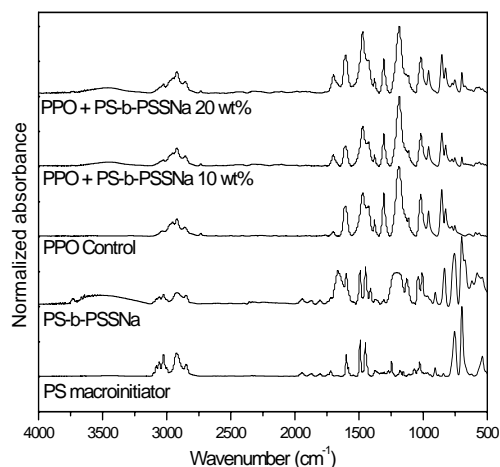


Figure 2. FT-IR spectra of blends and synthesized copolymers

Morphology of polymer films obtained from the blend was examined by atomic force microscopy (AFM). As in the **Figure 3** two phase morphology was developed well for the blend containing 20wt% block copolymer, and the size of dispersed domain is less than 100 nm. Proton conductivity, water uptake, and methanol permeability were measured, and these values showed good relationship with the wt% and the molecular weight of the block copolymer in the blends. Proton conductivity of the blends increased with the content of block copolymers. Some membranes showed high proton conductivities quite comparable to Nafion film. For a blend containing 50wt% of PS-PSSNa with molecular weight of 10K-5K, proton conductivity value of 5.27×10^{-2} S/cm was obtained. When the molecular weight of the block changed to 10K-10K, conductivity value changed to 1.24×10^{-2} S/cm. Detailed phase behavior and conductivity data will be presented.

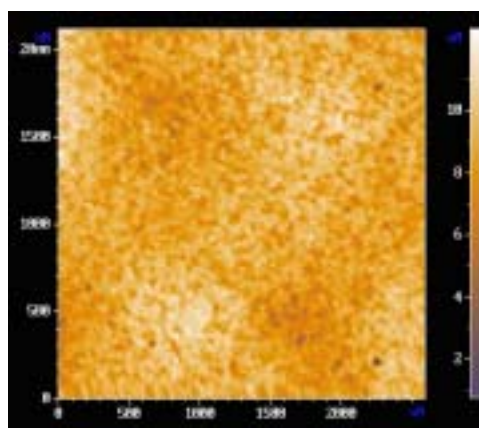


Figure 3. Atomic Force Microscopy of blend

Conclusions

Well-defined block copolymer was synthesized via stable free radical polymerization (SFRP) by using TEMPO. Blends of various compositions of block copolymer/MPPO were prepared, and their properties for proton exchange membrane were characterized. Blend

film showed well-defined two phase morphology. The molecular architecture of the block copolymer and the content of the block copolymer in the blend are important factors in controlling the properties of the film for proton exchange membrane.

Acknowledgment

This work was supported by Korea Research Foundation Grant (KRF-2003-41-D00207).

References

1. Appleby, A.J; Foulkes, R.L. Fuel Cell Handbook, Van Nostrand, New York, **1989**.
2. Ding, J; Chuy, C; Holdcroft, S. *Macromolecules* **2002**, 35, 1348.

SYNTHESIS AND CHARACTERIZATION OF SULFONATED POLY(ARYLENE ETHER SULFONE)/ZIRCONIUM PHENYLPHOSPHONATE COMPOSITE MEMBRANES FOR PROTON EXCHANGE MEMBRANE FUEL CELL APPLICATIONS

Melinda L. Hill¹, Brian R. Einsla¹, Yu Seung Kim², and James E. McGrath¹

¹Department of Chemistry and Institute for Polymeric Materials and Interfaces, Virginia Polytechnic Institute and State University, Blacksburg, VA 24061

²Los Alamos National Laboratory
Los Alamos, NM 87545

Email: jmcgrath@vt.edu

Introduction

High temperature hydrogen and methanol based fuel cells are of increasing interest due to environmental concerns and of the availability of fossil fuels. The proton exchange membrane (PEM), a protonically conductive polymer film, is an integral component of the fuel cell. New polymer materials are needed for these membranes because of the high cost and low conductivity at high temperatures (> 80°C) of the membranes currently in use. Sulfonated poly(arylene ether sulfone)s have good potential for use in fuel cells because of their excellent thermal stability, moderate water sorption, and sufficient conductivity at high temperatures. Addition of inorganic components to these membranes may enhance the high-temperature performance as well as other important properties of the membranes, such as water sorption.^{1,2} The *in-situ* formation of inorganic components results in small particle size and preservation of original membrane morphology.³ Herein we present the synthesis and characterization of disulfonated poly(arylene ether sulfone)/zirconium phenylphosphonate *in-situ* composite membranes for use as proton exchange membranes.

Experimental

Materials. The synthesis of the disulfonated poly(arylene ether sulfone)s with 35 mole % disulfonated moiety (BPSH-35) used for this work has been previously reported.⁴ The random copolymer structure is shown in Figure 1. Zirconyl chloride (30% solution in hydrochloric acid) and phenylphosphonic acid were obtained from Aldrich as used as received. HPLC-grade methanol was obtained from EMD Chemicals and used without further purification. Platinum-ruthenium and platinum black were used as received from Johnson-Matthey, and 5 wt. % Nafion dispersion with an equivalent weight of 1100 was obtained from Solution Technologies.

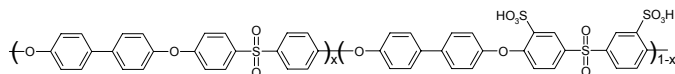


Figure 1. Structure of BPSH-35.

Synthesis of Composite Membranes. Copolymer membranes in the acid form were boiled in deionized water for one hour before use. The membranes were then immersed in zirconyl chloride solution at 80 °C (the concentration of the zirconyl chloride and the soaking time were varied). Upon removal from the zirconyl chloride solution, the membranes were briefly rinsed with deionized water and immersed in 0.2 M phenylphosphonic acid for 24 hours at room temperature. Finally, the membranes were thoroughly rinsed with deionized water and dried in a vacuum oven at 110 °C.

Characterization. The amount of zirconium phenylphosphonate (ZrPP) in the membranes was determined by weight difference after drying as follows: $(W_c - W_p)/W_c \times 100$ where W_c and W_p refer to the dry weights of the composite membrane and the pure copolymer membrane, respectively. The water uptakes of membranes are reported in weight percent as follows: $\text{water uptake} = (W_{\text{wet}} - W_{\text{dry}}) / (W_{\text{dry}}) \times 100$ where W_{wet} and W_{dry} are the weight of the wet and dry membranes, respectively. Thermogravimetric analysis (TGA) of dried, thin-film samples (10-15 mg) was performed on a TA Instruments TGA Q500 in air with a heating rate of 10 °C/min. Proton conductivity measurements were performed on the acid form of the membrane using a Hewlett-Packard 4192 Impedance/Gain-Phase Analyzer. The resistance of the film was taken at the frequency that produced the minimum imaginary response. The conductivity of the membrane was calculated from the measured resistance and sample dimensions. Magic angle spinning (MAS) ³¹P NMR spectroscopy was obtained on a Bruker MSL 300 instrument. The spectra were obtained using 100-200 scans using a spinning rate of 6.0-6.5 kHz. Membrane-electrode assemblies (MEA's) were prepared by painting using a 5 wt. % Nafion dispersion, water, and catalyst (platinum-ruthenium on the anode and platinum black on the cathode). The catalyst loadings were approximately 10 mg/cm² on the anode and 6 mg/cm² on the cathode. Direct methanol fuel cell (DMFC) performance was measured using a Fuel Cell Technologies fuel cell test stand using a standard 5 cm² test cell with 0.5 M methanol and a cell temperature of 80 °C.

Results and Discussion

The incorporation of zirconium phenylphosphonate was found to be dependent on the soaking time in the zirconyl chloride solution. The dependence of soaking time on incorporation is shown in Figure 2 for a zirconyl chloride concentration of 5%. The concentration of the zirconyl chloride solution may also be varied, and it was found that at constant time, varying the concentration resulted in a similar trend as that shown in Figure 2.

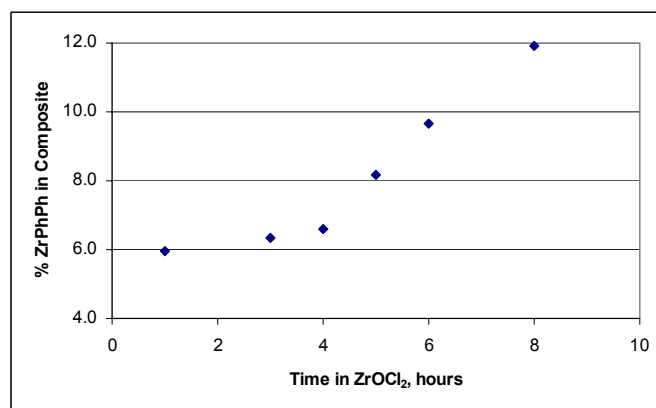


Figure 2. Incorporation versus soaking time in zirconyl chloride for a ZrOCl₂ concentration of 5%.

Solid-state ³¹P NMR was used to confirm the structure of the ZrPP in the membrane. The ³¹P NMR spectra of ZrPP and a BPSH-35/ZrPP composite membrane are compared in Figure 3.

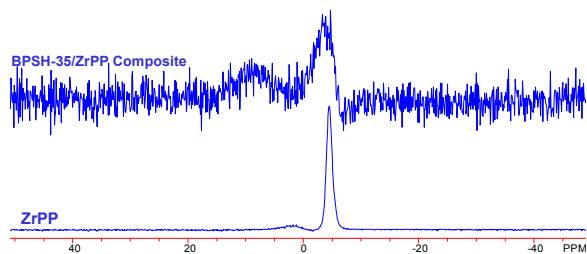


Figure 3. Solid-state ^{31}P NMR of BPSH-35/ZrPP composite and ZrPP powder.

The water uptake of the composite membranes was also studied as a function of ZrPP concentration at room temperature after three days of equilibration in liquid water. Figure 4 shows that the water uptake decreases with increasing ZrPP concentration.

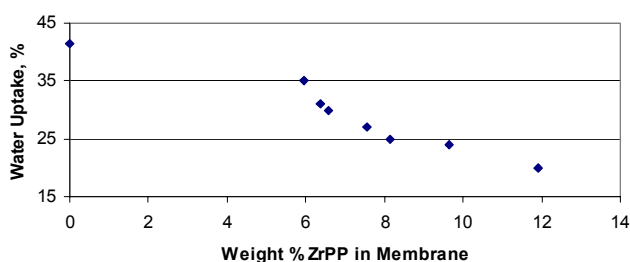


Figure 4. Water uptake as a function of ZrPP concentration in the composite membranes.

The TGA results in air at $10\text{ }^{\circ}\text{C}/\text{min}$ showed that the incorporation of ZrPP resulted in an increase in the decomposition temperature (T_d) and the char yield. These results are shown in Table 1.

Table 1. Thermal Behavior of BPSH-35/ZrPP Composites

	T_d , $^{\circ}\text{C}$	Char Yield at $800\text{ }^{\circ}\text{C}$, %
BPSH-35	304	1.5
BPSH-35/6.6% ZrPP	324	5.2
BPSH-35/7.6% ZrPP	348	7.3

Since this ZrPP additive is non-conductive, the proton conductivity of the composite membranes decreased with increasing ZrPP content, as shown in Figure 5.

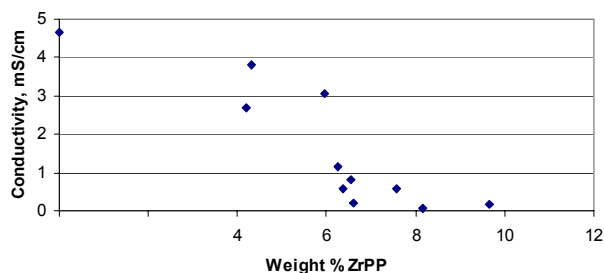


Figure 5. Proton conductivity of BPSH-35/ZrPP composite membranes.

The DMFC performance of several BPSH-35/ZrPP composites is shown in Figure 6. The composite membrane containing 3% of

ZrPP exhibits improved performance over pure BPSH-35. The thickness of the BPSH-35 and BPSH-35/ZrPP membranes was approximately 3 mil.

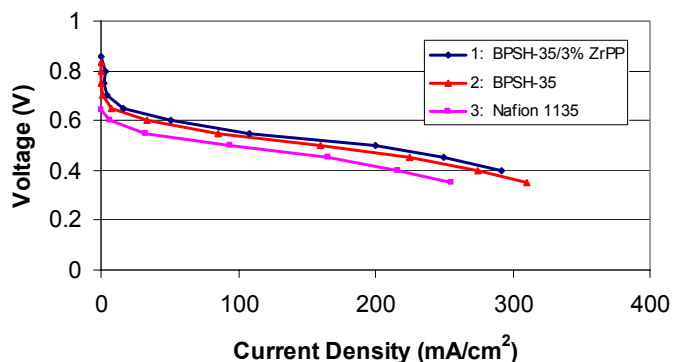


Figure 6. DMFC performance of virgin BPSH-35 and BPSH-35/ZrPP composite membranes.

Conclusions

Composite membranes of a disulfonated poly(arylene ether sulfone) and zirconium phenyl phosphonate were synthesized, and it was shown that the incorporation of the inorganic additive decreased the water uptake, although the conductivity decreased as well. The thermal stability, measured by TGA, was also improved after the ZrPP was added. The amount of ZrPP in the membrane can be controlled by varying the concentration of the zirconyl chloride solution and the amount of time the membrane is immersed in that solution. A composite membrane with 3% of ZrPP showed improved performance over pure BPSH-35 and Nafion 1135.

Future Research. The investigation of other additives, especially those exhibiting good proton conductivity, as well as blending with other polymer membranes is underway in cooperation with the research group of G. Alberti of the University of Perugia.⁵

Acknowledgement. The authors would like to thank the National Science Foundation "Partnership for Innovation" Program (HER-0090556) and the Department of Energy (DE-FC36-01G01086) for their support of this research effort.

References

- Yang, C.; Srinivasan, S.; Arico, A. S.; Creti, P.; and Baglio, V. *Electrochemical and Solid State Letters*, 2001, 4, A31.
- Zaidi, S. M. J.; Mickailenko, S. D.; Robertson, G. P.; Guiver, M. D.; Kaliaguine, S. *J. Membrane Sci.* **2000**, 173.
- Tchicaya-Bouckary, L.; Jones, D. J.; Roziere, J. *Fuel Cells* **2002**, 2, 40.
- Wang, F.; Hickner, M.; Kim, Y. S.; Zawodzinski, T. A.; and McGrath, J. E. *J. Mem. Sci.* **2002**, 197, 231.
- Alberti, G.; Casciola, M. *Annual Rev. Mater. Res.* **2003**, 33, 129.

SYNTHESIS OF SUBSTITUTED POLY(P-PHENYLENE)S BY NICKEL (0) CATALYZED COUPLING REACTION AND DERIVED MULTIBLOCK COPOLYMERS FOR PROTON EXCHANGE MEMBRANE FUEL CELLS

Hang Wang, William Harrison, Juan Yang, James E. McGrath

Department of Chemistry, Virginia Polytechnic Institute and State University, Blacksburg, VA 24061

Introduction

Poly(p-phenylene) (PPP) derivatives are a promising class of high-performance polymers because of their excellent thermal and mechanical properties. One main obstacle in synthesis of high molecular weight poly (1,4-phenylene) is the low solubility of the rigid-rod chains during polymerization. Lateral substituents afford substituted, high molecular weight PPPs with excellent solubility in polar, aprotic solvents¹.

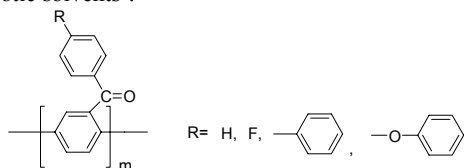


Figure 1. Structure of Poly(2,5-benzophenone) Derivatives

We have previously reported synthesis of poly(2,5-benzophenone) derivatives (shown in Figure 1) via nickel-catalyzed coupling polymerization of 4'-substituted 2,5-dichlorobenzophenones². These polymers were proven to be highly thermo-oxidative stable materials with good solubility and excellent mechanical properties. However, they do not form good films due to their extremely rigid rod-like chains. As an extension to our work, more flexible, film-forming, thermally stable terechelics, such as poly(arylene ether sulfone), poly(arylene ether ketone) oligomers were copolymerized with these PPPs to form multiblock copolymers which had both excellent thermo-oxidative stability and good film-forming ability.

Experimental

Materials. The synthesis of monomers via Friedel-Craft benzoylation of 1,4-dichlorobenzene has been previously reported³. N-methyl-2-pyrrolidone (NMP) were dried over calcium hydride, distilled under vacuum and stored under nitrogen before use. Triphenylphosphine (Aldrich) was recrystallized from Et₂O. Zn powder (Aldrich) was washed with acetic anhydride, filtered, washed with dry Et₂O, and dried under vacuum at 150°C. 2,2'-Bipyridine (BPY; Aldrich) and nickel (II) chloride (Aldrich) were used as received.

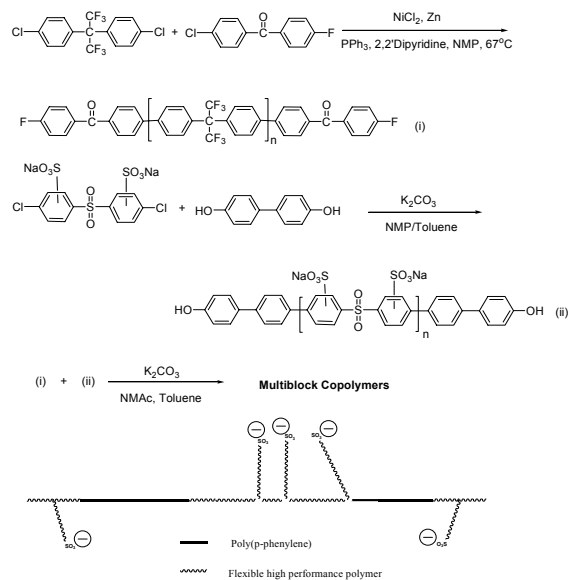
Polymerization. In a typical polymerization, a 100mL Schlenk flask was charged with NiCl₂, PPh₃, Zn, 2,2'-Bipyridine, monomer and a magnetic stir bar. The flask was sealed with a rubber septum, evacuated under flame for 10 minutes, and placed under an N₂ atmosphere by filling with N₂ followed by three evacuation-fill cycles. NMP (5mL) was added via syringe through the rubber septum. The mixture was stirred and heated at 67°C for 24 h. After cooling to room temperature, the reaction mixture was poured into 100mL methanol acidified with 25mL concentrated HCl. The resulting precipitate was collected by filtration and washed with 10% sodium bicarbonate solution (3 times) and deionized water (3 times).

After drying in a vacuum oven at 100°C overnight, the light yellow polymer was isolated and gave a yield of 85%.

The synthesis of hydroxyl terminated sulfonated poly (arylene ether sulfone) was same as reported earlier^{2c}.

Characterization

¹H-NMR experiments were performed using a Varian 400MHz instrument in deuterated chloroform. The intrinsic viscosity (IV) of the polymers was measured in NMP at 25°C using a Cannon Ubbelohde viscometer. Number average molecular weights (M_n) and molecular weight distributions (MWD) of polymers were determined by gel permeation chromatography based on polystyrene standards.



Scheme 1. Synthetic Scheme for Sulfonated Multiblock copolymers

Results and Discussion

As shown in Scheme 1, very rigid PPPs can be copolymerized with poly (arylene ether sulfone)s or poly(arylene ether ketone)s by nucleophilic aromatic reaction. Either the rigid PPP chains or relative soft poly (arylene ether sulfone)s or poly(arylene ether ketone)s can be sulfonated by directly polymerization of sulfonated monomers. In other words, PPP segments can either be a hydrophilic or hydrophobic phase. Besides, the degree of sulfonation can be controlled by varying composition of two macromolecules in the multiblock copolymers. We also expect that water uptake and conductivity of resulting multiblock copolymers can also be properly controlled.

Furthermore, since PPP molecules have extremely rigid chains and are reluctant to move, they may force some interesting morphology structures in the multiblock copolymers. The swelling properties and conductivity of the resulting membrane are expected to be greatly influenced by the morphology. The results will be discussing at the meeting.

Acknowledgements

The authors would like to thank the National Science Foundation "Partnership for Innovation" Program (HER-0090556) and the Department of Energy (DE-FC36-01G01086) for support of this research effort.

References

- ¹ (a) Schluter, A. D. *J Polym. Sci Part A: Polym Chem* 2001, 39, 1533-1556; (b) Phillips, R. W.; Sheares, V. V.; Samulski, E. T.; DeSimone, J. M. *Macromolecules* 1994, 27, 2354-2356; (c) Wang, Y.; Quirk, R. P. *Macromolecules* 1995, 28, 3495-3501; (d) Percec, V. Zhao, M.; Bae, J.; Hill, D. *Macromolecules* 1996, 29, 3727-3735; (e) Bloom, P. D.; Sheares, V. V. *J Polym. Sci Part A: Polym Chem* 2001, 39, 3505-3512
- ² (a) Ghassemi, H.; McGrath, J. E. *Polymer* 2004, accepted; (b) Ghassemi, H.; Ndip, G.; McGrath, J. E. *Polymer* 2004, accepted. (c) Ghassemi, H.; Harrison, W.; Zawodzinski, T. A., Jr.; McGrath, J. E. *Polymer Preprints* (American Chemical Society, Division of Polymer Chemistry) (2004), 45(1), 68-69; (d) Ghassemi, H.; Ndip, G.; McGrath, J. E. *Polymer Preprints* (American Chemical Society, Division of Polymer Chemistry) (2003), 44(1), 814-815.
- ³ Wang, Y.; Quirk, R. P. *Macromolecules* 1995, 28, 3495-3501

SYNTHESIS, CHARACTERIZATION AND FUEL CELL PERFORMANCE OF POLY (2,2'-(P-PHENYLENE) - 5,5'-BIBENZIMIDAZOLE) AS A HIGH TEMPERATURE FUEL CELL MEMBRANE

Haifeng Zhang, Ru Chen, L. S. Ramanathan, Eugene Scanlon, Lixiang Xiao, Eui-Won Choe and Brian C. Benicewicz*

NYS Center for Polymer Synthesis
Department of Chemistry and Chemical Biology
Rensselaer Polytechnic Institute
Troy, NY 12180
benice@rpi.edu

Introduction

Polymer electrolyte membrane fuel cells (PEMFC) are receiving attention for their potential application in both stationary and mobile devices. Traditional perfluorinated ionomers, such as Nafion[®] rely on water to conduct protons which results in cell operation temperatures lower than 100 °C and subsequent low carbon monoxide (CO) tolerance. Additional concerns are the high cost of the membrane and extra hardware related to water management issues.

Anhydrous proton-conducting polymers have the potential to extend the cell operation temperature of fuel cell devices. Phosphoric acid (PA) doped polybenzimidazoles (PBI) have been reported to be promising candidates for high temperature fuel cell membranes. The doped membranes exhibited good proton conductivity, low gas permeability and excellent thermal stability at elevated temperatures.^{1,2}

In our extensive evaluation of the PBI-PA system, we synthesized the homopolymer poly(2,2'-(p-phenylene) 5,5'-bibenzimidazole) (p-PBI) in polyphosphoric acid (PPA). Membranes were prepared using a novel membrane fabrication technique, called the PPA process, which produced acid-doped films with an excellent balance of thermal, mechanical and electrochemical properties. In this paper, we report on the polymer synthesis, membrane fabrication, composition, conductivity and cell performance based on the p-PBI homopolymer.

Experimental

Polymer Synthesis and Acid Doped Membrane Fabrication. As shown in **Scheme 1**, 3,3',4,4'-Tetraaminobiphenyl (TAB), terephthalic acid (TPA) and polyphosphoric acid (PPA) were added into a round bottom flask equipped with an overhead stirrer and nitrogen inlet/outlets. The monomer concentration was kept below approximately 4.5 wt %. The maximum temperature and polymerization time were varied to study the effects of polymerization conditions on ultimate molecular weight, as measured by inherent viscosity. After polymerization, the solution was cast directly onto a glass substrate using a casting blade with a 20 mil gap (510 μm). The substrate was allowed to stand in the laboratory atmosphere or controlled humidity glovebox for one to three days. Absorption of water from the atmosphere and subsequent hydrolysis of the PPA to phosphoric acid induced a sol-gel transition that produced gel membranes with a high acid doping level. These membranes were readily fabricated into MEAs and subjected to cell performance tests.

Characterization. Inherent viscosity was measured by a Ubbelohde viscometer in 96 % sulfuric acid at a concentration of 0.2 g/dL at 30 °C.

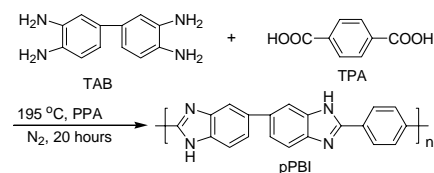
The acid content was determined by titrating three pieces of membranes using a standard base solution. After titration, the

polymer film was washed and dried in a vacuum oven and weighed to obtain the polymer content. Conductivity was measured by a four-probe ac impedance method using a Zahner IM6e electrochemical station in the frequency range of 1 Hz to 100 KHz at a temperature from 20 to 160 °C. The conductivity was calculated by fitting the experimental data with a model of a resistor in parallel with a capacitor.

Fuel Cell Testing. The cells were constructed with an active area of 44 cm² using commercially available electrodes. Pt catalyst loading was 1.0 mg/cm² on both anode and cathode.

The long-term tests were carried out on a test station constructed by Plug Power. Other performance tests were performed on a test station purchased from Fuel Cell Technologies.

Scheme 1 Synthesis of Poly (2,2'-(p-phenylene) 5,5'-bibenzimidazole in PPA solution



Results and Discussion

The low solubility of p-PBI in various solvents was reported previously.³ To obtain the high molecular weight polymer, the monomer concentration effect was investigated. **Figure 1** shows the effect of monomer concentration on the final polymer molecular weight. The polymer inherent viscosity increased with the increase of monomer concentration until around 4.5 wt%. At higher monomer concentrations, the solution was too viscous to stir and the solution became immobilized on the stirrer shaft. The polymerization was terminated early and only low molecular weight polymer was obtained due to the low mobility of the polymer chains. The inherent viscosity of p-PBI was approximately 3.0 (g/dL)⁻¹ at concentrations just below this critical concentration.

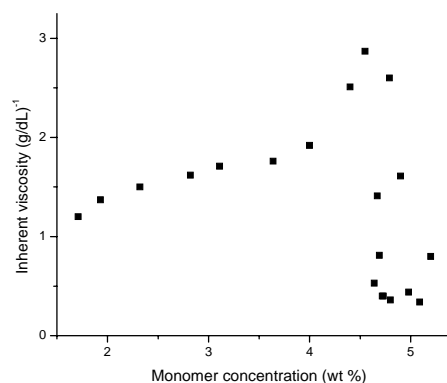


Figure 1. Effect of the monomer concentration on the polymer molecular weight.

Figure 2 shows the temperature dependent conductivity of phosphoric acid doped p-PBI membrane. Because the membrane initially contained water from the hydrolysis process, the first test run reflected the loss of water above 100 °C. To obtain the reliable and consistent data, the second conductivity test was performed after the first run or the preheating treatment. The conductivity measured on

the second heating run was about 0.23 S/cm at 160 °C, which is very high compared to the published data, usually reported at ~0.1 S/cm at 160 °C.⁴ This was attributed to the high acid content of this membrane. This membrane originally contained 70 (± 3) wt % of acid, 24 (± 2) wt % of water and 3.2 (± 0.5) wt % of polymer.

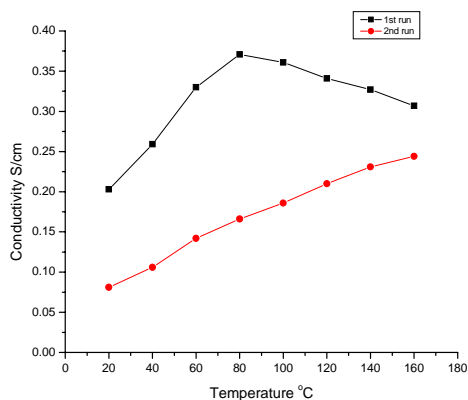


Figure 2. Temperature dependent conductivity of p-PBI membrane.

The cells based on the acid doped p-PBI membrane from the PPA process showed good performance at both low and high temperatures as shown in **Figures 3** and **4**. Cell temperatures ranged from 80 to 160 °C and cells were tested on hydrogen/air and hydrogen/oxygen gases at 1 or 2 atm (absolute) at fixed flow rates. As expected, performance and power densities increased with increasing temperature. **Figure 5** shows the results of a long-term test using hydrogen and air at ambient pressure and 160 °C. This preliminary test showed a drop of 53 mV, from 0.648 V to 0.595 V, after 2,500 hours' running at 160 °C and a current density of 0.2 A/cm².

Conclusions

A para-oriented PBI, poly (2,2'-(p-phenylene) 5,5'-bibenzimidazole), was synthesized at high molecular weights in polyphosphoric acid. Membrane fabrication using a novel sol-gel process produced films with high acid doping levels without isolation and redissolution of the polymer. The membrane showed high acid content (7,000 mole % acid per repeat unit), high conductivity (0.23 S/cm at 160 °C) and good mechanical and thermal properties. Fuel cells based on this acid doped membrane showed excellent performance and long-term durability at 160 °C for over 2,500 hours.

Acknowledgment. The authors thank Celanese Ventures, GmbH, Plug Power and NYSTAR for the financial and technical support.

References

- (1) Wainright, J. S.; Wang, J. T.; Weng, D.; Savinell, R. F.; Litt, M. *J. Electrochem. Soc.* **1995**, *142*, L121-L123.
- (2) Ma, Y. L.; Wainright, J. S.; Litt, M. H.; Savinell, R. F. *J. Electrochem. Soc.* **2004**, *151*, A8-A16.
- (3) Delano, C. B.; Doyle, R. R.; Miligan, R. J. *AFML-TR-74-22* **1974**.
- (4) Xing, B.; Savadogo, O. *J. New Mat. Electrochem. Systems* **1999**, *2*, 95-101.

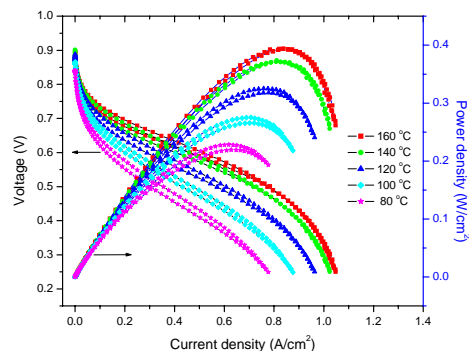


Figure 3. Performance curves for a hydrogen/air fuel cell based on p-PBI/PA membranes at different temperatures at ambient pressure. (Fuel cell operating conditions: constant flow rate, H₂ @ 400 sccm, air @ 1,000 sccm, no humidification.)

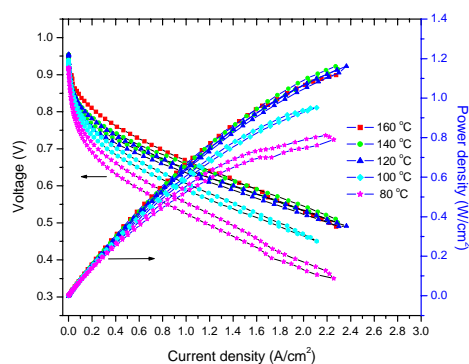


Figure 4. Performance curves for a hydrogen/oxygen fuel cell based on p-PBI/PA membranes at different temperatures at 30 psi(abs). (Fuel cell operating conditions: constant flow rate, H₂ @ 400 sccm, O₂ @ 400 sccm, no humidification.)

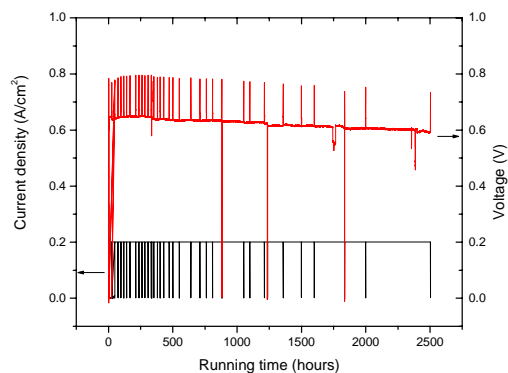


Figure 5. Long-term cell performance test (hydrogen/air) of a phosphoric acid doped p-PBI membrane at 160 °C, ambient pressure and no humidification. The cell voltage was recorded at a current density of 0.2 A/cm² with 1.2 stoic flow of hydrogen and 2.5 stoic flow of air.

THE USE OF HETEROPOLY ACIDS IN COMPOSITE MEMBRANES FOR ELEVATED TEMPERATURE PEM FUEL CELL OPERATION; LESSONS LEARNT FROM THREE DIFFERENT APPROACHES

Andrew M. Herring,¹ John A. Turner,³ Steven F. Dec,² Mary Ann Sweikart,^{1,3} Jennifer L. Malers,^{1,3} Fanqin Meng,¹ F. John Pern,³ James Horan² and David Vernon.³

Department of Chemical Engineering¹ and Chemistry and Geochemistry²
Colorado School of Mines
Golden, CO 80401-1887

Hydrogen and Electricity, Systems and Infrastructure Group³
National Renewable Energy Laboratory
Golden, CO 80401-3393

Introduction

There is increasing interest in using the heteropoly acids, HPA, as proton conducting components in PEM fuel cells for elevated temperature operation, 120 – 200 °C.¹⁻⁶ Operation of a PEM fuel cell at these elevated temperatures will allow the integration of the stack into existing vehicular cooling systems, as well as stationary CHP, and use of hydrogen with an elevated CO content, simplifying the overall design of the reformer needed to generate hydrogen from hydrocarbons. The heteropoly acids are a large and structurally diverse class of inorganic proton conducting materials⁷ with extremely high room temperature proton conductivities, as high as 0.2 S cm⁻¹ for 12-phosphotungstic acid.⁸ Importantly, for elevated temperature PEM fuel cell operation, the HPA are structurally stable to temperatures in excess of 600 °C and incorporate water molecules and protons to temperatures in excess of 300 °C depending on the system.

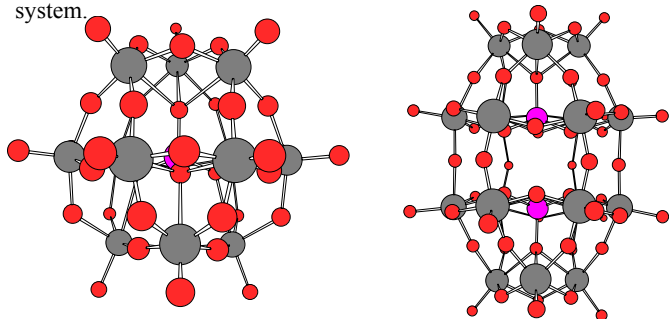


Figure 1. Structures of the Keggin anion, H₃PW₁₂O₄₀, 12-HPW, left and Dawson anion, H₆P₂W₁₈O₆₂, 18-HP2W, right.

Most studies to date have only considered the commercially available Keggin structures, consisting of a tetrahedral arrangement of three tungsten or molybdenum oxygen octahedral surrounding a central heteroatom, Figure 1. Many other structures are possible including the more thermally Dawson structure, Figure 1 and structures of increasing complexity. Importantly Lacunary structures may be derived from the parent Keggin or Dawson by the removal of 1, 2 or 3 metal oxygen octahedral leaving a vacant site that may be used as a covalent attachment point for the synthesis of hybrid materials or a coordination site for another metal center.

Because of their structural diversity these materials are particularly suitable for incorporation into a wide variety of membranes materials for which they can be specifically tailored. In addition, the HPA have interesting redox and catalytic properties that can be exploited for PEM fuel cell applications and must also be

fully understood before a practical system incorporating HPA can be developed. We have studied HPA in three systems: HPA cast in inert matrices such as polyvinylidene difluoride, PVDF, HPA infused into sulfonated perfluorinated polymers such as Nafion[®] and in polymer/silicate nanocomposites. All of these membranes were characterized by solid state NMR, IR, XRD and SAXS. Membrane electrode assemblies, MEAs, were constructed using standard E-tek electrodes, so that electrochemical measurements could be made, but the MEAs were not optimized for fuel cell operation.

Experimental

The HPA having the Keggin structure, 12-phosphotungstic acid, H₃PW₁₂O₄₀, 12-HPW, and 12-silicotungstic acid, H₄SiW₁₂O₄₀, 12-HSiW, were purchased (Aldrich) and used without further purification. All other HPA, 18-diphosphotungstic acid, H₆P₂W₁₈O₆₂, 18-HP2W, and 21-diarsenotungstic acid, H₆As₂W₂₁O₆₉, 21-HAs2W21 and the lacunary HPA H₈SiW₁₁O₃₉, 11-HSiW,⁹ were prepared by literature methods.

The PVDF/HPA membranes were formed by refluxing the PVDF-HFP co-polymer (Aldrich) and the HPA in acetone until dissolution was complete and casting the solution on Teflon blocks and allowing the solvent to evaporate.

Nafion[®] was cleaned by standard procedures, i.e. by boiling sequentially in concentrated nitric acid, deionized water, and hydrogen peroxide solution. The polymer was then doped by heating in a concentrated solution of the HPA at 80°C overnight.

Polymer/silicate/HPA nanocomposites were synthesized via a method³ based on Honma's reported method.² A Polyethylene glycol 400, PEG400, /SiO₂ sol-gel precursor was prepared by reacting PEG400 with a stoichiometric amount of 3-isocyanatopropyltriethoxysilane at 60-70 °C for 5 days under a N₂ atmosphere. The molecularly-hybridized precursor thus-obtained was then hydrolyzed and condensed with the addition of 11-HSiW, which served as a catalyst as well as a proton dopant. Monophenyltriethoxysilane, MPhTEOS, was added to the above mixture immediately under rapid stirring. Relative to the weight of the PEG400 precursor, 30 % of 11-HSiW and 60 % of MPhTEOS were added. The transparent and slightly brownish free-standing membranes were obtained and stored in air before further tests.

Membrane electrode assemblies, MEAs were fabricated by a standard hot press method¹⁰ using catalyzed E-TEK ELAT[®] electrodes with 0.35 mg Pt/cm² loading of 20 wt% Pt on Vulcan XC-72 carbon on carbon cloth gas diffusion backings with an active area of 5 cm². For the Nafion[®] MEAs, the electrodes were pretreated by brushing with one coating of 5 % Nafion[®] solution in mixed alcohols (Electrochem Inc.) and allowed to dry for 45 minutes under ambient conditions. The 5 cm² electrodes were hot pressed onto the membranes at 130 °C with a force of 360 psi for 90 seconds.

Results and Discussion

The most convenient method of studying the HPA in inert supports in fuel cell environments is to cast composite films of HPA in PVDF- HFP from acetone solution. These HPA/PVDF membranes can show very high current densities at ambient temperatures, a limiting current over 1 A cm⁻², with no external humidification has been achieved with 12-HPW. The polarization curve obtained with 18-HP2W at room temperature using dry O₂ and H₂ is shown in Figure 2. The open circuit value is poor, 0.7 V, as these membranes are quite porous and exhibit excessive cross-over. Attempts to achieve high current densities at elevated temperatures with a very limited set of HPA have so far failed. At 120 °C, similar membranes only exhibit a limiting current of 2 mA cm⁻², but as the lattice has shrunk on dehydration cross-over is expected to

deteriorate at these higher temperatures. Excess hydrogen applied to these porous membranes results in the reduction of the HPA and short circuiting of the cell as the reduced HPA can be electronically conducting in this system. As the library of HPA that we study increases we hope to discover HPA that are better suited to high temperature operation.

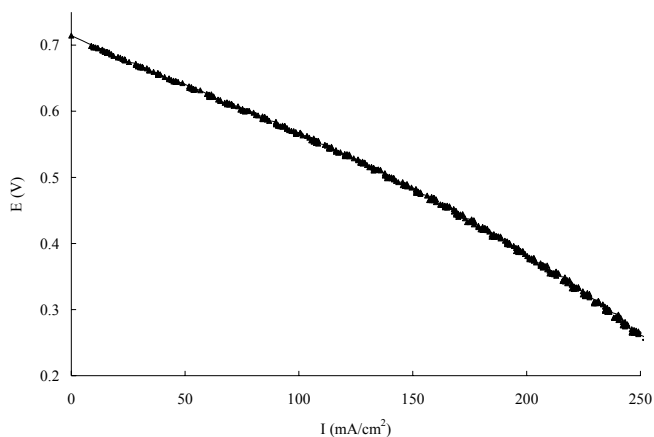


Figure 2. Typical polarization curve obtained for the PVDF-HFP/18-HP2W MEA using dry H₂ and O₂ and no back pressure at room temperature.

In contrast the addition of small amounts of HPA to sulfonated perfluorinated polymers such as Duponts Nafion[®] by infusion from aqueous solution dramatically increases the performance of the membranes at temperatures up to 150 °C depending on the HPA. The polarization for Nafion[®] doped with four different HPA at 120 °C with ca. 25% RH are shown in Figure 3. All doped samples show improved performance relative to the control membrane, the best performance is seen with 21-HAsW21, but it is currently unclear what the exact moiety involved in this system is as this HPA equilibrates in to a number of HPA species under the conditions of the experiment. These membranes have been studied in terms of understanding the interaction of the HPA with the polymer to enable a full understanding of this beneficial interaction. The HPA do not appear to be chemically reduced by hydrogen in these systems but are not immobilized and so may be leached from the membrane over time.

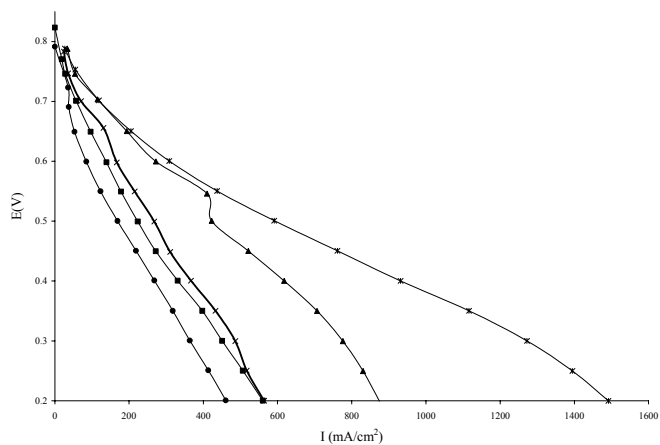


Figure 3. Polarization curves for HPA doped Nafion[®] at 120 °C using H₂ and O₂ humidified at 80 °C. • - control, ■ - 12-HPW, ▲ - 12-HSiW, x - 18-HP2W, * - 21-HAs2W21.

One approach to the leaching problem is to immobilize the HPA in a nanocomposite membrane using silicate sol-gel chemistry.¹⁻³ A number of polymer backbones have been investigated by us and ion exchange capacities, higher than 3 moleq g⁻¹, and diffusion coefficients as high as 1.2×10^{-6} cm² s⁻¹ have been achieved with these materials with excellent *exsitu* mechanical and thermal properties. The HPA are stable in these systems to leaching in boiling water. Tem analysis indicates that there is no ordering of proton conducting channels in these systems. In addition, preliminary data from MEA testing of these materials, Figure 4, indicates that significant optimization of the membrane/electrode interface will be required for these membranes to exhibit their full potential. This is manifested in the polarization curves, Figure 4, which lacks a clear kinetic loss region and show little improvement with the addition of Nafion[®] paint to the electrode surface.

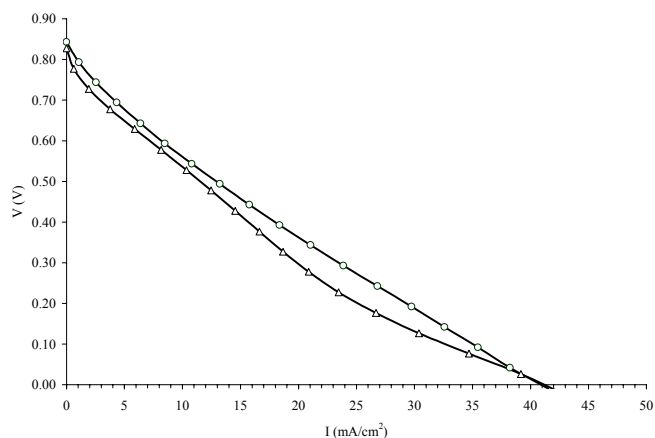


Figure 4. Polarization curves for a membrane with a ratio of PEG400 precursor:11-HSiW :MPhTEOS, of 100:40:100. △ - plain E-tek electrodes, ○ - E-tek electrodes painted with Nafion solution. Fuel cell at 47 °C, humidifier bottles at 80 °C.

Conclusions

HPA proton conducting systems hold much promise for PEM fuel cell operation at low humidity and elevated temperature, but challenges still exist in the development of fuel cell ready materials.

Acknowledgement. This work was supported by the US DOE science initiative, DE-FC02-0CH11088.

References

- (1) Honma, I.; Nakajima, H.; Nishikawa, O.; Sugimoto, T.; Nomura, S. *Journal of The Electrochemical Society* **2003**, *150*, A616.
- (2) Honma, I.; Takeda, Y.; Bae, J. M. *Solid State Ionics* **1999**, *120*, 255.
- (3) Vernon, D.; Meng, F.; Dec, S. F.; Williamson, D. L.; Turner, J. A.; Herring, A. M. *Journal of The Electrochemical Society* **2004**, submitted.
- (4) Kim, Y. S.; Wang, F.; Hickner, M.; Zawodzinski, T. A.; McGrath, J. E. *Journal of Membrane Science* **2003**, *212*, 263.
- (5) Ramani, V.; Kunz, H. R.; Fenton, J. M. *Journal of Membrane Science* **2004**, *232*, 31.
- (6) Staiti, P. *Journal of New Materials for Materials for Electrochemical Systems* **2001**, *4*, 181.
- (7) Pope, M. T.; Müller, A., Eds. *Polyoxometalate Chemistry: From Topology Via Self-Assembly to Applications*; Kluwer Academic Publishers: Dordrecht, 2001.
- (8) Nakamura, O.; Kodama, T.; Ogino, I.; Miyake, Y. *Chemistry Letters* **1979**, *1*, 17.
- (9) Tourne, C. M.; Tourne, G. F.; Malik, S. A.; Weakley, T. J. R. *Journal of Inorganic and Nuclear Chemistry* **1970**, *32*, 3875.
- (10) Mehta, V.; Cooper, J. S. *Journal of Power Sources* **2003**, *114*, 32.

ELECTRIC-FIELD-STRUCTURED PROTON EXCHANGE MEMBRANES

Jeffrey V. Gasa¹, R. A. Weiss,^{1,2} and Montgomery T. Shaw^{1,2}

¹Polymer Program and ²Department of Chemical Engineering
Institute of Materials Science, University of Connecticut, Storrs, CT
06269-3136

Introduction

Recent advancements in direct methanol fuel cell technology are quite dramatic and have placed this technology on the brink of commercialization. While there are several bottlenecks in current art, many regard the membrane, which must separate the methanol fuel and oxidant yet transport hydrogen ions, as the key polymer challenge because of the need for higher temperatures and greater chemical resistance for operation with methanol as the fuel.¹

This study has focused on methods for making highly acidic membranes based mainly on the high-performance polymer poly(ether ketone ketone) (PEKK), and its blends with poly(ether imide) (PEI).² We have reported recently that proton conductivities and MEA performance comparable to Nafion®, which is the benchmark, can be achieved with membranes based on sulfonated PEKK and its blends with PEI.^{2,3} In the case of blends, we have focused on the organization of the domain structure in the blend using mainly electric fields.⁴ An important factor for creating structures of high proton conductivity and low methanol permeability was the application of electric fields of selected magnitude and frequency during the formation of the membrane. We have also reported recently that the structured membranes have, in some cases, exhibited significantly increased conductivity relative to the equivalent isotropic material.⁵ The discussion in this paper is focused mainly on the influence of the magnitude and frequency of the applied field on the morphology of the resulting membranes.

Experimental

Materials. The acid polymer of principal focus in this study was sulfonated PEKK (SPEKK). The PEKK used was OXPEKK-SP (Oxford Performance Materials, New Britain, CT), which has a T/I ratio of 6/4. Sulfonation was achieved by dissolving the polymer (5% w/v) in a mixture of 53/47 (v/v) concentrated sulfuric acid and fuming sulfuric acid at room temperature. The sulfonation time and temperature were varied to achieve different levels of sulfonation, expressed here in terms of ion-exchange capacity (IEC).

Membrane Preparation. SPEKK and PEI were dissolved together (at various weight ratios) in N-methyl pyrrolidone (NMP) to form 7.5 wt% polymer solutions. These solutions were cast onto clean glass plates at 70 °C and air dried in a hood until most of the solvent had evaporated. The resulting membranes were dried in vacuum at 110-120°C for 48 h. After drying, the membranes were soaked in de-ionized water at 20°C for 48 h to remove residual solvent.

Electric-field-structured Membranes. The polymer solutions were cast under AC electric fields between two copper electrodes (2 x 3 x 50 mm) mounted on a microscope slide. This casting cell design was adopted from an earlier study conducted by Wnek and coworkers.⁴ In this cell, the field is applied along the plane of the membrane (in-plane). The solutions were cast at elevated temperatures (85 °C) for 1 h to evaporate most of the solvent and freeze in the morphology. The solutions were cast at various magnitudes and frequencies of the applied AC field.

Optical Microscopy. The morphology of the blend membranes was studied using a Nikon Labophot optical microscope in transmission mode. The size of the phase domains was distinct and large enough to be seen easily with the optical microscope.

Impedance Spectroscopy. The proton conductivity of the membranes was measured by impedance spectroscopy using a Solartron® 1260 impedance analyzer over a frequency range of 1-10⁶ Hz. The applied voltage was 50 mV. Membrane conductivities were measured using a cell described by Zawodzinski et al.⁶

Methanol Permeability. The methanol permeability was measured using a permeation cell. One side of the membrane was subjected to 50 wt% methanol solution in water, while pure water was put on the other side. The concentration of methanol was monitored as a function of time. Methanol concentrations were measured using gas chromatography. The methanol permeability was calculated using Fick's law of diffusion.

Results and Discussion

Proton Conductivity. The conductivities of the pure SPEKK membranes exhibited an exponential dependence on IEC, at 20 °C and 98 % humidity (Figure 1). In water, the higher IEC membranes dissolved, pointing to the need for modification by blending.

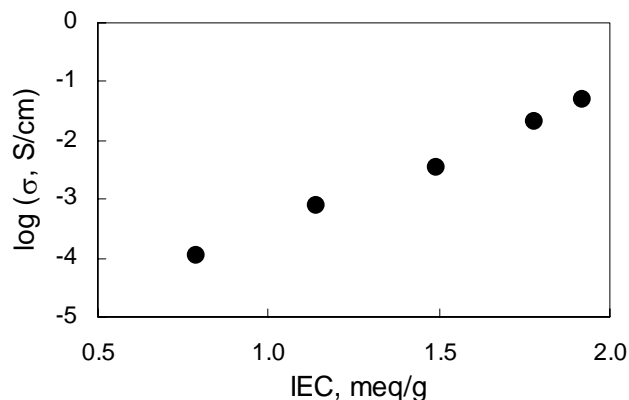


Figure 1. Proton conductivity of pure SPEKK membranes at various sulfonation levels. The measurements were made at 98% relative humidity and 20 °C.

Methanol Permeability. As shown in Figure 2, the methanol permeability increased with increasing IEC. The blend membranes containing 50% PEI had lower permeabilities than the pure SPEKK membranes.

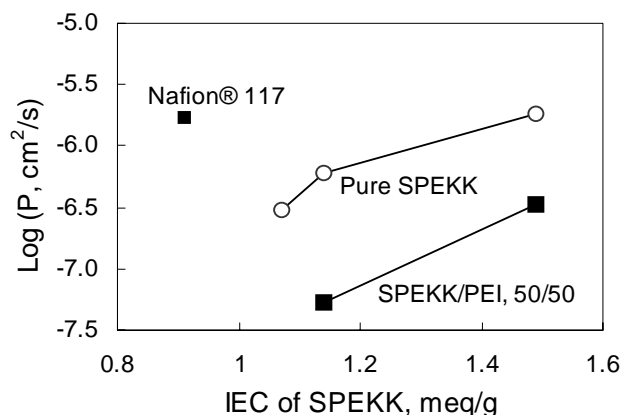


Figure 2. Methanol permeabilities of the membranes at room temperature

Morphology of Structured Membranes. Figure 3 shows the morphology of SPEKK-PEI blends cast at various field magnitudes and at a constant frequency of 10 kHz. Results clearly show that there is a threshold field magnitude (E_p) required to produce

structures that are preferentially aligned (anisotropic) along the direction of the applied field. Figure 5 suggests that E_p increases with increasing frequency. The E_p values for this blend system are much lower than those used by Wnek et al. (1 kV/mm) to align blends of non-sulfonated polymers.⁴ This is probably due to the increase in either the dielectric constant or the conductivity of PEKK upon sulfonation, which in effect increases the dielectric or conductivity contrast between the two phases. According to theory, the mutual attractive force due to interfacial polarization between the droplets decreases with increasing dielectric or conductivity contrast.⁷

At field magnitudes below E_p , the size of the dispersed phase was found to increase with increasing field magnitude (Figure 3). Above E_p , the diameter of the columnar structures was found to decrease when the frequency was increased (compare Figures 4B and 4C) and when the sulfonation level was decreased (compare Figures 4B and 4D). Application of DC field caused dielectric breakdown of the membrane as indicated by the presence of electrical trees (Figure 4A).

Conclusions

It has been demonstrated in this study that structured membranes for proton transport can be achieved by the application of electric fields during casting of these blend membranes. The size of the phase domains was found to depend on the magnitude and frequency of the applied field as well as the sulfonation level of the proton-conducting phase. With many other variables available (component structure and MW, temperature, composition, etc.) it is reasonable to imagine that membranes with superior properties can be made.

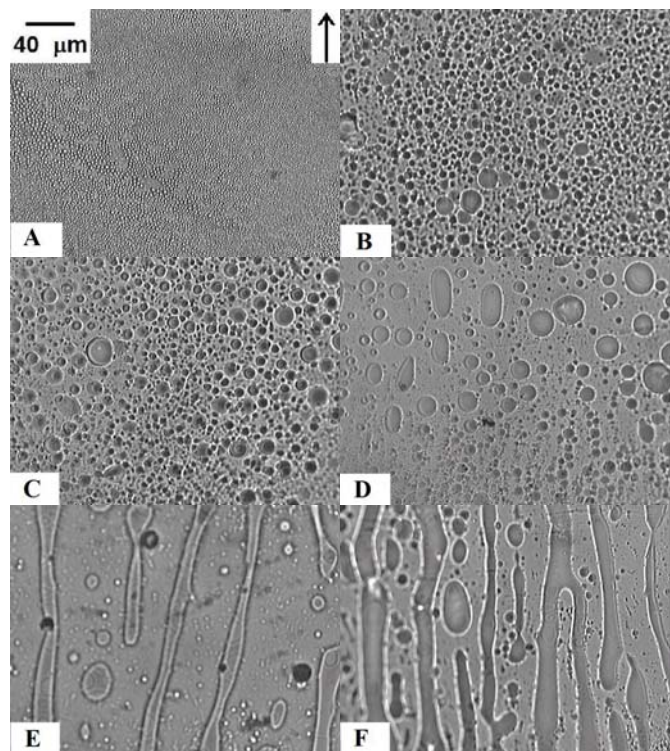


Figure 3. Optical Micrographs of SPEKK-PEI blends solvent cast at 85 °C under AC field with a frequency 10 kHz and at various field amplitudes: A) 5, B) 10, C) 15, D) 20, E) 25, and F) 30 V/mm. The arrow indicates the direction of the applied field. The weight fraction of SPEKK in the membrane was 0.2 with an IEC of 2.67 meq/g.

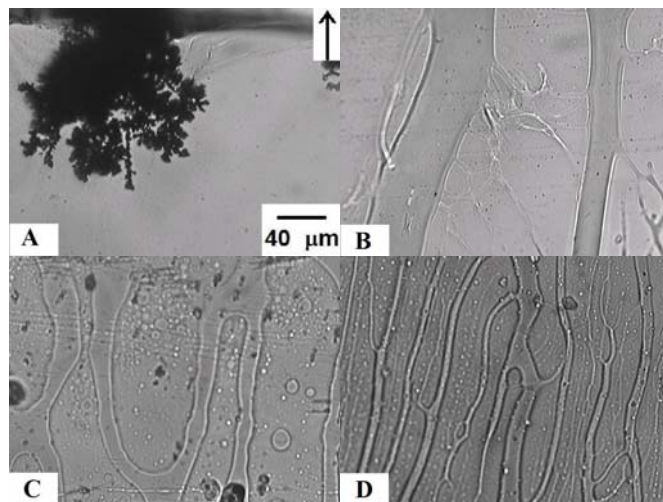


Figure 4. Optical Micrographs of SPEKK-PEI blends solvent cast at 85 °C under 50 V/mm AC electric field at various frequencies: A) DC, B) 10 Hz, and C) 10 kHz. The IEC of SPEKK was 2.67 meq/g. In D, the conditions were similar to B but the IEC of SPEKK was lower (1.26 meq/g).

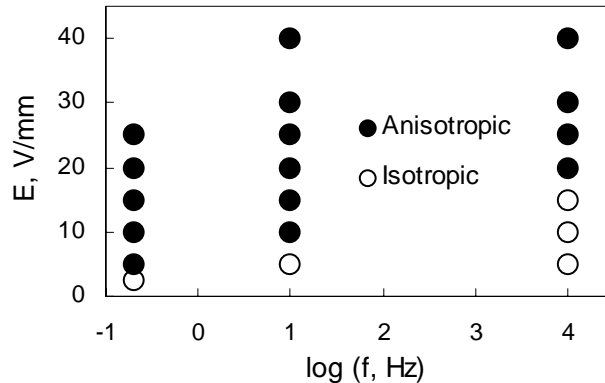


Figure 5. Influence of frequency on the threshold field magnitude required to produce structured (anisotropic) membranes.

Acknowledgement. The authors gratefully acknowledge financial support through the Connecticut Global Fuel Cell Center.

References

- Hoogers, G. *Fuel Cell Technology Handbook*. CRC Press LLC, 2003.
- Chun, S., Shaw, M.T., Weiss, R.A., "Sulfonated Poly(ether ketone ketone) Membranes," Asilomar Conference on Proton Exchange Membranes, February (2003).
- Swier, S., Gasa, J., Shaw, M.T., Weiss, R.A. "Proton-exchange membrane materials based on blends of poly(ether ketone ketone) and poly(ether imide)," Annual APS March Meeting, Montreal, Quebec, Canada, March (2004).
- Venugopal, G., S. Krause and G. Wnek, *Chem. Mater.*, **1992**, 4(6), 1334-43
- Gasa, J.; Shaw, M.T., "Conductivity enhancement of sulfonated poly(ether ketone ketone) blends using electric field structuring techniques," Annual APS March Meeting 2004, Montreal, Quebec, Canada, March (2004)
- Zawodzinski, T.A., M. Neeman, Jr., L.O. Sillerud and S. Gottesfeld, *J. Phys. Chem.*, **1991**, 95(15) 6040-6044.
- Pohl, H. A., *Dielectrophoresis*; Cambridge University Press: Cambridge, 1978.

MOLECULAR DESIGN OF RIGID ROD POLYELECTROLYTES: EFFECT OF STRUCTURE ON WATER RETENTION AND CONDUCTIVITY

Morton H. Litt*, Sergio Granados-Focil, Yue Zhang and Thomas Young

Macromolecular Sci. Dept., Case University, 10900 Euclid Ave., Cleveland, OH 44106-7202, U. S. A.

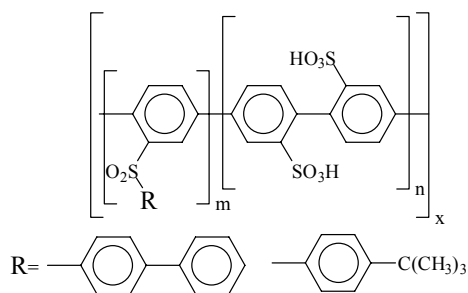
Introduction

My group has been working on polymers of the types shown below because they offer a unique opportunity to define molecular structure more precisely than is possible for most systems (1, 2, 3, 4, 5). The linear rigid rod structure causes the molecules to pack parallel to each other as liquid crystals. A small amount of co-monomer with a large cross-section, or one whose bonds are angled, forces the chains apart along their whole length, generating long pores lined with sulfonic acid groups that hold water very tightly. At low humidities the extra water raises conductivity over that of sulfonated flexible polymers. Recently, we have been studying rigid rod poly(p-phenylene sulfonic acids) (PPSA) polymers and copolymers to determine the effect of backbone structure on water retention and conductivity (6). A combination of TGA measurements with ^1H NMR for exact determination of the relative humidity dependence of the polymer water content enabled us to correlate the data and compare the two systems.

The polyimide structure is shown below. Comonomer nomenclature is detailed in **Experimental**.



The synthesis and properties of some PPSAs were reported earlier (6). The basic structure is given below. Here, copolymers were synthesized by post-reacting aromatic moieties with acid groups, creating sulfone links. Other preprints discuss the copolymers (6, 7).



Experimental

The following co-monomers were used as the **B** group: **1.** p-phenylene diamine (**P**), **2.** oxy-dianiline (**O**), **3.** 9,9-fluorenyl dianiline (**F**), **4.** 2', 3' 5', 6'-tetraphenyl 1, 4''-diamino p-terphenyl (**4PT**) and 2', 3'-di(biphenyl) 5', 6'-diphenyl 1,4''-diamino p-terphenyl (**D(BP)DPT**) (4). **O** and **F** are angled while the others are

linear. R in the acronym means random copolymer, B block, and the number is the mole% of co-monomer.

Water uptake measurements. Polyimide films in the acid form were dried at 80°C under vacuum for 72 hours. After weighing, they were equilibrated with LiCl solutions at given relative humidities until the weight was constant. One set of films, after equilibration at 50% relative humidity, was dried more thoroughly by heating under vacuum at 80°C for 72 hours, 100°C for 24 hours and at 150°C for 1 hour, and then weighed. Thermogravimetric analyses (TGA) were run at 20°C per minute under nitrogen using a T. A. Instruments TGA. Polyimide films were allowed to dry under a nitrogen stream at RT to get an initial weight and then heated. For PPSA, a film was equilibrated in the TGA pan with humidified nitrogen until its weight stabilized (Weight = 100%). Dry nitrogen was then passed over it at room temperature until the weight no longer changed, about one hour. It was then heated at 20°C/min. to 600°C. ^1H NMR measurements (Varian 300 MHz) were run on equilibrated PPSA films dissolved in D_2O , comparing the area from the aromatic H's to that of HDO.

Results and Discussion

Polyimides. Water retention for the polyimide sulfonic acids was determined using the TGA scans, showing the amount of water held by the polymers after nitrogen drying, Fig. 1. The trace derivative determined the maximum water loss rate temperature, T_{max} . As T_{max} rose, the activity coefficient of the bound water decreased. The bound water ranged from a minimum of 12% for the homopolymer to 21% for RO5, a calculated starting λ of 2 for homopolymer to 4.5 for RO5. T_{max} , Table 1, confirms this, it increased with increasing water retention, from 84°C for the homopolymer to 110°C for RO5. The water activity for RO5 is about 40% that of the homopolymer.

Normally, polymer was dried at 80°C for three days under vacuum. Stronger drying conditions, ending with one hour's heating at 150°C under vacuum, removed more water and gave values that agreed with the TGA values. Recalculation showed that homopolymer retained 1 water and the copolymers ~2.4 waters per acid group even after 3 days of drying at 80°C under vacuum.

Ionic conductivity showed a similar response; conductivity at 15% RH for the homopolymer was 0.4 mS/cm; rising to ~1.4 mS/cm. for the best copolymer (Nafion ~0.04 mS/cm.)(1,2,4). Interchain distances (WAXD), also increased for the bulky comonomers(1,4).

Poly(p-phenylene sulfonic acids). When the above approach was used for poly(phenylene sulfonic acids) the results were confusing. The weight loss up to 230°C by TGA, assumed to be water, was much smaller than the water content found by other methods. We needed an unequivocal way to measure water content. The best method used ^1H NMR. A solution of sodium acetate in D_2O was used to calibrate the system and to determine the amount of HDO in it. Weighed, equilibrated PPSA was dissolved in a measured volume of D_2O . The ratio of HDO to aromatic hydrogens could be measured easily. In addition, the acetate CH_3 group could be used to calculate an independent measure of water content. (The second method must be used when water insoluble films are measured.) The two approaches gave essentially identical results. These results could then be compared to the TGA data after conditioning at different RHs. For runs at 20°/min, much of their water was lost with N_2 drying at room temperature. After that, all the curves could be superimposed. Figure 2 shows TGA curves (equilibrated at 22% RH) run at different scan rates. The 20°/min. run is typical for the set used for the water determination. The TGA and NMR methods agreed only if the TGA transition at 335°C was taken as the end point for water loss. For PPSA T_{max} was 108°C, as high as that of the best polyimide homopolymer, Table 1, though less water was sequestered.

TGA water loss up to 250°C was analyzed using the thermodynamic concepts given in Ref. 5. Eq. 1, below, was used. ΔH_λ is the heat of vaporization of water from the polyelectrolyte. It is an average of the normal heat of vaporization at that temperature with the heat of solvation of the last water molecule evaporating under these conditions. B is the bulk modulus of the polymer. Water expands the volume and there is a compressive restoring force. a is the equilibrium amount of water held in the polymer free volume with no compressive stress. Minimizations for both 2 and 20°/min gave perfect fits with values of 60 KJ/mole for the heat of vaporization, $B \approx 1.4$ Gpa and $a \approx 0$. The data from four scans at 2, 5, 10 and 20°C/min. (ln(wt. loss rate) vs. 1/TK in this weight loss range) also gave a water heat of vaporization of 60 KJ/mole..

$$d(H_2O)/dt = -k_0 * K * T * \left(\frac{\lambda}{\lambda+1} \right) \exp\left(-\frac{\Delta H_\lambda}{R * T} + \frac{18 * (\lambda - a)}{100 + 18 * \lambda} * \frac{(18E - 6) * B}{R * T} \right) \quad 1$$

Conductivities of homo- and copolymers at different temperatures showed the expected behaviors. Copolymers held water tightly and were highly conducting at low RHs and elevated temperatures (7).

Conclusions

The water absorption data for two series of rigid rod, liquid crystalline polymers, were analyzed. The molecular design concept for building in free volume was validated for these linear, liquid crystal, rigid rod polymers. Water was held strongly; polyimides dried at room temperature had λ s of 2-4. PPSA homopolymer lost some water easily but held one water strongly (stable at RT but completely lost by 150°C) and two more waters so strongly that they were only removed at very high temperatures (200 to 335°C at 20°/min.) where one expects degradation. We are studying weight loss in this temperature range. Higher temperature weight loss is certainly from degradation.

Acknowledgements. We thank Drs. J. Wainwright and R. Savinell for helpful discussions and the use of the TGA. This work was supported by DARPA.

References

- Zhang, Yue; Litt, Morton H.; Savinell, Robert; Wainwright, Jesse. *Polymer Preprints* **40**(2), 480 (1999)
- Zhang, Yue; Litt, Morton H.; Savinell, Robert; Wainwright, Jesse; Vendramini, Jerome. *Polymer Preprints* **41**(2) 1561 (2000)
- Kim, H.-J.; Litt, M. H.; *Polymer Preprints (ACS)*, **42**(2), 486, (2001)
- Zhang, Yue. *Ph. D. thesis Case Western Reserve University*, 2001
- Litt, Morton H.; Zhang, Yue. *Polymeric Materials Science and Engineering* (2003), 89 21-22.
- Granados-Focil, Sergio; Litt, Morton H.; *Polymeric Materials Science and Engineering* (2003), 89 438-439.
- Granados-Focil, Sergio; Litt, Morton H, *Fuels, (ACS Preprints)* Aug. 2004

Table 1. Temperatures of maximum water loss rate, Tmax

Polyimide	Tmax, °C
Homopolymer	84
BP10	94
R(4P)T5	102
RF5	104
RO5	110

Table 2. Water content for PPSA as a function of RH, determined by NMR and TGA

Relative Humidity (%)	λ (TGA) ^a	NMR
22	4.6	3.7
42	5.0	4.7
58	5.9	5.2
75	6.7	6.6

a. Calculated after equilibrating at different RHs, (Wt. = 100%), 1 hr. dry N₂ flow at RT, and then heating at 20°/min. to 600°C. Weight loss at 335°C (end of a transition) agrees with NMR results.

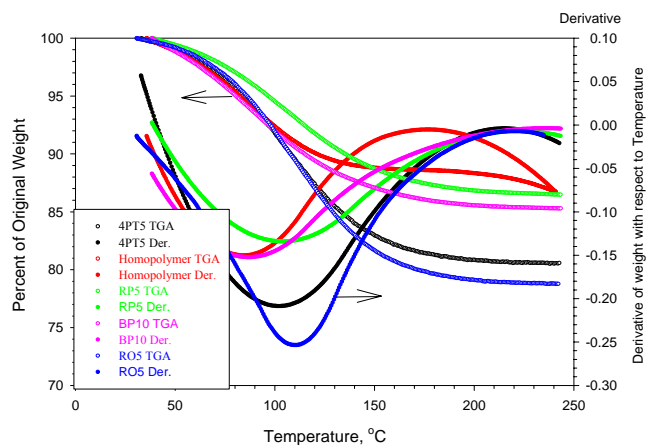


Figure 1. TGA weight loss (20°C/min.) and derivative curves for selected polyimides.

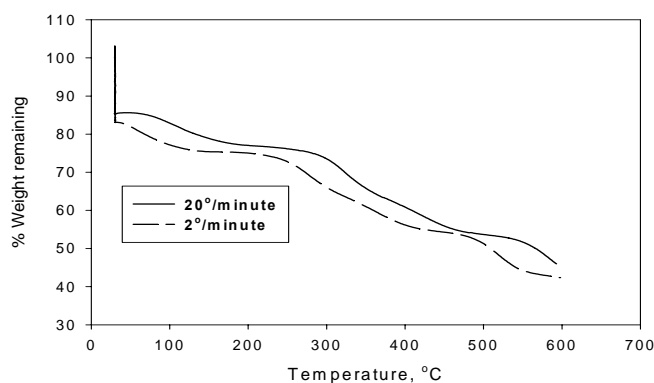


Figure 2. TGAs of PPSA after conditioning at 22% RH: Effect of heating rate on weight loss

New polymeric proton conductors for water-free and high temperature fuel cells

Xiao-Guang Sun, John B. Kerr, Gao Liu, Craig L. Reeder

Lawrence Berkeley National Laboratory, MS 62R0203, One Cyclotron Road, Berkeley, CA 94720

Introduction

Due to the considerable interest in PEM fuel cells for transportation purposes there has arisen a need to examine the feasibility of proton conducting membranes that do not depend on the presence of water for their performance. The most attractive option would involve a true solid-state material that contains no free solvent, can tolerate the presence of water, is conductive at low temperatures as well as high temperatures and can be tailored to provide desired gas permeabilities for both the separator and the membrane-electrode assembly. To accomplish this a somewhat complicated polyelectrolyte structure is necessary but an example of a candidate structure is shown in Figure 1 that illustrates some of the principles involved in proton transport in a solid polymer electrolyte.

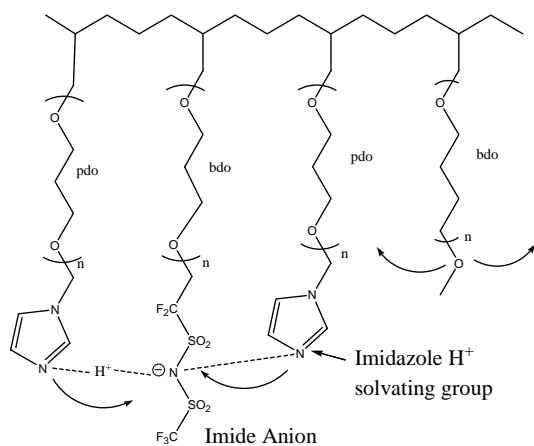


Figure 1. Schematic structure of polyether polyelectrolyte with attached imidazole groups showing mode of proton solvation.

Figure 1 shows the attachment of proton-solvating groups (imidazole) and acid groups (fluoroalkylsulfonimide) to a backbone by means of flexible side chains. The imidazoles are shown attached via an N-alkyl tether but they can easily be attached via one of the carbons (e.g. C2) so that both nitrogens would be available for proton solvation and to participate in a Grotthuss-type mechanism of proton transfer¹. The structure that is shown in Figure 1 is completely dependent on polymer side chain segmental motion which is dependent upon the flexibility of the side chains. The figure shows some modifications of the side-chain structure that can be easily made to achieve this and has already been reported for lithium ion transport in polymer electrolytes for lithium batteries. The nature of the backbone can be modified to provide a flexible structure (low T_g) with high gas permeability or a rigid chain with a high T_g (e.g. polystyrene) with low gas permeability. The structural changes that are possible in such a structure are virtually infinite if one considers side chain length, backbone flexibility concentration of proton solvation groups and acid groups, the nature of the acid groups and the role of cross-linking to provide improved mechanical properties.

The object of this work is to devise an easily modified polymer structure that will allow rapid elucidation of the role of these structural features in the determination of the properties of the membrane, bearing in mind that the needs are different in the separator and the MEA. We have chosen to study imidazole as the proton solvating group due to the successful development of the Polybenzimidazole-phosphoric acid system², the recent advances reported by Kreuer et al.^{3,4} and reports of remarkable stability of imidazole-containing polymer membranes that have been used for oxygen separation^{5,6}. The base polymer structure has been under development for use in lithium polymer batteries and uses a grafting chemistry that is shown in Figure 2 for lithium conductors. The grafting chemistry allows easy modification of the nature and length of the side chains, the nature of the backbone, the nature and concentration of the anions and the nature and density of cross-links. This chemistry has been recently reported^{7,8} and the strategy is extended to include proton conducting units in this work. The concentration of imidazole groups relative to that of the acid groups is critical not only for the possible operation of a Grotthuss-type mechanism but also to control possible poisoning interactions with the platinum electrocatalysts. Our experimental plan is to dope various acid polyelectrolytes such as Nafion® and the polyether polyelectrolytes shown in Figure 2 with imidazoles at different concentrations to determine the proton mobility and catalyst interactions and use the results as a guide to prepare the fully tethered polyelectrolyte proton conductors

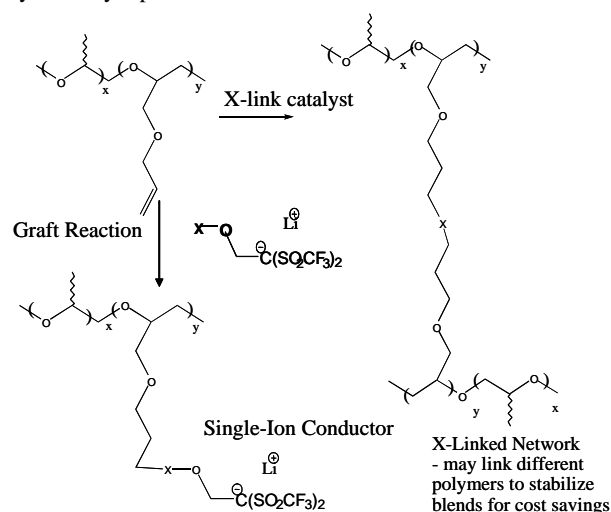


Figure 2. Grafting chemistry used to attach different acid groups (alkyl SO₃H, -CF₂SO₃H and imide -CF₂SO₂NHSO₂CF₃) and imidazole groups to the polymer matrix.

Experimental

The basic prepolymer synthesis and grafting chemistry for the lithium forms of polyether polyelectrolytes has been described previously⁷ and is also described in another article in this issue⁸. The acid forms were obtained by treatment with DOWEX[®] HCR-W₂ ion exchange resin. Anion groups were prepared from tetramethyldisilylyethane (Gelest, Inc), CH₂=CHCH₂OC₂H₄OC₂H₄SO₃Li and CH₂=CHCH₂C₂F₄OC₂F₄SO₃Li to give a nonfluorinated and a fluorinated acid group. The equivalent weights (EW) were about 1600-2000. Nafion (EW 1100) in the acid form was obtained from Aldrich as a dispersion in alcohols. The polyelectrolytes were prepared as solutions in alcohol with varying amounts of imidazole

added to the solution. The polymer solutions were then cast of Teflon sheets and dried over P_2O_5 dessicant to provide membranes suitable for conductivity and mechanical measurements. Conductivity measurements were carried out using ac impedance with membranes sandwiched between two stainless steel electrodes. The temperature was controlled by means of convection ovens and ambient humidity conditions were used. Mechanical measurements were carried out on a Rheometrics RSAII solids analyzer and DSC was performed using a Perkin-Elmer DSC7. The thermal and mechanical analysis showed that the presence of imidazole in the membrane lead to an increase in the main glass transition temperature.

Results and Discussion

The conductivities of the Nafion® membranes doped with imidazole and N-methylimidazole as a function of temperature are shown in Figures 3 and 4. These are all carried out in the absence of water and the conductivity of undoped Nafion® is shown for comparison. It is clear that the best conductivities occur at imidazole:acid ratios of 6-7 and that there is an apparent change in dependence once the imidazole is in excess over the acid group. The N-methylimidazole doped membranes, however, show a lower conductivity and the temperature dependence is similar to that of the low imidazole concentration system.

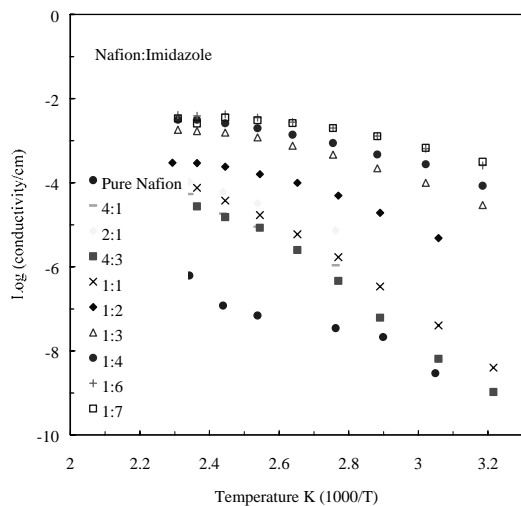


Figure 3. The conductivity of Nafion® doped with imidazole at different concentrations relative to the concentration of acid groups.

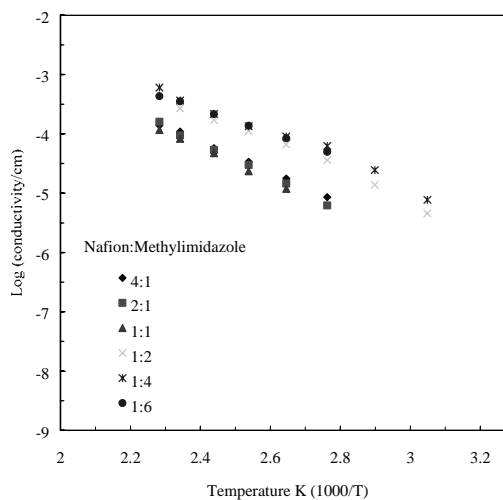


Figure 4. The conductivity of Nafion® doped with N-methyl imidazole at different concentrations relative to the concentration of acid groups.

Conductivities of the two polyether polyelectrolytes doped with imidazole are shown in Figure 5. These results illustrate the effect of the acid group. The alkyl sulfonate polymer has distinctly lower conductivities than the fluorinated alkylsulfonate, illustrating the effect of acid strength. At this time no data is available on the effect of EW. Cyclic voltammetry experiments carried out on a platinum electrode in sulfuric acid in the presence of imidazole shows no poisoning of the platinum activity until the imidazole is present in excess indicating that the imidazole base strongly interacts with platinum but the protonated form does not. This indicates that the polymer in the MEA must be completely protonated to avoid problems with catalyst activity.

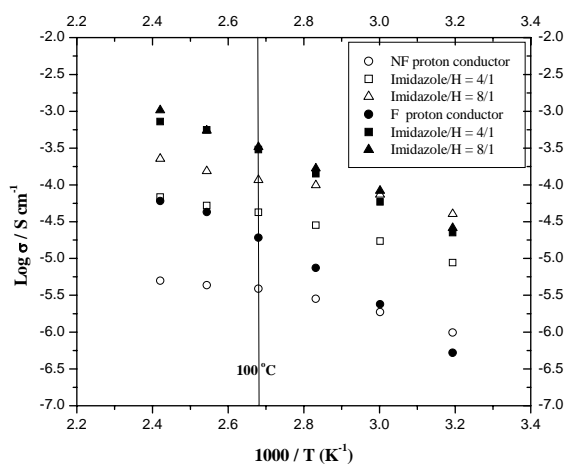


Figure 5. Proton conductivities of the proton conductors based on both non-fluorinated and fluorinated sulfonic acid with different amount of imidazole.

Conclusions

Conductivities of imidazole-containing polyelectrolyte membranes are sufficiently high to be of interest for fuel cell operation. The conductivity of membranes swollen with unsubstituted imidazole is higher than that of the N-methyl imidazole which may provide support for the participation of a Grotthuss mechanism of proton transport. Tethering of the imidazoles to the polymer matrix results in a solid state membrane with no mobile solvent that has lower conductivity than the solvent swollen systems. The polyelectrolyte structures are presently under construction and their conductivities will be reported on. The preliminary indications are that the stronger imide acid will provide higher conductivities and that optimization of the imidazole:acid ratio will provide conductivities that are of interest to fuel cell engineers.

Acknowledgement. This work was supported by the DOE Office of Hydrogen, Fuel Cells and Infrastructure and by NASA Glenn PERS program.

References.

1. Agmon, N. The Grotthuss Mechanism. *Chemical Physics Letters* **244**, 456-462 (1995).
2. Wang, J. T., Savinell, R. F., Wainright, J., Litt, M. & Yu, H. A H₂/O₂ Fuel Cell Using Acid Doped Polybenzimidazole as Polymer Electrolyte. *Electrochimica Acta* **41**, 193-197 (1996).
3. Herz, H. G. et al. New fully polymeric proton solvents with high proton mobility. *Electrochimica Acta* **48**, 2165-2171 (2003).
4. Schuster, M. F. H., Meyer, W. H., Schuster, M. & Kreuer, K. D. Toward a new type of anhydrous organic proton conductor based on immobilized imidazole. *Chemistry of Materials* **16**, 329-337 (2004).
5. Suzuki, Y., Nishide, H. & Tsuchida, E. Membranes of the picket fence cobalt porphyrin complexed with poly(vinylimidazole and -pyridine)s: Selective optical response to oxygen. *Macromolecules* **33**, 2530-2534 (2000).
6. Nishide, H., Tsukahara, Y. & Tsuchida, E. Highly selective oxygen permeation through a poly(vinylidene dichloride) cobalt porphyrin membrane: Hopping transport of oxygen via the fixed cobalt porphyrin carrier. *Journal of Physical Chemistry B* **102**, 8766-8770 (1998).
7. Sun, X. G., Reeder, C. L. & Kerr, J. B. Synthesis and characterization of network type single ion conductors. *Macromolecules* **37**, 2219-2227 (2004).
8. Sun, X. G., Reeder, C. L., Kerr, J. B. & DesMarteau, D. D. Synthesis and characterization of comb shape single ion conductors based on polyepoxide ethers and perfluorinated lithium salts, in *Polymer Preprints* (2004). This issue.

NOVEL INORGANIC/ORGANIC HYBRID ELECTROLYTE MEMBRANES

Zhiwei Yang, Decio Coutinho, Fangxia Feng, John P. Ferraris*,
Kenneth J. Balkus Jr.*

Department of Chemistry and The UTD Nanotech Institute,
University of Texas at Dallas
Richardson, Texas 75083-0688, USA

Introduction

Proton exchange membrane fuel cells (PEMFCs) hold promise as next generation clean energy sources for transportation as well as small-scale stationary power generation. The advantages of PEMFCs include high power density, fast startup and immediate response for power demand change.¹ Recently, the interest in high temperature (>130 °C) PEMFCs has grown because of possible advantages over low temperature PEMFCs. These include the enhanced ability of the FC system to directly use reformed fuels by increasing catalyst tolerance of impurities in the fuel feed stream, simplification of water-management for PEMFC systems, and reduction of radiator size in automotive applications due to enhanced rejection of heat by the FC system.

A key part of a PEMFC is the membrane that conducts protons and insulates electrons. Perfluorosulfonic acid (PFSA) polymers, such as Dupont's Nafion®, have been used as PEMs in PEMFCs for decades because of their superior performance and durability. The conduction of protons in the PFSA polymer is realized through the mobility of H⁺-nH₂O clusters among the -SO₃⁻ end groups, called the vehicular mechanism,^{2,3} which requires the PFSA polymers to be fully hydrated to perform well. This limits their applications under ambient atmosphere and elevated temperature (>100 °C) conditions. The previous efforts for high temperature PEM development mainly include modifying PFSA by compositing with hygroscopic materials and developing novel aromatic-based polymers, which directly incorporate sulfonic acid groups. Since H⁺ conduction in these membranes still depends on water (vehicular mechanism), they always suffer from low H⁺ conductivity at elevated temperature and low to zero humidity conditions because of the water loss, and/or swelling in the presence of water.

In recent years, Brønsted acid-base systems such as organic amine/ trifluoromethanesulfonimide (HTFSI) melting salts have been reported to be highly proton conducting at elevated temperatures (100–200 °C) and water-free conditions. The H⁺ conduction of these electrolytes could result from hopping of H⁺ from one amine/acid active site to another without transport of small molecules (Grotthuss mechanism).^{3,4}

In this study, novel inorganic/organic hybrid membranes containing immobilized amine/HTFSI groups were explored. Considering the activation energy of proton transport could depend upon the distance between the active sites as well as nature of electrolytes, a higher density of the active functional groups was introduced into the membranes to reduce the distance among active sites. The membranes are comprised of a 3-dimensional cross-linked silicon-oxygen backbone and organic amine groups. The silicon-oxygen backbone, which is stable to free radical attack, provides the PEM with the necessary thermal/chemical/mechanical properties. The organic amine groups were doped with HTFSI to form H⁺ conducting sites. The thermal stability and proton conductivities of these novel membranes were studied using TGA and ac impedance.

Experimental

Preparation of membranes.

HTFSI-doped PEI/SiO₂ membranes: Polyethylenimine (PEI) (linear, M.W. = 215K, prepared according to literature method⁵) was dissolved in absolute ethanol to form 10wt% solution. 3-glycidyl-oxypolypropyltrimethoxysilane (GLYMO) (97%, Fluka, 1:1 weight ratio vs. PEI) was added and stirred for ½ hour at room temperature. The desired amount of HTFSI (50wt% in ethanol) was added dropwise and stirred for another ½ hour at room temperature. The resultant solution was cast on a level PTFE surface, air dried at room temperature for 1 day, and then annealed at 80 °C, ambient atmosphere overnight to form a freestanding, flexible membrane.

Polysilsesquioxane membranes with amine/HTFSI groups: Three kinds of membranes comprising different types of organic amines were prepared through sol-gel processes by using N-[3-(trimethoxysilyl)propyl]-ethylenediamine (EDATMS) (97%, Aldrich), N-[3-(triethoxysilyl)propyl]-4,5-dihydroimidazole (IPTES) (Gelest Inc.) and N-[3-(trimethoxysilyl)propyl]-polyethylenimine hydrochloride (PEITMS) (Aldrich), respectively. In a typical membrane preparation, 0.5 g of IPTES was dissolved in 1 ml of methanol. 0.1 g of (GLYMO) (97%, Fluka) was added and stirred for overnight at room temperature. 1.3 g of HTFSI solution (50wt% in dry ethanol) was added and stirred for ~2 hours at room temperature. The resultant mixture was cast on a glass paper (HOVOSORB®, Hollingsworth & Vose Company), then dried in air for 2-3 days and annealed at 80 °C overnight to form a flexible membrane.

Thermal stability. The thermal decomposition of the membranes under O₂ atmosphere was evaluated by thermogravimetric analysis (TGA) using a Perkin Elmer Pyris 1 TGA. The heating rate was 10°C/min until no further weight loss was detected.

Proton conductivity measurements. Pt black (fuel cell grade, E-TEK) was symmetrically deposited on both sides of the membrane with a loading of ~5 mg/cm², followed by hot-pressing at ~85 °C and ~300 psig for 1-2 min to form crude MEA. The proton conductivities of MEA were measured by AC impedance using a PC controlled VoltaLab® PGZ301 (Radiometer Analytical S.A.) over the frequency range of 100 KHz to 0.1 Hz, using a 10 mV amplitude ac single. All measurements were carried out under ambient atmosphere. The experimental temperature and humidity were well controlled using a fuel cell testing station and 5 cm² single cell (Fuel Cell Technologies Inc.). The relative humidity of the cell was calculated from humidifier temperature against the cell temperature.

Results and Discussion

HTFSI-doped PEI/SiO₂ membrane. PEI has been chosen in this study because PEI has the highest amine density among the other polyamine polymers. Since the prepared linear PEI (cal. M.W.=215k) has a soft point of ~80 °C, GLYMO was used to cross-link PEI to increase its heat resistance. When mixed with PEI in alcohol solution, the epoxy ends of GLYMO covalently bonded to the amine groups of PEI, and the trimethoxysilane ends of GLYMO hydrolyzed and condensed together to form inorganic silica clusters through so called sol-gel processes, which greatly improved thermal stability of the composite membranes (Figure-1).⁶

Under water-free conditions, the proton conductivity of the membrane increased with increasing temperature, indicating that the proton conduction here follows Grotthuss mechanism only. Increasing relative humidity of the fuel cell operating atmosphere leads to an increase in the membrane's proton conductivity by introducing additional proton conduction through the vehicle mechanism (Figure 2).

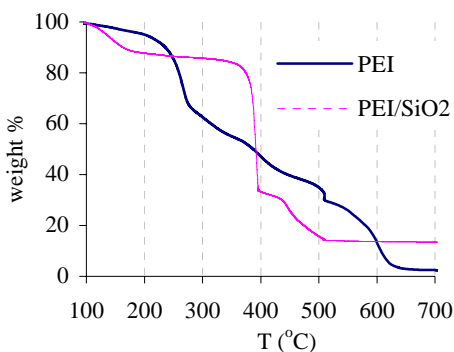


Figure 1. TGA of PEI polymer and GLYMO cross-linked PEI

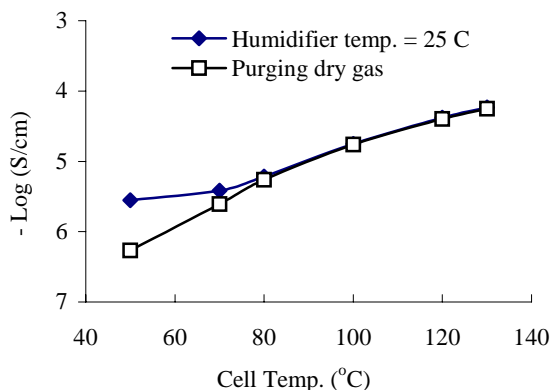


Figure 2. Proton conductivity of HTFSI doped PEI/SiO₂

Polysilsesquioxane membranes with amine/HTFSI groups.

The membrane precursors were organosilanes, which hydrolyze and condense to form a 3-dimensional cross-linked Si-O network with pendant organic amine groups that were doped with HTFSI to form proton-conducting sites. The mechanical properties of the membranes, especially flexibility and swelling in hot water, were greatly improved by adding GLYMO to increase the level of cross-linking. In this case, the epoxy end of GLYMO reacts with the amine groups to form covalent bonds, while the trimethoxysilane end of GLYMO hydrolyzes and condenses with the silane through a sol-gel process. The prepared membranes exhibited good thermal stability in an O₂ atmosphere (Figure 3), and hot water.

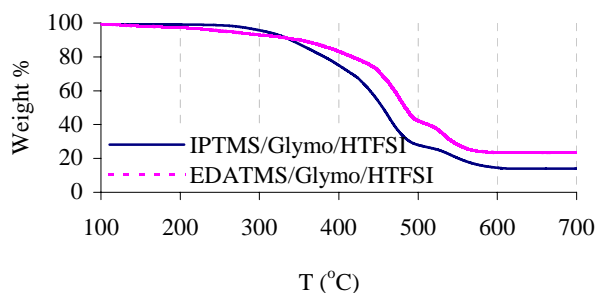


Figure 3. TGA of polysilsesquioxane hybrid membranes

Figure 4 shows the proton conductivities of an IPTES/GLYMO/HTFSI membrane with the corresponding molar ratio of 1.0 / 0.1 / 0.6 (per nitrogen site / GLYMO / HTFSI). Under water-free conditions, the membrane showed excellent proton conductivity, which increases with temperature, reaching a maximum of 10⁻³ S/cm at 130°C, while under fully hydrated conditions, the proton conductivity increased by ~1 order of magnitude. The proton conductivity of the membranes was also affected by GLYMO content and doping level. An increase of GLYMO content results in better mechanical strength but less proton conductivity. An increase in HTFSI content results in an increase in the doping level of organic amine groups, and a better proton conductivity but less mechanical strength. Membranes made from EDATMS/GLYMO/HTFSI and PEITMS/GLYMO/HTFSI showed similar behavior as IPTES/GLYMO/HTFSI membranes.

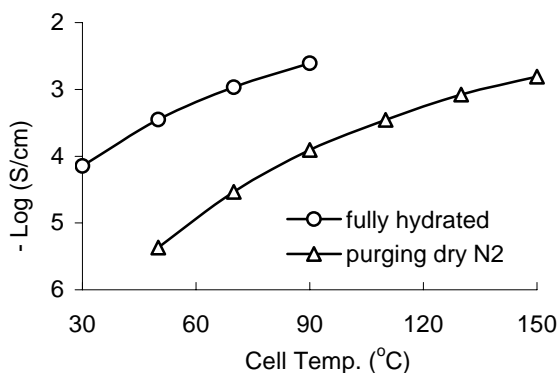


Figure 4. Proton conductivity of polysilsesquioxane membrane comprising IPTES/GLYMO/HTFSI in molar ratio of 1.0 / 0.1 / 0.6

Acknowledgment. We would like to thank R.A. Welch Foundation, THECB-ATP, DOE, LANL, SPRING, and the Clark Foundation for funding.

References

- 1 Cleghorn, S. J. C.; Ren, X.; Springer, T. E.; Wilson, M. S.; Zawodzinski, C.; Zawodzinski, T. A. and Gottesfeld, S. *Int. J. Hydrogen Energy*, **1997**, *22*, 1137.
- 2 Eikerling, M.; Kornyshev, A. A.; Kuznetsov, A. M.; Ulstrup, J. and Walbran, S. *J. Phys. Chem. B*, **2001**, *105*, 3646.
- 3 Hogarth, M. and Glipa, X. In *High Temperature Membranes for Solid Polymer Fuel Cells*, ETSU F/02/00189/REP DTI/Pub URN 01/893
- 4 Susan, Md. A. B. H.; Noda, A.; Mitsushima, S. and Watanabe, M. *Chem. Commun.*, **2003**, *8*, 938.
- 5 Tanaka, R.; Ueoka, I.; Takaki, Y.; Kataoka, K. and Saito, S. *Macromolecules*, **1983**, *16*, 849-853
- 6 Honma, I.; Takeda, Y.; Bae, J. M. *Solid State Ionics*, **1999**, *120*, 255-264

NOVEL SULFONATED PROTON EXCHANGE MEMBRANES FOR FUEL CELL APPLICATIONS: PARTIALLY FLUORINATED COPOLYMERS

Charles Tchatchoua, William Harrison, Brian Einsla, Mehmet Sankir, Yu Seung Kim*, Bryan Pivovar*, James E. McGrath

Department of Chemistry, Virginia Polytechnic Institute and State University, Blacksburg, VA 24061

* MST -11, Los Alamos National Laboratory, Los Alamos, New Mexico

Introduction

Currently there is great interest in cost effective and efficient fuel cells [1,2]. Proton exchange membranes (PEMs) are essential to the operation and the advancement of the of fuel cell technology [3,4]. The perfluorosulfonic acid polymer Nafion (DuPont) is the current state-of-the-art membrane, however, it is presently expensive, losses proton conductivity at low humidities, and has high methanol permeability. Our research group, and others, has developed alternative PEMs aimed to address noted short-comings of perfluorinated membranes—especially cost. In this presentation, we describe a two series of partially fluorinated, disulfonated poly(arylene ether sulfone) copolymers. The disulfonated copolymers were directly polymerized using the disulfonated monomer SDCDPS, dichlorodiphenyl sulfone (DCDPS), and either 3F bisphenol or 6F bisphenol A.

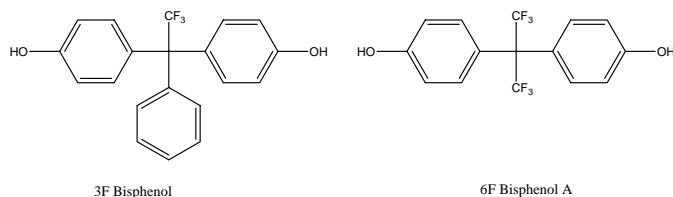


Figure 1. Structure partially fluorinated bisphenols

Experimental

Materials. All reagents were purified using typical laboratory procedures. The synthesis of 3F bisphenol and disulfonated dichlorodiphenyl sulfone have been reported previously by our group.

Copolymer Synthesis Direct syntheses of the copolymers were conducted using a 1:1 stoichiometry of each respective bisphenol to various ratios of activated dihalide monomers. As an example: In a three-necked flask, equipped with a nitrogen inlet, mechanical stirrer, a Dean-Stark trap and condenser, 10mmol of 3F bisphenol and a stoichiometric amount DCDPS and SDCDPS (the molar ratio was varied from 0 to 40%) were added to the flask, followed by K_2CO_3 in 20% molar excess (based on bisphenol). Polymerization was conducted at 20% solids concentration in dry NMP and toluene was used as azeotropic agent. The solution was allowed to reflux at 150°C for 4 hours to dehydrate the system then heated at 190°C overnight, for ~16 hours. The resulting solutions were diluted with NMP to reduce viscosity and then filtered to remove salt and finally precipitated in deionized water. The copolymers were isolated by filtration, washed with water and dried in the vacuum oven at 150°C overnight. All copolymers were isolated in high yields (>95%).

Characterization

1H -NMR experiments were performed using a Varian 400MHz instrument in deuterated chloroform. The intrinsic viscosity (IV) of the polymers was measured in NMP at 25°C using a Cannon Ubbelohde viscometer.

Membrane preparation. Membranes in the sodium sulfonate form were prepared by first redissolving the copolymer in DMAc to afford 5-10% transparent solutions followed by casting onto clean glass substrates. The films were carefully dried with infrared heat at gradually increasing temperatures (up to ~ 60 °C) under a nitrogen atmosphere, and then vacuum-dried at temperatures up to 150 °C for two days.

Acidification of Sulfonated Copolymers Membranes. The sulfonated poly(arylene ether) copolymer films were converted to their acid- form by boiling the cast membranes in 0.5 M sulfuric acid for 1.5 hours, followed by 1 hour extraction in boiling deionized water. The acidified membranes were either dried under vacuum at 90 °C in 48 hours or stored in deionized water at 30 °C.

Characterization Methods

Fourier Transform Infrared (FTIR) Spectroscopy Thin films of the copolymers were solvent cast from DMAc (~5%, w/v) and spectra were recorded for both the disodium-salt and diacid forms using a Nicolet Impact 400 FT-IR spectrometer to confirm the functional groups concentration of the copolymers.

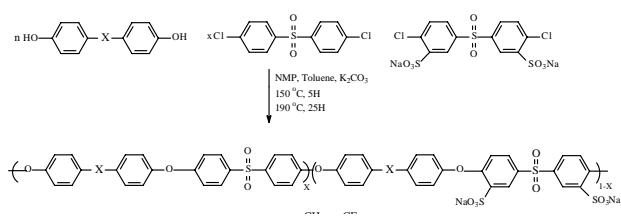
Nuclear Magnetic Resonance (NMR) Spectroscopy 1H and ^{13}C NMR analyses were conducted on a Varian UNITY 400 spectrometer. All spectra were obtained from a 10% solution (w/v) in dimethylsulfoxide- d_6 solution at room temperature. Monomer purity as well as copolymer compositions were analyzed via NMR spectroscopy.

Intrinsic Viscosity, Solution Properties and Water Uptake Homo- and sulfonated copolymer solubilities were determined at 10% concentration (w/v) in a number of solvents, including NMP, DMAc, DMSO, and chloroform. Intrinsic viscosities were determined in NMP at 25 °C using an Ubbelohde viscometer.

Water uptake was determined on films for all of the poly(arylene ether) copolymers in both the sulfonate and acidified forms. The films were first thoroughly dried at 150 °C under vacuum to a constant weight which was recorded. The dried film was then immersed in water at 30 °C and periodically weighed on an analytical balance until constant water uptake weight was obtained. Typically, the apparent equilibrium water sorption occurred within 48 hours. The water uptake is reported as a percentage and determined by taking the weight difference between the wet film and the dry film and dividing by the dry film weight.

Non-Aqueous Potentiometric Titration Non-aqueous potentiometric titrations were conducted using a MCI Automatic Titrator Model GT-05. The acidified membrane dissolved solutions in DMAc were titrated by standard tetramethyl ammonium hydroxide in isopropyl alcohol solution (TMAH). Quantitative determination of pendent sulfonic acid groups along the copolymer chain via titration confirmed the spectroscopic values and also allowed for the direct measurement of the ion exchange capacity (IEC, meq/g).

Thermogravimetric Analysis (TGA) The thermo-oxidative behavior of both the salt-form (sulfonate) and the acid-form copolymers was performed on a TA Instruments TGA Q 500. Samples were pieces of thin films and totaled a weight of 10 to 15 mg. The films were dried under vacuum for at least 12 hours prior to analysis to remove absorbed water. The samples were evaluated over the range of 30 to 800 °C at a heating rate of 10 °C/min in air.



Scheme 1 General synthesis of disulfonated poly(arylene ether sulfone) copolymers.

Results and Discussion

Nucleophilic aromatic substitution step polycondensation long been successfully employed to synthesize high molecular weight poly(arylene ether). Using typical polymerization conditions one may dehydrate the aprotic dipolar reaction system with toluene until a final polymerization temperature of 190 °C is reached. The high molecular weight sulfonated copolymers were isolated as swollen “strings” by precipitating in stirred deionized water after first diluting the viscous reaction solutions from 20 percent solids to ~10 percent solids with DMAc and filtering through filter paper to remove the salts. The copolymers demonstrated exceptional solubility in common polar, aprotic solvents. Interestingly, some of the 3F bisphenol based copolymers were soluble or swollen by chloroform, depending on degree of sulfonation.

Table 1. General characterization of selected partial fluorinated disulfonated poly(arylene ether sulfone) copolymer

Copolymer Type	$[\eta]^{NMP,30C}$	IEC (mmol/g)
3FS-0	0.7	--
3FS-20	0.9	0.5
3FS-30	1.4	0.81
3FS-40	1.4	1.0
6F-0	0.6	--
6FS-20	0.8	0.59
6FS-30	1.4	0.87
6FS-40	1.7	1.16
6FS-50	1.6	1.50

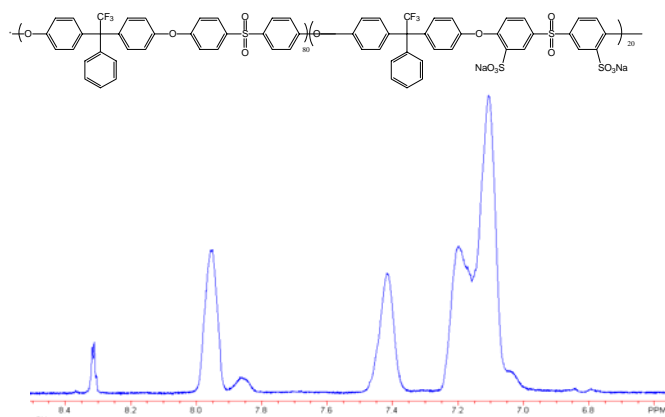


Figure 2. Proton NMR of 20mol% disulfonated 3F bisphenol based sulfonated poly(arylene ether sulfone) copolymer

Separate research from our group have shown that 6F bisphenol A containing membranes produced membrane electrode assemblies with lower high frequency resistance (HFR) than comparable wholly aromatic (biphenol based) membranes. The lower interfacial resistance was attributed to the partially fluorinated copolymer surface having better adhesion with the Nafion based electrodes. The 3F bisphenol was investigated to allow for insight on the ‘amount’ of fluorination needed in the copolymer composition (bulk and surface) to produced the observed performance enhancement.

Conclusion

New 3F bisphenol-based sulfonated poly(arylene ether sulfone) copolymers were synthesized and characterized. The sulfonated copolymers produced tough, ductile films.

Acknowledgements. The authors would like to thank the Department of Energy and the National Science Foundation for funding.

Polymer Electrolyte Membranes: Blends of Sulfonated Polystyrene and Poly(vinyl alcohol-co-ethylene)

Sarjit Kaur*, Ryan Callery, Sarah Tighe, Glenn Dale

*Chemistry Department, Vassar College, 124 Raymond Ave.,
Poughkeepsie, NY 12604-0287

INTRODUCTION

Many polymer electrolyte membranes, PEM, are obtained through post sulfonation of aromatic polymers with the goal to obtain both high ionic conductivity and mechanically strong films. This approach has some drawbacks that include difficulties in attaining high enough sulfonation, variability in sulfonation between batches and random sulfonation of aromatic rings. Sulfonated polystyrene (SPS), sodium salt, is available commercially and contains a para-substituted sulfonate group on each benzene. However, SPS is useless as a PEM because it is soluble in water. The goal of this work was to blend SPS with hydroxyl containing polymers to see if solubility of SPS can be reduced in water. Intermolecular polymeric interactions between hydroxyl groups and sulfonate groups can be expected to give miscible blends, with the added advantage that the polar environment will also contain OH groups that could endow a certain degree of inherent hydration. Blends of SPS were attempted using polyvinyl alcohol (PVA), 27 mol % PVACE (poly(vinyl alcohol-co-ethylene)) and 44 mol % PVACE. Three solvent systems were tried to cast the blends, and these included NMP, NMP/water and isopropanol/water. The blends were characterized by physical appearance before and soaking in water, thermal gravimetric analysis (TGA), differential scanning calorimetry (DSC), FTIR spectroscopy, SEM and water uptake studies.

EXPERIMENTAL

All materials were purchased from Sigma Aldrich Co, and used as received. PVACE is a copolymer, and 27 mol. % and 44 mol. % values correspond to the amount of the ethylene component in the polymer. FTIR spectra were collected using a Nexus FTIR model number 670 with an Attenuated Total Reflectance (ATR) thunderdome accessory. Spectra were collected using 32 scans and 2 cm^{-1} resolution. Thermal gravimetric analysis (TGA) and differential scanning calorimetry (DSC) were collected on Shimadzu TGA-50 and DSC-50 model instruments, respectively. The second runs on the DSC are reported.

Blends of SPS and PVA were cast from 5 wt. % polymer solutions to give a range of blends from 25 to 75 wt. % SPS. As expected, clear intact films were obtained upon evaporation of solvents, though these membranes absorbed water easily. The 75 wt. % blend came close to dissolving when soaked in water at room temperature (RT) for 24 hours, while the 25 wt. % and 50 wt. % SPS blends became gelatinous. Blends were also cast using 27 mol. % and 45 mol. % PVACE using a co solvent system (50/50 water/isopropanol). In this case, the polymer solutions were heated to 60 °C to allow dissolution, and different combinations of the two polymer solutions were mixed, warmed to 60 ° to obtain a homogenous solution, allowed to cool slowly to room temperature and left to evaporate at room temperature which generally took a day. (The stock solutions remained clear at room temperature for about 24 hours before becoming increasingly cloudy). All the blends from 44 mol % ethylene PVACE were opaque, while 25 wt. % SPS in 27 mol% PVACE was intact and slightly hazy (the higher wt.% SPS blends were significantly more cloudy, though remained intact). Following these results, lower SPS wt. % blends of 10, 15, 25 and 35 were cast using 27 mol% PVACE. The blends were also cast from polymer stock solutions in NMP and 50/50 NMP/water. Sodium SPS in NMP

was obtained by dissolving the polymer in water, addition of an equal amount of NMP, followed by removal of water at room temperature using high vacuum (0.2 mmHg).

RESULTS/DISCUSSION

Blend Appearance. Blends from PVA and sodium SPS were clear and intact upon casting but, not unexpectedly, absorbed water readily at RT. The 50 and 25 wt. % SPS blends did not completely dissolve but gave a slimy gelatinous material. To improve the mechanical integrity of the blends in water, copolymer PVACE were blended next with sodium SPS. PVACE was selected because it is readily available and the ethylene component lends a certain degree of hydrophobicity to the blends that would be expected to reduce solubility. The degree of hydrophobicity could be varied using different mol. % PVACE (the 27 % and 44% were selected for this study). Polymer blends in the range of 25 and 75 wt/ % of sodium SPS were cast from three different solvent systems (50/50 water/isopropanol, NMP and 50/50 NMP). Blends cast from 50/50 water/isopropanol solvent gave fairly brittle and opaque samples. It was thought that the solvent may have dried too quickly. Therefore, blends were cast from the other two solvent systems. All the blends from the 40 mol. % PVACE were opaque and initially intact films-became brittle upon standing, presumably when the blends are drier. With the 27 mol. % PVACE that has a higher content of hydroxyl groups, blends ≥ 50 wt % SPS were relatively opaque but intact films. The 35 and 25 wt. % blend sample were less opaque, with the latter only showing slight haziness. The results indicated increasing miscibility with lower wt. % sodium SPS in the blends. As a result, blends containing 10 and 15 wt. % SPS blends were also cast, and these were clear and intact films, suggesting miscibility. Water uptake studies were carried on the reasonably clear and intact blend films, the 10 and 15 wt. % samples absorbed 30-32 wt. % water, while the 25 wt. % SPS blend absorbed slightly higher (38%). The clear blends were also evaluated by soaking in water overnight at room temperature; blends remained intact, though become slightly cloudier that could be the onset of phase separation or development of crystallinity.

FTIR Studies. The blends that appeared to be miscible based on visual inspection were also characterized by FTIR ATR analysis (see OH region in Figure 1). There is an apparent decrease in the absorbance of the OH band with increasing wt. % of SPS, which is expected because of the varying OH concentration in the blends. However the OH region of the blends do not show any apparent shift or broadening upon blending, leading to the conclusion that the hydrogen bonding interactions in the blends are qualitatively comparable to intermolecular interactions present in PVACE. Given that the sulfonic acid form of SPS is most relevant for PEM applications, the 25 wt. % sodium SPS blend was converted to the acid form by soaking in 2 M sulfuric acid overnight at room temperature, followed by careful washing in distilled water and dried overnight at room temperature under high vacuum. Figure 2 shows the FTIR spectra of the 27 mol. % PVACE, and the sodium and acid forms of the 25 wt. % SPS blend. The sodium form of the blends shows a S=O asymmetric stretch at 1136 cm^{-1} (corresponding to salt form of sulfate) in addition to the expected PVACE peaks. Upon acidification, there are several changes: broadening of OH region; new peaks at 1389 and 1194 cm^{-1} corresponding to asymmetric S=O asymmetric and symmetric stretches; doublet at 861 and 898 cm^{-1} . The presence of the latter doublets is suggestive of S-O-C, which implies that there could be some condensation of OH and sulfonic acid.² Further studies are underway to clarify between organic sulfonate and sulfonic acid groups.

Thermal Studies. The thermal properties of the blends that appear miscible are reported in Table 1 and Figure 3 (peaks going

down are endothermic). TGA analysis showed some water loss about ~100 °C, followed only by degradation at higher temperatures. In terms of onset of degradation, the blends show a slightly earlier degradation (335- 366 °C) in contrast to 374 °C for PVACE copolymer. Presumably the presence of sulfonate groups appears to hasten degradation. DSC analysis showed two transitions, a glass transition that is fairly broadened (relatively difficult to discern in Figure 3) and a melting endotherm. The same two transitions are also observed in the blend samples. While no apparent change in T_g was observed, there is a decrease in the melting endotherm by about 7 °C that can be correlated to blending of the two polymers. The results indicate that SPS is being incorporated into the polar hydroxyl component of PVACE, and the hydrophobic is relatively undisturbed upon blending of the sodium SPS, as inferred by the lack a change in the T_g . Percent crystallinity and SEM studies are currently in progress to obtain further insight into the morphology of the blends.

CONCLUSION

Miscible blends containing between 10 to ~35 wt. % SPS were obtained with 27 mol. % PVACE. These blends remain intact when soaked in water, though became slightly more opaque, which could be attributable to phase separation or increasing crystallinity. Impedance studies will be conducted in future work to evaluate conductivity of membranes. For the most part, the higher hydrophobic content of 44 mol % in PVACE did not favor miscibility.

Table 1. Thermal Analysis of 27 mol% PVACE and Blends.

°C	Polymers		Blends (wt, % SPS)			
	PVACE	SPS	10	15	25	35
Degradation	374	395	351	335	366	346
T_g	58	-	59	58	58	-
T_m	187	-	182	181	181	-

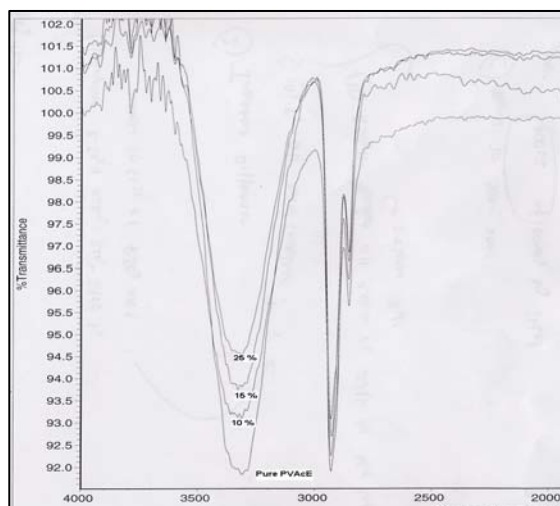


Figure 1. FTIR spectra of PVACE and 10, 15, 25 wt.% SPS blends.

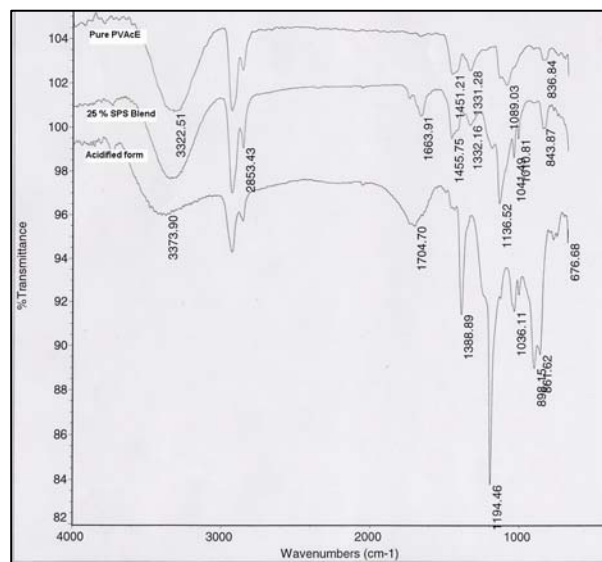


Figure 2. FTIR spectra of PVACE copolymer, 25 wt. % sodium SPS blend and acid form of 24 wt.% SPS blend.

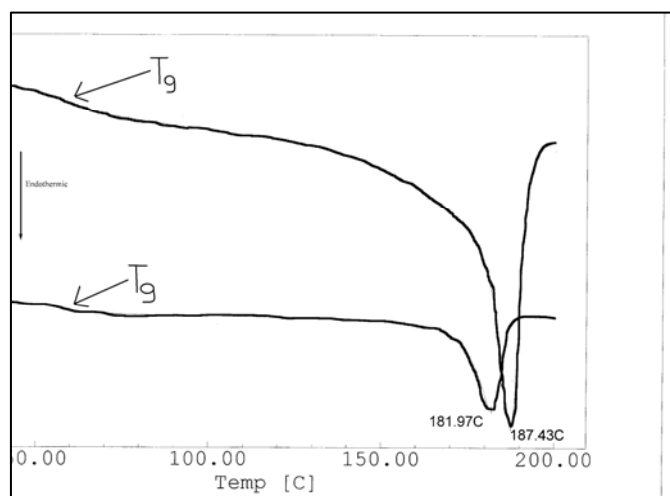


Figure 3. DSC scan of 27 mol. % PVACE (top scan) and 10 wt. % SPS blend (bottom scan)

References

- (1) Young, T.; Hsieh, C.; Chen L.; Huang, Y. *Journal of Membrane Science*, **1999**, 159 (1-2), pp 21.
- (2) Silverstein, R. M.; Bassler, G. C.; Morrill, T. C. *Spectrometric Identification of Organic Compounds*, 5th Edition Wiley: New York, 1991.

Sulfonated diels-alder polyphenylenes: Synthesis and properties of a novel polyelectrolyte

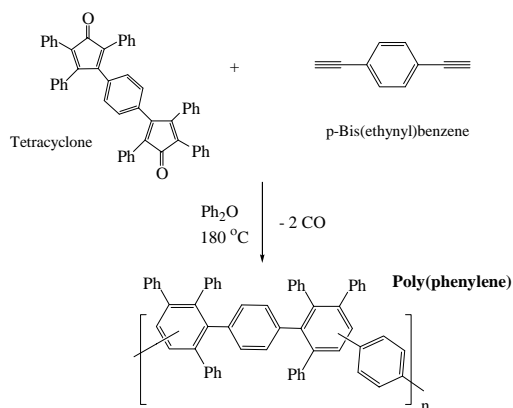
Chris J. Cornelius and Cy H. Fujimoto

Chem and Bio Technologies, Sandia National Laboratories,
Albuquerque, New Mexico 87185-0888.

Introduction

The physical property limitations of perfluorinated polymer electrolyte membrane (PEM) such as Nafion are represented by its poor mechanical properties at temperatures above 80°C, high methanol flux in DMFCs, proton conductivity at elevated temperatures, and material cost has driven research in the area of alternative polymer electrolytes.^{1,2,3}

Polyphenylenes represent a promising class of thermoplastics, which demonstrate the potential of being used as a PEM within a fuel cell. Furthermore, polyphenylenes synthesized through Diels Alder (DA) polymerizations have the advantages of thermal stability, while maintaining organic solubility making it possible to form mechanically robust films.^{4,5,6} The chemistry afforded by the parent DA polyphenylene represents a system that has tunable chemical structure and the potential of adding six sulfonic acid moieties per repeat unit.



Scheme 1. Preparation of DA Polyphenylene.

We report here some of the physical properties and preliminary hydrogen and methanol fuel cell performance data of this sulfonated Diels-Alder polyphenylene (SDAPP).

Experimental

Membrane Preparation. 0.5 g of sulfonated DA polymer was casted on a clean glass plate as the sodium salt form in 10 mL of NMP. The cast was left to evaporate at 80 °C under a constant flow of N₂ for 12 hrs. The film was then dried at 100 °C under vacuum for 24 hrs and acidified (soak in 2M H₂SO₄ for 24 hrs)

Ion-Exchange Capacity. 0.2 g of acidified polymer was dried and weighed. The sample was then treated with 10 mL of 0.1 M NaOH and stirred for 24 hrs. The sample was then filtered and titrated against 0.01 M HCl.

Water Uptake. The acidified films were immersed in DI water for 24 hrs. at 25 °C. They were then blotted dry and weighed (W_s). The films were then dried and weighted until a

constant weight was achieved (W_d). Water uptake was calculated by:

$$\text{Water uptake} = [(W_s - W_d) / W_d] \times 100\%$$

Proton Conductivity. The conductivities were determined in fully hydrated films by AC impedance spectroscopy over a frequency range of 1x10³ Hz to 1x10⁶ Hz using a Solartron 1260 gain phase analyzer and Solartron 1287 potentiostat at 25°C in deionized water.

Fuel Cell Testing. Polarization curves of the membranes were taken on a Fuel Cell Technologies instrument using ultra-pure H₂ and O₂ as reactant gases.

Results and Discussion

Sulfonated DA polymers were readily cast into films from NMP. These films were mechanically robust and were creasable after drying in a vacuum oven.

The films displayed proton conductivities ranging from 10-80 mS/cm while still maintaining mechanical stability.

IEC (meq/g)	Water uptake (weight %)	λ (H ₂ O/SO ₃ H)	Conductivity (mS/cm)
0.98	21	12	8
1.4	36	14	52
1.6	75	19	78
2.2	137	30	115

Fuel cell performance data indicated that the sulfonated DA polymers could obtain high power levels and current densities of 1000 mW/cm² at 2000 mA/cm² at 80°C with pure oxygen.

Acknowledgement. Sandia is a multiprogram laboratory operated by Sandia Corporation, a Lockheed Martin Company, for the United States Department of Energy's National Nuclear Security Administration under contract DE-AC04-94AL85000.

References:

1. Savadogo, O. J. *New Mater. Electrochem. Syst.* **1998**, 1, 47.
2. Rikukawa, M.; Sanui, K. *Prog. Polym. Sci.* **2000**, 25, 1463.
3. Steck, A.; Stone, C. Proceedings of the Second International Symposium on New Materials for Fuel Cell and Modern Battery Systems.
4. Stille, J. K. *J. Macromol. Sci. Chem.* **1969**, 3, 1043.
5. Neenan, T. X.; Kumar, U. *Macromolecules.* **1995**, 28, 124.
6. Fujimoto, C. H.; Loy, D. A.; Wheeler, D. R.; Jamison, G. M.; Cornelius, C. J. *Polymer Preprints.* **2002**, 43, 2, 1376.

Composite Membrane-Based PEMFCs for Operating at Elevated Temperature and Reduced Relative Humidity

Serguei N. Lvov, Mark V. Fedkin, Elena Chalkova, and Michael B. Pague

The Energy Institute & Department of Energy and Geo-Environmental Engineering, The Pennsylvania State University, 207 Hosler, University Park, PA 16802, lvov@psu.edu

Introduction

Proton exchange membrane fuel cells (PEMFCs) offer high promises as environmentally clean and highly efficient electric power sources for stationary and mobile applications. While the present-day PEMFCs are operated at temperatures below 100 °C, extension of the operating temperature range to 120-150 °C is desired for a number of technological reasons. Elevated temperature conditions are expected to reduce the need for noble metal catalysts, suppress CO poisoning, and eliminate water flooding at the cathode. High temperature fuel cell operation would also enhance the electrode reaction kinetics and thus boost the fuel cell efficiency. However, perfluorosulfonic acid polymer membranes (Nafion®), currently used in PEMFCs experience severe dehydration at temperatures above 100 °C, resulting in a decrease in proton conductivity and consequent drop of performance.

One of the approaches to suppress membrane dehydration is to impregnate the polymer with hygroscopic particles, e.g. metal oxides¹⁻³. Such composite solid oxide/Nafion membranes are known to have an increased water retention^{4,5} which helps the Nafion to preserve its functionality at high temperatures. In this study, we describe the properties of TiO₂/Nafion composite membranes and explore the limits of their applicability in PEMFCs over ranges of temperature and relative humidity (RH).

Experimental

TiO₂ properties. The TiO₂ (rutile) powder (Kronos Inc. 4020, Lot #60170) was sieved and cleaned under hydrothermal conditions (220°C) prior to use. The powder preparation was carried out at the Oak Ridge National Laboratory according to the procedure that was described in detailed elsewhere^{6,7}. Analytical characterization of the powder revealed the following properties: specific surface area - 2.914±0.004 m²g⁻¹ (BET); aggregates (3-50 μm in size) of anhedral or subhedral micron-size grains (SEM); phase - pure TiO₂ (rutile) with no detectable crystalline contaminants (XRD).

The Kronos TiO₂ was previously studied with respect to surface properties from 25 to 200 °C using the high temperature microelectrophoresis technique developed in our laboratory^{6,8}. According to these studies and also proton adsorption data obtained for a similarly treated TiO₂ powder sample^{7,9}, the TiO₂/water interface is positively charged under acidic conditions (pH<5.5 at 25 °C and pH<4.7 at 120 °C) and is characterized by a very high concentration of adsorbed protons. Based on several studies of the electrical double layer (EDL) at the TiO₂(rutile)/water interface including Multisite Complexation (MUSIC) modeling^{6,9,10} the terminal oxygen surface sites of rutile can accept up to two protons and are mainly protonated at the pH of the pore solution in the Nafion (~2-2.5). Since protons in the adsorption layer have hydration spheres of water molecules, TiO₂ is expected to be much more efficient water retainer compared to SiO₂, which remains virtually unchanged in acidic solutions.

Preparation of composite membranes and MEAs. The composite TiO₂/Nafion membranes were prepared using a procedure similar to that described elsewhere¹¹. An appropriate amount of commercial 5% Nafion solution (Aldrich) was mixed with a particular amount of TiO₂ powder (0, 5, 10, and 20 mass %), ultrasonicated, and cast in a Teflon dish. After solvent evaporation at 80 °C, resulting TiO₂/Nafion films were detached from the dish and hot-pressed at a pressure of less than 2 bars. The final treatment was at 150 °C for 10 minutes. The resulting membrane thickness was around 80 μm.

The membrane-electrode assemblies (MEAs) were prepared using a commercial gas diffusion solid polymer electrolyte electrode of Los Alamos type (ELAT) with double-side coatings. Electrode specifications were as follows: Pt loading 0.5 mg·cm⁻² with 20% Pt on Vulcan XC-72 as a catalyst, Nafion loading 0.8 mg·cm⁻², and standard PTFE loading. MEAs were prepared by pressing the electrodes onto the membrane in a Carver hot press at 130 °C and 50 bar for 40 seconds.

Membrane testing. The composite TiO₂/Nafion membranes were tested for proton conductivity and fuel cell performance.

The proton conductivity of the composite membranes fully hydrated in water was determined in a temperature range from 20 to 140 °C using four-electrode AC impedance spectroscopy (Gamry Instruments). Each sample was mounted in an electrochemical cell and submerged in deionized water inside a Parr Autoclave. The impedance measurements were carried out after the membrane was fully saturated with water, and the water was equilibrated with the vapor phase. The details of the experimental method are described elsewhere¹². The membrane conductivity, σ , was calculated as $\sigma=l/rS$, where l is the distance between the electrodes, r is the measured resistance of the membrane (at 1 kHz), and S is the cross-sectional area of the membrane perpendicular to the current flow.

The fabricated MEAs were tested in an ElectroChem H₂/O₂ fuel cell, which is capable of operating at temperatures up to 130 °C and at pressures up to 3.5 bar. To ensure the consistency of fuel cell operation, temperature, gas flow rate, H₂ and O₂ pressures, RH, and compaction force used for fuel cell arrangements were kept the same in parallel tests. The fuel cell tests were performed at 80 and 120 °C, at 26, 50, 80, and 100% RH with the total pressure (reactant gas and water vapor) of 3 bar.

Results and Discussion

The highest proton conductivity was obtained for the 5 mass % TiO₂/Nafion membrane. The conductivity value obtained for this membrane exceeded the conductivity of the unmodified Nafion membrane by 5-60% in the temperature range 20 to 140 °C (Fig. 1). The conductivity of the unmodified Nafion membrane was still higher than the conductivity of membranes with 10 and 20 mass % of TiO₂ at temperatures below 110 °C. For all studied membranes, the conductivity started to decrease as temperature was increased above 110 °C, however composite membranes showed much less degradation compared the unmodified Nafion membrane. The observed improvement in membrane conductivity is attributed to (1) hygroscopic effect of the TiO₂ particles (since the water retained in the EDL at the TiO₂/water interface can be used for proton solvation inside Nafion) and (2) surface proton conductivity of TiO₂ under the conditions of complete protonation¹³.

The performance of the TiO₂/Nafion composite membranes in the H₂/O₂ PEMFCs was evaluated based on cell voltage vs. current density (polarization) curves. The effects of the TiO₂ content and RH on the PEMFCs performance were studied at temperatures of 80 and

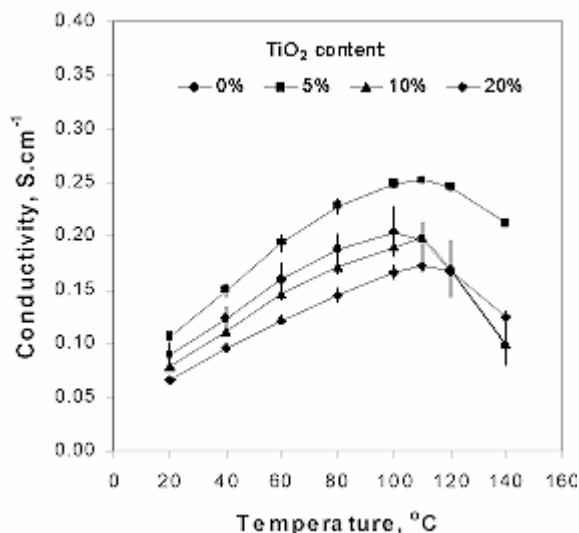


Figure 1. Proton conductivity of bare Nafion and TiO₂/Nafion composite membranes in water as a function of temperature.

120 °C. At 80 °C, the TiO₂ content had no significant effect on the PEMFC performance over the entire range of RH used (from 26 to 100%). However, the situation apparently changed when the same membranes were tested at 120 °C. In this case, the fuel cell performance was significantly affected by both TiO₂ content and RH (Fig. 2). When the TiO₂ content increased from 0 to 20%, the current density delivered at cell voltage of 0.6 V was increased, respectively, 3, 5.8, 1.6, and 1.1 times at 26, 50, 80, and 100% RH. The effect of RH (26 to 100%) was significant for the unmodified Nafion membrane, while the performance of the TiO₂/Nafion composite membranes was not affected by RH reduction within 50-100%. For the unmodified Nafion membrane, the maximum power density progressively dropped with decreasing RH from 100 to 26%. For the 10%-TiO₂/Nafion and 20%-TiO₂/Nafion membranes, the maximum power density stays on a plateau down to RH=50%. These results show that composite membranes are able to operate at RH 50% as efficiently as Nafion operates at RH 100%. This advantage can be attributed to the enhanced water retention properties of TiO₂ particles. Hydrophilic TiO₂ evidently improved the water retention properties of the membranes and, therefore, their hydration, which in turn favors the Nafion proton conductivity. Improvement of membrane water retention becomes more important at reduced relative humidity, when the Nafion polymer readily loses water.

Conclusions

The composite membranes showed a significant advantage over unmodified Nafion membranes, confirming that hydrophilic TiO₂ particles dispersed in the membrane provide better water retention than bare Nafion polymer at a reduced RH. The performance of the composite Nafion/20% TiO₂ membrane at 120 °C and 50% RH was comparable to the performance of the unmodified Nafion membranes at 80 °C and 100% RH, which means that the use of the new composite membrane allows increasing the operating temperature of the PEMFC from 80 to 120°C (at 50% RH) without significant performance loss.

Acknowledgement. This study was supported by DOE (Contract #DE-FC36-01GO11085). The authors thank David Wesolowski for providing TiO₂ powder and useful discussions.

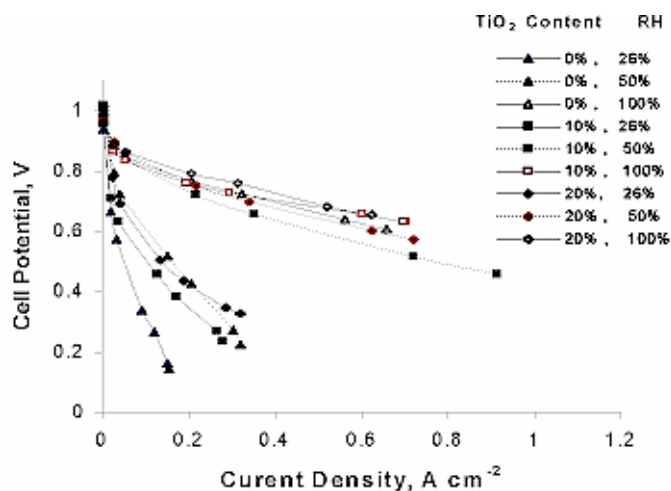


Figure 2. Performance of PEMFC operated with TiO₂/Nafion composite membranes at different relative humidities at 120°C.

References

- (1) P.L. Antonucci, A.S. Arico, P. Creti, E. Ramunni, V. Antonucci, *Solid State Ionics*, **1999**, *125*, 431.
- (2) N. Miyake, J.S. Wainright, R.F. Savinell, *J. Electrochem. Soc.* **2001**, *148*, A898.
- (3) K.T. Adjemian, S.J. Lee, S. Srinivasan, J. Benziger, A.B. Bocarsly, *J. Electrochem. Soc.* **2002**, *149*, A256.
- (4) A.S. Arico, V. Baglio, A. Di Blasi, P. Creti, P.L. Antonucci, V. Antonucci, *Solid State Ionics* **2003**, *161*, 251.
- (5) Li, Q., He, R., Jensen, J.O., and Bjerrum, N.J., *Chem. Mater.* **2003**, *15*, 4896.
- (6) M.V. Fedkin, X.Y. Zhou, J.D. Kubicki, A.V. Bandura, S.N. Lvov, M.L. Machesky D.J. Wesolowski, *Langmuir* **2003**, *19*, 3797.
- (7) M.L. Machesky, D.J. Wesolowski, D.A. Palmer, K. Ichiro-Hayashi, *J. Colloid Interface Sci.* **1998**, *200*, 298.
- (8) X.Y. Zhou, X.J. Wei, M.V. Fedkin, K.H. Strass, S.N. Lvov, *Rev. Sci. Instrum.* **2003**, *74*, 2501.
- (9) M.L. Machesky, D.J. Wesolowski, D.A. Palmer, M.K. Ridley, *J. Colloid Interface Sci.* **2001**, *239*, 314.
- (10) K. Bourikas, T. Hiemstra, W.H. van Riemsdijk, *Langmuir* **2001**, *17*, 749.
- (11) A.S. Arico, P. Greti, P.L. Antonucci, V. Antonucci, *Electrochim. Solid-State Lett.* **1998**, *1*, 66.
- (12) X.Y. Zhou, J. Weston, E. Chalkova, M.A. Hofmann, C.M. Ambler, H. Allcock, S.N. Lvov, *Electrochim. Acta* **2003**, *48*, 2173.
- (13) Lvov, S.N., Fedkin, M.V., Chalkova, E., Jayabalan, D.K., and Wesolowski, D.J., *Electrochim. Acta*, **2004** (submitted).

Degradation of PEMFC : sulfonated polyimides

Gilles Meyer, Carine Perrot, Laurent Gonon, Gérard Gebel, and Jean-Luc Gardette

Groupe Polymères Conducteurs Ioniques, DRFMC/SI3M UMR 5819
CEA-Grenoble, 17 rue des Martyrs, 38054 Grenoble cedex 9, France
* LPMM, UMR 6505, 63000 Aubière, France

Introduction

For the last decade Proton Exchange Membrane Fuel Cell (PEMFC) are of great interest for automotive and portable applications. Perfluorosulfonic acid membranes like Nafion are the reference materials because of their high ionic conductivities and chemical stability¹. On the other hand, these materials are too expensive, do not allow high temperature FC operation and exhibit a poor resistance to cycling FC conditions. As a consequence alternative nonfluorinated hydrocarbon membranes are developed, essentially by introduction of sulfonic acid groups on thermostable aromatic polymers^{1,2}. However, the chemical, electrochemical or physical evolution limits the lifetime in FC conditions. It is worth noting that the operating times are not always specified and never correlated to the ageing extent of the membrane.

Sulfonated polyimides (sPI) are considered as promising ionic conductive polymers for fuel cell applications³. While most sulfonated polymers are prepared by post-sulfonation² sPI used in this study were obtained by direct polymerization using sulfonated monomers. It allows the control of the quantity and distribution of ionic groups along the polymer chains.

To take into account the influence of the molecular structure of the macromolecules, a series of sPI membranes were studied in FC under stationary operating conditions. The membrane lifetimes were determined and the chemical modifications induced on the macromolecule were quantified by IR spectroscopy. In addition, after *ex-situ* ageing experiments, IR and mechanical analyses were performed to confirm the degradation mechanism involved in FC.

Experimental

Materials. The synthesis of sPI block copolymers (**Figure 1**) is described in details elsewhere⁴. These polymers are characterized by X=5 as sulfonated block size and the size of the hydrophobic sequence (Y) is adjusted to control the Ionic Exchange Capacity (IEC) of the membrane. IEC is defined as the molar amount of sulfonated groups per gram of polymer. The membranes tested have a Y value of 5, 12 or 21 to reach an IEC of 2, 1.3 and 0.9 meq.g⁻¹, respectively. The membrane will be referenced as follow : IEC/X-Y.

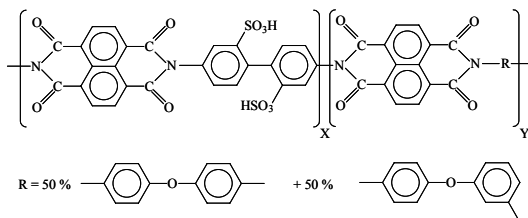


Figure 1. sPI chemical structure

Fuel cell experiments. The lifetimes of sPI in FC were determined using a specially designed bench and a 25 cm² active area single cell. The electrodes were provided by Sorapec, and the catalyst loading was 0.1 mg.cm⁻² at the anode and 0.2 mg.cm⁻² at the cathode. A gasket of 0.28 mm surrounded each electrode to avoid

leaks of gases. The cell was pressed with a couple of about 7 N.m to enhance the electrode-membrane contacts and therefore to minimise the ohmic drops at the interface. The gas inlets were 27 cm³/min for hydrogen and 42 cm³/min for oxygen. The tests were performed under a constant current density of 200 mA.cm⁻², at 3 bar absolute gas pressure and a cell temperature ranging from 60 to 90°C. The end of each test corresponded to the mechanical rupture of the membrane evidenced by an abrupt potential drop to 0 V due to a H₂/O₂ gas mixing.

Characterization methods. The mechanical properties were determined on test pieces 0.95 mm width and 4.25 mm long using an Instron 4301 tester, with a traction speed of 3 mm per minute. The samples were studied soaked in water at room temperature in order to control the swelling degree of the membrane. Plastic extensions were calculated as the difference between extensions at rupture and at the beginning of the plastic zone.

FTIR-ATR spectra were recorded on a Nicolet 55XC spectrometer, with a Thunderdome accessory and a germanium crystal. The surface analysis was about 5 mm².

Ionic conductivities of membranes equilibrated in water were measured by impedancemetry using a cell equipped of mercury electrodes.

Results and Discussion

The properties of the polymer membranes tested in the present study and their performances in FC are summarized in **Table 1**. As expected, the cell voltages are directly connected to the ionic conductivity of the membrane. The cell voltage thermal dependence observed for the sPI 1.3/5-12 can be attributed to a non optimized water management. Both the lifetime and performances are strongly related to the IEC value, but in opposite ways. Based on the three studied samples, the lifetime dramatically decreases for IEC values larger than 1.3. Correlatively, the FC performances drops for IEC values lower than 1.3. As a consequence, the IEC value of 1.3 appears as the best compromise for FC operation.

sPI	Thickness (μm)	Conductivity (S/cm)	T (°C)	U (mV) (200 mA.cm ⁻²)	Lifetime (hours)
0.9/5-21	87	0.6.10 ⁻²	80	400	600
			70	670	600
1.3/5-12	75	1.9.10 ⁻²	80	640	300
			90	580	150
			60	700	270
2/5-5	60	2.6.10 ⁻²	70	700	100
			80	690	30
			80	690	30
			90	695	10

Table 1. Results of ionic conductivity and fuel cell measurements

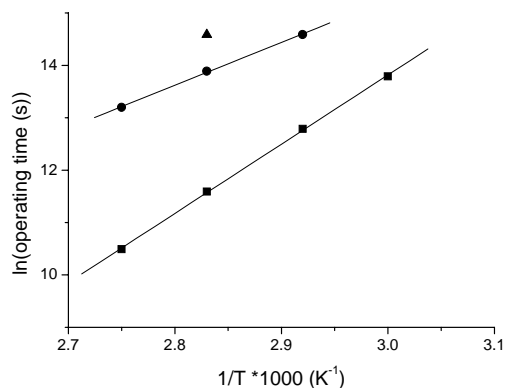


Figure 2. Evolution of the operating times with temperature on an Arrhenius graph for sPI 0.9/5-21 (▲), 1.3/5-12 (●) and 2/5-5 (■) membranes.

The lifetimes represented in an Arrhenius plot exhibit a linear trend (**Figure 2**) characteristic of a thermo-activated process. The activation energies are 72 and 111 $\text{kJ}\cdot\text{mol}^{-1}$ for an IEC of 1.3 and 2 $\text{meq}\cdot\text{g}^{-1}$ respectively. From **Figure 2**, the lifetime of the membrane can be extrapolated to lower temperatures (4000 hours at 40°C for a IEC = 1.3 $\text{meq}\cdot\text{g}^{-1}$). Ion of the curve at low temperatures suggests that these polymers can be used for low temperature PEMFC since it gives an operating time of sPI.

The water produced after fuel cell operation is lyophilized and the residues were analyzed by IR spectroscopy. The absence of the characteristic absorption bands from the hydrophobic sequence suggests the degradation mainly occurs on the sulfonated blocks.

FTIR-ATR analyses were performed on both sides of the 0.9/5-21 sPI tested 600 hours at 80°C . Difference spectra (aged – reference) for both anode and cathode sides are reported on **Figure 3**. Significant differences appear between the two spectra. On the cathode side, the major phenomenon is a decrease of the absorption bands characteristic of the polymer, particularly the one at 1350 cm^{-1} revealing a hydrolysis of imide functions. Assuming that hydrolysis is limited to the ionic segments, the loss of imide groups of these blocks can be estimated to 74%. On the anode side, the same phenomena is detected. However one can notice the appearance of new absorption bands in the carbonyl region suggesting either an oxidative process or a partial hydrolysis of the imide rings.

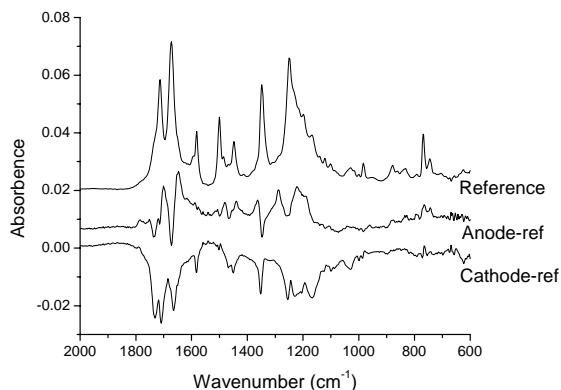


Figure 3. Infra-red spectra (ATR, crystal Ge) of the sPI 0.9/5-21 before and after 600 hours at 80°C of operation in fuel cell.

IR determination of the IEC from the absorption at 1580 cm^{-1} revealed a quasi total disappearance of the sulfonic groups at the cathode side, whereas it is nearly unchanged at the anode one. As water is produced at the cathode, an elution process of the degradation products can take place.

The mechanical properties of sPI membranes were determined after *ex-situ* ageing in water at 70 and 90°C . The plastic extensions measured as function of degradation time are given in **Figure 4**. As expected, the hydrolysis of the imide functions leads to chain scissions and as a consequence to a loss of the mechanical properties.

The evolution of the mechanical properties versus IEC and temperature exhibits the same trend than the results obtained in FC tests and *ex-situ* degradation kinetics by IR.

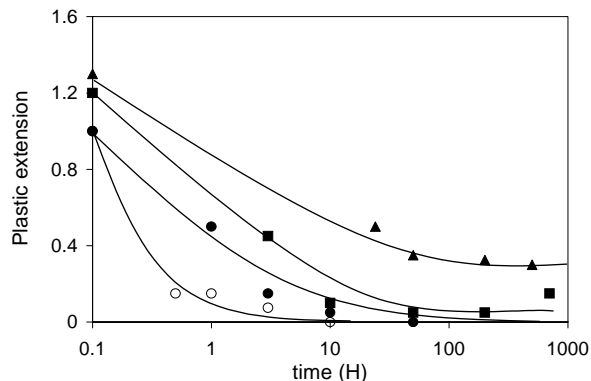


Figure 4. Evolution of the plastic extension with hydrolysis time : sPI 0.9/5-21 at 70°C (▲), 1.3/5-12 at 70°C (■), 2/5-5 at 70°C (●) and 90°C (○)

Conclusions

The stability of sPI was studied in FC and *ex-situ* conditions. While a good correlation between an in-situ and *ex-situ* experiments was established, ageing appears accelerated in FC. IR and mechanical experiments have pointed out that hydrolysis of the imide ring leading to polymer chain scissions is the major degradation process. Therefore, the sPI stability can be significantly improved by reducing hydrolytic sensitivity.

Acknowledgements. The authors would like to acknowledge the LMOPS (R.Mercier) for the polymer synthesis, the CEA-Le Ripault/DMAT for the membrane preparation and the CEA Grenoble /DTEN for their help in membrane FC testing.

References

- (1) Savadogo, O.; *J. Power Sources*, **2004**, *127*, 135.
- (2) Rozière, J.; Jones, D.J.; *Annu. Rev. Mater. Res.*, **2003**, *33*, 503
- (3) Besse, S.; Capron, P.; Diat, O.; Gebel, G.; Jousse, F.; Marsacq, D.; Pinéri, M.; Marestin, C.; Mercier, R.; *J. New Mat. Electrochem. Syst.*, **2002**, *5*, 109
- (4) Genies, C.; Mercier, R.; Sillion, B.; Cornet, N.; Pinéri, M. *Polymer*, **2001**, *42*, 359

PROTON EXCHANGE MEMBRANES BASED ON COMPOSITES OF SULFONATED POLY(ETHER KETONE KETONE) AND CROSSLINKED SULFONATED POLYSTYRENE PARTICLES

Jeffrey V. Gasa¹, S. Boob¹, R.A. Weiss,^{1,2} and Montgomery T. Shaw^{1,2}

¹Polymer Program and ²Department of Chemical Engineering
Institute of Materials Science, University of Connecticut, Storrs, CT
06269-3136

Introduction

An elegant solution to the fueling problem of proton-exchange membrane (PEM) fuel cells running on hydrogen is to modify the cell design for operation on a liquid fuel, for example, methanol. This is of particular importance to transportation and portable power supply applications. For portable fuel cells, polymers can provide simplicity of design and reliable performance, in addition to the usual attributes of light weight and low cost. The main polymer challenge for fuel cells operating on methanol is the improvement of the methanol/oxygen barrier properties of the proton-exchange membrane without compromising other essential properties, specifically, proton conductivity.¹

We have reported recently that proton conductivities and MEA performance comparable to Nafion®, which is the benchmark, can be achieved with membranes based on the high-performance polymer poly(ether ketone ketone) PEKK, and its blend with poly(ether imide).^{2,3} At present, our research has focused mainly on improving the transport and mechanical properties of sulfonated PEKK (SPEKK) membranes. The approach of the research presented herein was to use relatively low sulfonation levels of SPEKK (about 1 meq/g) to minimize water uptake and maintain low methanol/oxygen permeability of the membrane. However, SPEKK with low sulfonation level also has low proton conductivity.^{2,3} To enhance proton conductivity, crosslinked sulfonated polystyrene (XLSPS) particles that have very high sulfonation levels (about 5 meq/g) were used as an additive. It has been demonstrated in the past by Chen et al. that non-conductive polymer blends can have excellent proton conductivities when mixed with XLSPS microspheres.^{4,5} However, they did not include sulfonated matrices in their study. Our hypothesis is that the sulfonic acid groups in the matrix will tend to cluster around the particles to reduce interfacial energy, and provide a highly acidic path for proton movement.

Experimental

Materials. The acid polymer of principal focus in this study was sulfonated PEKK (SPEKK). The PEKK used was OXPEKK-SP (Oxford Performance Materials, New Britain, CT), which has a T/I ratio of 6/4. Sulfonation was achieved by dissolving the polymer (5% w/v) in a mixture of 53/47 (v/v) concentrated sulfuric acid and fuming sulfuric acid. The sulfonation time and temperature were varied to achieve different levels of sulfonation, expressed here in terms of ion-exchange capacity (IEC). Crosslinked sulfonated polystyrene (XLSPS) beads used were Dowex Marathon® C (Aldrich Chemical Company, Inc). These 380-500 μm beads were thoroughly washed with de-ionized water to remove residual sulfuric acid. After drying these beads at 100 °C in vacuum for 1 day, they were ground in a mill and sifted. Particle sizing was done in a 400 mesh sieve to obtain particles of size 37 μm and smaller. The ion exchange capacity of the particles was measured by titration and was found to be about 5.2 meq/g.

Membrane Preparation. SPEKK and XLSPS particles (at various weight ratios) were mixed using N-methyl pyrrolidone (NMP) as a solvent to form 5% polymer solutions. The SPEKK dissolved while the XLSPS particles remained in suspension. These

solutions were cast onto clean glass plates at 60 °C and air dried in a hood until most of the solvent had evaporated. After drying, the membranes were soaked in de-ionized water at 60°C for 6 h to remove residual solvent.

Impedance Spectroscopy. The proton conductivity of the membranes was measured by impedance spectroscopy using a Solartron® 1260 impedance analyzer over a frequency range of 1-10⁶ Hz. The applied voltage was 50 mV. Membrane conductivities were measured using a cell described by Zawodzinski et al.⁶

Water Uptake Measurements. The membranes were kept in a controlled humidity environment and weighed every 24 h until the mass of the membranes reached equilibrium values. The membranes were then dried in vacuum at 100 °C for 24 h and weighed. The water uptake values reported were calculated on a wet basis.

Electron Microscopy. The morphology of the composite membranes was studied using an environmental scanning electron microscope (ESEM). The composite membranes were cryo-fractured in liquid nitrogen and micrographs of the cryo-fractured section through the thickness were taken.

Results and Discussion

Proton Conductivity. The conductivities of the SPEKK-XLSPS composite membranes at 20 °C and 98 % relative humidity (Figure 1) exhibited a sigmoidal dependence on XLSPS weight fraction for both sulfonation levels of the SPEKK matrix.

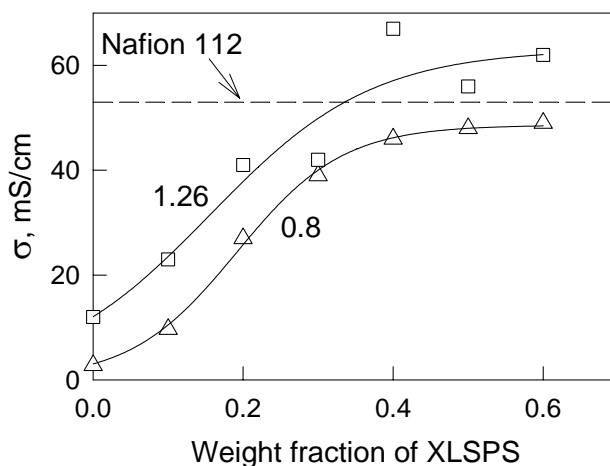


Figure 1. Proton conductivity of the membranes at 98% relative humidity and 20 °C. The values indicated in the graph pertain to the IEC of the SPEKK matrix in meq/g. The solid lines represent 3-parameter sigmoidal fits of the data.

Water Uptake. As shown in Figure 2, the relationship between water uptake and XLSPS weight fraction is almost linear, although there is a slight curvature. The slopes of the λ values (proportional to the second derivatives of the water uptake curves) for both sulfonation levels were significant ($P < 0.01$) and were statistically the same. As expected, the composites containing higher-IEC SPEKK (1.26 meq/g) matrix have higher water uptakes than the lower-IEC (0.8 meq/g) counterpart but there was no significant difference in the λ values, which is the water to sulfonic acid mole ratio. Figure 4 compares the water uptakes of the pure SPEKK membranes with those of the composite membranes. The IEC of the composites shown in Figure 4 are weight-average values calculated from the ion-exchange capacities of the pure components. At low IEC values

(below 1.5 meq/g), the water uptake of the composites is almost identical to that of pure SPEKK. However, at IEC values above 1.5 meq/g, the slope of the latter increases with increasing IEC while the slope for the former has an opposite trend.

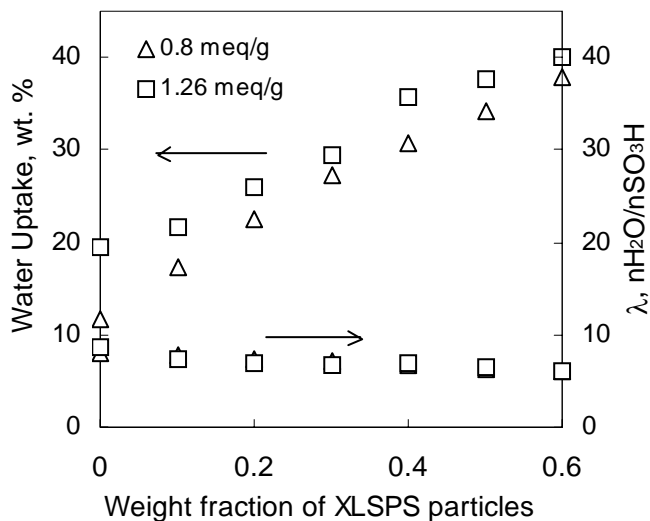


Figure 2. Water uptake of the SPEKK-XLSPS composite membranes at 98% relative humidity and room temperature. The IEC values indicated in the graph pertain to the IEC of the SPEKK matrix.

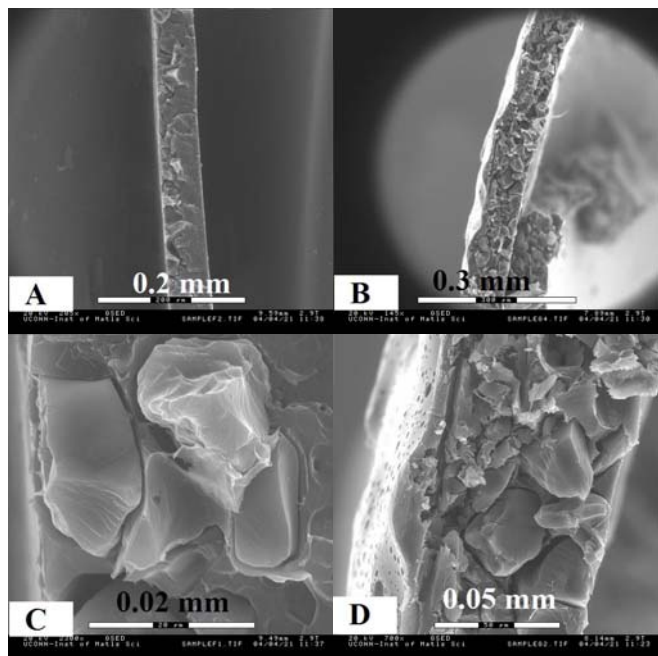


Figure 3. ESEM micrographs of a cryo-fractured section of SPEKK-XLSPS composite membranes at two different weight fractions of XLSPS: A) 0.2 and B) 0.5. The micrographs labeled C and D are the same micrographs as A and B, respectively, but at a higher magnification.

Morphology of the Composite Membranes. ESEM micrographs of cryo-fractured sections of the composite membranes are shown in Figure 3. For high weight fractions of particles (above 0.2), the dispersion of the particles in the SPEKK matrix was fairly uniform. However, at low weight fractions, the particles settled and

accumulated on one side of the membrane. This can be beneficial if it is desired that the particles be concentrated on just one side (cathode or anode) of the fuel cell. For example, if the particles are less stable in oxygen environment than the SPEKK matrix, it is desirable that the particles concentrate on the side opposite to the oxygen side.

Conclusions

It has been demonstrated in this study that conductivity of low-IEC SPEKK membranes can be enhanced dramatically by the addition of highly acidic polymeric particles (XLSPS). We are presently investigating the mechanical properties of these composite membranes, as there are some indications of increase in toughness upon addition of the particles.

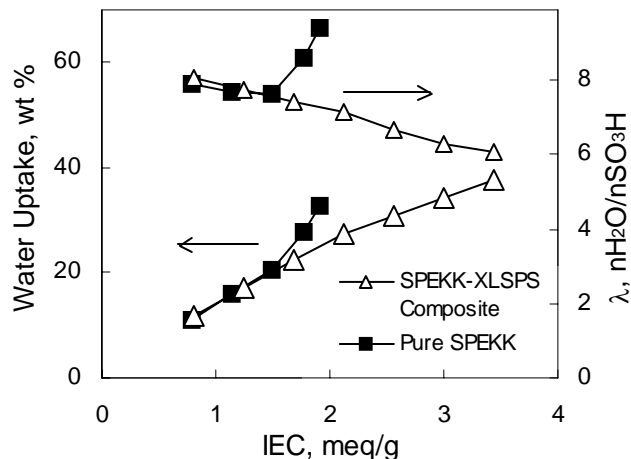


Figure 4. Comparison between the water uptake of pure SPEKK and that of the SPEKK-XLSPS composite membranes. The IEC of XLSPS was 5.2 meq/g while the SPEKK was 0.8 meq/g.

Acknowledgement. The authors gratefully acknowledge financial support from the Army through the Connecticut Global Fuel Cell Center.

References

1. Hoogers, G. *Fuel Cell Technology Handbook*. CRC Press LLC, 2003.
2. Chun, S., Shaw, M.T., Weiss, R.A., "Sulfonated Poly(ether ketone) Membranes," Asilomar Conference on Proton Exchange Membranes, February (2003).
3. Swier, S., Gasa, J., Shaw, M.T., Weiss, R.A. "Proton-exchange membrane materials based on blends of poly(ether ketone) and poly(ether imide)," Annual APS March Meeting, Montreal, Quebec, Canada, March (2004).
4. Chen, N.; Hong, L. *Solid State Ionics* **2002**, *46*, 377-385.
5. Hong, L.; Chen, N. *J. of Polym. Sci.: Part B: Polym. Phys.* **2000**, *38*, 1530-1538.
6. Zawodzinski, T.A., M. Neeman, Jr., L.O. Sillerud and S. Gottesfeld, *J. Phys. Chem.*, **1991**, *95*(15) 6040-6044.

PROTON-CONDUCTING COMPOSITE MEMBRANE DERIVED FROM SULFONATED POLY (ETHER ETHER KETONE) AND POLYACRYLONITRILE

Jinwen Wang, Zhongren Yue, and James Economy

Department of Materials Science and Engineering
University of Illinois at Urbana-Champaign
1304 West Green St.
Urbana, IL 61801

Introduction

Up to now perfluorinated membranes from Dupont, Dow and Asahi Chemical companies have been used exclusively as proton conductors in membrane fuel cells. They possess outstanding chemical and mechanical stability and high proton conductivity (10^{-2} S/cm) and perform excellently not only in PEMFCs but also in direct methanol fuel cells (DMFCs).

However, they have two major drawbacks: 1) high cost due to the toxic and complicated production process and 2) high methanol cross over in DMFCs reducing the fuel utilization efficiency and the cathode performance. These limitations have prompted research into alternative membranes based on partially fluorinated ionomers and hydrocarbon polymer.

A large number of arylene mainchain polymers with chemical and mechanical stabilities approaching the fluorinated polymers have been sulfonated in order to obtain proton-conducting membranes. These included polyethersulfone (PSU) and poly (ether ether ketone) (PEEK). The general problem of homogeneous sulfonated aromatic polymers is that they begin to swell too easily and thus lose their mechanical stability. This happens when the degree of sulfonation exceeds 1.4–1.6 meq $\text{SO}_3\text{H/g}$ or the operating temperatures are in excess of 60–80°C. Therefore, it is essential to reduce the swelling of the membranes without lowering their proton conductivity¹.

In this study, composite membranes from sulfonated PEEK (sPEEK) and polyacrylonitrile (PAN) were prepared by heating under nitrogen at 380°C. Methanol permeability and the swelling in hot water of the membranes were significantly reduced by the treatment.

Experimental

Sulfonation of PEEK. PEEK Victrex® was sulfonated according to procedures described in the literature². The polymer (60 g) was dissolved in 95–97% H_2SO_4 (330ml) at room temperature for 24hrs and raised to 70°C for 20mins. The reaction temperature was decreased to 60°C and the reaction mixture stirred for a further 6 hrs. The sulfonated polymer was precipitated in 5 l water, filtered off and washed in (1) 1 M HCl at 80°C and (2) H_2O at 50–60°C until a pH of 7 was attained. The polymer was dried to constant weight at 80°C.

Preparation of composite membrane. The sPEEK was converted from acid form to salt form (KPEEK) in 0.5MKCl solution for 24 hrs according to $-\text{SO}_3\text{H}:\text{KCl} = 1:10$ (molar ratio). KPEEK and PAN were solution blended in DMF at 80–90°C to get a homogenous solution. The resulting solution was spread on a smooth glass plate and kept at 40°C for 24hrs and 150°C for 1hr to form a membrane. Hereafter the temperature was increased to 200°C and PAN in the membrane was pre-oxidized in air for 24 hrs. Finally the membrane was heated at 380°C for 1hr in the furnace under N_2 . The $-\text{SO}_3\text{H}$ was recovered from $-\text{SO}_3\text{K}$ by heating the membrane in 1M HCl at 80°C and H_2O at 50–60°C for several hours.

Characterization Methods. Proton conductivities of membranes were measured in a two terminal configuration along the membranes rather than perpendicular to them³. Before measurement

Nafion 117 was refluxed in 1M HNO_3 and the composite membrane in 1M HCl for 1hr and then both in DI water for another hour. The humidity was kept 100% using a sealed bottle in which membranes were suspended above the water surface. The ends of the membranes were connected to an HP4284A analyzer through stainless steel clamps. The frequency range was 20Hz–1MHz and the voltage amplitude 10mV. The impedance (R) with the minimum imaginary part was used to calculate the proton conductivity:

$$\text{Conductivity} = \text{length} / (\text{width} * \text{thickness} * R)$$

Methanol permeability of the membranes was determined using the diaphragm diffusion cell described in the literature⁴. Concentration of methanol in the initially pure water cell was measured versus time using 5890 Series II GC with crosslinked methyl siloxane capillary column and helium as carrier. The temperature of the injection and FID was kept at 120°C and the oven temperature at 35°C for 25mins and 100°C for 2mins.

Results and Discussion

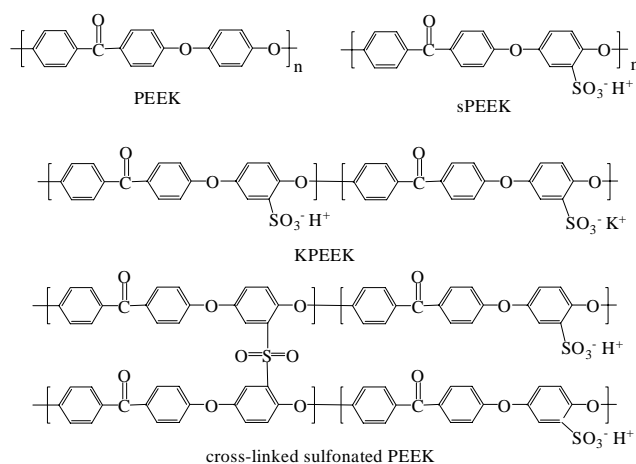


Figure 1. Repeat units of PEEK, sPEEK, KPEEK, cross-linked sulfonated PEEK

In **Figure 1** the chemical changes in PEEK in the composite membrane are described. During sulfonation the $-\text{SO}_3\text{H}$ was introduced into the diether benzene ring and most $-\text{SO}_3\text{H}$ groups were converted to $-\text{SO}_3\text{K}$ after soaked in 0.5MKCl solution. According to thermal analysis about 15% $-\text{SO}_3\text{H}$ formed sulphone crosslink in the membrane when treated at 380°C⁵. If the temperature were below 360°C, the membrane would dissolve in hot water (60°C) showing that 360°C was the minimum temperature the crosslinking reaction could occur. The $-\text{SO}_3\text{K}$ was stable even at 400°C and provided protection for the remaining 85% $-\text{SO}_3\text{H}$ at 380°C. The

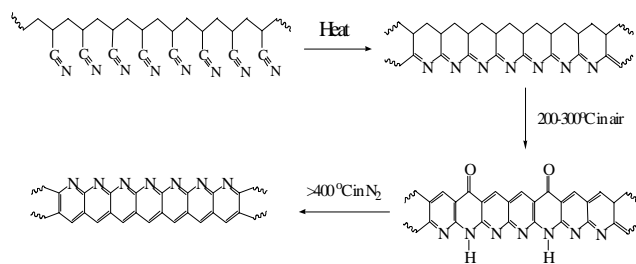


Figure 2. Heat treatment of PAN

-SO₃H groups could be easily recovered by ion exchange with 1M HCl after the thermal treatment. The other reason to choose 380°C is related to the reaction of PAN at this temperature shown in **Figure 2**. By heat treatment the stable ladder structure of PAN could be obtained, in which nitrogen atoms may interact with -SO₃H. Some sections within the ladder chains even have structure very similar to imidazole and pyrazole that could act as a vehicle to transport proton in anhydrous membranes⁷.

The incorporation of thermally treated PAN could also reduce the swelling of membranes in water. We swelled membranes completely in 80°C water and cut the wet membranes into small disks with the same diameter. After drying, the diameter increased with the increase of PAN in membranes. This could be observed clearly from **Figure 3**.



Figure 3. Changes in the diameter of composite membranes with increasing PAN after drying

In **Figure 4** proton conductivities of composite membranes first increased with the addition of PAN. This may result from the interaction between nitrogen atoms in PAN and protons in sPEEK. At 5% there was a maximum (0.52S/cm), which was similar to that of Nafion 117 (0.053S/cm). This is promising because sPEEK has 1/4 of the thickness of Nafion. As shown in **Figure 4**, above 5%, the conductivities decreased quickly. This could be due to larger PAN region in composite membranes blocking the proton transport. When PAN exceeded 10%, there was phase inversion between PAN and sPEEK, i.e., PAN became the continuous phase. Therefore, proton conductivity would be further reduced.

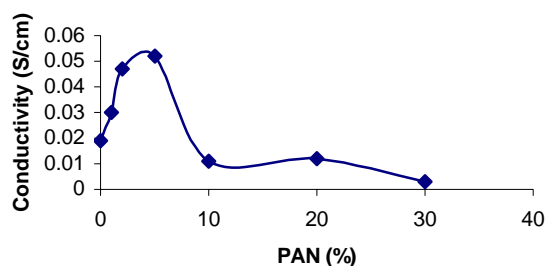


Figure 4. Proton conductivity versus PAN in composite membranes

A typical diffusion curve derived from GC is illustrated in **Figure 5**. Methanol permeability was calculated from the slope of the linear fit line in **Figure 5** based on the equation: methanol permeability = (flux / thickness) / concentration difference, where flux = (slope / cell volume) / membrane area. In **Table 1** methanol permeability of these membranes are listed and compared to Nafion

117. The sPEEK membrane without PAN displayed methanol permeability of 39% of Nafion 117. The composite membranes with thermally treated PAN resulted in lower methanol permeability because the micro-sized dispersion of rigid ladder PAN chains prevented methanol from transferring through the membrane. The membrane (95:5) had 20% methanol permeability compared to Nafion 117 while the proton conductivity was similar to Nafion 117. These properties would make it a possible low cost alternative to Nafion 117 in DMFCs.

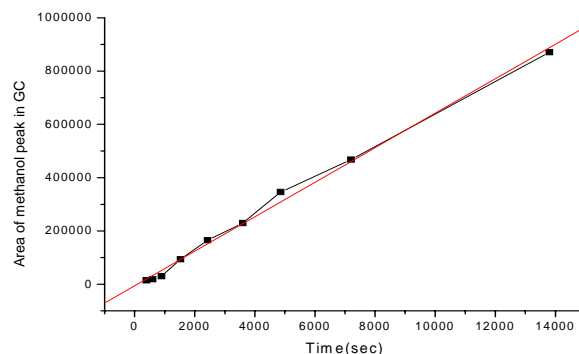


Figure 5. Typical diffusion data at room temperature: the methanol-water solution was 50vol%.

Table 1. Methanol permeability of membranes

Membranes	Thickness (cm)	Slope	Methanol permeability (10 ⁻⁷ cm ² /s)
Nafion	0.022	2051	27.4
100:0	0.0027	6474	10.6
95:5	0.0035	2562	5.4
80:20	0.0047	1588	4.5
70:30	0.0047	595	1.7

References

1. Kerres, J.A., *J. Membr. Sci.*, **2001**, *185*, 3-27
2. Cui, W.; Kerres, J.A.; Eigenberger, G., *Separation and Purification Technology* **1998**, *14*, 145-154
3. Fontanella, J.J.; McLin, M.G.; Wintersgill, M.C.; Calame, J.P.; Greenbaum, S.G., *Solid State Ionics*, **1993**, *66*, 1-4
4. Pivovar, B.S.; Wang, Y.; Cussler, E.L., *J. Membr. Sci.*, **1999**, *154*, 155-162
5. Yen et al., *US 5795496*, **1998**
6. Memetea, L.T.; Billingham, N.C.; Then, E.T.H., *Polymer Degradation and Stability*, **1995**, *47*, 189-201
7. Kreuer, K.D.; Fuchs, A.; Ise, M.; Spaeth, M.; Maier, J., *Electrochimica Acta*, **1998**, *43(10-11)*, 1281-1288

SYNTHESIS AND CHARACTERIZATION OF HYDROQUINONE BASED DISULFONATED POLY (ARYLENE ETHER SULFONE)S VIA DIRECT COPOLYMERIZATION

Abhishek Roy, Brian R. Einsla, William L. Harrison and James E. McGrath(jmcgrath@vt.edu)

Department of Chemistry, Virginia Polytechnic Institute and State University, Blacksburg, VA 24061

Introduction

The integral part of the fuel cell is considered to be proton exchange membrane (PEM). There has been enormous ongoing research for the development of suitable candidates for PEM fuel cells. Among the promising candidates, poly(arylene ether sulfone)s are the well noted. Poly(arylene ether sulfone)s are important engineering thermoplastics possessing excellent thermal and chemical resistance.^{1,2,3} Our group has reported the synthesis of sulfonated poly(arylene ether sulfone)s based on biphenol and other bisphenol systems via direct copolymerization. This paper is focused on the synthesis and characterization of hydroquinone based poly(arylene ether sulfone)s.

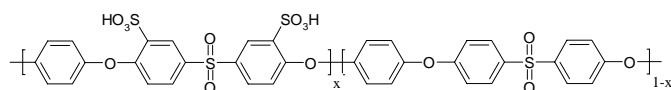


Figure 1. Structure of Hydroquinone-Based Poly(arylene ether sulfone)s (HQS-x)

Experimental

Materials. Highly purified, commercially available, 4,4' dichlorodiphenyl sulfone (DCDPS) and hydroquinone were obtained from Solvay Advanced Polymers and Eastman Chemical Company, respectively. DCDPS was dried at 60 °C under vacuum for 12 h and hydroquinone was dried under vacuum at room temperature for 12 h. The preparation SDCDPS was previously reported. The reaction solvent n-methyl-2-pyrrolidone (NMP) was distilled from calcium hydride under vacuum before use. Potassium carbonate was obtained from Aldrich and was dried under vacuum at 120 °C for 12 h.

Polymerization. A typical direct copolymerization of DCDPS, SDCDPS and hydroquinone was conducted in a three necked round bottomed flask. The reaction was carried out in presence of nitrogen inlet, overhead stirrer, a Dean-Stark trap fitted with condenser and thermocouple sensor. For the 25% sulfonated copolymer, 3.24 g (6 mmol) of SDCDPS, 2.79 g (25 mmol) of hydroquinone, 5.47 g (19 mmol) of DCDPS and 4.037 g of potassium carbonate was charged into the flask. Distilled NMP (38 mL) was added as solvent and 20 mL of toluene was added as refluxing solvent. The Dean-Stark trap was filled with toluene and the reaction flask was heated to 150 °C and allowed to reflux for 4 h. After that the toluene was gradually removed, the reaction temperature was raised to 190 °C. The reaction was continued for about 20 h, cooled to room temperature and then the copolymer was precipitated into deionized water. The fibrous precipitate was collected by filtration and dried under vacuum for 2 days at 100 °C.

Membrane Preparation. The dried copolymer was dissolved in 10 weight % solution of DMAC and casted onto clean glass plates. The films were dried under a infrared lamp in a nitrogen atmosphere. The film formed was removed from the plate by submersion in deionized water. The membranes were treated with 0.5 M boiling sulfuric acid to convert the sulfonate salt of the copolymer to proton conductive acid form.³ To remove the residual sulfuric acid, the

membrane was extracted with boiling water for 2 h and then dried under vacuum at 100 °C for 16 h.

Characterization. The Proton NMR spectrum of the copolymers was obtained using a Varian 400 MHz instrument in deuterated dimethylsulfoxide. ATR-FTIR analysis was done in DuraSamplR instrument. Intrinsic viscosity measurements were measured in NMP at 25 °C using a Cannon Ubbelohde viscometer. To determine the water uptake of the membranes, the dry weights of the membranes was taken and then the membranes were immersed in deionized water for 48 h at room temperature. The wet membranes were blotted dry and weighed immediately. The ratio of the weight gain to initial weight was taken as the water uptake. Thermogravimetric analysis was conducted in air at a heating rate of 10 °C per min using a TA instrument. DSC measurements were performed on a TA instrument in presence of nitrogen at a heating rate of 10 °C per min. Proton conductivity of the acid form membranes was determined using a Solatron 1260 Impedance /Gain-Phase Analyzer.

Results and Discussion

Hydroquinone based disulfonated poly(arylene ether sulfone)s copolymers were successfully synthesized by nucleophilic aromatic substitution. A series of copolymers (Table I) were prepared with varying degrees of disulfonation (SDCDPS content) and were characterized by ¹H NMR, intrinsic viscosity (IV), thermogravimetry (TGA), differential scanning calorimetry (DSC), IR, water uptake and proton conductivity measurements.

Table 1. Properties of Disulfonated Poly(arylene ether sulfone) Copolymers

Copolym er	Yield (%)	% DS by ¹ H NMR	IV (dL/g)	IEC	Water Uptake (%)	σ (S/cm)
20	94	19.5	0.75	1.12	19	-
25	97	23.4	1.12	1.37	35	0.05
30	93	30.3	1.60	1.61	46	0.06
35	95	33.2	1.50	1.84	68	0.07

The high IV values suggest formation of high molecular weight disulfonated copolymers. From the water uptake values, it is apparent that water uptake increases with increased degree of sulfonation. Also it was noted that there was a huge jump in water uptake from the 30% disulfonation level to the 35% sulfonation level, which may be associated with a change in morphology (i.e., percolation threshold).¹⁻³ As apparent from the conductivity data, the conductivity increases with increase in percent sulfonation and water uptake. The structure of copolymers was confirmed by ¹H NMR as shown in the Figure 2. The degree of disulfonation was calculated from ¹H NMR spectra, and agreed with the theoretical values. ATR-FTIR analysis (Figure 3) confirmed the successful incorporation of sulfonate groups. The strong characteristic peaks at 1030 cm⁻¹ and 1098 cm⁻¹ were assigned to symmetric and asymmetric stretching of the sulfonate group.

Thermogravimetric analysis (Figures 4 and 5) showed the increased thermo-oxidative stability of the salt form copolymers compared to their sulfonic acid form. Also, it can be concluded that the thermo-oxidative stability of the polymer decreases with increased sulfonation level. The initial drop in weight around 300 °C is attributed to the loss in sulfonic groups. DSC measurements (Figure 6) conducted on acid form membrane (25% sulfonation) showed a high dry glass transition temperature (~240 °C).

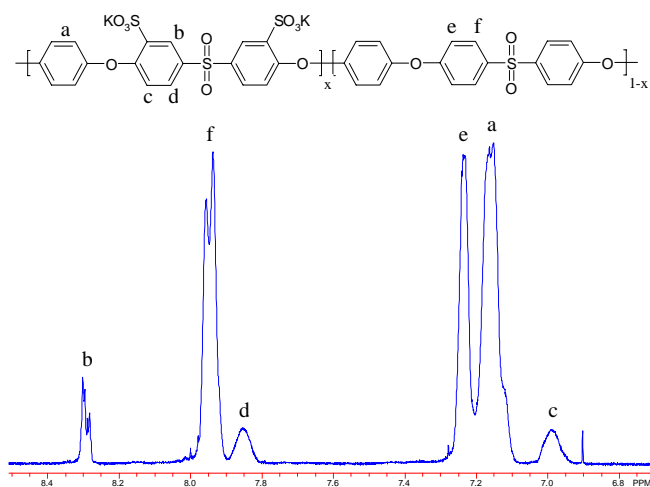


Figure 2. ^1H NMR of HQS25 copolymer.

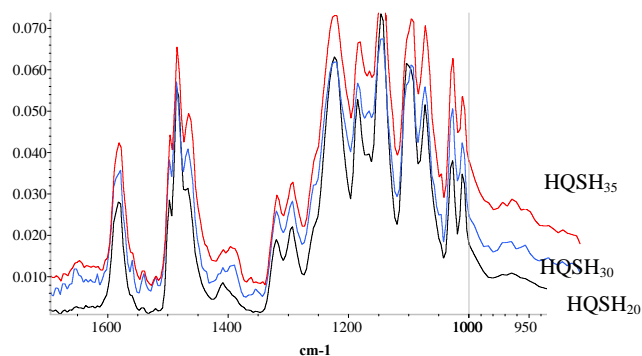


Figure 3. ATR of HQSH_{xx} copolymers.

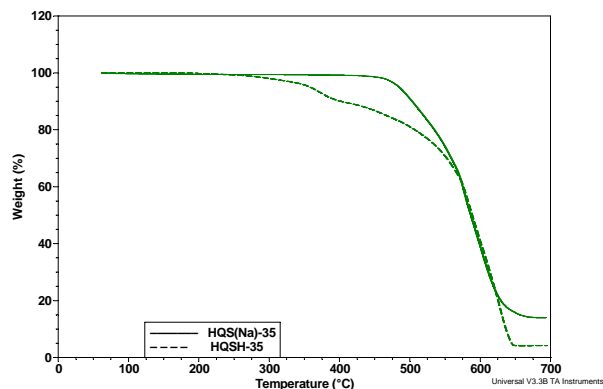


Figure 4. TGA of HQS-35 salt form (—) and HQSH-35 acid form (---)

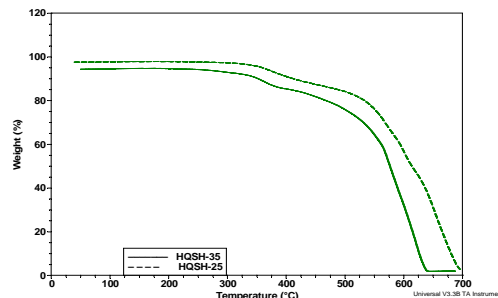


Figure 5. Influence of copolymer composition on thermo-oxidative stability (acid form membranes).

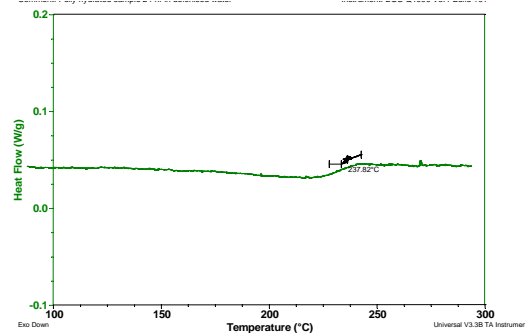


Figure 6. DSC of the acid form HQSH-25 membrane (2nd heat).

Conclusions

Hydroquinone bases sulfonated poly(arylene ether sulfone) copolymers were successfully synthesized and characterized. The structure was confirmed by ^1H NMR analysis. Water uptake values demonstrate an increase in water uptake with increased degree of disulfonation, as expected. The proton conductivity value was found to increase with increase in degree in sulfonation. From the TGA, it can be concluded that the salt form membranes are more stable than their corresponding acid form. The high glass transition of the membrane may be for high temperature fuel cell applications.

Acknowledgement. The authors would like to thank the National Science Foundation “Partnership for Innovation” Program (HER-0090556) and the Department of Energy (DE-FC36-01G01086) for support of this research effort.

References

1. W. L.Harrison, F. Wang, J.B. Mecham, V. A. Bhanu, M. Hill, Y. S. Kim, J. E. Mcgrath.; Influence of the Bisphenol Structure on the Direct Synthesis of Sulfonated Poly(arylene ether) Copolymers; *Journal of Polymer Science: Part A: Polymer Chemistry*, Vol. 41, 2264–2276 (2003)
2. F. Wang, M. Hickner, Y.S. Kim, T. Zawodzinski and J.E. McGrath, “Synthesis and Characterization of Sulfonated Poly(arylene ether sulfone) Random (Statistical) Copolymers Via Direct Polymerization: Candidates for New Proton Exchange Membranes,” *Journal of Membrane Science*, 197 (2002), 231-242
3. ; Y. S. Kim ,F. Wang, M. Hickner, S.Mccartney, Y. Taik Hong,W. Harrison, T. A. Zawodzinski, J.E Mcgrath; Effect of Acidification Treatment and Morphological Stability of Sulfonated Poly(arylene ether sulfone) Copolymer Proton-Exchange Membranes for Fuel-Cell Use above 100 °C *Journal of Polymer Science: Part B: Polymer Physics*, Vol. 41, 2816–2828 (2003)

SYNTHESIS AND CHARACTERIZATION OF HYDROXY-FUNCTIONALIZED POLY(ARYLENE ETHER SULFONE)S AND CONVERSION TO PROTON CONDUCTING MEMBRANES FOR FUEL CELLS

Brian R. Einsla and James E. McGrath

Institute for Polymeric Materials and Interfaces, Virginia Polytechnic Institute and State University, Blacksburg, Virginia 24061
jm McGrath@vt.edu

Introduction

Recently, there has been considerable interest in the development of high performance and potentially lower cost proton exchange membrane (PEM) fuel cells for transportation, stationary and portable power applications.^{1,2} The interest in fuel cells is largely due to their ability to continuously convert chemical energy into electric energy and heat with high efficiency and low emission of pollutants.³ In PEM fuel cells, the membrane must transport protons from the anode to the cathode, and act as a barrier to oxygen and the hydrogen-rich fuel. At the anode, hydrogen is oxidized to protons and electrons by platinum or platinum/metal catalysts. The resulting protons are transported across the electrolyte to the cathode. Useful electrical energy is harnessed by moving the electrons through an external circuit before allowing them to reach the cathode. At the cathode, gaseous oxygen from the air is reduced and combined with the protons and electrons to form water.⁴

Promising PEM fuel cell systems include high temperature hydrogen/air and direct methanol fuel cells (DMFC). In hydrogen/air-based fuel cells, high temperature (>120 °C) provides benefits such as faster electrode kinetics and greater tolerance to impurities in the fuel stream.⁵ To operate at these high temperatures, new and improved mechanisms for conductivity above the boiling point of water are needed.⁶ DMFC's offer reasonably high fuel energy density, readily stored liquid fuel, ease of refueling, and direct and complete electro-oxidation of methanol at moderate temperatures.⁷ Nafion[®] perfluorosulfonic acid copolymers are the state-of-the-art membranes for DMFC and hydrogen/air fuel cells due to their high conductivity when hydrated and chemical stability. However, there is much interest in alternative PEM's because of Nafion's reduced performance above 80 °C, significant methanol crossover and cost.^{8,9,10}

One method to achieve proton conductivity in PEM's is to incorporate sulfonic acid sites along the polymer chain. As an example, sulfonated poly(arylene ether sulfone)s (PAES) can be synthesized via post-sulfonation of the parent polymer, or direct copolymerization of sulfonated monomers. The properties of the resulting copolymer membrane depend on the preparation method as well as the processing steps.^{11,12,13} Direct copolymerization of sulfonic acid-containing monomers allows for improved control of the ion-exchange capacity (IEC), and therefore control over the proton conductivity, water sorption, and morphology of the membrane.

It is well known in the area of nonlinear optics (NLO) that polyimides with NLO chromophore side chains can be incorporated into the polymer chain by direct copolymerization or post-derivatization. A common synthetic route for nonlinear optical polyimides is the condensation polymerization of dianhydrides with diamines containing an NLO chromophore via a poly(amic acid) prepolymer.¹⁴ This method, however, often involves a tedious synthesis of the chromophore-containing diamine monomers. Sometimes, the fact that few chromophores can survive the relatively harsh chemical conditions of the monomer synthesis limits the kind

of chromophores that are incorporated in the polyimide backbone.¹⁵ To avoid the synthesis of chromophore-containing diamine compounds, an alternate synthetic route was developed by Chen *et al.*^{9,16} A one-pot preparation of a preimidized, hydroxy-containing polyimide was developed, followed by the covalent attachment of a chromophore to the backbone of the polyimide.

This post-derivatization method may also have an application in the synthesis of proton exchange membranes for fuel cells. Instead of bonding the NLO chromophore to the polymer backbone, ion-conducting sites could be introduced. Unfortunately, the hydrolytic stability of sulfonated polyimides under fuel cell conditions is unsatisfactory. On the other hand, sulfonated poly(arylene ether sulfone)s have attracted much attention as suitable membranes for PEM fuel cells. Herein, we report the synthesis of hydroxyl-functionalized PAES and derivatization to sulfonated copolymers.

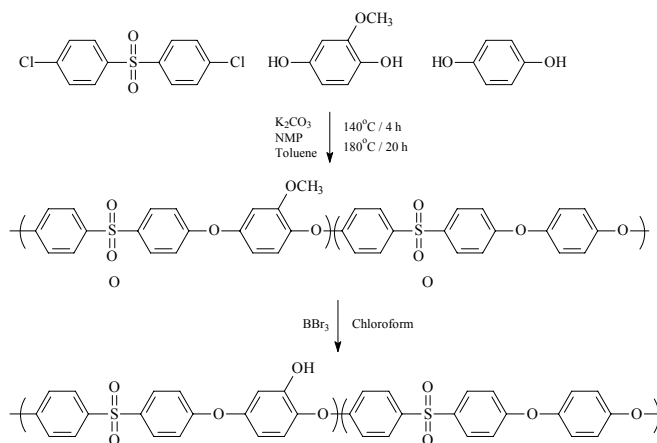


Figure 1. Copolymerization of Methoxy-PAES and Conversion of Methoxy Groups to Hydroxyl.

Experimental

Materials. 4,4'-Dichlorodiphenylsulfone (DCDPS, Solvay Advanced Polymers) was used as received. Hydroquinone, methoxyhydroquinone, potassium carbonate, toluene, boron tribromide, and chloroform were used as received from Aldrich. N-methylpyrrolidone (Aldrich) was distilled from calcium hydride under vacuum before use.

Methoxy-Poly(arylene ether sulfone) Copolymerization. A typical copolymerization of a methoxy-PAES with 50 mol % methoxy groups is discussed (MHQS-50). DCDPS (4.000 g, 14 mmol), hydroquinone (0.7669 g, 7 mmol), and methoxyhydroquinone (0.9760 g, 7 mmol) were introduced to a 250-mL, three neck flask equipped with a mechanical stirrer, Dean-Stark trap, condenser, and a nitrogen inlet/outlet. Potassium carbonate (2.22 g, 16 mmol) and 29 mL of NMP were added to the reaction flask to afford a 20% (w/v) solid concentration. Toluene (15 mL) was added to the flask as an azeotroping agent. The Dean-Stark trap was filled with toluene and the reaction mixture was heated to 140 °C to dehydrate the system. After 4 h at 140 °C, the Dean-Stark trap was emptied and the oil bath temperature was heated to 180 °C for 20 h. The resulting viscous solution was cooled to room temperature and precipitated into an excess of deionized water. The precipitated copolymer was collected by filtration and purified in a Soxhlet extractor with deionized water for 2 days. The resulting white, fibrous copolymer (MHQS-50) was dried under vacuum at 110 °C for at least 24 h.

Conversion of Methoxy to Hydroxyl Groups. A typical reaction for converting MHQS-30 to HOHQ-30 is given. MHQS-30 (1.000 g) was dissolved into 20 mL of chloroform in a 100-mL, three neck flask equipped with a stirbar and nitrogen purge. BBr₃ (0.5 mL in 10 mL chloroform) was added dropwise to the reaction via a syringe. The reaction mixture was allowed to stir overnight at room temperature. The copolymer was isolated by filtration, washed with methanol (2x) and deionized water (2x), and finally dried under vacuum at 120 °C.

Preparation of Sulfonated Poly(arylene ether sulfone) Copolymer. HOHQ-30 (1.0000 g) and 4-nitrophenylsulfonic acid sodium salt (0.6100 g) were introduced to a 100-mL, three neck flask equipped with a mechanical stirrer, Dean-Stark trap, condenser, and a nitrogen inlet/outlet. Potassium carbonate (0.48 g) and 10 mL were added to the reaction flask to afford a 15% (w/v) solid concentration. The reaction mixture was heated to 80 °C 72 h. The resulting viscous solution was cooled to room temperature and precipitated into an excess of deionized water. The precipitated copolymer was collected by filtration and purified in a Soxhlet extractor with deionized water for 2 days. The resulting white, fibrous copolymer (MHQS-30) was dried under vacuum at 110 °C for at least 24 h.

Characterization. ¹H NMR spectra were recorded on a Varian Unity 400 instrument operating at 399.952 MHz in deuterated dimethylsulfoxide (DMSO-*d*₆). Intrinsic viscosity (IV) measurements were conducted in NMP at 25 °C using a Cannon Ubbelohde viscometer.

Results and Discussion

PAES's with pendant methoxy groups were synthesized by nucleophilic substitution reactions (Figure 1). The high molecular weight copolymers were characterized by intrinsic viscosity (Table 1) and ¹H NMR (Figure 2). The incorporation of the methoxyhydroquinone was found to be quantitative through integration of the peak at 3.6 ppm with respect to one in the aromatic region (7.9 ppm) (Table 1). All of the MHQS-XX copolymers were soluble in chloroform; therefore the conversion of the methoxy groups to hydroxyl groups using BBr₃ was conducted in chloroform. Due to the polar nature of the hydroxyl groups, the subsequent HOHQ-XX copolymers were not soluble in chloroform allowing for straightforward isolation. The intrinsic viscosity of the HOHQ-XX copolymers was higher than the MHQS-XX copolymers in all cases. Perhaps this effect is due to hydrogen bonding of the hydroxyl groups. The quantitative conversion of methoxy groups to hydroxyl groups was determined by ¹H NMR. The complete disappearance of the protons of the methoxy group (3.6 ppm) and appearance of a peak at ~10 ppm (due to -OH) was observed for all three copolymers. Additionally, an increase in the glass transition temperature of the HOHQ-XX copolymers with respect to the MHQS-XX copolymers can be attributed to hydrogen bonding which decreases chain mobility (Table 1).

As an example, HOHQ-30 was reacted under nucleophilic conditions with 4-nitrobenzenesulfonic acid sodium salt (NBS) to prepare a 30% sulfonated copolymer. The derivatization reaction was heated to 80 °C to reduce the ether-ether interchange that could possibly lower the molecular weight of the copolymer. The resulting high molecular weight sulfonated copolymer formed a tough, ductile membrane when solution cast from *N,N*-dimethylacetamide. The ¹H NMR of the sulfonated copolymer is shown in Figure 4. The incorporation of the NBS was shown by the ¹H NMR peaks at 7.85 ppm and 8.4 ppm.

Table 1. Copolymer Properties

Copolymer	I.V. (dL/g)*	¹ H NMR		T _g (°C)**
		%-OCH ₃	%-OH	
MHQS-30	0.83	31.4	-	195
MHQS-40	0.84	39.5	-	195
MHQS-50	0.81	52.3	-	-
HOHQ-30	1.09	-	29.2	211
HOHQ-40	1.02	-	40.8	216
HOHQ-50	1.30	-	52.2	-

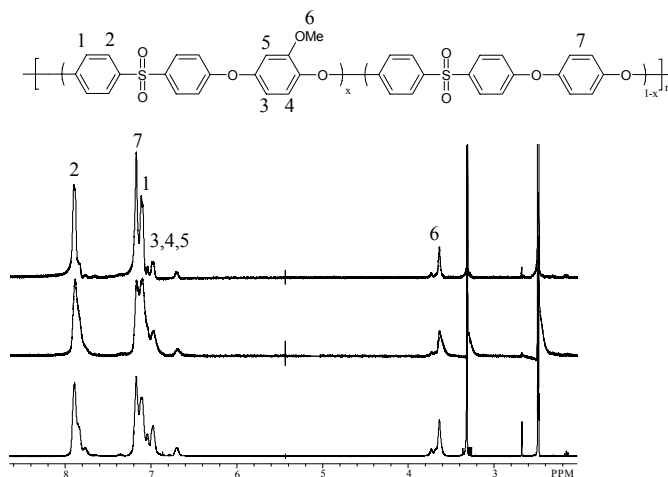


Figure 2. ¹H NMR of MHQS-XX Copolymers in DMSO-*d*₆

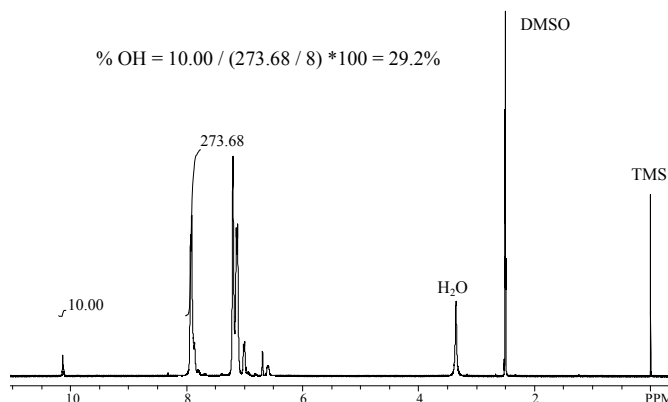


Figure 3. ¹H NMR of HOHQ-30 to Determine the % Hydroxyl Groups

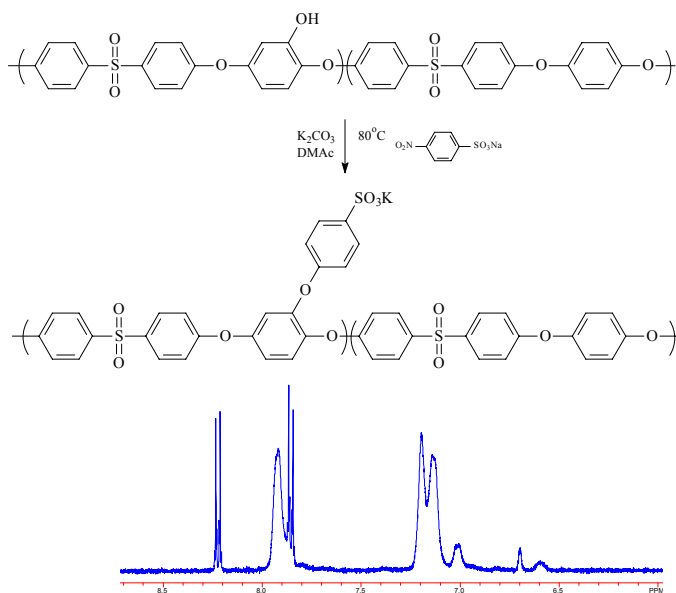


Figure 4. Preparation and ^1H NMR of Sulfonated PAES.

Conclusions

A series of high molecular weight PAES's were synthesized with pendant methoxy groups which were completely converted to reactive hydroxyl groups. The hydroxyl functionalized copolymers showed higher intrinsic viscosities and T_g 's due to hydrogen bonding. A 30% sulfonated copolymer was prepared by post-derivatization of the 30% hydroxyl copolymer, and this sulfonated copolymer formed a tough, ductile film after solution casting. Further work is ongoing to study the properties of these sulfonated copolymers for use as PEM fuel cells and this will be discussed at the meeting.

Acknowledgements. The authors would like to thank the Department of Energy (DE-FC36-01G01086) for support of this research effort.

References

- G.J.K. Acres, Recent Advances in Fuel Cell Technology and its Applications, *J. Power Sources* 100 (2001) 60-66.
- B.C.H. Steele, A. Heinzel, Materials for Fuel-Cell Technologies, *Nature* 414 (2001) 345-352.
- L. Carrette, K.A. Friedrich, U. Stimming, Fuel Cells: Principles, Types, Fuels, and Applications, *Chem. Phys. Chem.* 1 (2000) 162-193.
- M. Jacoby, Fuel Cells Heading For Sale, *C&E News*, June 14, 1999, 31.
- G. Alberti, M. Casciola, L. Massinelli, B. Bauer. *J. Membrane Sci* 185 (2001) 73-81.
- S. Thomas, M. Zalbowitz, Fuel Cells: Green Power, Los Alamos National Laboratory, Los Alamos, NM.
- A.S. Arico, S. Srinivasan, V. Antonucci. *Fuel Cells* 1 (2001) 133-161.
- F. Wang, M. Hickner, Q. Ji, W. Harrison, J. Mecham, T.A. Zawodzinski, J.E. McGrath. *Macromol. Symp.* 175 (2001) 387-395.
- F. Wang, M. Hickner, Y.S. Kim, T.A. Zawodzinski, J.E. McGrath. *J. Membrane Sci.* 197 (2002) 231-242.
- W.L. Harrison, F. Wang, J. Mecham, V.A. Bhanu, M. Hill, Y.S. Kim, J.E. McGrath. *J. Polym. Sci.: Part A: Polym. Chem.* 41 (2003) 2264-2276.
- F. Lufitano, I. Gatto, P. Staiti, V. Antonucci, E. Passalacqua. *Solid State Ionics*, 145 (2001) 47-51.
- W.L. Harrison, K. O'Connor, N. Arnett, J.E. McGrath. *Polym. Prepr. (Am. Chem. Soc. Div. Polym. Chem.)* 43 (2002) 1159.
- Y.S. Kim, L. Dong, M.A. Hickner, B.S. Pivovar, J.E. McGrath. *Polymer* 44 (2003) 5729-5736.
- S. Yang, Z. Peng, L. Yu. *Macromolecules* 27 (1994) 5858-5862.
- T.-A. Chen, A.K.-Y. Jen, Y. Cai. *J. Am. Chem. Soc.* 117 (1995) 7295-7299.
- T.-A. Chen, A.K.-Y. Jen, Y. Cai. *Macromolecules* 29 (1996) 535-539.

PROMISING COMPONENTS FOR HIGH-TEMPERATURE PEM FUEL CELLS: THERMALLY STABLE AND HIGHLY PROTON CONDUCTING HETEROPOLY ACIDS

Fanqin Meng,^{1,3} Jennifer L. Malers,^{1,3} James Horan,² Steven F. Dec,² Andrew M. Herring,¹ John A. Turner.³

Department of Chemical Engineering¹ and Chemistry and Geochemistry²
Colorado School of Mines
Golden, CO 80401-1887

Hydrogen and Electricity, Systems and Infrastructure Group³
National Renewable Energy Laboratory
Golden, CO 80401-3393

Introduction

Heteropoly acids (HPAs) have attracted attention of PEM fuel cell community because of their exceptionally high proton conductivities, for example, 0.2 S cm^{-1} for 12-phosphotungstic acid at room temperature.^{1,2} Studies conducted in our laboratory as well as by other researchers have revealed the high thermal stabilities of these materials. Moreover, we have found that proton diffusion coefficients of various HPAs increase with temperature till $100 \text{ }^\circ\text{C}$ or higher. These discoveries are especially encouraging for the use of HPAs in PEM fuel cells operating at desirable elevated temperatures ($120 - 200 \text{ }^\circ\text{C}$). Besides the many well-know advantages in terms of economy, high temperature operation actually minimizes, if not eliminates, the conventional obstacle to implementing solid acids in fuel cells: at temperatures above $100 \text{ }^\circ\text{C}$, H_2O is in the form of steam and is thus harmless to the otherwise water-soluble electrolyte.

The family of HPAs adopts a wide variety of compositions and structures. The central heteroatom has been located in a large area of the periodic table, from transitional metals to main group elements. Diverse molecular structures have been discovered, including the most common Keggin and Dawson types, their lacunary structures, and derivatives by various condensation of the lacunary moieties. However, only the four commercially available Keggin-type HPAs, 12-phosphotungstic, 12-phosphomolybdic, 12-silicotungstic, and 12-silicomolybdic acids have been studied to any great extent and the study of proton conduction in these materials has been limited. There is, therefore, a need to correlate proton conducting properties of the HPAs with the vast number of structures and hydration states available in order to choose or design the best materials for fuel cell applications. To this end, our group has been using TGA, DRIFTS, MAS and PFGSE NMR techniques to investigate a variety of HPAs with respect to their thermal stability, hydrogen bonding, proton acidity and proton diffusion coefficients.

Experimental

The Keggin-type HPAs, 12-phosphotungstic acid, $\text{H}_3\text{PW}_{12}\text{O}_{40}$ (12-HPW) and 12-silicotungstic acid, $\text{H}_4\text{SiW}_{12}\text{O}_{40}$ (12-HSiW), were purchased from Aldrich and used as received. All other HPAs, such as 18-diphosphotungstic acid, $\text{H}_6\text{P}_2\text{W}_{18}\text{O}_{62}$ (18-HP2W), and 21-diarsenotungstic acid, $\text{H}_6\text{As}_2\text{W}_{21}\text{O}_{69}$ (21-HAs2W) etc, were prepared by literature methods.³⁻⁶

All TGA data were taken on samples that had been heated in an oven at *ca.* $120 \text{ }^\circ\text{C}$ for several days. The temperature was run from ambient to $600 \text{ }^\circ\text{C}$ (heating rate $5 \text{ }^\circ\text{C}/\text{min}$) under helium flow of $162 \text{ mL}/\text{min}$.

All MAS ^1H spectra were recorded on a two-channel Chemagnetics CMX Infinity 400 NMR spectrometer operating at

400.0 MHz , using a Chemagnetics 5mm double-resonance MAS probe equipped with a Pencil spinning module, sample spinning at 10 kHz . Proton diffusion measurements were obtained with the use of a 5mm Doty Scientific, Inc. #20-40 z-gradient pulsed-field gradient NMR probe. The stimulated-echo pulse sequence⁷ was used and the gradient coil was calibrated using water at $25 \text{ }^\circ\text{C}$. The resulting NMR spectra were integrated and fit to a two-Gaussian decay using Spinsight[®] software available from Varian, Inc.

DRIFTS samples were heated *in situ* (ambient temperature to $350 \text{ }^\circ\text{C}$) under constant helium flow, the spectra were recorded on a Thermo Nicolet Nexus 670 FT-IR spectrometer using the Omnic[®]6.0 software package and with a specially designed Harrick Praying Mantis diffuse reflection attachment (DRA).

Results and Discussion

TGA measurements indicate the HPAs in interest maintain a considerable amount of water and proton up to $>400 \text{ }^\circ\text{C}$. The remarkable observation here is the high temperatures to which some of the HPAs retain water in their secondary structure. Should water presence be required for high temperature proton conduction a great many of these materials would be suitable candidates. Temperature-dependent DRIFTS spectra are consistent with TGA results. Figure 1 shows that the heteropoly anions keep intact above $300 \text{ }^\circ\text{C}$, and more importantly, water molecules are present in the structure at temperatures appreciably higher than $100 \text{ }^\circ\text{C}$.

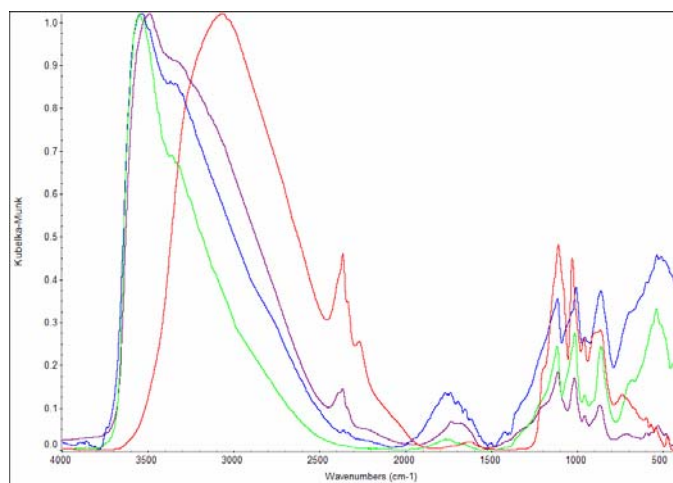


Figure 1. DRIFTS spectra of 18-HP2W at 50(blue), 100(green) 200(purple), and 300(red) $^\circ\text{C}$.

MAS ^1H chemical shifts of HPAs are in the range of 8-11, compounds with main group elements in the center consistently showing lower values than those with transition metal elements as the heteroatom. Diffusion coefficients of the HPAs are mostly in the order of $10^{-6} \text{ cm}^2/\text{sec}$, much higher than those of other types of proton conducting solids. As shown in Figure 2, all the HPAs in this work showed increasing proton mobility with temperature until a maximum was reached. Interestingly, while the maxima for most of the materials are at approximately $100 \text{ }^\circ\text{C}$, the proton diffusion coefficients for 12-HZnW kept rising till $140 \text{ }^\circ\text{C}$, and 21-HAs2W repeatedly showed a second peak around $150 \text{ }^\circ\text{C}$ although at a lower value.

Conclusions

Highly proton conducting HPAs are promising components for PEM fuel cells operating at elevated temperatures. Certain compositions and structures seem to exhibit higher proton acidity and favor proton diffusion.

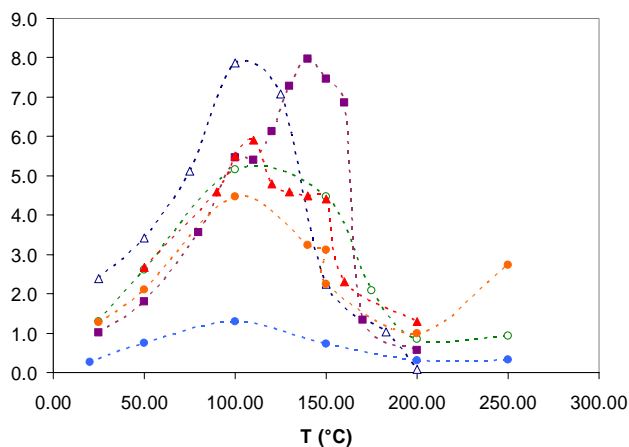


Figure 2. Diffusion coefficients as a function of temperature, 21-HB3W (navy), 11-HSiW (green), 18-HP2W (blue), 21-HP2W (orange), 12-HZnW (purple), and 21-HAs2W (red).

Acknowledgement. This work was supported by the US DOE science initiative, DE-FC02-0CH11088.

References

- (1) Nakamura, O.; Kodama, T.; Ogino, I.; Miyake, Y. *Chemistry Letters* **1979**, *1*, 17.
- (2) Pope, M. T.; Müller, A., Eds. *Polyoxometalate Chemistry: From Topology Via Self-Assembly to Applications*; Kluwer Academic Publishers: Dordrecht, **2001**.
- (3) Brown, D. H., Mair, J. A., *J. Chem. Soc.* **1958**, 2597-9.
- (4) Tourné, C. M., Tourné, G. F., Malik, S. A., Weakley, T. J. R., *J. Inorg. Nucl. Chem.* **1970**, *32*, 3875-90.
- (5) Tézé, A., Michelon, M., Herve, G., *Inorg. Chem.* **1997**, *36*, 505-9.
- (6) Jeannin, Y., Martin-Frere, J., *Inorg. Synth.* **1990**, *27*, 111-2.
- (7) Tanner, J. E. *The Journal of Chemical Physics* **1970**, *52*, 2523.

Synthesis of proton conducting tungstosilicate mesoporous materials (WMM) and organic/WMM composite membranes for high temperature PEM fuel cells

Fangxia Feng, Decio Coutinho, Zhiwei Yang,
John P. Ferraris and Kenneth Balkus Jr.

Department of Chemistry and
The UTD NanoTech Institute
The University of Texas at Dallas
P O Box 830688 MS BE26
Richardson, TX 75083-0688

Introduction

Proton-conducting solid materials have grown in interest due to their potential applications in electrochemical devices, such as batteries, chemical sensors, fuel cells, and supercapacitors. Heteropolyacids (HPAs) are one of the more promising inorganic based ionic conductors (1,2). The direct application of HPAs as solid proton conductor is somewhat limited by highly solubility in water and alcohols (1,3). This is further complicated by the fact that the proton conductivity is significantly influenced by the relative humidity. In order to overcome these limitations, there have been attempts to disperse HPAs in polymers as inorganic/organic composite membranes for high temperature fuel cells (1,3). However, high proton conductivity normally required high relative humidity (mostly 100%). Additionally, the HPAs are mobile and could partially diffuse out of the membrane.

An alternative strategy for immobilizing HPAs is to construct nanoporous frameworks based on the HPA composition. Mesoporous molecular sieves have several promising properties, such as uniform pore size (in the range of 20 – 500 Å), high specific surface area ($\geq 1000 \text{ m}^2/\text{g}$), large dimension open channels, and relative high thermal stability.

In this paper, we report the synthesis of tungsten-containing mesoporous materials (WMM) and an evaluation of their proton conductivity. The surfactants employed in the study include the ionic template CTMABr, and the non-ionic Brij surfactants, $\text{C}_{12}\text{E}_{10}\text{OH}$, $\text{C}_{16}\text{E}_{10}\text{OH}$, and $\text{C}_{18}\text{E}_{10}\text{OH}$. The effect of different acids including HCl, H_3PO_4 , and $\text{CF}_3\text{SO}_3\text{H}$ was also studied. Additionally, the influence of the surfactant type on the synthesis and the proton conductivity of WMM product was investigated. A free-standing film grown from the $\text{C}_{12}\text{E}_{10}\text{OH} - \text{H}_3\text{PO}_4$ system was prepared but too brittle to employ a membrane-electrode-assembly (MEA) for fuel cell test. Therefore, a WMM/PEI-Glymo-HTFSI composite membrane was prepared and evaluated.

Experimental

Materials. Cetyltrimethylammonium bromide (CTMABr, Aldrich), hydrochloric acid (37 wt.%, Mallinckrodt), phosphoric acid (H_3PO_4 , 85%, EM), trifluoromethanesulfonic acid ($\text{CF}_3\text{SO}_3\text{H}$, 98%, Aldrich), sodium tungstate dihydrate ($\text{Na}_2\text{WO}_4 \cdot 2 \text{H}_2\text{O}$, 99%, Aldrich), tetraethyl orthosilicate (TEOS, 99%, Aldrich), polyoxyethylene 10 lauryl ether (Brij 56, $\text{C}_{12}\text{EO}_{10}\text{OH}$, Sigma-Aldrich), polyoxyethylene 10 cetyl ether (Brij 56, $\text{C}_{16}\text{EO}_{10}\text{OH}$, Sigma-Aldrich), polyoxyethylene 10 stearyl ether (Brij 76, $\text{C}_{18}\text{EO}_{10}\text{OH}$, Sigma-Aldrich), tungstosilicic acid hydrate ($\text{H}_4\text{SiW}_{12}\text{O}_{40} \cdot \text{aq}$, Fluka), poly(2-ethyl-2-oxazoline) (average Mw = 500,000, Aldrich), 3-glycidy—oxypropylmethoxysilane (GLYMO, 97%, Fluka), trifluoromethanesulfonimide (3M company), methanol (98%, Aldrich), Pt black (fuel cell grade, E-TEK), and carbon layer (ELAT[®], E-TEK Div. of De Nora N.A., Inc) were used as received.

Synthesis of mesoporous tungstosilicates. The syntheses of tungsten-containing mesoporous materials (WMM) were based on a

modification of the method reported by Piquemal et al. (5). The molar composition of the final reaction mixture was $\text{SiO}_2 : 0.2 \text{ T} : \text{A} : (0 \sim 30) \text{ WO}_3 : 150 \text{ H}_2\text{O}$, in which T = CTMABr, $\text{C}_{12}\text{EO}_{10}\text{OH}$, $\text{C}_{16}\text{EO}_{10}\text{OH}$, and $\text{C}_{18}\text{EO}_{10}\text{OH}$, respectively; A = HCl, H_3PO_4 , and $\text{CF}_3\text{SO}_3\text{H}$, respectively. A typical procedure involved combining 2.19 g of CTMABr in 81 ml of deionized water, with 2.4 ml of concentrated HCl. To this clear solution, 0.25 g of $\text{Na}_2\text{WO}_4 \cdot 2 \text{H}_2\text{O}$ and 6.69 ml of TEOS were added. A light yellow gel was formed and was stirred vigorously at room temperature for 1 ~ 6 days. At elevated temperature, the dense WO_3 was easily formed as an impurity. The resulting product was filtered, washed with deionized water, and then dried at 50°C overnight. Some samples were calcined in air at 500°C for 2 days to remove the surfactant. For the samples obtained in the CTMABr - H_3PO_4 system, the template was removed by ethanol extraction under reflux for 44 hours (0.1 g of as-synthesized material per 100 ml of ethanol).

Preparation of composite membrane. Linear polyethyleneimine (PEI) was prepared by a published procedure (6). Trifluoromethanesulfonimide (HTFSI) was also prepared according to a reported procedure (7).

A typical preparation of a composite membrane was conducted as follows: 0.087 g of linear PEI was dissolved into 0.5 g of methanol, followed by mixing with a mixture of desired amount of as-synthesized (or calcined) tungstosilicate (FF40) dispersed in 0.5 g of methanol. To the above mixture, 0.093 g of Glymo was added and stirred 30 mins. Then, 1.145 g of 50 wt.% HTFSI in methanol was added and stirred until a viscous gel was formed. The gel was casted on Teflon and dried for 12 hours at room temperature and then annealed at 50°C for 12 hours.

Fabrication of Membrane-Electrode-Assembly (MEA).

Before the fabrication of MEA, the thickness of the membrane was measured using Mitutoyo IP 54 digimatic micrometer. 20-25 mg of Pt black (fuel cell grade, E-TEK) was dispersed into ~3 mL of hexanes by sonication. Then the Pt was symmetrically deposited on both sides of the membrane with a loading of $\sim 5 \text{ mg}/\text{cm}^2$, followed by hot-pressing at $\sim 85^\circ\text{C}$ and $\sim 300 \text{ psig}$ for 2 mins.

Characterization. X-ray powder diffraction (XRD) patterns were collected using a Scintag XDS 2000 X-ray diffractometer, using CuK_α radiation. Scanning electron microscopy (SEM) images were recorded on a LEO 153VP electron microscope from samples coated with Au/Pd.

The conductivity measurements were made following a published procedure (8). Measured amounts of the dry solid powder and water were mixed completely. The water was added until a maximum conductivity was observed. The water content was calculated by the percentage of the water to the total of the water and the dry solid powder. The resulting wet mixture was placed into a glass tube with the surface area of 1 cm^2 , which was clamped between two stainless-steel pistons as the electrodes.

For the proton conductivity measurement of the composite membrane, the MEA was sandwiched between two pieces of gas-diffusion carbon layers and placed into a 5 cm^2 single cell (Fuel Cell Technologies Inc.). A fuel cell testing station (Fuel Cell Technologies Inc.) was used to control the single cell's temperature and humidity. The relative humidity of the cell was calculated from humidifier temperature against the cell temperature. The humidifier temperature was kept at 22°C. The cell temperature was varied. The relative humidity varied in the range of 35 to 95%.

The AC impedance measurements were carried out using a PC controlled frequency response analyzer--VoltaLab[®] PGZ301 (Radiometer Analytical S.A.) over the frequency range of 100 KHz to 1 Hz, using a 10 mV amplitude AC single throughout the experiments.

Results and Discussion

CTMABr template. Using CTMABr as a template, the product obtained with H_3PO_4 was not stable after calcination at 500°C . The dense WO_3 impurity was detected in the calcined products prepared with HCl and $\text{CF}_3\text{SO}_3\text{H}$, respectively. The proton conductivities for these samples are given in Table 1. The proton conductivity increased with an increase in water content and finally reached a maximum value of 10^{-2} S/cm. The as-synthesized product showed a higher proton conductivity than the calcined product, which could be attributed to acid trapped in the micelles. The order of the conductivity for as-synthesized products in acid was $\text{CF}_3\text{SO}_3\text{H} > \text{H}_3\text{PO}_4 > \text{HCl}$.

Table 1. Proton conductivity of WMM using CTMABr.

Acid	Water content (%)		Conductivity ($\times 10^{-2}$ S/cm)	
	as-made	calcined	as-made	calcined
HCl	50.4	58.4	1.00	0.50
H_3PO_4	33.8	-	1.78	-
$\text{CF}_3\text{SO}_3\text{H}$	42.4	64.1	2.24	1.38

Brij template. Using non-ionic Brij surfactants, all of products except the one obtained in $\text{C}_{18}/\text{H}_3\text{PO}_4$ system were thermal stable and no dense WO_3 impurity was detected. The proton conductivities are list in Table 2. The conductivity was influenced by the acid type and the length of the chain of Brij template. The product synthesized in $\text{C}_{18}/\text{CF}_3\text{SO}_3\text{H}$ system showed the highest conductivity of 4.0×10^{-2} S/cm.

Table 2. Proton conductivity of WMM using Brij.

T.	Acid	Water content (wt%)		Conductivity ($\times 10^{-2}$ S/cm)	
		As-made	Calcined	As-made	Calcined
C_1	HCl	50.4	58.3	0.07	0.26
C_1	H_3PO_4	23.4	28.1	0.19	0.31
C_1	$\text{CF}_3\text{SO}_3\text{H}$	40.5	51.8	3.31	0.30
C_1	HCl	42.4	46.5	0.57	0.30
C_1	H_3PO_4	34.0	25.5	0.03	0.20
C_1	$\text{CF}_3\text{SO}_3\text{H}$	39.8	63.2	0.03	0.08
C_1	HCl	43.9	53.1	0.06	0.35
C_1	H_3PO_4	35.7	a.	0.09	a.
C_1	$\text{CF}_3\text{SO}_3\text{H}$	38.8	61.1	3.98	0.66

a.= amorphous

Composite membranes. The composite membrane was continuous as shown in Figure 1 by the SEM image of the cross-section. At 100% relative humidity, the composite membrane with 10 wt.% WMM showed higher conductivity the PEI-Glymo-HTFSI membrane. The difference in conductivity decreased with an increase in the cell temperature, shown in Figure 2. The conductivity increased with increasing the relative humidity.

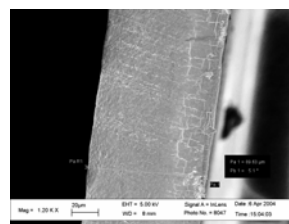


Figure 1. SEM image of the cross-section of the composite membrane.

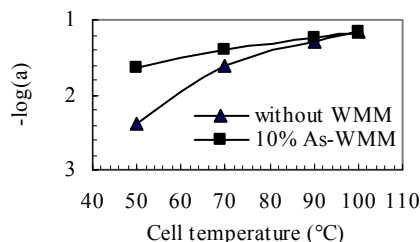


Figure 2. Effect of WMM on the conductivity.

Conclusions

Using CTMABr, $\text{C}_{12}\text{EO}_{10}\text{OH}$, $\text{C}_{16}\text{EO}_{10}\text{OH}$, or $\text{C}_{18}\text{EO}_{10}\text{OH}$ as the structure-directing agent, tungstosilicate mesoporous materials (WMMs) were synthesized with HCl, H_3PO_4 or $\text{CF}_3\text{SO}_3\text{H}$. Compared to CTMABr, the samples synthesized with the non-ionic surfactant showed higher tungsten incorporation, showed much thicker wall structure ($34 \sim 39\text{\AA}$), higher thermal stability, and higher proton conductivity (4.0×10^{-2} S/cm). In CTMABr- H_3PO_4 system, the conductivity was found to increase with an increase in the W/Si molar ratio. The preliminary results of the composite membrane suggest tungstosilicates are promising additives for high temperature PEM fuel cell applications.

Acknowledgements. We thank the DOE, THECB/ATP and SAMSUNG for financial support

References

- (1) Nakamura, O.; Kodama, T.; Ogino, I.; and Miyake, Y. *Chem. Letts.*, **1979**, 17.
- (2) Alberti, G. and Casciola, M. *Solid State Ionics*, **2001**, 145, 3.
- (3) Kim, Y. S.; Wang, F.; Hickner, M.; Zawodzinski, T. A.; and McGrath, J. E. *J. Membr. Sci.*, **2003**, 212, 263.
- (4) Tazi, B. and Savadogo, O. *Electrochim. Acta* **2000**, 45, 4329.
- (5) Piquemal, J. Y.; Briot, E.; Chottard, G.; Tougne, Manoli, P. J. M.; and Brégeault, J. M. *Micropor. Mesopor. Mater.*, **2003**, 58, 279.
- (6) Tanaka, R.; Ueoka, I.; Takali, Y.; Katapka, K.; and Saito, S. *Macromolecules*, **1983**, 16, 849.
- (7) Desmarteau, D. D. and Witz, M. *J. Fluorine Chem.* **1991**, 52, 7.
- (8) Mikhailenko, S.; Desplantier-Giscard, D.; Danumah, C.; and Kaliaguine, S. *Micropor. Mesopor. Mater.*; **2002**, 52, 29.

CATALYSTS FOR DIRECT ETHANOL FUEL CELLS

Jonathan Mann, M. Scott Daubin, and Andrew B. Bocarsly

Chemistry Department
Princeton University
Princeton, NJ 08544

Background

Of the two existing pre-market proton exchange membrane fuel cells: hydrogen-oxygen and direct methanol, H₂/O₂ is suggested for applications involving high energy density, while direct methanol holds pragmatic promise for small low power application where ease of fuel handling is critical. Of equal importance, is the energy per unit volume when matching an application to a fuel, since available volume for a mobile application is often a limiting consideration.

A simple review of the thermochemical parameters (provided in Table 1) indicates that ethanol has fuel characteristics similar to methanol. However, it substantially exceeds methanol with respect to volumetric energy density providing 68% of the volumetric energy density of gasoline. Thus, from an energy storage point of view, ethanol appears to be a preferred fuel over methanol.

**Table 1. Energy Content of Fuel Cell Fuels
Assuming Complete Combustion**

Thermochemical Parameter	Ethanol	Methanol	Gasoline
ΔH° , kJ/mol	-1406	-658	
ΔG° , kJ/mol	-1324	-702	
Specific Energy, MJ/kg	26.8	19.9	44.4
Energy Density, MJ/L	21.2	15.8	31.1

Likewise, a strong environmental argument can be made for ethanol over methanol. Methanol is water soluble and rather toxic. As recently seen with the withdrawal of MBTE as a gasoline additive this combination of properties represents an environmental threat. Ethanol though water soluble, is much less toxic than methanol, thus the environmental threat is dramatically attenuated.

Introduction

Ethanol oxidation at the anode of a fuel cell requires the development of a catalyst. The complete anode reaction (1) involves the breaking of C-H bonds and C-C bonds as well as the formation of C=O bonds. New alloys for this catalysis were investigated.



Preliminary fuel cell studies at elevated temperature have shown that ethanol can be oxidized to CO₂ with a yield of 96% above 140°C.¹ It has also been reported that the concentration of ethanol at the electrode surface has a significant effect, with ethanol concentrations much higher than 1 M resulting in catalytic poisoning by adsorbed, partially oxidized ethanol species. This is easily explained by understanding that a high ethanol concentration also means a lower water concentration. It is easy to see from reaction (1) that a decrease in water concentration at the electrode interface will result in incomplete oxidation.²

In addition, studies³ have shown that a variety of bimetallic catalysts containing platinum and a second post-transition metal may be catalytically superior to a pure platinum electrocatalyst. Three different types of broad-based systems have been suggested: bulk alloys, surface ad-atom composites and (quite recently) intermetallic phases.⁴

To date, alloy base systems have received the most attention. Though similar, different trends are noticed for methanol and hydrogen oxidation than for ethanol. Specifically, Pt/Sn alloy systems have been shown to demonstrate higher activity than Pt/Ru, the preferred alloy for methanol and reformed hydrogen oxidation. This finding has been correlated with the need for a large quantity of adsorbed oxygen in the case of ethanol oxidation. Tin adopts an oxidized state while platinum and ruthenium remain in more reduced states. This added oxygen promotes the ethanol oxidation on the Pt/Sn surface over others. It is well established from electrochemical studies that bulk ethanol is oxidized only partially, while surface adsorbed ethanol undergoes complete oxidation to CO₂. As might be expected, the complete oxidation of ethanol requires a higher potential than does the partial oxidation to acetaldehyde or acetic acid; surface adsorbed species do not diffuse away from the electrode before the higher potential is reached. This conclusion not only suggests a strategy for the development of new catalysts, but also indicates that electrochemical studies (which typically utilize low surface area electrodes in contact with an aqueous electrolyte) may not faithfully model the fuel cell environment that incorporates a supported nanoparticulate catalyst bed in contact with a polymer electrolyte.

Experimental

Electrodes. Anodes were prepared from a commercial carbon cloth with a single gas diffusion layer (E-TEK). Catalysts (E-TEK) were Pt binary and ternary alloys on carbon. They were suspended in a solution of iso-propanol and sprayed onto the diffusion layer of the electrode. The catalytic loading was aimed at 0.4 mg/cm², and the exact loading was calculated by mass difference. The same procedure was used to impregnate Nafion into the newly deposited active layer of the anode electrodes. Loadings of 0.6 mg/cm² were the aim for the Nafion.

Cathodes were prepared from commercial carbon cloths with a pre-applied active layer of 0.4 mg/cm² of Pt (E-TEK). Nafion was impregnated into the active layer of the catalysts at a loading of 0.6 mg/cm².

Membranes. Nafion 115 membranes were used after a boiling in successive baths of 0.5 M H₂SO₄, H₂O, 3% H₂O₂, and H₂O twice. Membranes made from dissolved Nafion (Ion Power) combined with metal oxide particles and cast into membranes were also used. This second type of membrane underwent the same kind of treatment before being assembled into the cell.

Cell Testing. The membrane and electrodes were assembled according to existing procedures.⁵ The membrane electrode assembly (MEA) was then inserted into a GlobeTech single cell test station where the potential on each electrode was independently cycled from 0.1 to 1.0 volts at 100 mV/s under nitrogen.

The cell was then moved to a modified GlobeTech single cell test station equipped to deliver liquids to the anode. The liquid at the anode was 1.0 M ethanol flowing at 0.2 mL/min. The cathode was pure oxygen with a flow rate of 150 mL/min. Both sides of the cell were pressurized above 60 psig.

Polarization curves were used to evaluate cell performance as a function of temperature and anode catalyst material. The dependence on flow rate, membrane, and pressure was also considered.

Preliminary Results

Polarization curves for the tested cells confirmed that the Pt:Sn alloy (3:1 atomic ratio) is the preferred catalyst among Pt:Ru (1:1) and Pt (not shown). Both open circuit voltages and activation over potentials are more favorable for the Sn alloy. (Fig. 1.)

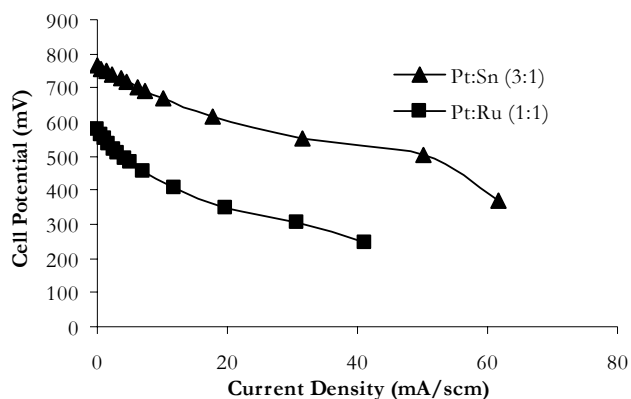


Figure 1. Reproducible comparison of performance of Pt:Sn catalyzed cell with Pt:Ru catalyzed cell.

The standard cell potential for the ethanol reaction is 1.14 V, about 90 mV less than the H_2/O_2 cell, while the open circuit of the ethanol cell, measured as high as 808 mV, is less than 200 mV below that of the common H_2/O_2 cell. This reasonably high open circuit potential is a promising number considering the relatively unresearched array of possible catalytic particles available. However, the extraordinarily low current densities demonstrate that the presently employed catalysis is insufficient at extracting power from the fuel.

Summary

The study of ethanol as a fuel in fuel cells is a relatively new exploration in the field. The motivation to use it over hydrogen or methanol is several-fold, while its demonstrated abilities leave something to be desired. Continued exploration into the vast array of catalytic particles will reveal the most ideal catalytic system which then can be combined with the most successful *in situ* conditions to produce a power source capable of competing with existing electrochemical cells.

References

- 1 (a) Arico, A.S., Creti, P., Antonucci, P.L. and Antonucci V., *Electrochemical and Solid-State Letters*, **1998**, *1*, 66, (b) S. Srinivasan and C. Yang, Private Communication, Princeton University **2000**.
- 2 Wang, J., Wasmus, S., and Savinell, R.F., *Journal of the Electrochemical Society* **1995**, *142*, 4218.
- 3 Zhou, W.J, et al. *Journal of Power Sources*, **2004**, *126*, 16.
- 4 Casado-Rivera, E., et al. *Journal of the American Chemical Society*, **2004**, *126*(12) 4043.
- 5 Adjemian, K.T., et al. *Journal of The Electrochemical Society* **2002**, *149*, A256.

WHAT MATTERS AFTER FIRST ELECTRON TRANSFER IN OXYGEN REDUCTION: A KINETIC STUDY OF Pt(111) AND Pt/C THIN LAYER CATALYSTS ON ROTATING DISK ELECTRODES

Jia X. Wang, Junliang Zhang, and Radoslav R. Adzic

Materials Science Department, Building 555
Brookhaven National Laboratory
Upton, NY 11973

Introduction

Oxygen reduction is one of widely studied reactions because it is the cathodic reaction in fuel cells, corrosion, and several other important processes. From the catalytic point of view, the reaction mechanism on a Pt electrode has attracted most attention because Pt and Pt-alloys are still the most active cathode catalysts for low temperature fuel cells. In electrocatalytic reduction of oxygen, the first electron transfer appears to occur simultaneously with the adsorption of oxygen molecules since there is no evidence for oxygen adsorption at potentials higher than the onset of oxygen reduction reaction (ORR). Although this step may have the highest activation energy and is hence considered to be the rate-determining step, many experimental observations show that the Pt-OH formation and other anion adsorption played an important role in determining catalytic performance.

In this study, we carried out a kinetic analysis of the rotating disk electrode (RDE) polarization curves obtained for Pt(111) in HClO₄ and H₂SO₄ solutions using the adsorption isotherms measured from the voltammetry curves. A negative electronic effect on ORR kinetics was found for both OH and bisulfate adsorbates in addition to site blocking¹. To further study the role of OH adsorption on nanoparticle catalysts, RDE measures of thin-layer catalysts were carried out. The surface oxidation of Pt, was found more irreversible and occurs over wider potential region on nanoparticles than on bulk Pt. The time dependent polarization curves in HClO₄ were measured and the roles of the reaction intermediates and the dynamic equilibrium coverage of Pt-OH in determining the quasi-stable kinetic current of ORR will be demonstrated.

Experimental

The carbon-supported Pt catalyst (20%Pt/C HP, E-TEK) was deposited on a glassy carbon electrode by placing 15 μl catalyst suspension over 0.168 cm² electrode area with Pt loading between 30 and 60 nmol/cm². The 0.1 M HClO₄ solution was prepared from ultrapure perchloric acid and MilliQ UV-plus water (Millipore). An Ag/AgCl/(3M KCl) reference electrode was used with a double-junction reference chamber and all potentials are quoted with respect to reversible hydrogen electrode (RHE).

Results and Discussion

Intrinsic kinetic parameters and anion adsorption effects on the Pt(111) electrode. In analysis of the RDE polarization curves for Pt(111) in HClO₄ and H₂SO₄ solutions, the Tafel slope and the exchange current on an adsorbate-free surface were defined as the intrinsic kinetic parameters. The site blocking and electronic effects of adsorbed anions were evaluated with the adsorption isotherms incorporated in the model. As shown in Fig. 1, a reversible OH (in HClO₄) adsorption occurs at potentials positive of 450 mV and (bi)sulfate ions adsorb above 370 mV, which blocks the OH adsorption up to 900 mV. The anion adsorption isotherms were

obtained by integrating the corresponding current curves above these potentials.

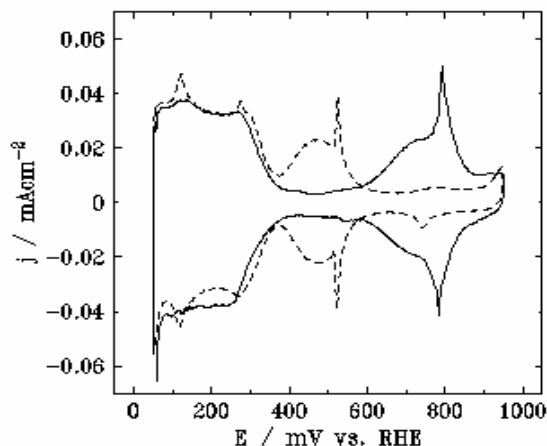


Figure 1. Linear sweep voltammetry curves for Pt(111) in Ar-saturated 0.1 M HClO₄ (solid line) and 0.05 M H₂SO₄ (dashed line) solutions. Sweep rate 50 mV/s.

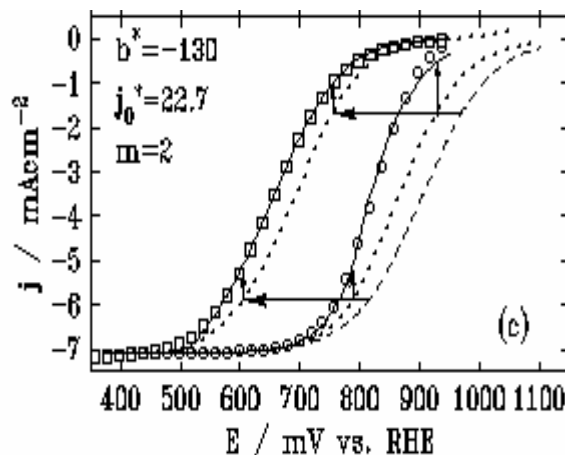


Figure 2. Polarization curves for Pt(111) in 0.1 M HClO₄ (circles) and 0.05 M H₂SO₄ (squares) solutions with calculated curves discussed in the text.

With the intrinsic kinetic parameters kept to the same values for the RDE polarization curves in both solutions, the anion adsorption effects were quantitatively evaluate using the following equation for the kinetic current:

$$j_k(E) = -j_0^*(1 - \gamma_A \theta_A(E))^m \exp(2.303(E - E^0 - \varepsilon_A \theta_A(E))/b^*)$$

where γ and ε are the site-blocking and energy coefficients for either OH or bisulfate anion, and m is the number of Pt sites involved in the rate determining step. The best fits, shown by the solid lines in Fig. 2, yielded the intrinsic Tafel slope in the range from -118 to -130 mV/dec, supporting single electron transfer in the rate-determining step with the corresponding transfer coefficients equal to 0.50 and 0.45, respectively.

To illustrate the effect of anion adsorption on the ORR kinetics, additional lines were provided in Fig. 2. The dashed line is obtained with the intrinsic kinetic parameters without any adsorption effects and the dotted lines are calculated with the electronic effect included. The differences between the dashed and dotted lines show the

electronic effect of adsorbed anions on the activation energy causing a potential shift indicated by the horizontal arrows. Since the solid lines include both the site-blocking and electronic effects while the dotted lines excludes the site-blocking effect, the differences between the two curves show the site blocking effects as marked by the vertical arrows. For HClO_4 solutions, both effects increase at higher potentials, which cause the slope of the ORR polarization curve, or the apparent Tafel slope, deviates from the intrinsic value. Since bisulfate adsorption saturates at a low potential, both site-blocking and electronic effects are nearly constant over the mixed kinetic-diffusion controlled region in H_2SO_4 solutions, and thus the apparent Tafel slope remains close to the intrinsic value.

These analyses also show that the catalytic performance of Pt for ORR is largely constrained by the OH adsorption and surface oxidation in the absence of other specifically adsorbed anions. Further studies of these effects were carried out on Pt nanoparticle catalyst as discussed below.

OH adsorption and surface oxide formation on Pt nanoparticles. Recently, we demonstrated that a thin-layer of a carbon-supported Pt nanoparticle catalyst can be deposited onto a glassy carbon rotating-disk electrode without using Nafion to stabilize it, and that to extract useful kinetic information from rotating-disk electrode's measurements, it is important to have a small enough loading so that full utilization is reached². For the oxygen-reduction, we found that the suitable Pt loading is 30-50 nmol/cm^2 .

Fig. 3a shows several voltammetry curves with different positive potential limits. When the potential was swept to more positive limits, the current in the reversed sweep increases below 100 mV, which indicates that OH adsorption on nanoparticles occurs over a wide potential region and the corresponding reduction requires a very low potential. This behavior is reflected on the dependence of the ORR polarization curve on the sweep rate. As shown in Fig. 3b, the curve taken at 50 mV/s exhibits higher activity than that measured at 10 mV/s.

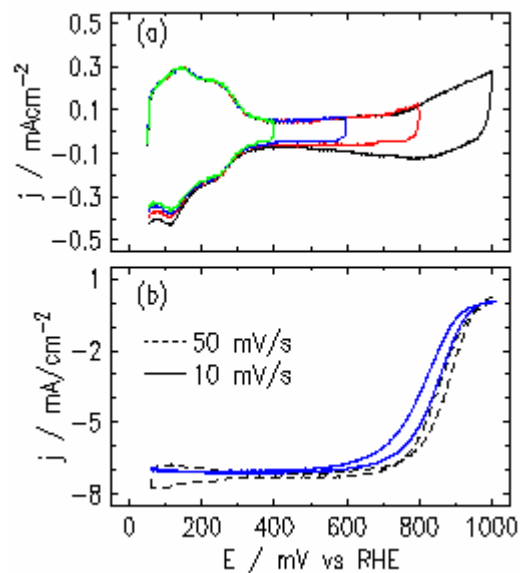


Figure 3. (a) Linear sweep voltammetry curves for Pt/C (20% wt, E-TEK, 30 nmol/cm^2) in Ar-saturated 0.1 M HClO_4 . Sweep rate 50 mV/s. (b) Polarization curves in oxygen saturated 0.1 M HClO_4 .

To obtain time-dependent polarization curve, we measured current at 2500 rpm as a function of time after stepping the potential from 50 mV to a given value as shown in Fig. 4. For all measured potentials, the maximum ORR current was reached within 1 sec and a gradual decay of activity follows. The maximum currents near 1 sec, and the currents at 1 and 5 min are plotted as a function of potential in Fig. 5.

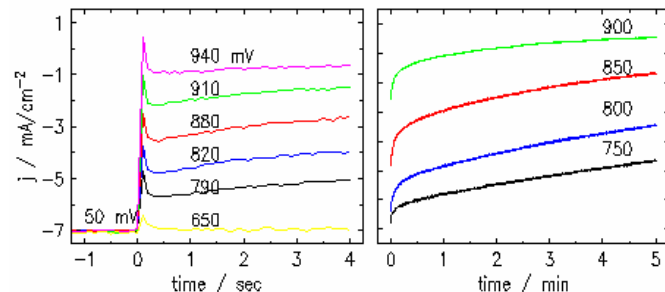


Figure 4. ORR currents at 2500 rpm as a function of potential after stepping the potential from 50 mV to the given potentials in 0.1 M HClO_4 solution.

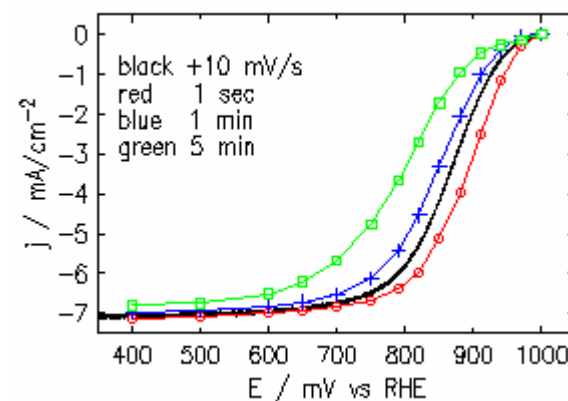


Figure 5. Time-dependent polarization curves for ORR at 2500 rpm in 0.1 M HClO_4 solution.

More data will be provided to identify the cause of the activity decay, which has also been studied by Uribe et. al in polymer electrolyte fuel cells³. The implications of the findings will be discussed.

Acknowledgement. This work is supported by U.S. Department of Energy, Divisions of Chemical and Material Sciences, under the Contract No. DE-AC02-98CH10886.

References

1. Wang, J.X.; Markovic, N.M.; Adzic, R.R., *J. Phys. Chem. B* **2004**, *108*, 4127.
2. Wang, J.X.; Brankovic, S.R.; Zhu, Y.; Hanson, J.C.; Adzic, R.R., *J. Electrochem. Soc.*, **2003**, *150*, A1108.
3. Uribe, F. A.; Zawodzinski Jr., T. A., *Electrochimica Acta* **2002**, *47*, 3799.

FUNCTIONALIZED NANOSTRUCTURED CARBONS FOR FUEL CELL ELECTRODES

Mark W. Perpall, Ibrahim Shaban, Hua Mei, Stephen E. Creager,
Darryl D. Desmarteau, Dennis W. Smith, Jr.*

Department of Chemistry, Clemson University, Clemson, SC 29678

Introduction

Bis-ortho-diyne arene or BODA monomers¹ have been used to fabricate nanostructured carbon materials² through their unique combination of excellent processability and high carbon yield. The enediyne functionality of the monomers undergo a thermal Bergman cycloaromatization reaction that yields reactive naphthalene diradicals which polymerize to form polynaphthalene. (Figure 1) The tetrafunctionality of the monomers allows for both a higher processing window due to extensive branching and ultimately the formation of network polymers. The high carbon yield results in less shrinkage of the polymer upon pyrolysis to the glassy carbon state. This allows for the faithful templating of carbon structures from a polymeric precursor.

Hydrogen fuel cell electrodes require several properties for optimum performance. An ideal electrode would have as high a surface area as possible with a uniform dispersion of nano-scale catalyst particles attached to the surface. The electrode must be electrically conductive and have good mass transport for products and reactants. Carbon supported platinum is the best known catalyst for the oxidation of hydrogen at the anode and the reduction of oxygen at the cathode of a proton exchange membrane fuel cell (PEMFC)³. The material also must have good compatibility with the material used for the proton exchange membrane in the membrane electrode assembly (MEA), usually a sulfonated fluoropolymer such as Nafion.

We have undertaken a study to prepare a high surface area carbon material through a BODA templating method which can then be functionalized with both well dispersed platinum nanoparticles to act as catalysts and fluorophilic groups to facilitate the compatibility of the membrane and electrodes in the MEA.

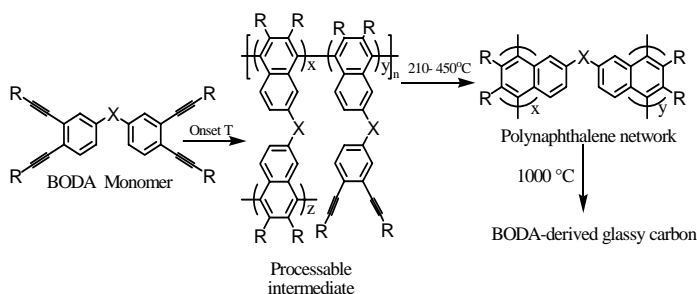


Figure 1. Polymerization of BODA monomers

Experimental

Materials. All BODA monomers were synthesized as previously reported.^{1,2b} H₂PtCl₆ was purchased from Strem Chemicals. Karstedt's catalyst was purchased from GFS Chemicals. 4-acetylamino-phenol was purchased from Avocado Research Chemicals. All chemicals were used as received, unless otherwise noted.

Fabrication. BODA derived carbon materials were templated with a disordered monolith composed of nanoparticles of silica synthesized from a sol-gel and sintered together at 900 °C. The BODA monomer was melted into the free space in the monoliths to replicate the disordered porosity of the template into the polymer. The polymer was fully cured by heating under nitrogen. Further heating leads to pyrolysis of the polymer network and glassy carbon formation. The template was then removed with HF.

Platinum Functionalization. Platinum functionalization was attempted by several different methods. The platinum particles can be preliminarily synthesized and adsorbed onto the carbon surface, or the particles can be formed from an adsorbed platinum precursor with in situ reduction methods. Further attempts have included the adsorption of Pt(0) species which theoretically would lose the organic ligands and coalesce into Pt(0) particles. **Method 1.** Platinum sol formed from H₂PtCl₆ reduced with sodium citrate, then adsorbed onto carbon.⁴ **Method 2.** H₂PtCl₆ adsorbed onto carbon then

reduced with formaldehyde.⁴ **Method 3.** H₂PtCl₆ adsorbed onto carbon then reduced with sodium borohydride.³ **Method 4.** H₂PtCl₆ adsorbed onto carbon then reduced under H₂ flow in tube furnace.⁵ **Method 5.** Karstedt's Catalyst [Pt₂((CH₃)₂C₂H₃Si₂O)₃] (1 mL 10 % in xylene) was adsorbed onto 0.029 g carbon, dried and heated under N₂ at 300 °C in a tube furnace for 1h.

Fluorine Functionalization. Incorporation of fluorine containing groups onto the surface of the carbon materials was attempted in several different ways. Direct fluorination of aromatic groups is possible using certain classes of electrophilic fluorine reagents. Alternatively, incorporation of fluorine containing groups can be achieved through reaction of carbon or functional groups on carbon. A few methods have already been attempted. N-fluorobenzene sulfonimide (NFSi) reacted with carbon samples from Aerogel and templated BODA samples.⁶ Diethylamino Sulfur trifluoride (DAST) was reacted with oxidized carbon aerogel sample (refluxed in HNO₃, 13h) at -78 °C to room temperature.⁷ Carbon reacted with diazonium salt⁸. Diazonium salts were all synthesized from their corresponding amines.⁹ The Trifluorovinylether aniline was first synthesized by Harris et al.¹⁰

Surface Area Measurements. BET surface area measurements were performed using N₂ gas adsorption on a Micromeritics instrument.

Results and Discussion

BODA-Derived Carbon Foams. The carbon used in a fuel cell electrode must have high specific surface area for maximum efficiency in facilitating the redox reactions at the catalyst. BODA monomers were therefore templated with colloidal silica nanoparticles and thermally polymerized and carbonized in situ to yield an open shell three dimensional carbon foam with very high specific surface area (Figure 3). The templating fidelity of the monomers is dependent on its wettability with the template material. This can be controlled through the variability of the terminal group R on the monomer (Figure 2). Templated carbon materials were prepared using the same process from several different monomers. The BET surface area was then measured using N₂ gas adsorption. The results are summarized in Table 1. The carbon templated using monomer 1 yielded the highest specific surface area of 275 m²/g.

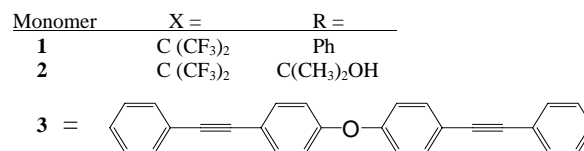


Figure 2. BODA monomers 1, 2 and Bisacetylene 3.

Table 1 Composition of Precursor BODA Polymer Network and BET Specific Surface Area of Templated Carbon Foams

Monomer composition	BET Surface Area, (m ² /g)
100 % 1	275
100 % 2	135
80% 1, 20% 3	51
100 % 3	95

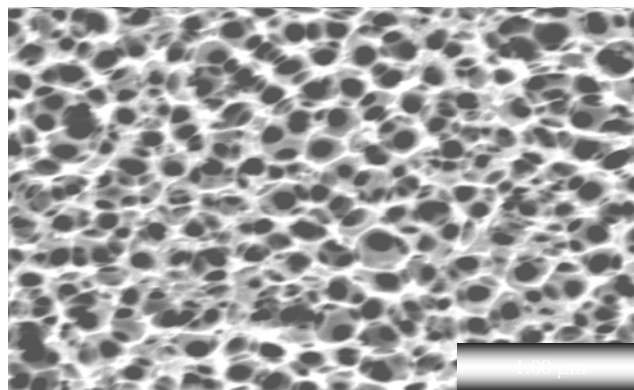


Figure 3. SEM of Templated BODA Carbon Material.

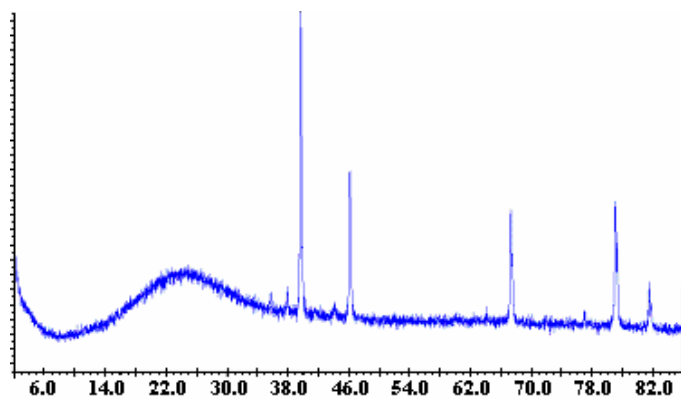


Figure 4. X-ray diffraction of Pt particles on BODA derived carbon

Platinum Incorporation. The platinum nanocatalyst syntheses can be divided into two basic paradigms: 1) pre-synthesis/ adsorption and 2) in situ reduction. Methods 1 and 5 represent the pre-synthesis/ adsorption route, where a Pt (0) species is adsorbed directly onto the surface of the carbon. This technique ensures that all of the platinum incorporated into the material will be surface bound and accessible for reaction in the fuel cell. Particle size is also better controlled and more monodisperse. Methods 2, 3, and 4 are all variations of the in situ reduction of a platinum salt method. This method involves immersing the carbon in a solution of a platinum salt and then using a chemical reducing agent to form the Pt (0) species within the framework of the carbon. This approach leads to a good dispersion of platinum particles over the entire surface of the carbon material.

Each method was attempted using enough platinum or platinum precursor to yield a final Pt loading of 20 % by weight with a carbon aerogel material. The samples were then analyzed using scanning electron microscopy (SEM) to determine catalyst size and dispersity and energy dispersive x-ray spectroscopy (EDX) for elemental analysis. The nanoparticles of platinum were not observed in any of the samples due either to too small of size for the resolution of the microscope or due to coalescence of the particles together on the surface. The EDX data, as summarized in **Table 2** support the conclusion that the loading of platinum was too high for the surface area of the carbon and the size of particle formed. There is a greater than expected loading of platinum observed on the surface of the carbon for three of the methods. Method 1 seems to suffer from a poor adsorption of the platinum sol onto the carbon surface. The lack of control over loading is a major drawback for this method. Method 4 showed a platinum content very close to the expected platinum loading value. This indicates either good dispersity throughout the sample or a low yield of Pt (0) species from the precursor salt. In future experiments, the loading of the platinum should be related to the available surface area of the carbon support to prevent coalescence of the platinum nanoparticles on the limited surface.

The platinum nanoparticles may also be analyzed using wide angle x-ray scattering (WAXS) techniques, such as the pattern shown in **Figure 4**, which shows the platinum particles remaining after thermal oxidative removal of the carbon support. The large broad reflection indicates the presence of some carbon that was not fully removed. The sharp lines indicate the platinum that is left after the oxidation step. It is uncertain exactly what species is indicated. The peak width may be exploited to determine particle size. Unfortunately the particles are not visible in WAXS unless the carbon is removed, in a step which may also effect either the platinum species that exists or the particle size

Table 2. EDX-Derived Elemental Analyses for Surfaces of Platinum Incorporated Carbon Samples.

Platinum incorporation method	C content (%)	Pt content (%)
1	86.5	2.7
2	16.2	80.9
3	15.1	83.1
4	72.3	16.8
5	27.5	53.7

Fluorine Incorporation. The incorporation of fluorine onto the carbon electrode material to aid in compatibilizing the electrode with the proton exchange membrane for close contact can be achieved by either the direct fluorination of the carbon material or incorporation of another fluorine containing functionality. Attempts at analyzing carbon materials with diamond ATR-IR have had only moderate success due partially to the inherent absorption of light by carbon. New peaks are detected around 1100 cm^{-1} that may be attributable to new aromatic C-F bonds formed by the direct fluorination of carbon using DAST. No such peaks are visible for the other direct fluorination methods. The incorporation of fluorine may also be possible by including it with another group that can readily be attached to carbon such as a diazonium salt. Diazonium salts add to carbon materials, by dediazonium to form a reactive phenyl cation which then adds to the carbon.¹¹ Several diazonium salts have been prepared as shown in **Figure 5** with $R = \text{CF}_3$ and OCFCF_2 . The latter species is a reactive species from which high molecular weight fluoropolymers may be grown from the surface of the carbon. This allows for high fluorine content to be achieved from even moderate carbon functionalization yields.

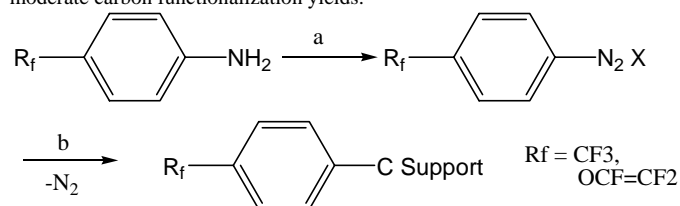


Figure 5. Synthesis of Diazonium Salts and functionalization of carbon support. a) NaNO_2 , HCl , H_2O b) Carbon powder, H_3PO_2 , 5°C , 40 min.

Conclusions

Through the right combination of a suitable platinum nanoparticle formation technique, a suitable surface fluorine incorporation technique and the templated BODA carbon fabrication method, a very attractive approach for fabricating hydrogen PEM fuel cell electrodes should show promise for reducing some of the efficiency depriving faults in today's fuel cells technology.

Acknowledgement. The authors would like to recognize the financial support of NSF/ NER for funding the project. We would also like to recognize the assistance of Dr. K. Prasanna Perera, Dr. Suresh Iyer, Dr. Sibylle Glaser, and Dr. Chris Topping.

References

- Smith, Jr., D.W.; Babb, D.A.; Snelgrove, R.V.; Townsend, III, P.H.; Martin, S.J. *J. Am. Chem. Soc.* **1998**, *120*, 9078-9079.
- a) Perpall, M.W.; Zengin, H.; Perera, K.P.U.; Zhou, W.; Shah, H. Wu, X.; Creager, S.E.; Smith, Jr., D.W.; Foulger, S.H.; Ballato, J. *Proc. of SPIE*, **2003**, *4979*, 307-316. b) Perpall, M.W.; Perera, K.P.U.; Dimaio, J.; Ballato, J.; Foulger, S.H.; Smith, Jr., D.W. *Langmuir* **2003**, *19*, 7153-7156.
- Ye, S.; Vijn, A.K.; Dao, L.H. *J. Electrochem. Soc.* **1996**, *143*, L7-L9.
- Frelink, T.; Visscher, W.; van Veen, J.A.R. *J. Electroanal. Chem.* **1995**, *382*, 65-72.
- Joo, S.H.; Choi, S.J.; Oh, I.; Kwak, J.; Liu, Z.; Terasaki, O. Ryoo, R. *Nature* **2001**, *412*, 169-172.
- Singh, S.; Desmarteau, D.D.; Zuberi, S.S.; Witz, M.; Huang, H.-N. *J. Am. Chem. Soc.* **1987**, *109*, 7194-7196.
- Middleton, W.J. *J. Org. Chem.* **1975**, *40*, 574-578.
- Pandurangappa, M.; Lawrence, N.S.; Compton, R.G. *Analyst* **2002**, *127*, 1568-1571.
- Finger, G.C.; Oesterling, R.E. *J. Am. Chem. Soc.* **1956**, *78*, 2593-2596.
- Choi, W.-S.; Harris, F.W. *Polymer* **2000**, *41*, 6213-6221.
- Zollinger, H. *Diazo Chemistry I*; VCH: New York, NY, 1994; Vol. 1, pp 161-212.

DEVELOPMENT OF AIR-BREATHING DIRECT ETHANOL FUEL CELLS WITH PtSn AS ANODE

Luhua Jiang^a, Zhenhua Zhou^b, Suli Wang^a, Jianguo Liu^a,
Xinsheng Zhao^a, Gongquan Sun^a, Qin Xin^{ac*}, Bing Zhou^b

^aDirect Athanol Fuel Cells Laboratory, Dalian Institute of Chemical Physics, CAS, P.O. Box 110, Dalian 116023, China

^bHeadwaters Nanokinetix, 1501 New York Avenue, Lawrenceville, NJ 08648, USA

^cState Key Laboratory of Catalysis, Dalian Institute of Chemical Physics, CAS, P.O. Box 110, Dalian 116023, China

Introduction

In the past decades direct methanol fuel cells (DMFCs) have been studied extensively as promising power sources for portable devices, electric vehicles due to their high power density, simplified system and the ease of fuel transportation and storage. Although great progress has been made in this field¹⁻⁷, the commercialization process of the direct methanol fuel cell is postponed due to the sluggish methanol oxidation kinetics, methanol crossover and the toxicity of methanol. Compared to methanol, ethanol with reduced crossover is cleaner, safer and available from fermentation of sugar-containing raw materials. These features make ethanol more attractive than methanol for direct alcohol fuel cells operating at lower temperatures^{8,9}. Great efforts have been made so far¹⁰⁻¹³. However, difficulties and challenges for crack of C-C bond via optimal PtRu based electrocatalysts are great¹⁴⁻¹⁶. In this paper, with PtSn as anode, the performance of DEFCs with two different electrode structures was measured using pure oxygen and air as oxidant, respectively. More importantly, a comparable performance of air-breathing DEFC to DMFC is supplied for the first time¹⁷.

Experimental

PtSn/C (with different Pt/Sn atomic ratios of 2:1, 3:1, 4:1, denoted as Pt₂Sn/C, Pt₃Sn/C, Pt₄Sn/C, respectively) and Pt/C employed in the present paper were all homemade according to literature¹⁸. Electroactivities of the homemade PtSn/C catalysts were measured first by cyclic voltammetry using an EG&G model 273 potentiostat/galvanostat and a three-electrode test cell at room temperature. The conventional membrane electrode assemblies (MEAs) were fabricated according to the method described in the literature¹⁹. The improved CCM MEAs were prepared by spraying the catalyst on the Nafion membrane. MEAs were made by hot-pressing the diffusion layer on either side of Nafion membranes with catalyst layers at 140 °C for 90 s. Nafion 115 (DuPont) was used as the electrolyte membrane for all the MEAs reported here. MEAs were tested using a homemade 4 cm² single cell with reservoir. The ethanol was injected into the fuel reservoir using a micro syringe. The cathode was opened to air. The load was varied using a rheostat when voltage (V)-current density (*I*) curves were collected. The MEAs had been activated by 1 M ethanol for 2 hours before all the data were collected.

Results and Discussion

The TEM images of homemade 20 wt.% Pt/C, 50 wt. % Pt/C and 20 wt.% Pt₃Sn/C catalysts are shown in Fig. 1.

Fig. 2 shows the cyclic voltammogram of ethanol electrooxidation with PtSn/C as electrode. It can be seen clearly that the ethanol oxidation current peaks with different PtSn/C catalysts all started at around 500 mV, but the Pt₃Sn/C catalyst brought the highest oxidation current in contrast to the Pt₄Sn/C with the lowest oxidation current. This result indicated that Pt₃Sn/C might be a better catalyst for ethanol oxidation.

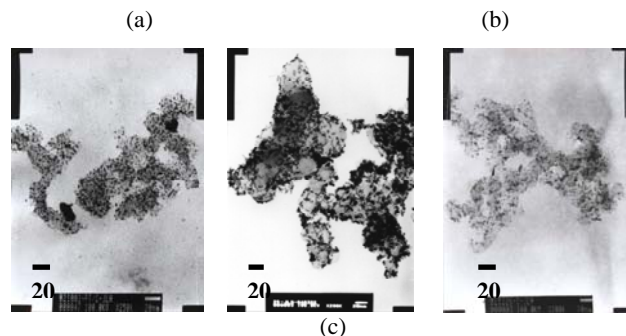


Figure 1. TEM images of (a) 20 wt.% Pt/C (b) 50 wt.% Pt/C (c) 20 wt.% Pt₃Sn/C

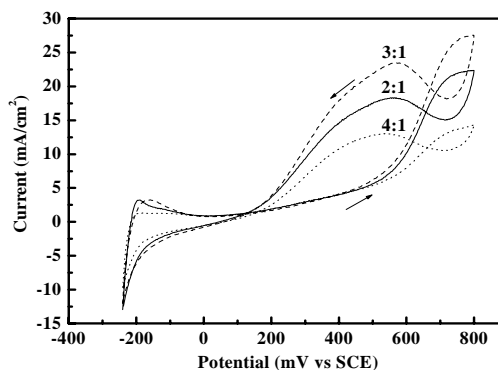


Figure 2. The CV results of PtSn/C catalysts with different atomic ratio for ethanol electro-oxidation. Operation Temperature: 25 °C. Scan rate: 50 mV/s. Electrolyte: 0.5 M EtOH + 0.5 M H₂SO₄

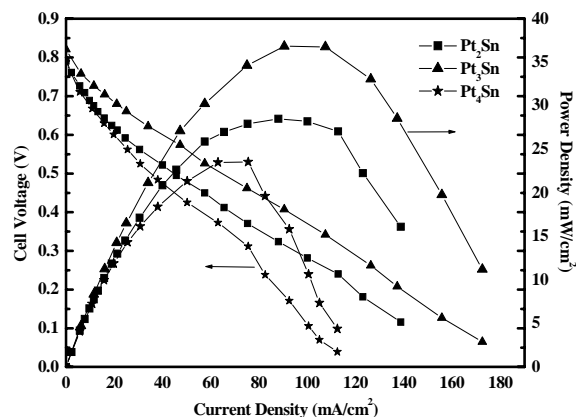


Figure 3. Performance of the active direct ethanol fuel cell with conventional electrode structure operated at 90 °C. Anode catalyst and metal loading: PtSn/C, 1.5 mg Pt/cm², cathode catalyst and metal loading: 1.0 mg Pt/cm² (20 wt. % Pt/C), ethanol concentration and flow rate: 1 M & 1.0 ml/min, oxidant: O₂

Fig. 3 shows the performance for electrodes with conventional electrode structure. It can be seen that the Pt₃Sn/C electrode shows the best performance and the maximum output power density is about 38 mW/cm². The next is Pt₂Sn/C, which shows a maximum power density of 27 mW/cm². Pt₄Sn/C electrode presents the worst performance. This result is in good agreement with the above CV screening results. Another interesting phenomenon could be observed in Fig. 3. As are known, the cell voltage of DMFCs decreases sharply at high current density, which might be due to the mass transport limitation rising from anode or cathode. However, unlike the V-I curves of DMFCs, the I-V curves of DEFCs decrease linearly with current density increasing. This might suggest that for DEFCs, mass transport limitation whether from anode or from cathode might be not the rate-determining step (RDS). It is not surprising that the mass transport is not the RDS for the slow dynamics of ethanol oxidation at such temperature.

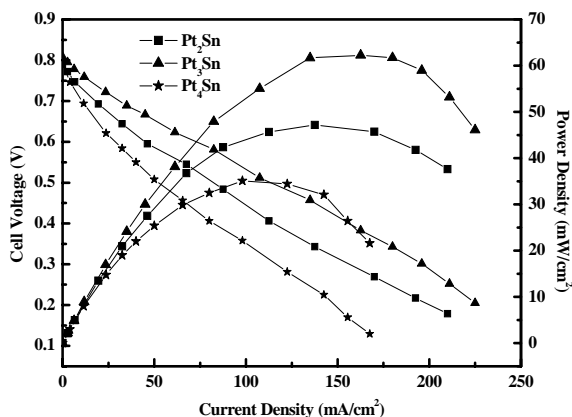


Figure 4. Performance of the active direct ethanol fuel cell with CCM electrode structure operated at 90 °C. Anode catalyst and metal loading: PtSn/C, 2.0 mg Pt/cm², cathode catalyst and metal loading: 1.0 mg Pt/cm² (50 wt.% Pt/C), ethanol concentration and flow rate: 1 M & 1.0 ml/min, oxidant: O₂

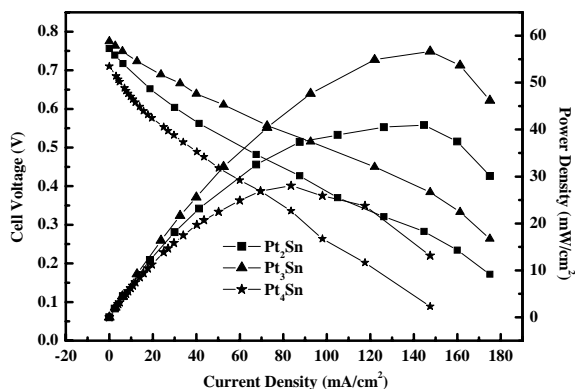


Figure 5. Performance of the active direct ethanol fuel cell with CCM electrode structure operated at 90 °C. Anode catalyst and metal loading: PtSn/C, 2.0 mg Pt/cm², cathode catalyst and metal loading: 1.0 mg Pt/cm² (50 wt.% Pt/C), ethanol concentration and flow rate: 1 M & 1.0 ml/min, oxidant: air

Fig. 4 shows the performance of DEFCs with CCM electrode

structure. It can be observed that the performance of DEFCs with CCM electrode structure was enhanced greatly in comparison with the performance of DEFCs with the conventional one. The best performance is still presented by Pt₃Sn/C, which brought the maximum power density of 62 mW/cm². Even the worst catalyst Pt₄Sn with CCM electrode structure in this research shows a comparable performance (the maximum output power density is 35 mW/cm²) with the best catalyst Pt₃Sn/C with conventional one. While even with the CCM electrode structure, mass transport limitation phenomenon is not observed yet. This might indicate that the ethanol oxidation is still the RDS at the operation temperature, although the CCM electrode structure enhances the DEFCs performance.

Fig. 5 is the performance of DEFCs with CCM electrode structure operated with air as oxidant. It can be observed that the change of oxidant from O₂ to air brought a little decrease of the performance. The maximum output power density is 57 mW/cm² (Pt₃Sn/C), 41 mW/cm² (Pt₂Sn/C) and 28 mW/cm² (Pt₄Sn/C), respectively. It is understandable that there is only a little drop of cell performance with the oxidant changing from O₂ to air on the premise of ethanol oxidation being the RDS as the above discussion. Based on this premise, the oxygen in air is enough to meet the reaction requirement. So it is extremely suitable for ethanol to act as air-breathing fuel considering the insensibility of ethanol oxidation to the concentration of oxygen.

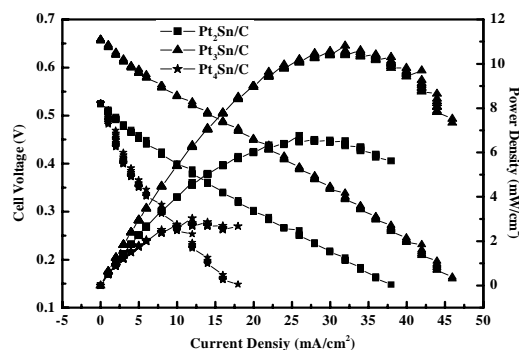


Figure 6. Performance of the passive air-breathing direct ethanol fuel cell operated at 30 °C. Anode catalyst and metal loading: PtSn/C, 2.0 mg Pt/cm², cathode catalyst and metal loading: 1.0 mg Pt/cm² (50 wt.% Pt/C). The ambient air was used as oxidant.

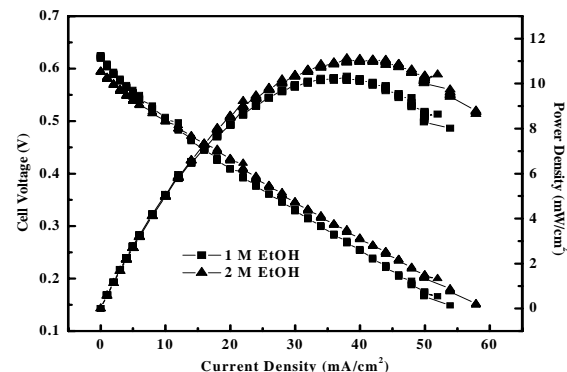


Figure 7. The effect of ethanol concentration on the performance of the passive air-breathing DEFCs operated at 30 °C. Anode catalyst and metal loading: Pt₃Sn/C, 2.0 mg Pt/cm², cathode catalyst and metal loading: 1.0 mg Pt/cm² (50 wt.% Pt/C). The ambient air was used as oxidant.

The air-breathing performance tests were conducted at room temperature under static feed conditions: air was fed only through natural convection and the methanol solution was stored in the reservoir that contacted the MEA on the anode side. Different ethanol concentrations were employed to test the cell performance. The results were shown in Fig. 6. It can be seen that the cell performance with Pt₃Sn/C as the anode catalyst showed the best performance. The maximum output power density with Pt₃Sn/C, Pt₂Sn/C and Pt₄Sn/C as the anode catalyst are 10 mW/cm², 6 mW/cm² and 2.5 mW/cm², respectively.

Fig. 7 shows the influence of ethanol concentration on the performance of DEFCs with CCM electrode structure. It can be seen that the concentration increase of ethanol from 1 M to 2 M only brought a little performance improvement of 1 mW/cm². It can be seen that the cell performance is insensitive to the ethanol concentration in the studied range. This suggests that the anode mass transport has little influence on the performance of DEFCs. But usually, it is believed that the performance of DMFCs with the CCM electrode structure is enhanced via improving the mass transport in MEAs. It was observed that the delamination of the catalyst layer and the electrolyte membrane in DEFCs with CCM electrode structure is not so serious as those with conventional one after performance tests. In order to quantify the effect of cell internal impedance on the improvement of DEFCs performance, the impedance of the DEFCs with different electrode structures was measured. The results showed that all the DEFCs with CCM electrode structure present much smaller internal impedance than those with conventional one. The improvement of the DEFCs performance might be mainly derived from the decreased internal impedance of the former.

Highly active PtSn/C electrocatalyst was employed to the anode of DEFCs with a CCM electrode structure. This electrodes exhibited excellent performance. Using homemade 20 wt.% PtSn/C and 50 wt.% Pt/C yielded the best performance. With the CCM electrode structure, power density as high as 62 mW/cm² and 57 mW/cm² were achieved with pure O₂ and air as oxidant at cell temperature of 90 °C, respectively, for a cathode with a Pt loading of 1 mg Pt/cm² and anode with 2 mg Pt/cm². With the same anode and cathode noble metal loadings, power density of air-breathing DEFCs is about 10 mW/cm² at 30 °C. The improvement of the DEFCs performance might be mainly derived from the decreased internal impedance in the DEFCs with the CCM electrode structure. Further research on the optimal electrode structure for DEFCs and the reaction mechanism of ethanol on PtSn catalysts is being carried out.

Acknowledgment. The present work was partly supported by National Natural Science Foundation of China (Grant No 29976006, Grant No 29876040) and Innovation Foundation of Dalian Institute of Chemical Physics (K2003D2). The authors are grateful to Engineer Fengliang Zhao and Likang Chen for kindly offering the air-breathing test device. We are also grateful to Professor Shaohua Yang for discussion and revision.

References

1. Ren, X.; Zelenay, P.; Thomas, S.; Davey, J.; Gottesfeld, S., *J. Power Sources*, **2000**, 86, 111.
2. Lamy, C.; Lima, A.; LeRhun, V.; Delime, F.; Cutanceau, C.; Leger, J-M., *J. Power Sources*, **2002**, 105, 283.
3. Ren, X.; Wilson, M.; Gottesfeld, S., *J. Electrochem. Soc.*, **1996**, 143, 12.
4. Wasmus, S.; Kuver, A., *J. Electroanal. Chem.*, **1999**, 461, 14.
5. Wei, Z.B.; Wang, S.L.; Yi, B.L.; Liu, J.G.; Chen, L.K.; Zhou, W.J.; Li, W.Z.; Xin, Q., *J. Power Sources*, **2002**, 106, 364.
6. Surampudi, S.; Narayanan, S.R.; Vamos, E.; Frank, H.; Halpert, G.; Lacont, A.; Kosek, J.; Prakash, G.; Olah, G., *J. Power Sources*,

7. Liu, J.G.; Sun, G.Q.; Zhao, F.L.; Wang, G.X.; Zhao, G.; Chen, L.K.; Yi, B.L.; Xin, Q., *J. Power Sources*, **2004**, in press.
8. Ianniello, R.; Schmidt, V.M.; Rodriguez, J.L.; Pastor, E.; *J. Electroanal. Chem.*, **1999**, 471, 167.
9. Chen, G.L.; Chen, S.P.; Zhou, Z.Y.; Zhen, C.H.; Sun, S.G., *J. Electrochem.(Chinese)*, **2001**, 7, 96.
10. Arico, A.S.; Creti, P.; Antonucci, P.L.; Antonucci, V., *Electrochem. Solid-State Lett.*, **1998**, 1, 66.
11. Tremiliosi-Filho, G.; Gonzalez, E.R.; Motheo, A.J.; Belgsir, E.M.; Leger, J.-M.; Lamy, C., *J. electroanal. Chem.*, **1998**, 444, 31.
12. Lamy, C.; Belgsir, E.M.; Leger, J-M., *J. Appl. Electrochem.*, **2001**, 31, 799.
13. Ha, S.; Adams, B.; Masel, R.I., *J. Power Sources*, **2004**, in press.
14. Zhou, W.J.; Zhou, Z.H.; Song, S.Q.; Li, W.Z.; Sun, G.Q.; Tsiakaras, P.; Xin, Q., *Appl. Catal.*, **2003**, 46, 273.
15. Zhou, W.J.; Zhou, B.; Li, W.Z.; Zhou, Z.H.; Song, S.Q.; Sun, G.Q.; Xin, Q.; Douvartzides, S.; Goula, M.; Tsiakaras, P., *J. Power Sources*, **2004**, 126, 16.
16. Zhou, W.J.; Li, W.Z.; Song, S.Q.; Zhou, Z.H.; Jiang, L.H.; Sun, G.Q.; Xin, Q.; Poulitanis, K.; Kontou, S.; Tsiakaras, P., *J. Power Sources*, **2004**, in press.
17. Dillon, R.; Srinivasan, S.; Arico, A.S.; Antonucci, V., *J. Power Sources*, **2004**, in press.
18. Zhou, Z.H.; Wang, S.L.; Zhou, W.J.; Wang, G.X.; Jiang, L.H.; Li, W.Z.; Song, S.Q.; Liu, J.G.; Sun, G.Q.; Xin, Q., *Chem. Comm.*, **2003**, 3, 394.
19. Zhou, Z.H.; Wang, S.L.; Zhou, W.J.; Jiang, L.H.; Wang, G.X.; Sun, G.Q.; Zhou, B.; Xin, Q., *Phys. Chem. Chem. Phys.*, **2003**, 5, 5485.

ELECTROCATALYST MATERIALS FOR PEM FUEL CELLS BASED ON HETEROPOLY ACIDS

Andrew M. Herring,¹ Mei-Chen Kuo,¹ Ronald J. Stanis,¹
Brad R. Limoges¹, John A. Turner.

Department of Chemical Engineering¹
Colorado School of Mines
Golden, CO 80401-1887

Hydrogen and Electricity, Systems and Infrastructure Group²
National Renewable Energy Laboratory
Golden, CO 80401-3393

Introduction

One of the major barriers to the commercialization of proton exchange membrane, PEM, fuel cells is the expense of the platinum needed to catalyze the electrodes. In addition the kinetics of oxygen reduction is slower than desirable and the platinum anode is easily poisoned by carbon monoxide a by-product of hydrogen production from hydrocarbon reforming. The ideal electrode materials for a commercially viable fuel cell would be inexpensive, have fast kinetics and not be poisoned by small molecules.

The Heteropoly acids (HPA) a large and diverse class of polyoxometallates that can act as redox catalysts when substituted by a transition metal, are proton conductors, and can be reduced to form electronically conducting materials [1]. This makes the HPA ideal candidates for an electrode material in a PEM fuel cell as the catalyst would ideally enable fast transfer of protons and electrons as well as be a selective catalyst. Some heteropolyoxometalates have been explored as possible electrocatalysts for PEM fuel cell applications [2]. Functionalized heteropoly acids, HPA, based on iron and vanadium have the potential to act as cost effective catalysts for fuel cell oxidations as well as facilitate both proton and electron conduction. The goal of this research is to develop a non-platinum electrocatalyst based on an HPA or to enhance the catalytic activity of a conventional platinum catalyst in a co-catalyst system and so reduce the amount of precious metals.

Experimental

The HPA and lacunary HPA and iron and vanadium substituted HPA were prepared by literature methods. The materials were characterized by IR, NMR, TGA, Mössbauer, and ICP-AA elemental analysis. Cyclic voltammetry was measured using a polished glassy carbon disk electrode in 1M H₂SO₄.

The Nafion[®] membrane (Ion Power) was cleaned and converted into the acid form by successively boiling the membranes for at least one hour in each of the following solution: 3% H₂O₂, deionized (DI) water, 0.5 M H₂SO₄, and DI water again. The acid form Nafion[®] 117 was stored in DI water in the dark prior to use. Approximately 1 g of the catalyst was dissolved in 40 mL of DI water and heated at about 60 °C with stirring. A 5 cm² piece of uncatalyzed thick gas diffusion electrode (GDE) (the DGE was developmental gas diffusion electrodes-Type V 2.33-very thick standard ELAT-all hydrophilic, E-tek) was floated in the catalyst solution overnight. The GDE was removed from the solution, washed with DI Water, and dried in the oven. HPA loading was about 0.08 mg/cm². The catalyzed GDE layer and a 5 cm² piece of GDE which is hand fabricated single side coating standard 0.5 mg/cm² TM loading using 20 % Pt on Vulcan XC-72 were hand painted with Nafion[®] solution and allowed to dry in the air. The maximum Nafion[®] loading is 1.9 mg/cm² when pure oxygen was employed as the oxidant. [3]. These two electrodes were

pressed into Nafion[®] 117 with heated plates at 115 °C and 75 psi for 90 seconds. The MEAs were conditioned to achieve constant polarization curve prior to use. Polarization curves in H₂/O₂ were measured at 80°C with humidified gasses using standard 5 cm² active area fuel cell hardware.

Results and Discussion

The loadings of HPA on the XC-72 carbon based ELAT GDEs are very low, typically 0.1 mg/cm². After conditioning the MEA current densities are typically on the order of 100 mA/cm² at 0.1 V using H₂/O₂, but the OCV of 0.75 V is somewhat low presumably due to the poor activation of the iron catalyst compared to platinum. When the MEA is turned over and the iron-substituted HPA is run as the anode an electrochemical wave is observed. After exposure to H₂ as the anode the catalyst improves to give close to 150 mA/cm² under the same conditions on the cathode, **Figure 1**. This activity appears to be stable, multiple polarization curves can be run after the reduction step.

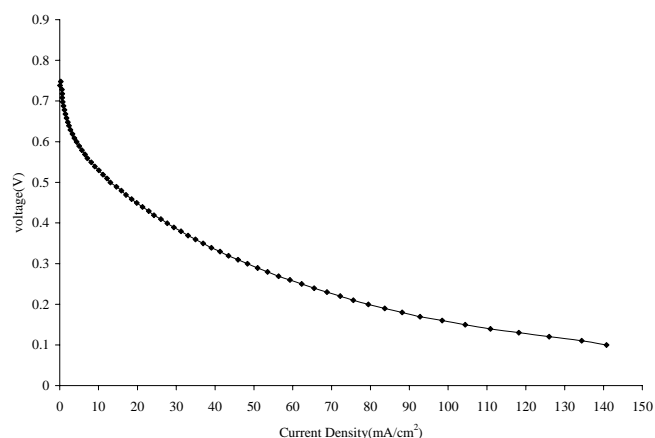
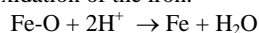


Figure 1. Polarization curve for a iron substituted HPA after reduction on the cathode and Pt on the anode on ELAT GDE at 80 °C, using H₂/O₂ humidified at 90 °C.

We speculate that the mechanism involves fast protonation of an oxygen atom bonded to an iron center, followed by a slow chemical re-oxidation of the iron:



When O₂ is switched for N₂ on the cathode and successive polarization curves are run the limiting current density falls, initially rapidly and then more slowly, **Figure 2**. As there is no oxygen to regenerate the catalyst the activity is diminished with each successive sweep. The rapid fall of current density is due to the reversible depletion of the oxygen from the iron centers. The slow fall in activity at longer times/lower current densities is due to the irreversible depletion of skeletal tungsten bound oxygen. This is borne out in experiments in which the catalyst is run under N₂ to exhaustion, on exposure to O₂, the catalyst does not recover all of its activity. When the catalyst is depleted under N₂ only to the end of the rapid reversible current density loss we would expect it to recover all its activity on re-exposure to O₂. Interestingly the catalyst performs better and better on each successive cycle of experiments. From these results we speculate that electrochemical or chemical reduction of these iron substituted HPA results in the formation of iron/tungsten oxide nanoparticles that may be the true catalyst.

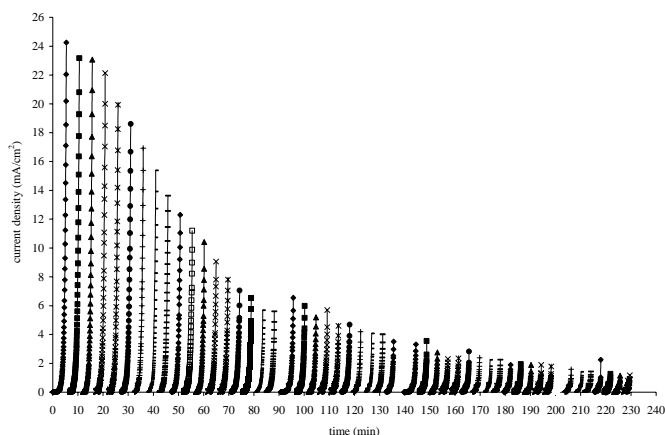


Figure 2. Successive polarization curves for an iron substituted HPA after O_2 exposure on the cathode and Pt on the anode on ELAT GDE at $80\text{ }^\circ\text{C}$, using H_2/N_2 humidified at $90\text{ }^\circ\text{C}$.

We have also investigated vanadium substituted HPA [5]. These materials exhibit very similar behavior to the iron-substituted HPA, but limiting current densities achieved on the cathode are only 24 mA cm^{-2} at $80\text{ }^\circ\text{C}$. The temperature dependence of the catalytic activity improves dramatically with temperature leading us to believe that these may be very interesting catalysts for higher temperature PEM fuel cells.

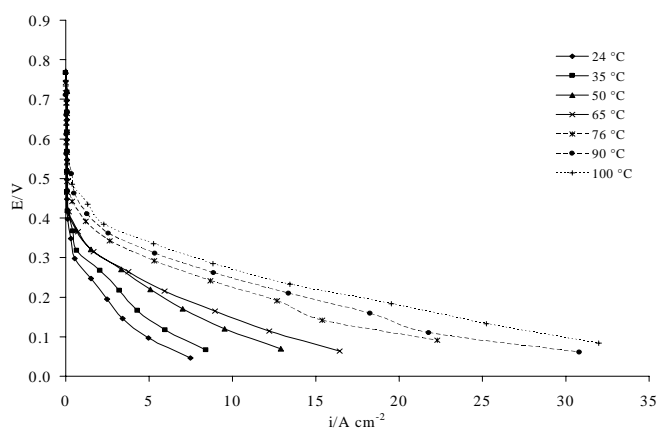


Figure 3. Temperature dependence of a vanadium substituted HPA as a cathode catalyst.

These vanadium substituted HPA materials are much more interesting when used as a co-catalyst on the fuel cell anode, **Figure 4**. A 30% improvement in current density and power is seen with the vanadium HPA/Pt versus the Pt catalyst. Control experiments with and without Nafion[®] in the electrodes indicate that at least some of this activity is due to the proton conducting ability of the HPA. Additional controls with unsubstituted HPA and V_2O_5 indicate that the catalytic activity only originates from the vanadium substituted HPA and in addition the catalyst must contain more than two vanadium atoms.

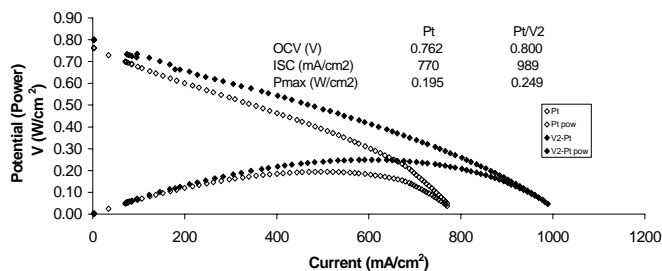


Figure 4. Polarization and power curves for Pt on ELAT electrodes as both anode and cathode catalysts and for a vanadium substituted HPA/Pt co-catalyst system as anode with a Pt cathode.

Conclusions

Heteropoly acids may be immobilized on carbon supports and used in PEM fuel cells as catalysts. Iron substituted HPA exhibit catalytic activity comparable to the best non-platinum catalysts so far discovered. Vanadium substituted materials may be useful as co-catalysts for Pt systems. Co tolerance of the co-catalyst anodes will be investigated in the future and further characterization will be performed on the iron cathodic catalyst to determine then exact nature of the catalyst.

Acknowledgement. This work was supported by the Xcel Energy renewable development fund, project No. CB07.

References

- (1) Mizuno, N.; Misono, M. *Chem. Rev.*, **1998**, *98*, 199-217.
- (2) Savadogo, O.; Bartolacci, G. *Int. J. Hydrogen Energy* **1992**, *17*, 109-114.
- (3) Ren, X.; Wilson, M. S.; Gottesfeld, S. In "Proton Conducting Membrane Fuel Cells I", Gottesfeld, S.; Halpert, G.; Landgrebe, A. Editors, *95* (23), p. 252, The Electrochemical Society Proceedings Series, Pennington, NJ (**1995**).
- (4) Litster, S.; McLean, G. *J. Power Sources*, **2004**, *109*, 61-76.
- (5) Limoges, B. R.; Herring, A. M.; Turner, J. A. *Electrochimica Acta*, Submitted.

FLUORINATED SULFONIMIDE ELECTROLYTES GRAFTED ONTO CARBON: A POTENTIAL ROUTE TO HIGH-PERFORMANCE PEM FUEL CELL ELECTRODES

Stephen E. Creager, Hua Mei, Bing Liu, Mark W. Perpill, Ibrahim Shaban, Dennis W. Smith, Jr, Darryl D. Desmarteau

Department of Chemistry, Clemson University, Clemson, SC 29634-0973

Introduction

Proton-conducting polymer electrolytes based on fluorinated sulfonimide superacids (1-4) are being developed as alternatives to fluorinated sulfonic acid-based polymer electrolytes such as Nafion™ that are commonly used in PEM fuel cell technology. The sulfonimide group can be incorporated into a rich variety of functional derivatives which provides opportunities for making crosslinked ionomers and ionomers with greater TFE character to provide dimensional stability at high ionic content, as is desired to achieve high conductivity and usefulness in PEM fuel cells.

An important issue in PEM fuel cell technology is the integration of electrolyte with electrode. Present technology involves simple mixing to achieve good contact between ionomer and electrode. Improvements are needed to provide for greater integration and contact with electrocatalyst, and also longer life by preventing phase segregation between the carbon electrode support and the electrolyte.

This contribution concerns one such derivative in which a sulfonimide functional group is attached at the para-position of an aryl diazonium inner salt. The resulting compound has structure ${}^+\text{N}_2\text{-C}_6\text{H}_4\text{-SO}_2\text{N-SO}_2\text{CF}_3$, and we show that the aryl diazonium portion of the molecule may be used to graft a sulfonimide anion onto the surface of carbon electrodes by formation of a covalent carbon-carbon bond. In this contribution we consider the formation of grafted electrolytes on carbon formed by electroreduction of the diazonium inner salt at glassy carbon electrodes, and also by thermal treatment of porous carbon aerogels with solutions of the diazonium salt in organic solvents.

Experimental

Synthesis of the target compound will be described in detail separately. (5) Cyclic voltammetry was accomplished using a CH Instruments model 660 Electrochemical Workstation. Conditions were as follows: 3-electrode cell: carbon plate working electrode, Ag/AgCl reference electrode, Pt auxiliary electrode. Diazonium salt was present at 10^{-3} M in acetonitrile solution containing 0.10M TEABF₄. Scans were from 0 to -0.9 V, 20–30 cycles.

Results and Discussion

Figure 1 presents a crystal structure of the fluorosulfonamide diazonium salt studied in this work. The presence of the diazonium functionality on one side and the fluorosulfonamide on the other are clearly evident.

Figure 2 presents a series of cyclic voltammograms of the compound from Figure 1 at a glassy carbon plate electrode. The diminishing current with continues scanning indicates coating of the electrode with a grafted, covalently bonded coating of the target molecule. XPS analysis of the carbon plate confirms that coating has occurred; the survey XPS scan indicates the coated surface composition is approximately 73.5% C, 14.7% O, 3.2% N, 4.2% F, 2.8% S. In contrast, the uncoated surface composition by XPS is 92.7% C and 7.2% O, with no other elements present.

It is of interest to extend the approach above to nanoporous carbon aerogels being developed at Clmeson and elsewhere for use as electrodes in PEM fuel cells. Figure 3 presents an SEM micrograph of a carbon aerogel sample, showing the pore structure on submicrometer length scales. TO modify the interior pore surfaces of this aerogel with fuorsulfonimide electrolyte, we impregnated dry ground-up particles of carbon aerogel (40-200 micrometers particle size) with the solution and allowed them to react for 2 hours at ambient temperature or 55 °C). EDX analysis of the resulting particles showed the binding had occurred, e.g., for an aerogel sample modified at 55 °C the EDX analysis indicated an aerogel bulk composition of 84.6% C, 3.2% N, 7.2% O, 2.0% F, and 2.9% S.

Conclusions

We have synthesized a fluorosulfonimide aryl diazonium salt and used it to modify the flat surface of a glassy carbon plate electrode and the surface of the interior pores of a carbon aerogel sample. XPS and EDX analysis confirm immobilization of F, N, and S, which indicates grafting of the fluorosulfonimide electrolyte.

Acknowledgement: Financial support of this work by the National Science Foundation, DMI-0303645, is gratefully acknowledged.

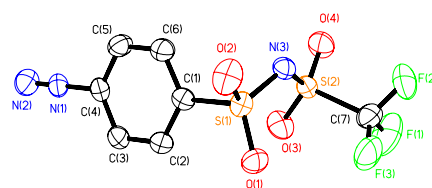


Figure 1. X-ray crystal structure of structure ${}^+\text{N}_2\text{-C}_6\text{H}_4\text{-SO}_2\text{N-SO}_2\text{CF}_3$, that was used in this work to chemical modify carbon surfaces.

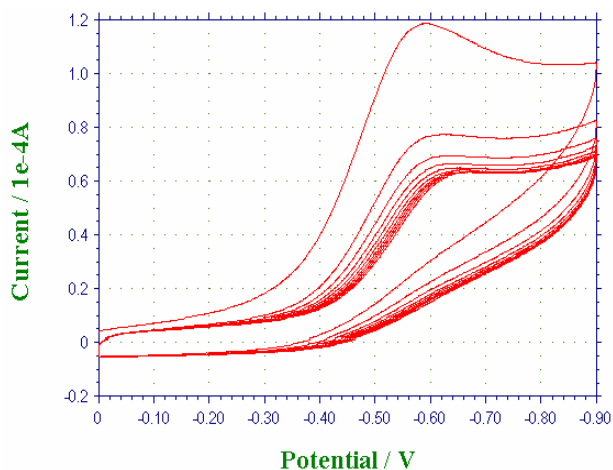


Figure 2. Cyclic voltammograms of a solution of fluorosulfonamide aryl diazonium salt at a glassy carbon plate electrode.

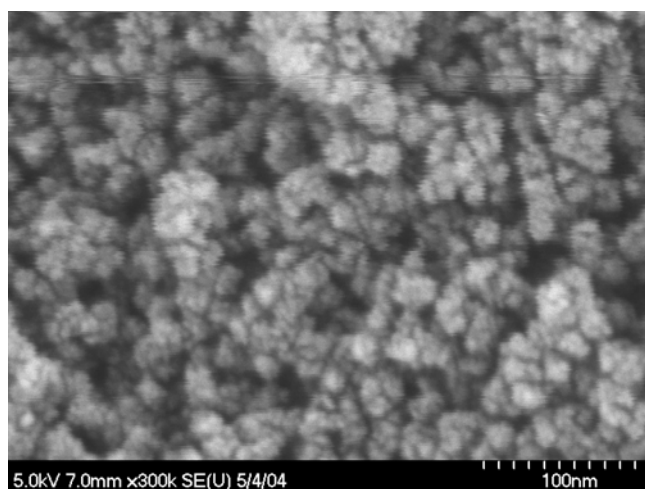


Figure 3. Field-emission SEM micrograph of an RF carbon aerogel prepared using literature methods.(6)

References

1. Atkins, J.R., C.R. Sides, S.E. Creager, J.L. Harris, W.T. Pennington, B.H. Thomas, and D.D. DesMarteau, Effects of Equivalent Weight on Ionic Conductivity in Bis[(perfluoroalkyl)sulfonyl]imide Perfluorinated Ionomers. *Journal of New Materials for Electrochemical Systems*, 2003. 6: p. 9-16.
2. Savett, S.C., J.R. Atkins, C.R. Sides, J.L. Harris, B.H. Thomas, S.E. Creager, W.T. Pennington, and D.D. DesMarteau, A Comparison of bis[(perfluoroalkyl)sulfonyl]imide Ionomers with Perfluorosulfonic Acid Ionomers for Applications in PEM Fuel Cell Technology. *Journal of the Electrochemical Society*, 2002. 149(12): p. A1527-1532.
3. Creager, S.E., J.J. Sumner, R.D. Bailey, J.J. Ma, W.T. Pennington, and D.D. Desmarteau, Effects of water uptake and ionomer crystallinity on proton conductivity in bis[(perfluoroalkyl)sulfonyl]imide-based perfluorinated ionomers. *Electrochemical and Solid-State Letters*, 1999. 2: p. 434-436.
4. Sumner, J.J., S.E. Creager, J.J. Ma, and D.D. DesMarteau, Proton conductivity in Nafion 117 and in a novel bis[(perfluoroalkyl)sulfonyl]imide ionomer membrane. *Journal of the Electrochemical Society*, 1998. 145(1): p. 107-110.
5. Hua Mei, Bing Liu, Stephen E. Creager, Mark W. Perpall, Dennis W. Smith, Jr, Darryl D. Desmarteau. " Novel Diazonium Salts for Grafting Fluorinated Polyelectrolytes to Fuel Cell Electrodes", preprint, Fuel Division, ACS National Meeting, Fall 2004.
6. Saliger, R., V. Bock, R. Petricevic, T. Tillotson, S. Geis, and J. Fricke, Carbon aerogels from dilute catalysis of resorcinol with formaldehyde. *Journal of Non-Crystalline Solids*, 1997. 221: p. 144-150.

Multifunctional Composites Containing Molybdenum Carbides as Potential Electrocatalysts

Erich C. Weigert^a, Joseph South^b, Jingguang G. Chen^c

^a Center for Catalytic Science and Technology, Department of Materials Science and Engineering, University of Delaware, Newark, DE 19716

^b Army Research Laboratory, Building 4600, Aberdeen Proving Ground, MD 21005

^c Center for Catalytic Science and Technology, Department of Chemical Engineering, University of Delaware, Newark, DE 19716

Introduction

Currently, the most widely used electrocatalysts for Proton Exchange Membrane (PEM) and Direct Methanol Fuel Cells (DMFC) are platinum (Pt) containing alloys such as Pt-Ru [1-3] and Pt-Sn [1-5]. The primary disadvantages of these Pt alloys are their relative scarcity and high cost. In the case of functionalized RVC carbon foam, it is not economically feasible to simply coat the foam surfaces with Pt. Furthermore, because Pt does not bond strongly with carbon foam, Pt would most likely be in the form of clusters instead of being highly dispersed on the foam surfaces. Solutions to these problems are to either produce cost-effective electrocatalysts using less expensive components, or to reduce the Pt loading by improving its dispersion on the carbon foam.

Early transition metal carbides have been shown in previous studies [6,7] to behave similarly to the Pt group metals (Pt, Pd, Ir, Rh, Ru). For example, research done by our group has shown that carbide modified W(111) and W(110) surfaces showed high activity toward the dissociation of methanol, although about 14% of the adsorbed methanol decomposed to produce methane [8,9], an undesirable process for the application in DMFC. An additional study from our research group on the carbide modified Mo(110) surface showed that the methane formation pathway was not present on C/Mo(110) [10]. In addition, this study indicated that the C/Mo(110) surface was more active toward the dissociation of water than the C/W(111) or C/W(110) surfaces. Overall, these surface science studies suggest the possibility of using molybdenum carbides as an alternative electrocatalyst for DMFC.

In the present study we have investigated using molybdenum carbides, and platinum modified molybdenum carbides as potential electrocatalysts for DMFC's. In particular, we are interested in determining the feasibility of the integration of the electrocatalytic functionality on the surfaces of carbon foam. If successful, the multifunctional composite materials would provide the fuel cell functionality into the structural components in many military and domestic applications.

Experimental

Deposition. Sample preparation was performed in a stainless steel vacuum system with a typical base pressure of 3×10^{-8} Torr. The system was equipped with Mo and Pt metal sources for physical vapor deposition (PVD). The PVD deposition was conducted on reticulated vitreous carbon (RVC) foam. Samples were introduced into the vacuum chamber individually and coated with Mo and/or Pt by PVD to produce samples of Mo-C/foam, Pt/foam and Pt/Mo-C/foam. For all samples to be tested in the electrochemical cell, exposure time and metal source current were adjusted such that the surface ratio of Mo/C was approximately 0.17, based on standard XPS sensitivity factors [11]. Molybdenum

carbides were formed on the surface by resistive heating of the Mo/carbon samples in vacuum to temperatures between 823 and 973 K. Pt modified surfaces were prepared by PVD of Pt on either foam or Mo-C/foam surfaces. The Pt PVD deposition current and time were controlled to achieve a surface atomic ratio of 0.17 Pt/C.

Techniques. The PVD system was equipped with an Al/Mg dual anode X-ray source and a concentric hemispherical analyzer (CHA) for in-situ XPS. Studies using XPS enabled us to control the surface concentrations of Mo and Pt as well as to verify carbide formation. Other characterization techniques used to examine the synthesized samples were Near Edge X-ray Absorption Fine Structure (NEXAFS) at Brookhaven National Laboratory and SEM. These two techniques provided additional and complementary information about the Mo-C thin films. The Pt/foam and Pt/Mo-C/foam samples were also evaluated using Cyclic Voltammetry (CV). The CV measurements were performed in an electrochemical half-cell. The half-cell was a glass vessel containing 1 Liter of 0.05M H₂SO₄ electrolyte, equipped with a Saturated Calomel Electrode (SCE) and a Pt counter electrode.

Results and Discussion

Deposition on RVC foam. Following metal deposition on the RVC foam samples, the annealing was allowed to continue for an extended period of time at 973 K to ensure uniform heating of the sample. The results from XPS show no clear evidence of carbide formation on the Mo modified RVC surface, as suggested by the observation that the C 1s signal does not shift significantly after sample heating.

It was unclear whether the lack of a characteristic carbide peak at 284.0 eV was the result of insufficient sample heating, insufficient surface coverage of Mo, or a dominance of the graphitic C 1s signal from the channels in the carbon foam. As described in a review, NEXAFS is much more sensitive than XPS in detecting the carbidic carbon in transition metal carbides [12]. Newly prepared samples of RVC foam were analyzed with NEXAFS, shown in Figure 1. The presence of the carbon K-edge feature at 285.5 eV in spectrum b is indicative of carbidic carbon, confirming the formation of Mo-C on the foam surface.

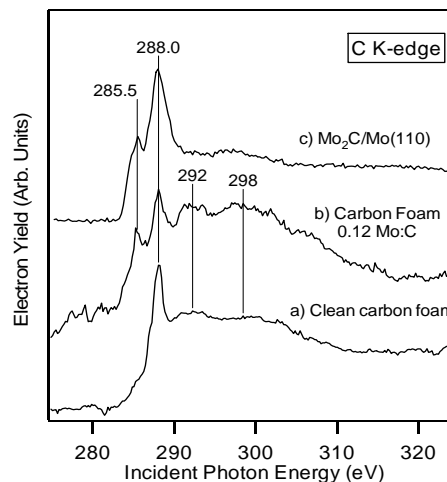


Figure 1. NEXAFS spectrum of clean and carbide modified carbon and Molybdenum substrates.

Cyclic Voltammetry (CV) Characterization of Electrochemical Stability. Figure 2 shows results of a preliminary study conducted on Pt/foam and Pt/Mo-C/foam samples to determine their electrochemical stability. Each sample, partially immersed in a dilute H₂SO₄ environment purged with either N₂ or H₂ gas, was subjected to a voltage sweep between -0.05 and 0.8 V. All CV data were collected with the assumption that the sample surface was uniform.

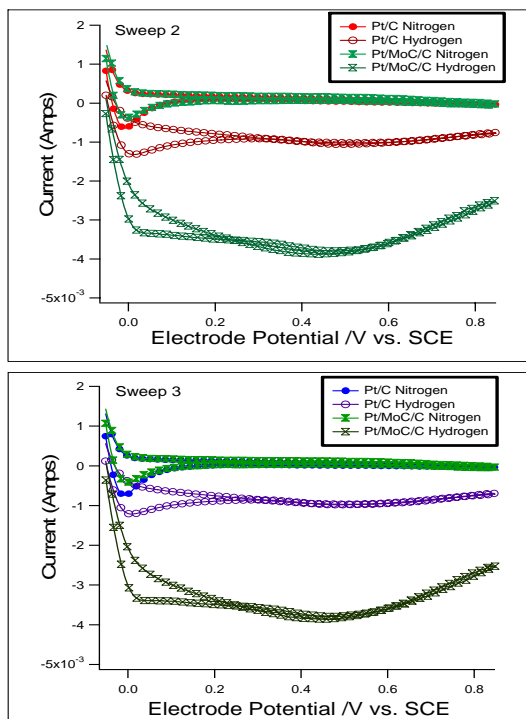


Figure 2. Cyclic Voltammograms of Pt/foam and Pt/Mo-C/foam partially immersed in a 0.05M H₂SO₄ solution.

The dissimilarity of these CV curves to those obtained from other studies on Pt modified carbon surfaces [13, 14] is not well understood at this time. Overall, the initial electrochemical study suggests that the Pt/foam and Pt/Mo-C/foam samples have significantly distinguishable performances, and that they possess some level of electrochemical stability in the sulfuric acid electrolyte solution.

Conclusions

From the results described above, the following conclusions can be made regarding the functionalization of carbon foams by Mo carbides:

(1) The formation of molybdenum carbides on the surface of RVC substrates has been found using XPS and NEXAFS.

(2) Preliminary CV measurements on the Pt/foam and Pt/Mo-C/foam samples indicate that there is an increase in the electrocatalytic activity when the carbon foam surface is functionalized with Pt and Pt/Mo-C. Multiple sweeps of the CV experiments show identical CV curves, indicating the electrochemical stability of the PVD films.

References

- (1) M.M.P. Janssen, J. Moolhysen, *Electrochim. Acta* 21 (1976) 869.
- (2) M.M.P. Janssen, J. Moolhysen, *Electrochim. Acta* 21 (1976) 861; *J. Catal.* 46 (1977) 289.
- (3) K. Wang, H.A. Gasteiger, N.M. Markovic, P.N. Ross Jr., *Electrochim. Acta* 41 (1996) 2587.
- (4) C. Panja, N. Saliba, B.E. Koel, *Surf. Sci.* 395 (1998) 248.
- (5) A.N. Haner, P.N. Ross, *J. Phys. Chem.* 95 (1991) 3740.
- (6) J.G. Chen, *Chem. Rev.* 96 (1996) 1477, and references therein.
- (7) S.T. Oyama, *The Chemistry of Transition Metal Carbides and Nitrides*, Blackie, Glasgow, 1996.
- (8) N. Liu, K. Kourtakis, J.C. Figueroa, J.G. Chen, *J. Catal.* 215 (2003) 254.
- (9) H. Hwu, J.G. Chen, *J. Phys. Chem. B* 105 (2001), 10037.
- (10) H. Hwu, J.G. Chen, *Surf. Sci.* 536 (2003) 75.
- (11) Moulder J.F., Stickle W.F., Sobol P.E., Bomben K.D. *Handbook of X-ray Photoelectron Spectroscopy*. Physical Electronics, Eden Prairie MN. 1995.
- (12) J.G. Chen, *Surf. Sci. Reports*, 30 (1997) 1.
- (13) L.M. Roen, C.H. Paik, T.D. Jarvi, *Electrochem. and Solid-State Lett.* 7 (2004) A19-A22.
- (14) H. Tang, J. Chen, L. Nie, D. Liu, W. Deng, Y. Kuang, S. Yao, *J. of Colloid and Interface Sci.* 269 (2004) 26-31.

Pt-BASED CATALYSTS FOR DIRECT ETHANOL FUEL CELLS

S. Song¹, Q. Xin^{1,2*}, G. Sun¹, P. Tsiakaras^{3*}

¹Direct Alcohol Fuel Cell Lab, ²State Key Lab of Catalysis, Dalian Institute of Chemical Physics, CAS P. O. Box 110, Dalian 116023, China

³Department of Mechanical and Industrial Engineering, School of Engineering, University of Thessaly Pedion Areos, 383 34, Greece

Introduction

Direct ethanol fuel cells (DEFCs) have spurred more and more interest in recent years due to ethanol intrinsic advantages such as its low toxicity, renewability, and its easy production in great quantity by the fermentation from sugar-containing raw materials. The main challenge for DEFC is to break the C-C bond, which is difficult to occur at low temperatures. Sn has been found to be a good modifier to enhance the electrocatalytic activity of Pt to ethanol oxidation [1]. Sn's valence state [2] and Sn content [3] play an important role in ethanol electrooxidation and consequently in the single DEFC performance. From the practical point of view, the development of DEFC depends on the progress in the electrocatalytic materials for ethanol electrooxidation to a great extent. Ethanol adsorption, dissociation and oxidation are mainly affected by the composition and structure of electrocatalysts and the catalyst preparation procedure plays a crucial role in electrocatalysts' composition and structure, especially in the interaction between different components. In the present work, a PtSn/C catalyst synthesized by the direct decoration of commercial Pt/C with Sn as anode electrocatalyst in direct ethanol fuel cell. The techniques of cyclic voltammetry, anode polarization curve and single DEFC tests were applied to compare the electrocatalytic activity of the prepared PtSn/C and the commercial PtRu/CPt to ethanol oxidation.

Experimental

PtSn/C catalyst with a Pt to Sn atomic ratio of 2 was prepared by using 20 wt.% Pt/C (Johnson Matthey Corp.) as support and SnCl₂ as tin precursor by a modified poly method [4]. The catalysts were characterized by XRD on a Rigaku X-3000 X-ray powder diffractometer using Cu K α radiation with a Ni filter. Cyclic voltammetry of as prepared PtSn/C and commercial PtRu/C was performed in a conventional three-electrode cell with saturated calomel electrode and Pt wire as the reference electrode and counter electrode respectively in 1.0 M C₂H₅OH+1.0 M H₂SO₄ aqueous solutions at room temperature. The anode polarization curves of ethanol oxidation on PtSn/C and PtRu/C were obtained by supplying the cathode of the DEFC with humidified H₂ instead of O₂, which was used both as a *dynamic hydrogen reference electrode* (DHE) and as the counter electrode. The anode potential was controlled with a potentiostat/galvanostat (EG&G Model 273A) at a scan rate of 2.0 mV/s. The DHE was made by feeding 40 mL/min of H₂ humidified at 90°C at atmospheric pressure. The anode compartment was pumped by the preheated 1.0 mol/L ethanol aqueous solution at a flow rate of 1.0 ml/min, acting as the working electrode for the electrochemical measurements. Single DEFC tests were carried out with MEAs prepared according to the method described in literature [5] by pumping 1.0 mol/L ethanol aqueous solution at 1.0 ml/min to the anode and at the same time feeding 2 atm oxygen to the cathode at 90°C. The polarization curves were obtained by an Arbin fuel cell test station in a galvanodynamic state.

Results and Discussion

XRD characterization results showed that after the modification by Sn, there is no change in Pt (fcc) characteristic and Sn exists in oxidative state. Fig. 1 shows cyclic voltammograms for ethanol electrooxidation over PtSn/C and PtRu/C catalysts. It can be clearly seen from Fig. 2 that in the investigated potential range, there are two oxidation peaks during the forward sweep in both cases of PtSn/C and PtRu/C and these two oxidation peaks of ethanol over PtSn/C are higher than those over PtRu/C. This means from the current density point of view, PtSn/C presents higher catalytic activity to ethanol electrooxidation in comparison with PtRu/C. The oxidation peak during the backward sweep could be attributed to the further oxidation of the adsorbed intermediate species of ethanol. From Fig. 2, it can also be seen that, in the case of PtSn/C, this backward oxidation peak is higher with respect to PtRu/C. This could be attributed to the more promoting role of Sn in the oxidative removal of the adsorbed intermediate species of ethanol oxidation over platinum. On the other hand, the shift of the oxidation peak potential for PtSn/C to more negative with respect to that of PtRu/C indicates that in the case of PtSn/C, the energy necessary for ethanol electrooxidation is lower, which could be attributable to both the synergetic role of tin in platinum catalytic activity to ethanol electrooxidation and the structural modification of Sn to Pt. CV results show that PtSn/C is more suitable electrocatalyst for ethanol oxidation in comparison with PtRu/C.

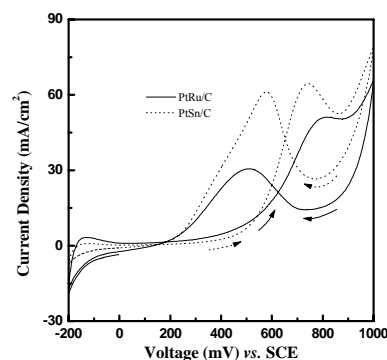


Figure 1. Cyclic voltammetry spectra of PtSn/C and PtRu/C in 1.0 mol/L CH₃CH₂OH/ 1.0 mol/L HClO₄ aqueous solution at room temperature. The potential sweep rate was 50 mV/s.

Anode polarization curves can eliminate the other factors except the electrochemical activity of Pt-based catalysts to ethanol electrooxidation and the results are illustrated in Figure 2. It can be clearly seen that the onset potential of ethanol electro-oxidation over PtSn/C is shifted by about 100 mV negatively in comparison with that over PtRu/C. The negative potential shift of the beginning of ethanol oxidation on PtSn/C could be attributable to the oxidation of the adsorbed residues formed during its dissociative adsorption by adsorbed OH species present on Sn sites in oxidized states [6]. Figure 2 also shows that when the potential is less than about 80 mV (vs. DHE), PtSn/C presents a lower activity while it exhibits steeply increment in current density from about 80 mV (vs. DHE) until about 300 mV (vs. DHE) with a maximum $i(\text{PtSn/C})/i(\text{PtRu/C})$ ratio of about 5 at about 200 mV (vs. DHE). And then the increment of the polarization current on PtSn/C slows down while the corresponding value on PtRu/C becomes obvious. Along with the potential increment, PtSn/C shows inferior activity for ethanol oxidation to PtRu/C again.

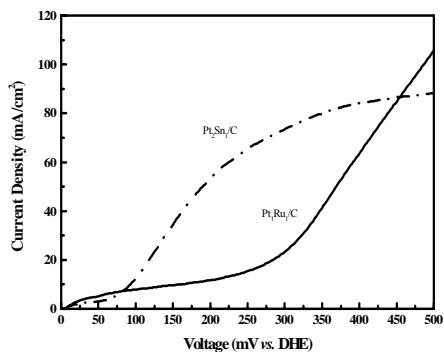


Figure 2. Anode polarization curves of ethanol electro-oxidation over in-house PtSn/C and commercial PtRu/C at 90°C. Anode: PtSn/C or PtRu/C with a loading of 1.3 mg/cm², C_{ethanol} = 1.0 mol/L, flow rate: 1.0 ml/min. Cathode: Pt/C (20 wt.%, Johnson Matthey Corp.), the metal loading: 1.0 mg Pt/cm², P_{H₂} = 1 atm, flow rate: 40 mL/min T_{H₂-humidified} = 90°C. Electrolyte: Nafion[®]-115 membrane.

Figure 3 compares the cell performances of direct ethanol fuel cells with PtSn/C and PtRu/C as anode catalysts. Obviously, the single cell performance with the PtSn/C is better than that of PtRu/C.

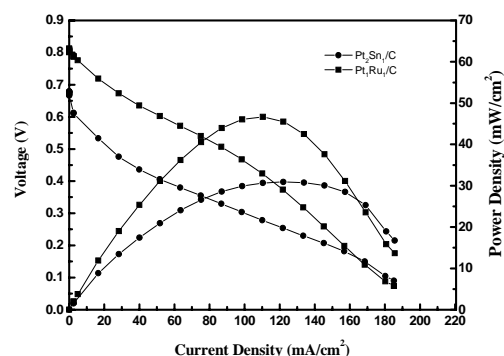


Figure 3. Performance comparison of DEFCs adopting in-house PtSn/C and commercial PtRu/C as anode respectively at 90°C. Anode: PtSn/C or PtRu/C with a loading of 1.3 mg/cm², C_{ethanol} = 1.0 mol/L, flow rate: 1.0 ml/min. Cathode: Pt/C (20 wt.%, Johnson Matthey Corp.), the metal loading: 1.0 mg Pt/cm², P_{O₂} = 2 atm. Electrolyte: Nafion[®]-115 membrane.

The voltages are about 0.81 V and 0.68 V at open circuit condition, and 0.46 V and 0.31 V at 100 mA/cm² for PtSn/C and PtRu/C, respectively. The maximum power densities are about 46 mW/cm² for PtSn/C and 30 mW/cm² for PtRu/C respectively. It can also be seen from Figure 3 that there is a rapid initial fall in voltage with PtRu/C as anode catalyst but the voltage falls less with PtSn/C as anode catalyst in the low current density. The rapid initial fall in voltage is caused by the slow reaction of ethanol oxidation taking place on the surface of the electrode. A proportion of the voltage generated is lost in driving the electrochemical reaction that transfers the electrons to or from the electrode. Activation overvoltage is the most important cause of voltage drop. As for DEFC, with the same conditions except for different anode catalysts, the slower initial voltage drop can be attributed to the more effective and active catalytic ability of PtSn/C than PtRu/C to ethanol electrooxidation. However, above about 160 mA/cm², the cell performance with PtSn/C as anode catalyst is slightly less than that obtained with

PtRu/C, which may be due to the higher internal resistance of fuel cell with PtSn/C as anode catalyst. This can also be observed from Figure 3, the voltage drops more significantly with PtSn/C than with PtRu/C in the ohmic control region. In this region, the voltage drop is simply proportional to current. Therefore, the more significant the voltage drops, the bigger the area specific resistance is in the ohmic control region of I-V characteristics of fuel cells. The higher internal resistance of fuel cell with PtSn/C as anode catalyst may be attributed to that tin is in the oxidized state is less conductive. Accordingly, the electrical resistance of the anodic electrode increases.

Conclusions

Pt/C catalyst modified by Sn shows superior electrocatalytic activity to ethanol oxidation than commercial PtRu/C. Even if considered as the most active electrocatalyst for methanol electrooxidation, PtRu/C is not considered as a suitable one for ethanol electrooxidation. The results of cyclic voltammetry and anode polarization are coordinated with those of single DEFC tests. PtSn/C can exhibit a more negative ethanol oxidation onset potential and a higher oxidation current density.

Acknowledgement. The authors would like to thank the "Greece-China Joint Research and Technology Programme 2003-2005" and the National Natural Science Foundation of China (Grant No.: 20173060) for funding.

References

- (1) Zhou, W., Zhou, Z., Song S., Li, W., Sun, G., Tsiakaras, P., Xin, Q. *Appl. Catal. B: Environmental*, **2003**, *46*, 273.
- (2) Jiang, L., Zhou, Z., Li, W., Zhou, W., Song, S., Li, H., Sun, G., Xin, Q. *Fuel & Energy*, **2004**, accepted for publication.
- (3) Zhou, W., Song, S., Li, W., Zhou, Z., Sun, G., Xin, Q., Douvartzides, S., Tsiakaras, P. *J. Power Sources*, **2004**, submitted.
- (4) Wang, Y., Ren, J., Deng, K, Gui, L., Tang, Y., *Chem. Mater.* **2000**, *12*, 1622.
- (5) Li, W., Liang, C., Zhou, W., Qiu, J., Li, H., Sun, G., Xin, Q. *Carbon*, **2002**, *42*(2), 436.
- (6) Delime, F., Léger, J-M., Lamy, C. *J. Appl. Electrochem.*, **1999**, *29*, 1249.

Novel high performance platinum and alloy catalysts for PEMFC & DMFC

Yu-Min Tsou *, Lixin Cao, and Emory De Castro

E-TEK, a Division of De Nora North America, Somerset, NJ, USA; Tel (732)545-5100; Fax (732)545-5170; yu.min.tsou.dnna@denora.com

ABSTRACT

In the past two years, E-TEK has advanced the technologies in manufacturing Pt-based catalysts to meet the increasing demand for catalysts in the fuel cell industry. The application of the new method leads to enhanced catalyst performance as the results of dramatic decrease in Pt crystalline size and poisoning impurities as well as uniform spatial distribution on supports. Supported platinum catalysts (10-80 wt% Pt) on various carbon blacks as well as pure platinum black with a controlled size of 5.3 nm have been readily prepared for proton exchange membrane fuel cells (PEMFC) and direct methanol fuel cells (DMFC). By combining novel platinum and ruthenium chemistry, we have succeeded in developing a new process for making thoroughly mixed Pt:Ru alloy at all loadings as evidenced by XRD analysis. Electrochemical experiments indicated that the newly developed Pt:Ru catalysts exhibited the best performances among all commercial products for CO tolerance and methanol oxidation.

INTRODUCTION

The first commercial Pt catalyst on Vulcan XC-72 for phosphoric acid fuel cells was supplied by E-TEK scientists in the 1980's. The traditional E-TEK method for Pt and Pt:Ru catalyst preparation was based on platinum and ruthenium sulfite compounds that undergo redox chemistry to form absorbable fine particles on carbon supports [1]. Other published methods include formation of surfactant-shell stabilized Pt colloidal particles in an organic solvent [2] and reduction of metal chlorides with LiBH_4 in THF [3]. The disadvantages of these published methods include toxic solvents, tedious procedures, contaminants, poor size control, and Pt/Ru phase separation.

In this presentation we will describe the characterization of supported and unsupported platinum catalysts prepared from a novel chemistry and process. The new method resulted in excellent catalyst particle size control, electrochemical activity, and low contaminants. Also included in the discussion is the characterization of supported and unsupported platinum ruthenium alloy catalysts prepared from a novel chemistry and process. Besides the advantage described above for the new Pt catalysts, the Pt:Ru alloy catalysts exhibit good mixing on atomic scale which is crucial for methanol oxidation activity.

RESULTS

The goal of developing the unique platinum chemistry in this work is to ensure the formation and deposition of catalyst particles on the support with uniform size and exhibit minimum growth in subsequent treatments. These catalysts (HP, high performance) were shown to have smaller XRD crystalline sizes and larger surface areas than the previous E-TEK catalysts (Table 1). At a loading higher than 40% on Vulcan XC-72, the XRD size of the previous catalysts increases dramatically but that of the new catalyst increases very slightly with the loading. Besides having

controllable crystalline size, the new catalysts also have more uniform size distribution and spatial distribution over the support. These features give rise to enhanced current distribution and performance in comparison with other commercial products, and essentially no poisoning contaminants. Pt black and 60-80% Pt/C are good candidates for cathode catalysts in DMFC cells. The new Pt chemistry affords Pt black with smaller XRD size (5.3 nm) and higher surface area than other commercial products (Table 2). Figure 1 compares the polarization curve of a gas diffusion electrode with the E-TEK new HP 30% catalyst and that of a commercial 30% Pt/C catalyst.

Synthesis of PtRu methanol catalysts usually follows similar procedures as those for Pt catalysts. Fundamental studies in our lab as well as others indicate that the following factors are crucial for catalytic activity: (i) Pt/Ru alloying degree; (ii) minimum separate Ru phase in XRD spectra, which is ineffective for methanol oxidation. XRD peaks were found to probe alloying degree in Pt:Ru catalysts. The closeness of XRD derived Pt:Ru ratios and bulk Pt:Ru ratio indicates good alloying. E-TEK's new HP Pt/Ru chemistry leads to thorough alloying of the two elements in the catalysts without Ru phase separation; whereas other commercial products give significant deviations (Table 3) and some have single Ru phase. Rotating disk electrode (RDE) experiments (Figure 2) show that the electrochemical activities of E-TEK HP PtRu catalysts for methanol oxidation are better than other commercial products. These new HP PtRu catalysts have replaced the previous versions on the market. These new PtRu catalysts are also excellent for CO tolerance. Crystalline and morphological factors which might affect the performance of catalysts along with electrochemical diagnosis tool to predict performance will be discussed.

Table 1. Crystalline Size (XRD, nm) of E-TEK Pt Catalysts on Vulcan XC-72

Pt loading(%)	Previous catalyst	New catalyst
10	2.2	1.8
20	2.5	2.4
30	3.2	2.7
40	6.4	3.3
60	8.8	4.1
80	25.0	4.9
100	--	5.3

Table 2. Crystalline Size (XRD, nm) and BET Surface Area of Pt Blacks

	XRD size(nm)	BET surface area (m ² /g)
New E-tek	5.3	34
Company 1	10.0	20
Company 2	6.4	27

Table 3. Pt:Ru Alloying Degree and XRD Size (nm), Bulk Pt:Ru ratio: 50:50 Except Company 2, 40:60.

Pt:Ru loading(%)	E-TEK HP Pt:Ru catalyst		Company 1 Pt:Ru catalyst		Company 2 Pt:Ru catalyst	
	ratio	size	ratio	size	ratio	size
30	52:48	2.6	47:54	2.4	25:75	3.7
60	46:54	2.8	39:61	2.7	20:80	3.8
100	48:52	2.7	38:62	2.7	--	--

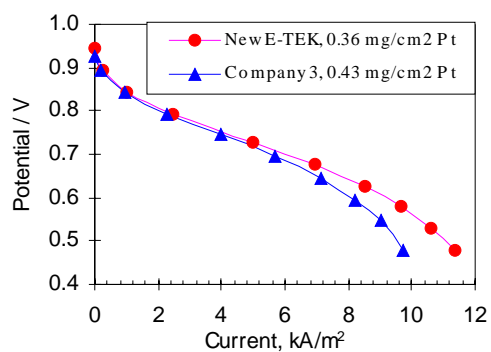


Figure 1. Comparison of 30% cathode catalysts, 70 °C.

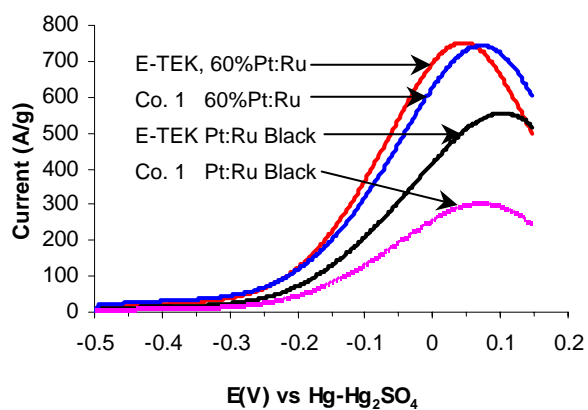


Figure 2. RDE results of methanol oxidation on Pt:Ru (1:1) catalysts, 1M CH₃OH, 50 °C, 1600 rpm.

REFERENCES

1. Petrow, H.G.; Allen, R. J. *US Patent 4,044,193*, August 23, **1977**.
2. Bonnemann, H.; Brijoux, W. in “*Advanced Catalysis and Nano-structured Materials*”, Ed., W. Moser, Academic Press, **1996**, p. 165.
3. Lee, A.S.; Park, C. Y.; Choi, J.H.; Kwon, B. K.; Sung, E. Y. *J. Electrochem. Soc.*, **2002**, 149 (10), A1299.

Novel, Size-controlled Pt Cluster Electrocatalysts for H₂ Fuel Cells

Eric N. Coker, William A. Steen, Michael J. Kelly, Ion C. Abraham, and James E. Miller

Sandia National Laboratories
PO Box 5800, Albuquerque NM 87185-1349

Introduction

One of the biggest hurdles to market acceptance of fuel cell-powered vehicles is the precious metal (PM) requirement; a commercially viable fuel cell electrocatalyst will require almost an order-of-magnitude reduction in PM usage compared to current state of the art to meet both cost and PM availability issues. Therefore, reducing or eliminating the need for Pt as an electrocatalyst is paramount. Another important attribute for a versatile fuel cell catalyst is its durability to poisons such as CO and S, which may be real concerns when reformat is considered as a H₂-source. Alloys of platinum with, *e.g.*, ruthenium, have received considerable attention, due to their higher CO-tolerance.

Studies of cluster chemistry have shown that the physics and chemistry of nanoparticles is extremely sensitive to the number of atoms comprising the cluster, especially when they contain less than a few dozen atoms. For example, the rate of adsorption of H₂ onto a cluster of ten iron atoms is almost three orders of magnitude greater than that of a 17 atom cluster¹. We are developing a Fourier Transform Ion Cyclotron Resonance Mass Spectrometer (FT-ICR-MS), similar to others in the literature,² in an effort to identify electrocatalyst cluster sizes with increased H₂ adsorption (and ideally lowered CO adsorption). Initial efforts have focused on Pt but Pt alloys and other alternatives are being considered. Concurrent with the cluster chemistry studies, we are synthesizing catalysts containing Pt or Pt-alloy clusters of precisely controlled size and narrow size-distribution. Once ideal cluster sizes have been identified by FT-ICR-MS, we will be able to prepare the appropriate catalyst materials for evaluation.

The electrocatalyst synthesis protocol we have adopted utilizes a microporous zeolite as a sacrificial host for the PM clusters. This approach was chosen for a number of reasons: a) to introduce good spatial distribution of the PM-cluster precursors (*i.e.*, (NH₃)₄Pt²⁺); the precursor complex is molecularly dispersed at ion exchange sites which are homogeneously distributed throughout the zeolite structure; b) to restrict cluster growth due to the volume limitation of the zeolite cavities (in the case of zeolite X, the largest cavities are 1.3 nm in diameter), and; c) to impose restriction of cluster-migration during thermal processing due to the constraints of the zeolite porosity (*i.e.*, reduction of sintering). It is known that the rate of heating a (NH₃)₄Pt²⁺-exchanged zeolite can influence the size of the resulting Pt clusters, and clusters as small as *ca.* 1nm have been reported.³

Experimental

To prepare a platinum-on-carbon electrocatalyst with the desired control over cluster size, the following general protocol was adopted: 1) tetra-ammine platinum(II) nitrate (50.29 wt.-% Pt, Alfa Aesar) was ion exchanged from 0.05M solution into zeolite X (Molecular Sieve 13X powder, Aldrich) to the desired loading (typically between 1 and 20 weight percent); 2) the (NH₃)₄Pt²⁺-exchanged zeolite was then heated in air to 350-400°C to decompose the Pt complex to a mixture of Pt(0) and Pt(II)/Pt(IV) oxides, depending on the cluster size. These materials are referred to as PtX(n), where n is the heating rate in °C min⁻¹; 3) the PtX(n) material was degassed to remove adsorbates and water from the pore volume, and was then impregnated with furfuryl alcohol (99%, Aldrich or Acros); 4) after evacuation to

ensure complete infiltration of the monomer into the zeolite pores, the sample was heated in air to 80 – 120°C to induce polymerization; 5) the PtX(n)/polymer composite was then carbonized at between 400°C and 1200°C under an inert and/or reducing atmosphere to convert the polymer to conductive carbon and ensure the platinum was fully reduced; 6) the insulating zeolite template was removed by acid or base digestion, leaving a conductive platinum-on-carbon (Pt/C) electrocatalyst.

The above procedure is currently being adapted for the preparation of Pt-alloys, as well as clusters of other PMs.

Characterization Techniques. The PtX(n), Pt/C, and intermediate materials have been characterized using a variety of techniques, including Transmission Electron Microscopy (TEM), X-ray diffraction (XRD), EXAFS and ¹³C MAS-NMR. Electrocatalyst evaluation has been performed using standard voltammetric techniques.

Results and Discussion

Figure 1 shows TEM micrographs of two different PtX(n) samples, prepared from the same (NH₃)₄Pt²⁺-X precursor (containing 20 wt.-% Pt), but heated in air to 400°C at different rates. The sample heated at 2°C min⁻¹ (PtX(2), Fig. 1A) possesses Pt clusters ~3-6nm in diameter, while the sample heated at 0.1°C min⁻¹ (PtX(0.1), Fig. 1B) contains almost exclusively sub-nm clusters with a very narrow size distribution (most clusters are between 0.6 and 0.9nm). By heating the precursor at intermediate rates, Pt clusters of intermediate size were synthesized. XRD analysis indicated that PtX(2) contained Pt metal and amorphous silica-alumina; clearly the growth of Pt particles beyond the size of the zeolite cavities had contributed to the amorphization of the host. The XRD pattern of PtX(0.1), however, revealed the zeolite to have retained its crystallinity, while the Pt clusters were too small to diffract X-rays coherently. Preliminary EXAFS data corroborate those from TEM and XRD and indicate that the Pt clusters are fully oxidized in air, but readily reduce to Pt⁰ under H₂ at 250°C. Thus, by heating the (NH₃)₄Pt²⁺-X precursor at a specified rate, control over Pt cluster size is garnered. Further control is realized by adjusting the platinum loading; a slight decrease in Pt-Pt coordination number (hence cluster size) was observed by EXAFS on identical heat-treatment of precursors with decreasing Pt-loading in the range 20 wt.-% down to 5 wt.-% Pt.

After impregnation, polymerization and carbonization to 600°C, the Pt clusters in PtX(0.1) were observed by TEM to have increased slightly in size to *ca.* 0.7 to 1.2nm. For comparison, identical heat treatment of PtX(0.1) without introducing the polymer resulted in a doubling of the cluster diameter. The carbon matrix resulting from the 600°C carbonization was identified by ¹³C MAS-NMR to be mostly sp² carbon (*i.e.*, graphene sheets), however, measurements of electrical conductivity after carbonizing at temperatures between 400 and 1200°C indicated that carbonization temperatures in excess of 700°C were required for optimal electron transport.

Figure 2 shows representative cyclic voltammograms of one of our Pt/C materials derived from PtX(0.1) compared with a Pt Black standard. Approximately 10μg Pt-equivalent of each catalyst was deposited onto a glassy carbon electrode and cycled at 50mV s⁻¹ in 0.5M H₂SO₄. Features characteristic of H₂ adsorption and desorption can be seen at *ca.* -200mV_{Ag/AgCl} for each electrode and have comparable charge (*i.e.*, comparable electroactive surface area). Fundamental kinetic studies are also being conducted as the cluster chemistry studies reveal how to optimize the nanostructure of the Pt/C catalyst allowing performance beyond that of standard fuel cell electrocatalysts.

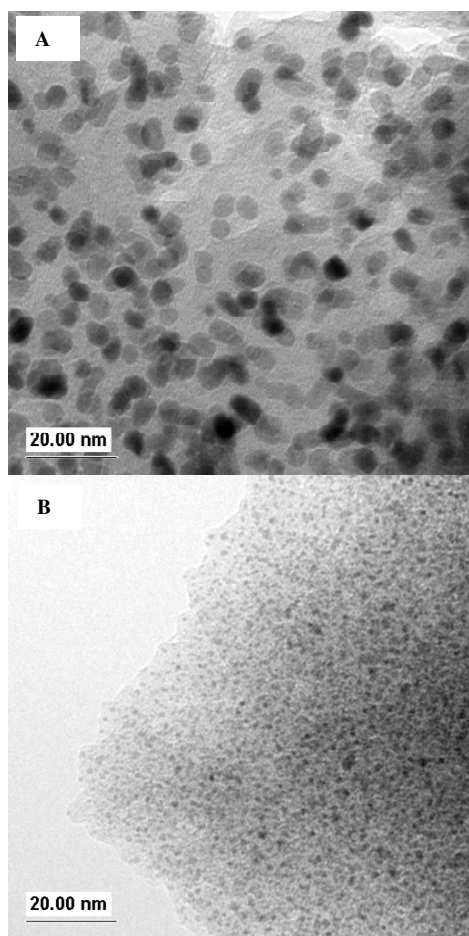


Figure 1. TEM images of PtX samples after heating $(\text{NH}_3)_4\text{Pt}^{2+}$ -zeolite X (20 wt-% Pt) to 400°C in air at (A) 2°C min⁻¹, and (B) 0.1°C min⁻¹.

Conclusions

Controlled heat-treatment of $(\text{NH}_3)_4\text{Pt}^{2+}$ -exchanged zeolite X, followed by reduction under reducing atmosphere, produces small Pt clusters, which can be tuned in size from < 1 nm to > 3 nm depending on the heating rate and Pt loading. Electro-active H₂ oxidation and O₂ reduction catalysts have been prepared from these Pt zeolites through impregnation of a carbonaceous material into the pores of the zeolite, followed by polymerization and carbonization. The zeolite host may be removed by acid or base digestion to yield a Pt/C catalyst with unprecedented control over the size and uniformity of Pt clusters. Electrochemical tests have verified the activity of these catalysts, which compare favorably with state of the art commercial materials.

Acknowledgement. Sandia is a multiprogram laboratory operated by Sandia Corporation, a Lockheed Martin Company, for the United States Department of Energy's National Nuclear Security Administration under contract DE-AC04-94AL85000. EXAFS measurements were conducted at sector 10 (MRCAT) of the Advanced Photon Source (APS), Argonne, IL. Use of the APS was supported by the U.S. Department of Energy Basic Energy Science, under Contract No. W-31-109-Eng-38. Work performed at MRCAT is supported, in part, by funding from the Department of Energy under grant number DEFG0200ER45811.

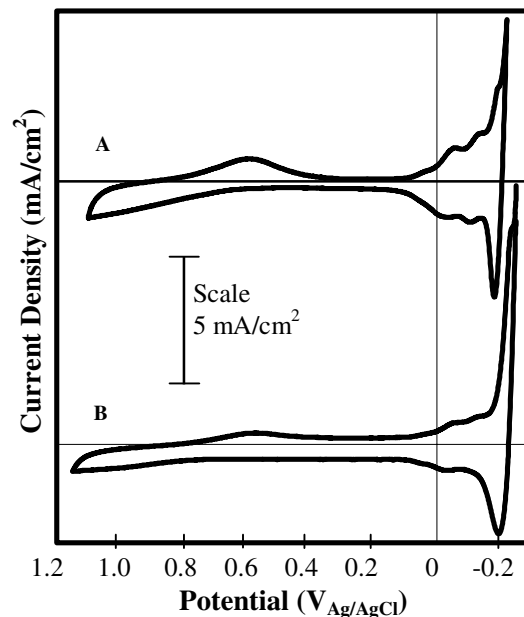


Figure 2. Cyclic voltammograms of a Pt Black standard (A), and of Pt/C prepared from PtX(0.1) (B). Scan rate in 0.5M H₂SO₄ is 50mV/s. Current density is per surface area of substrate, a glassy carbon electrode. Pt loading is ca. 10µg for each electrode.

References

- 1 Riley, S.J. In *Clusters of Atoms and Molecules II*, Haberland, H. Ed.; Springer Verlag, Berlin, 1994; p.226.
- 2 Maruyama, S.; Anderson, L.R. and Smalley, R.E., *Rev. Sci. Instrum.* **1990**, 61(12), 3686; Vakhtin, A.B. and Sugawara, K., *Chem. Phys. Lett.* **1999**, 299, 553; Jarek, R.L. and Thornberg, S.M., *IEEE Trans. Semiconductor Manuf.*, **2001**, 14(1), 20; Jeong, S.; Fisher, K.J.; Howe, R.F. and Willett, G.D., *Microp. Mesop. Materials* **1998**, 22, 369.
- 3 de Graaf, J; van Dillen, A.J.; de Jong, K.P. and Koningsberger, D.C., *J. Catal.*, **2001**, 203, 307.

In-situ pH measurement in a Nafion® based Polymer electrolyte fuel cell by fluorescence spectroscopy

Yatin P. Patil¹, Thomas A. P. Seery^{1,3}, Montgomery T. Shaw^{1,2} and Richard S. Parnas^{1,2}

¹Polymer Program, Institute of Materials Science, ²Department of Chemical Engineering and ³Department of Chemistry
University of Connecticut
Storrs, CT 06269-3136

Introduction

Proton conductivity of the most often used polymer electrolyte membrane, Nafion®, manufactured by du Pont de Nemours & co., depends on its water content. The ionic domains swell with water adsorption and form interconnected proton-conducting channels above a critical water content. The membrane water content depends on the humidity of the gases and the interplay between electro-osmotic drag and back diffusion. Also, uneven gas distribution and uneven electrochemical reactions can lead to uneven water distribution in the membrane. Water management is therefore very important for the optimum functioning of fuel cells. With change in the membrane water content, the pH inside the membrane will change. We have incorporated a pH sensitive fluorescent molecule inside the membrane, which responds to the change in the pH and hence the water content inside the membrane. By introducing a bare fiber optic we are able to measure the fluorescence response and hence the pH inside the membrane.

Experimental

A commercially available 20 wt% Nafion® solution in water-Isopropanol was obtained from Solution Technology Inc. (equivalent weight 1100 g/mol sulfonic acid groups). Rhodamine-6G was obtained from Sigma-Aldrich and was used without further purification. A very dilute dye solution in Nafion® was made by mixing the 20 wt % Nafion® solution with a 4.12×10^{-4} mol/L ethanol solution of Rhodamine-6G. The membrane was cast by pouring the 20 wt% Nafion® solution on a 4-cm \times 4-cm glass plate with a 350- μ m bare optical fiber (OZ Optics) in it. The end of the fiber was positioned at the center of the membrane. Before embedding the bare optical fiber, its tip was coated with the Nafion® dye solution. The final concentration of the dye in the dry membrane at the tip of the fiber was calculated to be 5.75×10^{-7} mol/g. The thickness of the cast membrane was 400- μ m. The membrane was coated with the catalyst obtained from Tanaka Kikinokogyo K. K., Japan by the decal transfer process. The catalysts, 46.5 wt.% Pt/C on the cathode and 30.1% Pt-23.4% Ru/C on the anode were impregnated with Nafion® solution. The electrodes were first screen printed on a Teflon sheet and then hot pressed with the membrane between two rubber sheets at 150 °C for 10 min. under 207×10^3 Pa (30 psig). The membrane electrode assembly was assembled in a 5 cm² fuel cell with series sweep flowfields (Electrochem Inc.; model no. FC05-01SP). The cell was closed by applying a uniform torque of 3.5 N m to each of the eight bolts. High purity hydrogen and oxygen, passed through water-filled sparger bottles, were used. The humidity of the gases was controlled by controlling the temperature of the sparger. The cell temperature was maintained at 80 °C for all the experiments.

Fluorescence spectra were recorded using an Ocean Optics fiber optic fluorescence spectrometer (HR 2000) equipped with an attachment to connect bare optical fiber. UV-Vis spectra were recorded with a Perkin-Elmer Lambda 6 UV-Vis spectrometer.

Results and Discussion

To study the effect of Nafion® membrane water content on the fluorescence behavior of Rhodamine-6G, a membrane was cast from the Nafion® dye solution at 60°C in an oven. A piece of the membrane was vacuum dried and weighed at room temperature. It was soaked in deionised water and patted dry to remove excess water. The water soaked sample was placed on a balance to monitor the water weight loss with simultaneous fluorescence measurements. The fiber optic was oriented at an angle of 60° with respect to the membrane. The fluorescence behavior of the wet Nafion® membrane containing Rhodamine-6G with loss of water and the experimental geometry is shown in the figure 1. At high water content the fluorescence exhibited a maximum at 552 nm, whose intensity initially increases and then decreases with loss of water. This behavior was observed in two different fluorescence spectrometers.

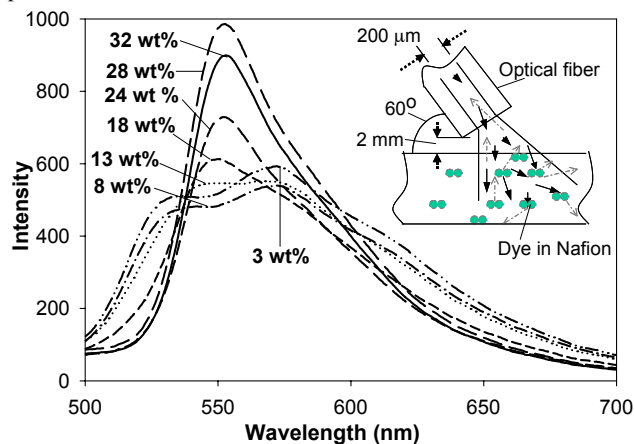


Figure 1. Fluorescence spectra of rhodamine-6G in Nafion® with loss of water and the geometry for fluorescence measurement.

Not only does the intensity of the peak at 552 nm decrease with loss of water, but also it disappears and new peaks appear with further loss of water. Similar behavior of Rhodamine-6G in Nafion® membranes has been reported in the literature¹⁻³. Zhu et al.¹ has proposed that Rhodamine-6G forms a complex with water that has higher absorbance compared to an uncomplexed form, and hence the fluorescence intensity increases with the water content. Mohan et al. reported similar behavior of rhodamine-6G in Nafion®. When the wet membrane containing the dye dried out in air the intensity at 550 nm decreased and new peaks appeared^{2,3}.

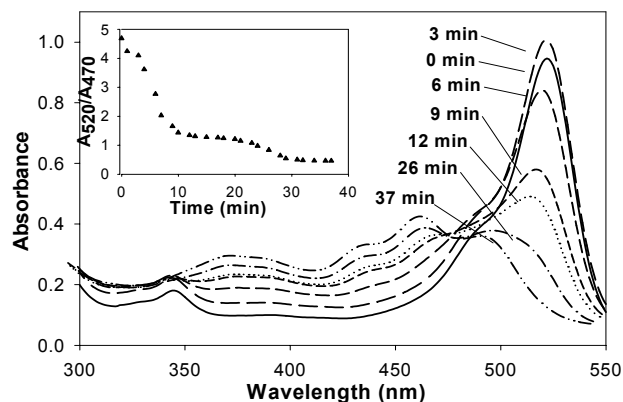


Figure 2. Absorption spectra of Nafion® containing Rhodamine-6G with loss of water.

They proposed that Rhodamine-6G in Nafion® exists in two equilibrium forms, protonated and non-protonated. The protonated form absorbs at 470 nm and has low absorbance whereas the non-protonated form absorbs at 525 nm and has high absorbance. The relative fraction depends on the concentration of H⁺ ions i.e. pH. At high pH the non-protonated form dominates whereas at low pH the protonated form dominates. They have verified this by monitoring the absorbance ratio A₅₂₅/A₄₇₀ of a membrane immersed in aqueous acidic solutions; the absorbance ratio decreased with increasing concentration of the H⁺ ions. They reported a similar trend during the drying of the Nafion® membrane. In Nafion®, the number of sulfonic acid groups does not change unless the membrane undergoes degradation. However, with change in its water content the pH changes and hence the absorbance and fluorescence behavior will change. The absorbance trend of the dye-containing membrane during drying is shown in figure 2. As reported we found that the intensity ratio decreased with loss of water. The absorbance below 480 nm increased with the loss of water.

The absorbance shows a drastic change at 520 nm but to avoid excitation and emission overlap we chose an excitation band from 400-460 nm as the dye emits in the 500-700 nm range. The fluorescence intensity decreases with decreasing pH but we chose to follow intensity ratio as the fluorescence intensity depends on the source intensity and orientation of the fiber with respect to the sample. The fluorescence intensities at 552 and 620 nm were used. The intensity ratio as a function of membrane water content is shown in figure 3. Based on the membrane weight and its water content one can approximate the concentration of H⁺ ions inside it. The intensity ratio shows a sigmoidal trend as a function of membrane water content.

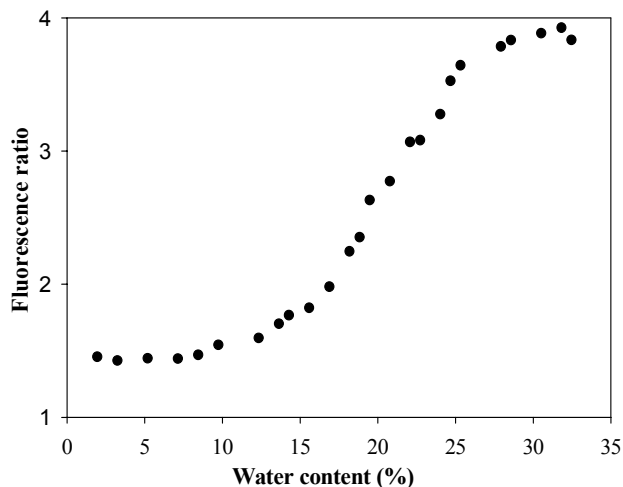


Figure 3; Fluorescence intensity ratio as a function of Nafion® water content

For in-situ fluorescence measurements, the cell temperature was raised from room temperature to 80 °C and was fed with 100% humidified hydrogen and oxygen gases. For proper humidification of the membrane, the cell was operated at steady state for 12 h. The current, drawn at a constant voltage of 0.2 volts, was measured until it reached a steady state. Figure 4 shows the fluorescence ratio and the current response of the cell from its start until it reached a steady state. As the cell temperature increased the membrane lost water, which reduced its conductivity and the current. The fluorescence ratio decreased as the pH fell down. The membrane subsequently adsorbed water from the humidified gases and its conductivity increased, which increased current. The fluorescence ratio increased

as a result of increase in pH inside the membrane. Increased current corresponds to increased amount of proton transfer; however, protons are transported as hydronium ions, where each proton is accompanied by at least one water molecule⁴. Thus, increased current does not lower the pH as water content also goes up due to membrane water uptake and electro-osmotic drag. The fluorescence response is very fast and sensitive towards the change in the pH of the membrane as the peaks in the current match well with the peaks in the fluorescence.

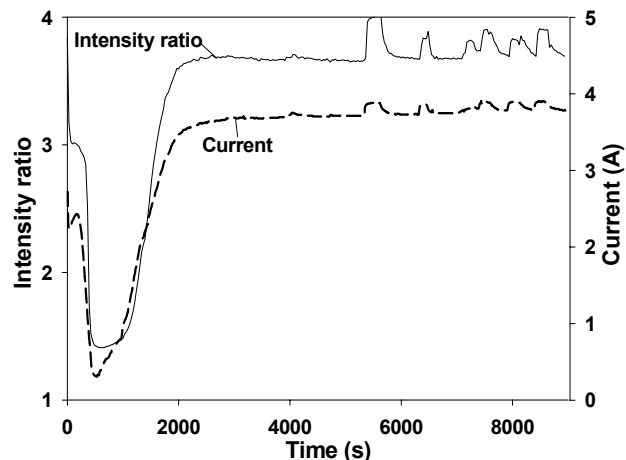


Figure 4; Fluorescence ratio and current as a function of time.

Similar experiments were performed by changing the relative humidities of the hydrogen and oxygen gas. The fluorescence response and current decreased with the decrease in the humidities of the gases. Also at different relative humidities we found a step change in the fluorescence signal corresponding to a step change in the current drawn. To quantify the pH corresponding to the in-situ measured fluorescence signal, we need to establish a correlation curve similar to figure 3 at the cell operating temperature.

The fluorescence technique outlined above may be useful for understanding fuel crossover, membrane degradation, and membrane phase specific behavior. Since there are many fluorescent dye molecules, a variety of physical and chemical phenomena can now be accessed during fuel cell operation using embedded optical fiber fluorescence spectroscopy. In particular, current work is focused on integrating the probe with porous nanoparticles with a localized fluorescence molecule on it.

Acknowledgement This work was supported by the Army Research Office and through the Connecticut Global Fuel Cell Center. We would like to thank Prof. James Fenton and Vijay Ramani for letting us use their fuel cell set.

References

- (1) Zhu, C.; Bright, F. V.; Wyatt, W. A.; Hieftje, G. M. *Proceedings - Electrochemical Society* **1987**, 87-9, 476-483.
- (2) Mohan, H.; Iyer, R. M. *Journal of the Chemical Society, Faraday Transactions* **1992**, 88, 41-45.
- (3) Mohan, H.; Iyer, R. M. *Analyst (Cambridge, United Kingdom)* **1993**, 118, 929-932.
- (4) Zawodzinski, T. A.; Davey, J.; Valerio, J.; Gottesfeld, S. *Electrochimica Acta* **1995**, 40, 297-302.

DOE FE DISTRIBUTED GENERATION PROGRAM

Mark C. Williams and Bruce Utz

US Department of Energy, National Energy Technology Laboratory,
PO Box 880, 3610 Collins Ferry Road, Morgantown, WV 26507-0880

Abstract

The U.S. Department of Energy's (DOE) Office of Fossil Energy's (FE) National Energy Technology Laboratory (NETL), in partnership with private industries, is leading the development and demonstration of high efficiency solid oxide fuel cells (SOFCs) and fuel cell turbine hybrid power generation systems for near term distributed generation (DG) market with emphasis on premium power and high reliability. NETL is partnering with Pacific Northwest National Laboratory (PNNL) in developing new directions in research under the Solid-State Energy Conversion Alliance (SECA) initiative for the development and commercialization of modular, low cost, and fuel flexible SOFC systems. The SECA initiative, through advanced materials, processing and system integration research and development will bring the fuel cell cost to \$400/kilowatt (kW) for stationary and auxiliary power unit (APU) markets. The use of fuel cells is expected to bring about the hydrogen economy. FutureGen is a major new Presidential initiative to produce hydrogen from coal.

Solid State Energy Conversion Alliance

The SECA Program is the main thrust of the DOE FE DG Fuel Cell Program. SECA is also recognized as part of the Hydrogen Program. Achieving the SECA goals should result in the wide deployment of the SOFC technology in large high volume markets. This means benefits to the nation are large and cost is low, which is the SECA goal. Less expensive materials, simple stack and system design, and high volume markets are the three criteria that must be met by a fuel cell system to compete in today's energy market. Near zero emissions, fuel flexibility, modularity, high efficiency, simple CO₂ capture will provide a national payoff that gets bigger as these markets get larger.

The SECA program is dedicated to developing innovative, effective, low-cost ways to commercialize SOFCs. The program is designed to move fuel cells out of limited niche markets into widespread market applications by making them available at a cost of \$400 per kilowatt or less through the mass customization of common modules. SECA fuel cells will operate on today's conventional fuels such as natural gas, diesel, as well as coal, gas, and hydrogen, the fuel of tomorrow. The program will provide a bridge to the hydrogen economy beginning with the introduction of SECA fuel cells for stationary (both central generation and distributed energy) and auxiliary power applications.

The SECA program is currently structured to include competing industry teams supported by a crosscutting core technology program. SECA has six industry teams working on designs that can be mass-produced at costs that are ten-fold less than current costs. The SECA core technology program is made up of researchers from industry suppliers and manufacturers as well as from universities and national laboratories all working towards addressing key science and technology gaps to provide breakthrough solutions to critical issues facing SECA. Delphi, in partnership with Battelle, is developing a 5 kW, planar, 700 °C – 800 °C, anode supported SOFC compact unit for the DG and APU markets. Delphi is expert at system integration and high volume manufacturing and cost reduction. They are focused on making a very compact and light weight system suitable for auxiliary power in transportation applications. General Electric is

initially developing a natural gas 5 kW, planar, 700 °C – 800 °C, anode supported SOFC compact unit for residential power markets. GE is evaluating several stack designs and is especially interested in extending planar SOFCs to large hybrid systems. They also have a radial design that can simplify packaging by minimizing the need for seals. GE has made good progress in achieving high fuel utilization with improved anode performance using standard materials by optimizing microstructure. SWPC is developing 5-10 kW products to satisfy multiple markets. SWPC has developed a new tube design for their 5 kW units that use flat, high power density tubes. This allows for a shorter tube length and twice the power output compared to their current cylindrical tube. Cummins and SOFCo-EFS are developing a 10 kW product initially for recreational vehicles that would run on propane using a catalytic partial oxidation reformer. The team has produced a conceptual design for a multilayer SOFC stack assembled from low cost "building blocks." The basic cell, a thin electrolyte layer (50 75 micron), is fabricated by tape casting. Anode ink is screen printed onto one side of the electrolyte tape, and cathode ink onto the other. The printed cell is sandwiched between layers of dense ceramic that will accommodate reactant gas flow and electrical conduction. The assembly is then co fired to form a single repeat unit. FuelCell Energy and Acumentrics represent additional industry design alternatives that will enhance the prospects of success of SECA fuel cells for a broader market.

SECA Core Research Issues

Developing the solid oxide fuel cell which meets both performance and cost targets is a matter of complex trade-offs. Within each sub-system and its components there exist research needs. The needs may be different for the various system alternatives and their design – anode supported, cathode supported, and electrolyte supported; planar, radial tubular. While progress has been made in power density and utilization, the cathode remains an important area of research if low temperatures are to be achieved. To achieve low overpotentials at reduced temperature requires optimization over composition and structure. Mixed ionic and electronic conducting cathodes with sufficient catalytic activity are being considered. Seals are a long-standing issue in some SOFC designs. The requirements on the seal are demanding to ensure thermal cyclability and gas tightness. The use of low-cost metallic interconnects is highly desirable for some designs.

SOFC's and Hydrogen

One of the ways in the U.S. to produce hydrogen may be with coal. Coal is a very abundant resource in the U.S. and for energy independence should be used as the primary fuel in the U.S. Coal must be in our future for energy independence. Over 50 percent of the electricity in the U.S. comes from coal, and coal use is increasing. The President recently announced the FutureGen project to produce hydrogen from coal. From the perspective of fuel cells, the goal is to aggregate SECA fuel cells into larger systems and to produce a very high-efficiency fuel cell-turbine hybrid module. The SOFC hybrid is a key part of the FutureGen plants. The highly efficient SOFC hybrid plant will produce electric power and other parts could produce hydrogen and sequester CO₂. The hydrogen produced can be used in fuel cell cars and for large SOFC DG applications. The fuel cell or hybrid could operate on syngas or hydrogen and segregation/isolation of CO₂ if operating on syngas is possible with some fuel cell designs.

References

- (1) Fuel Cells--A Handbook (Revision 4, November 1998), Report Number DOE/FETC-99/1076 (CD).
- (2) M. Williams, "Status of SOFC Development and Commercialization in the US", 6th International SOFC Symposium, in Proceedings, pp. 3-9 (1999).
- (3) M. C. Williams, "Fuel Cells - Realizing the Potential", Fuel Cell Seminar, Portland, November 1, 2000, in Proceedings Fuel Cell Seminar, pp. (2000).
- (4) M. Williams, "Energy Decision Magazine Roundtable on DG", during Electric Power 2000, Cincinnati, Ohio, in Energy Decision, June pp. 26-32, 2000.
- (5) M. Williams, "Energy Futures: Advanced Fuel cell Power Systems," Brookings Institute Seminar, "Science and Technology Policy: Current and Emerging Issues," June 14, 2000.
- (6) "SECA Workshop Proceedings," June 1-2, 2000, Baltimore, MD.
- (7) N. Minh, et. al., in Solid Oxide Fuel Cells VI, S. C. Singhal and M Dokiya, Editors, PV 99-19. p.68, The Electrochemical Society Proceedings Series, Pennington, NJ (1999).
- (8) J. Thijssen, et.al., Conceptual Design of POX SOFC 5 kW net System, Arthur D. Little, Inc. Report # 71316 (to be published), Cambridge MA (2000).
- (9) M. Williams and S. Singhal, "Mass-produced ceramic fuel cells for low-cost power," in Fuel Cell Bulletin, no. 24, pp. 8-11 (September 2000).
- (10) M. Williams, "Fuel Cells: Realizing the Potential for Natural Gas," Key Note Address in Proceedings Fuel Cells 2000, Philadelphia, PA, September 27, 2000.
- (11) M. C. Williams, "Fuel Cells - Realizing the Potential", Fuel Cell Seminar, Portland, Oregon, November 1-3, 2000, in Proceedings Fuel Cell Seminar, pp. .
- (12) M. Williams, "Status of SOFC Development and Commercialization in the US", 7th International SOFC Symposium, Japan, in Proceedings, (2000).
- (13) M. C. Williams, "Distributed generation fuel cells and power reliability," #1605, Energy 2001, Baltimore, Md., 2001.
- (14) M. Williams, "Fuel Cells and the World Energy Future," in Proceedings PowerGen, Orlando, FL, 2001.
- (15) David A. Berry, Wayne A. Surdoval, and Mark C. Williams, "The solid state energy conversion alliance - program to produce mass manufactured ceramic fuel cells," in Proceedings ACS Fuel Cell Symposium, Chicago August 2001.
- (16) M. C. Williams, "New Direction in the US Fuel Cell Program," in Proceedings 7th Grove Fuel Cell Symposium, September 11, 2001.
- (17) Catherine Greenman, "Fuel Cells: Clean, Reliable (and Pricey) Electricity," *The New York Times*, May 10, 2001, p. D8.
- (18) "SECA Workshop Proceedings," March 29-30, 2001, Arlington, VA.
- (19) "SECA Workshop Proceedings," March 21-22, 2002, Washington, DC.
- (20) "SECA Workshop Proceedings," April 15-16, 2003, Seattle, WA.

Defect chemistry of p-type perovskite conductor used in solid oxide fuel cells

Xiao-Dong Zhou and Harlan U. Anderson

Department of Ceramic Engineering, Electronic Materials Applied Research Center, University of Missouri-Rolla, Rolla, MO 65409

Introduction

The development of solid oxide fuel cells (SOFCs) has been driven by both industry and academy for the purpose of searching for the alternative energy sources. Over last several years, operation of SOFCs in the intermediate temperature regime (500 – 700°C) is of particular interest, which seems mandatory for SOFC commercialization. Strict materials requirements are of great importance for the electrode of SOFCs operated over the intermediate temperature region. Therefore, it is necessary to study the electrode materials by understanding the mechanisms for the conductive and catalytic behavior and developing reliable and stable experimental methods to measure defect density and catalytic ability. Perovskite type oxides are of great interest for use as the electrodes in SOFCs because (1) site occupancy is determined mainly by ionic radius so lattice site location of a particular cation is fairly certain; (2) electronic conductivity (σ) is determined by B site ion; and (3) ionic conductivity results from the presence of oxygen vacancies. Thus, this family of oxides was tailored to use as mixed ionic and electronic conductors, superionic conductors, and superconductors. Defect chemistry is a particularly powerful technique in understanding the mass and charge transfer properties by determining defect type, density, association and mobility. In this article, it is our intent to report the global solutions to defect chemistry models, with an emphasis on the p-type perovskite conductors which are being considered as the electrodes of SOFCs. The global defect chemistry models allow us to better understand and predict the electrochemical properties of perovskite type p-type conductors.

Defect Chemistry Modeling

The procedure is to write the defect formation reactions: 1) list the basic defect types and reactions which can occur: intrinsic, stoichiometric, oxygen excess and oxygen deficient; 2) write the overall neutrality relation and 3) combine the resulting equations to yield a relationship which can be solved for particular temperature and oxygen activity regimes. Considering a general type perovskite type oxide (ABO_3), the occupants at A site can be (Kroger-Vink notation is used) A_A^x , V_A^m and Sr_A' (for simplicity, assume Sr is the low valence element substituting at the A site). The occupants at the B site are B_B^x , B_B' , B_B^{\bullet} and V_B^m , where B_B^x indicates a majority of B cations which are in valence of 3+, B_B' represents that some B site cations are in 2+ state and B_B^{\bullet} shows some B site cations are in 4+ valence state. The oxygen site can have two type of occupants, V_O^{\bullet} and O_O^x .

Since there exist nine variables, nine equations are needed to obtain these values. Two methods can be used to solve the resulting equations: 1) divide into regions of particular neutrality conditions and solve for that particular region or 2) do not use limiting conditions, but allow a computer to make a numerical solution to the overall equation using the total neutrality condition. More detailed equations and solutions can be found elsewhere.¹ A global solution will be discussed in this article, in which the overall electron neutrality expression is used results in a term named as the

ability for oxygen vacancy generation (AOG). This method is considered as a model based on delocalized electron holes.

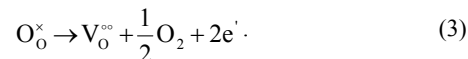
The total electrical conductivity, σ , is given by

$$\sigma = N\mu q \quad (1)$$

where μ is the mobility, q is the carrier charge and N is the carrier concentration. Because of the mobility of either the electrons or holes is much higher than that of oxygen ions, the total conductivity in ferrites is dominated by hole conduction. The carrier concentration, N is:

$$N = [Sr_{La}'] - 2[V_O^{\bullet}] \quad (2)$$

where $[Sr_{La}']$ is the acceptor level and $[V_O^{\bullet}]$ is the oxygen vacancy concentration. For simple analysis, it is assumed that all doping centers are dissociated. Generation of oxygen vacancy, V_O^{\bullet} , follows:



The reaction constant (K_1) of reaction in Eq. (3) is:

$$K_{V_O^{\bullet}} = [V_O^{\bullet}] pO_2^{1/2} n^2 \quad (4)$$

where, pO_2 is the oxygen partial pressure and n is the electron concentration. Assuming this reaction follows the Arrhenius law:

$$K_{V_O^{\bullet}} = K_{V_O^{\bullet},0} \exp\left(-\frac{E_{V_O^{\bullet}}}{kT}\right), \quad (5)$$

where $E_{V_O^{\bullet}}$ is the activation energy for oxygen vacancy generation

and k is Planck's constant. Considering $np = K_i$, then the expression can be rearranged to yield

$$\ln\left(\frac{[V_O^{\bullet}]}{([Sr_{La}'] - 2[V_O^{\bullet}])^2}\right) = \ln\left(\frac{K_{V_O^{\bullet},0}}{K_i^2}\right) - \frac{1}{2}\ln(pO_2) - \frac{E_{V_O^{\bullet}}}{kT} \quad (6)$$

From this expression the oxygen vacancy concentration can be derived as a function of substitution level ($[Sr_{La}']$), temperature, and materials properties:

$$[V_O^{\bullet}] = \frac{(4MN + 1) - \sqrt{1 + 8MN}}{8A} \quad \text{where} \quad (7)$$

$$M = \frac{K_{V_O^{\bullet},0}}{K_i^2} \cdot \exp\left(-\frac{E_{V_O^{\bullet}}}{kT}\right) \cdot P_{O_2}^{-1/2} \quad \text{and} \quad N = [Sr_{La}']$$

The term M can be expressed as $AOG \cdot pO_2^{-1/2}$, where AOG stands for the ability for oxygen vacancy generation, which is a function of temperature and intrinsic materials properties. Fig. 1 shows a plot of carrier concentration calculated from Eqs. (2), (6) and (7). The ability for oxygen vacancy generation as a function of temperature and oxygen activity can be determined by simulating experimental conductivity data with the current defect chemistry. Fig. 2 shows a plot of the experimental and simulated conductivity of LSM, LSF and LSCF. Table 1 lists the AOG values of these compounds. It is worthwhile to note again that the B site cation can be easily driven from 4+ to 3+ for the perovskites which possess high values of AOG, such as $(La,Sr)FeO_{3-\delta}$. For instance, $\delta \sim 0.2$ takes place at $\sim 1500^\circ\text{C}$ for $La_{0.60}Sr_{0.40}FeO_{3-\delta}$ in air, which indicates that all of the Fe ions are in the 3+ valence state. If the temperature is lowered to 1000°C , the oxygen activity has to be lowered to $\sim 10^{-14}$ atm to observe this state. Activation energy values for AOG of manganites and chromites are larger than those of ferrites, hence, it is expected that Cr and Mn cations can be reduced to 3+ in air only if the temperature is sufficiently high.

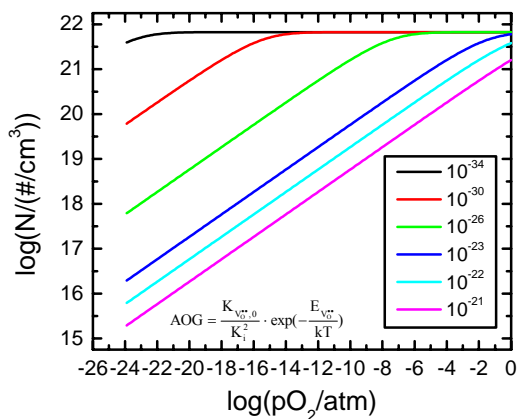


Figure 1. A plot of carrier concentration as a function of oxygen activity with various AOG values

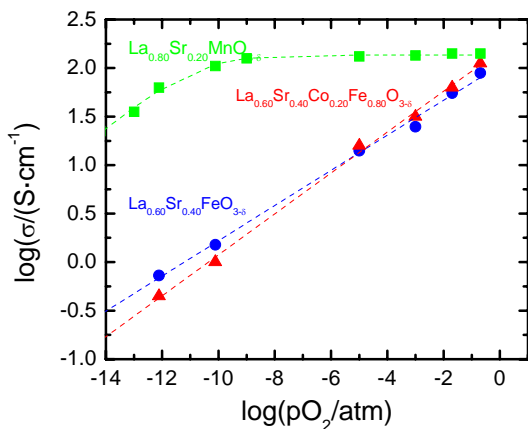


Figure 2. Plot of $\log(\sigma)$ vs. $\log(pO_2)$ for LSM, LSF and LSCF. The solid points are experimental data. The dash lines are fitting results from the global defect chemistry model.²⁻⁴

The knowledge of the values for the AOG terms can enable us to understand the maximum conductivity of many p type conductors. For example, from the previous results, we know that at temperatures $< 600^\circ\text{C}$ in air LSF possesses nearly stoichiometric oxygen occupancy. Thus it can be expected that the oxygen vacancy concentration is extremely low at relatively low temperature (\sim room temperature), therefore conductivity should increase with increasing temperature because of the increasing mobility. At elevated temperature, more oxygen vacancies are generated which will decrease the total carrier numbers because of the increasing oxygen vacancy concentration. The mobility, however, continuously increases with increasing temperature. Hence, a maximum conductivity at a specific temperature is expected due to an increasing mobility and decreasing carrier concentration. A shift of the temperature corresponding to the maximum conductivity is observed as shown in Table 1. As discussed previously this maximum in conductivity represents the temperature at which the oxygen vacancy concentration starts to influence the carrier concentration. It does not mean that the oxygen vacancy concentration is negligible at this temperature, but on the other hand, the influence of oxygen vacancy concentration on total carrier concentration is negligible below this temperature and the

concentration of oxygen vacancies is so small that their contribution to transport processes becomes minimal.

The values of AOG and understanding of the maximum conductivity are of particular importance in the search for materials for energy conversion devices. Since oxygen vacancies are required for lower cathodic overpotentials, this temperature also represents the temperature below which a cathode can be expected to have high overpotentials. Therefore, when pure LSM is used as the cathode, it will be expected to work well when the operation temperature is $\sim 1000^\circ\text{C}$ because the oxygen vacancy concentrations are sufficiently high to support the required transport processes of the cathode. Below this temperature range, overpotential problems are commonly encountered. It has been found that the addition of a second ionic conducting phase to the cathode enhances the ionic transport processes, which allows lower temperature operation. Thus the use of cathodes consisting of mixtures of LSM and YSZ or LSM and CGO has become common practice in the SOFC industry, but these mixtures will not extend the temperature much below $750\text{--}800^\circ\text{C}$ before cathodic overpotentials become too large because the concentration of oxygen vacancies is insufficient to support the transport processes which are required for oxygen reduction and transport of the oxygen ions to the electrolyte.

Conclusions

The understanding of the defect chemistry in the perovskite family p type conductors allows us to search for the novel materials for use in fossil energy conversion system, which requires a sufficient vacancy density, a mixed ionic and electronic conductance, high catalytic ability and stability. Examples include the electrodes used in SOFCs where the cathode component which requires high oxygen vacancy density and electronic conductance and the anode requires stability in a very reducing atmosphere, electronic conductance, and oxygen vacancy density.

Acknowledgement. This work was supported by contracts DE-FC26-02NT41563 and DE – FC36 – 01G011084.

References

- (1) Zhou X D and Anderson H U. unpublished.
- (2) Kuo J H, Anderson H U, Sparlin D M, "Oxidation-reduction behavior of undoped and strontium-doped lanthanum manganese oxide (LaMnO_3): defect structure, electrical conductivity, and thermoelectric power," *J. Solid State Chem.* (1990) **87**, 55-63.
- (3) Tai L W, Nasrallah M M, Anderson H U, Sparlin D M, Sehlin S R, "Structure and electrical properties of $\text{La}_{1-x}\text{Sr}_x\text{Co}_{1-y}\text{Fe}_y\text{O}_3$, part 2. The system of $\text{La}_{1-x}\text{Sr}_x\text{Co}_{0.2}\text{Fe}_{0.8}\text{O}_3$," *Solid State Ionics* (1995), **76**(3,4), 273-83.
- (4) Kaus I, Anderson H U, "Electrical and thermal properties of $\text{La}_{0.2}\text{Sr}_{0.8}\text{Cu}_{0.1}\text{Fe}_{0.9}\text{O}_{3-d}$ and $\text{La}_{0.2}\text{Sr}_{0.8}\text{Cu}_{0.2}\text{Fe}_{0.8}\text{O}_{3-d}$," *Solid State Ionics* (2000), **129**(1-4), 189-200.

Table 1 AOG and T_{max} for four p type conductors

	LSM	LSF	LSCF	LSCFu
AOG	2.9×10^{-27}	3×10^{-21}	3×10^{-20}	
T_{max} ($^\circ\text{C}$)	900	600	550	400

Peculiar Properties of Novel Self-stabilized NiO-YSZ Nanocomposite Materials for Solid Oxide Fuel Cell Anode

Ming-Yao Cheng and Bing-Joe Hwang

Dept. Chemical Engineering
National Taiwan University of Science and Technology
106, Taipei, Taiwan,
ROC

Introduction

In electrochemical systems, for example, an electrochemical sensor, the length of three-phase-boundary at electrode/electrolyte interface governs its sensitivity and selectivity. Although it is difficult to estimate the length of three-phase-boundary, smaller particles, proper ratio and well dispersion of electrode and electrolyte materials would create larger three-phase-boundary length. Similarly, it would be helpful to improve the power density of solid oxide fuel cell (SOFC) by increasing three-phase-boundary length. Meanwhile, utilization of fuel would be more efficient as well.

Liu et al. have fabricated nanostructured electrode materials by combustion chemical vapor deposition technique and shown excellent performance at low temperatures [1]. Structure stabilities of the nanostructured electrode materials were not shown in this work. Mamak et al. have synthesized mesoporous electrode materials for SOFC applications, indicating the three-phase-boundary length of the synthesized materials can be improved [2-5]. However, collapse nature of mesoporous materials should be considered during its preparation process. Nevertheless, the sintering of nanostructured materials in SOFC applications might be extremely serious and result in losing great quantity of three-phase-boundary length. Therefore, it is of great importance to stabilize the structure of nanostructured materials in SOFC applications. In this work, self-stabilized NiO-YSZ nanocomposite materials were synthesized for SOFC applications. The grain growth of the synthesized NiO-YSZ SOFC anode materials is significantly inhibited during high-temperature treatment. The properties of the self-stabilized NiO-YSZ nanocomposite anode materials are also characterized and discussed here.

Experimental

Synthesis. Nickel hydroxide was chosen as the precursor for self-stabilized NiO-YSZ nanocomposite (referred as S.S. NiO-YSZ) powders. Proper amounts of nickel hydroxide (Acros, USA) were added into 100ml 1-propanol solution with stirring. 70wt% zirconium propoxide dissolved in 1-propanol solution (Aldrich, USA) was then added into the above solution. The molar ratio of nickel hydroxide to zirconium propoxide was fixed to 10/3 to make the volume ratio of Ni to YSZ as 1/1. Yttrium nitrate (Acros, USA) was dissolved into 1-propanol first followed by adding into the above solution. The molar ratio of zirconium to yttrium was fixed to 92/8. The solution was sealed and kept at room temperature with stirring. Reaction of zirconium propoxide with nickel hydroxide took place until totally evaporation of 1-propanol in the solution. The reaction was processed for several days. After reaction, the precursors were transferred into furnace immediately for preventing hydrolysis of the precursors. The furnace was operated with a heating rate of 5 °C/min to 600 °C and held for 1 hour and the said S.S. NiO-YSZ powders were synthesized. For comparison, NiO-YSZ powders by a traditional route [6] were synthesized from NiCO₃·Ni(OH)₂ (Showa, Japan) and 8YSZ powders (TOSOH, Japan) as precursors. The

mixed precursors were ball-milled for 12 hours followed by heat treatment at 600 °C for 1 hour and denoted as t-NiO-YSZ later.

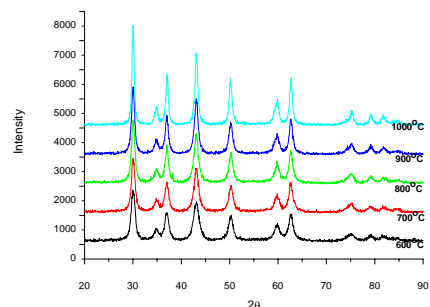
Characterization. For characterizing the synthesized materials, XRD was performed with Rigaku diffractometer and Cu K_α was taken as radiation source. The sweeping rate was 10 degree/min in the 2θ range of 20~90°. In order to investigate the behavior of grain growth, S.S. NiO-YSZ powders were further heated to higher temperature step by step up to 1000 °C and held for 1 hour for each step.

To understand the morphologies of the synthesized materials, electron microscope was performed with JEOL-2010 field emission SEM with 40-second Pt coating on the surfaces of the samples.

Results and Discussion

XRD patterns of S.S. NiO-YSZ and t-NiO-YSZ powders were shown in figure 1(a) and (b), respectively. From 1(a), it exhibited that cubic-fluorite YSZ materials were obtained and the doping process of yttrium ions into zirconia crystalline structures was confirmed. In addition, the cubic NiO peaks are still broad in the S.S. NiO-YSZ materials even after 1000 °C calcination, indicating their grains are still very fine.

(a)



(b)

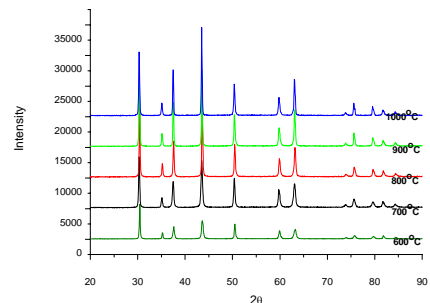


Figure 1. XRD patterns of (a) self-stabilized and (b) traditional NiO-YSZ materials of various calcination temperatures

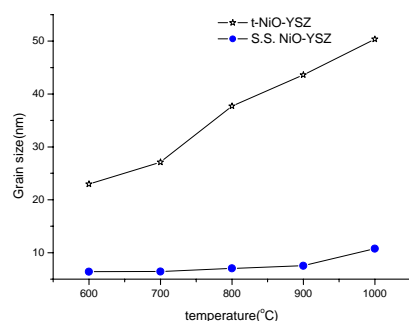


Figure 2. Calculated grain sizes of NiO in S.S. NiO-YSZ and t-NiO-YSZ to various calcinations temperatures

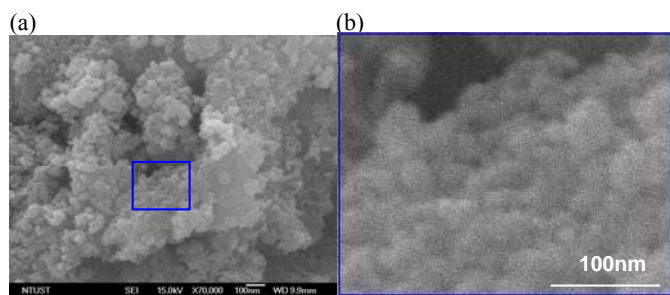


Figure 3. SEM morphologies of S.S. NiO-YSZ material (a) 70,000 \times (b) Enlarging part of blue-line area in (a)

Scherrer equation was used to further analyze the grain growth behaviors of NiO in the S.S. NiO-YSZ materials according to the FWHM of NiO (200) peak in figure 1. The calculated grain sizes of NiO in the S.S. NiO-YSZ and t-NiO-YSZ were shown in figure 2. The grain size of NiO in the S.S. NiO-YSZ was found to be 6.4 nm at 600 and 10.7 nm at 1000. It is interesting that the grain size of NiO in S.S. NiO-YSZ almost no changes until 1000. For the t-NiO-YSZ, however, the grain size of NiO was around 22.3 nm at 600 and 50.4 nm at 1000. It was found that the synthesized S.S. NiO-YSZ materials showed better structural stability than the t-NiO-YSZ materials even though sintering effect of nanostructured materials should be more serious in general. Undoubtedly, the length of three-phase-boundary of SOFC anode would be much larger in the S.S. NiO-YSZ materials.

From morphology observation by FESEM shown in figure 3, nanocrystalline nature of the S.S. NiO-YSZ materials was revealed. Even though it was hard to resolve NiO and YSZ grains individually from FESEM, other techniques were still underway for resolution of NiO distribution in the microstructure.

Acknowledgment. The authors would like to thank National Science Council (NSC 92-2214-E-011-010) for financial support and National Taiwan University of Science and Technology for XRD and FESEM assistances.

References

1. Mamak, M., Coombs, N. and Ozin, G. A., *Chem. Mater.* **2001**, *13*, 3564-3570.
2. Mamak, M., Coombs, N. and Ozin, G. A., *J. Am. Chem. Soc.* **2000**, *122*, 8932-8939.
3. Mamak, M., Métraux, G. S., Petrov, S., Coombs, N., Ozin, G. A., and Green, M. A., *J. Am. Chem. Soc.* **2003**, *125*, 5161-5175.
4. Mamak, M., Coombs, N. and Ozin, G. A., *Adv. Mater.* **2000**, *12*, 198-202.

5. Liu, Y., Zha, S., and Liu, M., *Adv. Mater.* **2004**, *16*, 256-260.
6. Negishi, H., Sakai, N., Yamaji, K., Horita, T. and Yokokawa, H., *J. Electrochem. Soc.* **2000**, *147*, 1682-1687.

Solid Oxide Fuel Cell Exhaust Studies of Simple and Complex Fuels with FTIR Spectroscopy

Michael B. Pomfret^a, Oktay Demircan^a, Mary Sukeshini^a, Robert A. Walker^{a,b}

^aDepartment of Chemistry and Biochemistry, University of Maryland, College Park, MD 20742

^bChemical Physics Program, University of Maryland, College Park, MD 20742

Introduction

Solid oxide fuel cells (SOFC) have long been viewed as a potential source of clean, reliable, efficient electrical power. While progress has been made in fuel cell development and fabrication numerous questions exist about the actual mechanism(s) by which fuel is oxidized in SOFCs. Most studies have focused on engineering and electrochemical issues to improve the overall efficiency.¹⁻³ Considerably less attention has focused on the way in which complex fuels (i.e. butane and toluene) are oxidized to CO₂ and H₂O.

Standard SOFC designs use a nickel or Ni/YSZ (yttria stabilized zirconia) anode to oxidize fuel.⁴ Oxidation occurs as O²⁻ ions are created at the cathode and transported through the electrolyte – most commonly YSZ – to the anode. Most models of fuel cell operation postulate that the fuel is oxidized at the three-phase boundary. The anode then carries the resulting electrons out of the cell to an exterior circuit. Recently, hydrocarbon fuels have taken on increased importance as C₄H₁₀ has been shown to increase cell productivity if used as a fuel. Specifically, power densities for H₂ operation increase greatly after C₄H₁₀ has been used as a fuel.⁵

SOFC efficiencies that depend on fuel type raise concerns about both anode poisoning and enhanced conductivity. To fully understand the effect hydrocarbon fuels have on fuel cell performance detailed, molecular mechanisms of the chemistry occurring at the anode surface during oxidation must be developed. One means of building this understanding is by monitoring the products of oxidation in SOFCs. This strategy can be pursued by analyzing the exhaust, as well as any deposits that remain in the cell, using Fourier-transform infrared (FTIR) spectroscopy.

The present work employs FTIR to study samples of SOFCs using hydrogen, methane and butane as fuels. The resulting spectra demonstrate the important role that spectroscopy can play in identifying chemistry that occurs in SOFCs.

Experimental

Fuel Cell Operation. Experiments described in this work use two types of fuel cells. Both cells have 0.8 mm thick, 8% polycrystalline YSZ electrolytes and lanthanum strontium manganate (LSM) cathodes. One cell has a Ni/YSZ cermet anode to be used for H₂ and CH₄ fuels, while the other has a Cu/CeO₂ cermet anode to be used for H₂ and C₄H₁₀ fuels. The fuel cell rig is comprised of Hastelloy-X Ni alloy and the electrolyte operational temperature is 800°C.

The three fuels are diluted with argon to regulate the number of H₂ atoms in the reaction zone at a single time for all fuels. The H₂ flow is 139 sccm H₂ and 275 sccm Ar. The CH₄ flow is 69.79 sccm CH₄ and 137.46 sccm Ar. The C₄H₁₀ flow is 13.4 sccm C₄H₁₀ and 26.8 sccm Ar. This results in residence times of 0.800 s for H₂, 0.662 s for CH₄ and 3.52 s for C₄H₁₀. Open circuit voltages are -1.03 V for H₂, -0.89 V for CH₄, and -0.79 V for C₄H₁₀. Typical currents drawn were on the order of 10 mA.

Both cells are first operated with the H₂ mixture and allowed to equilibrate for 30 min. After stable operation has been achieved the fuel is switched to the hydrocarbon mixtures and again allowed to equilibrate for 30 min.

Exhaust Collection and IR Characterization. A custom-built glass collection manifold with auxiliary exhaust outlets is attached to the anode exhaust outlet. An IR gas cell with a volume of 35.0 cm³ and NaCl crystal windows is evacuated and then attached to the collection chamber and the auxiliary outlets closed. The valves on the IR cell are then opened and the exhaust flow of the fuel cell is flowed through the collection system for 10 min. After this time the IR cell's valves are closed, the cell detached, and the spectrum taken.

Spectra are obtained using a ThermoNicolet Nexus 670 FTIR Spectrometer with a tungsten source. Each spectrum consists of 64 scans. All reported spectra have been corrected for any background features arising from the evacuated cell.

Results and Discussion

Figure 1 shows exhaust spectra of all three fuels. They all exhibit well resolved bands that can be readily assigned to stable, low molecular weight species. The H₂ exhaust spectrum (**a**) shows only water stretching and bending bands, as expected. The CH₄ exhaust (**b**) also shows water peaks. In addition, the spectrum shows carbon dioxide bands (2360 and 2341 cm⁻¹) from the full oxidation of the hydrocarbon. The other bands (CH₄ at 3015 and 1303 cm⁻¹, and carbon monoxide at 2170 and 2119 cm⁻¹) indicate incomplete oxidation of the fuel and intermediate species. This observation is illustrated even more dramatically by the C₄H₁₀ exhaust spectrum (**c**).

Complete oxidation would lead to only water and carbon dioxide peaks in the IR spectra of the exhaust. In the C₄H₁₀ case many other species are present, most notably CH₄. There also appear to be other small hydrocarbons (≤ 4 carbons) as well as larger, polyaromatic hydrocarbons – in agreement with previous studies.^{6,7}

The 2500-3500 cm⁻¹ region of the spectra is expanded in **Figure 2**. Both the CH₄ (**a**) and C₄H₁₀ (**b**) exhausts contain a significant amount of CH₄ in the exhaust, with easily distinguishable, identical P, Q, and R branches. Additional lines in the C₄H₁₀ spectrum reflect the presence of both aromatic and aliphatic C-H stretching from other hydrocarbon species. The most important aspect of Figures 1 and 2 is that incomplete oxidation of C₄H₁₀ results in the formation of overwhelming amounts of CH₄. An outstanding question is whether CH₄ is formed on the metal electrolyte anode assembly itself or through a gas phase reforming reactions.⁸ The answer to this question carries important consequences for evaluating SOFC operation. If CH₄ is being created due to incomplete oxidation at the anode, then the chemical composition of the anode assembly surface is likely to be substantially different from the original material.⁹ However, should the reforming happen in the gas phase starting fuel identity should not matter as complex hydrocarbons will simply decompose to create CH₄ before reaching the anode.

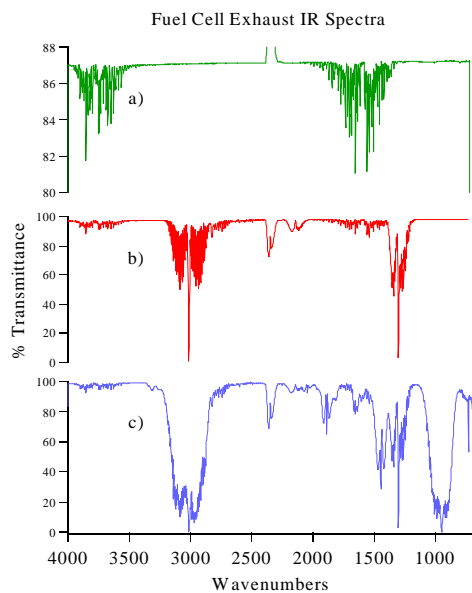


Figure 1. The IR spectra of the exhaust of the three SOFC fuels; a) H₂, b) CH₄, c) C₄H₁₀. Note the different % transmittance scales.

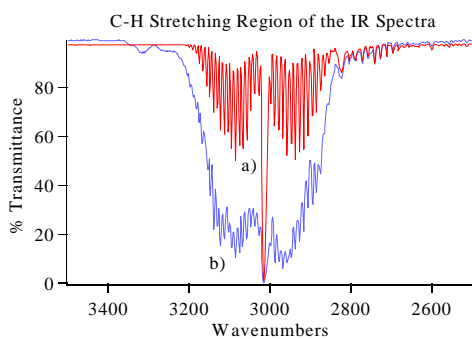


Figure 2. The 3500 – 2500 cm⁻¹ region of the IR spectra of the hydrocarbon fuels; a) CH₄, b) C₄H₁₀.

Figure 3 displays the 1900-2500 cm⁻¹ region in the IR spectra of the CH₄ (a) and C₄H₁₀ (b) exhausts. This part of the IR shows an interesting detail. The CH₄ spectrum has a CO/CO₂ peak area ratio of 0.58, while the C₄H₁₀ spectrum's ratio is 0.30. This result suggests that although both fuels experience incomplete oxidation, C₄H₁₀ is at least slightly more efficient in the SOFC in terms of its ability to react to completion implying that C₄H₁₀ does not pyrolyze to form CH₄ quantitatively.

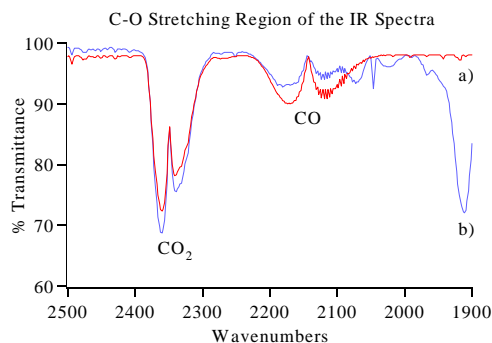


Figure 3. The 1900 – 2500 cm⁻¹ region of the IR spectra of the hydrocarbon fuels; a) CH₄, b) C₄H₁₀.

Conclusion

The present experiment clearly demonstrates the utility and importance of optical spectroscopy in the study of solid oxide fuel cells. This work clearly shows how infrared spectroscopy can aid in the determination of the products of the fuel cell process and the evaluation of the efficiency of oxidation of various fuels. Isotopically labeled fuels as well as GC/MS analysis of effluent gases will greatly assist in interpreting oxidation chemistry in SOFCs.

Acknowledgements. This work is supported by the Office of Naval Research through the Multiple University Research Initiative Grant # 0110138816, in association with the Colorado School of Mines and the California Institute of Technology.

References

- (1) Weber, A.; Ivers-Tiffée, E. *J. Power Sources* **2004**, *127*, 273-283.
- (2) Srikanth, V.T.; Turner, K.T.; Ie, T.Y.A.; Spearing, S.M. *J. Power Sources* **2004**, *125*, 62-69.
- (3) Ormerod, M.R. *Chem. Soc. Rev.* **2003**, *32*, 17-28.
- (4) Zhu, W.Z.; Deevi, S.C. *Mat. Sci. Eng. A-Struct.* **2003**, *362*, 228-239.
- (5) McIntosh, S.; Vohs, J.M.; Gorte, R.J. *J. Electrochem. Soc.* **2003**, *150*, A470-A476.
- (6) McIntosh, S.; He, H.P.; Lee, S.I.; Costa-Nunez, O.; Krishnan, V.V.; Vohs, J.M.; Gorte, R.J. *J. Electrochem. Soc.* **2004**, *87*, 331-336.
- (7) Demircan, O.; Suresh, M.; Pomfret, M.; Jackson, G.; Walker, R.; Eichhorn, B. *J. Electrochem. Soc.* **2004**, submitted.
- (8) Naik, C.; Cartensen, H.-H.; Dean, A.M. *Proceedings of the 3rd Joint Meeting of the U.S. Sections of the Combustion Institute* **2003**.
- (9) Pomfret, M.; Suresh, M.; Stoltz, C.; Eichhorn, B.; Walker, R. *J. Electrochem. Soc.* **2004**, submitted.

SOLID OXIDE FUEL CELLS FOR DIRECT UTILIZATION OF HYDROCARBONS PREPARED BY LAMINATION METHODS

Kipyung Ahn, Shung-Ik Lee, Yingyi Huang, John M. Vohs, and Raymond J. Gorte

Department of Chemical and Biomolecular Engineering
University of Pennsylvania, Philadelphia, PA 19104 USA

Introduction

Solid oxide fuel cells (SOFCs) show great promise for power generation in a wide range of applications. Because they are based on a ceramic, oxygen ion-conducting membrane, a SOFC can theoretically operate on any combustible fuel, including CO [1,2] and hydrocarbons [3-5], allowing them to be used with fuels that are readily available today. However, in order to operate on hydrocarbon fuels, it is necessary to choose the materials that are used in the anode with great care. For example, Ni, which is commonly used in anodes on fuel cells that utilize H₂, tends to form carbon fibers in the presence of hydrocarbons.

In general, the first step in fabricating SOFC electrodes involves high-temperature sintering of mixed oxides including electrolyte materials. This approach limits the choice of materials that can be used for the electrode since the oxides may decompose or undergo unwanted solid-state reactions at high temperatures. Therefore, alternative methods are required for preparation of electrode composites in order to incorporate a wide range of materials that may have superior catalytic or current collection properties.

Recent work in our laboratory has demonstrated that it is possible to prepare SOFC electrodes from a wide range of materials by using low-temperature methods in which the electronically conductive component is added by impregnation with soluble salts to a porous matrix of the electrolyte material [6,7]. The primary advantage of producing electrodes in this manner is that the porous matrix can be sintered together with the electrolyte to very high temperatures before the active component is added, allowing the processing temperatures for the two components to be decoupled.

In this paper, we describe the fabrication of SOFCs with high-performance electrodes, having controlled structures and capable of producing electrons directly from hydrocarbon fuels, without reforming. These SOFCs were produced using a single, high-temperature sintering step in which the initial structure consists of a dense layer of YSZ separating two porous layers and is produced by lamination of green ceramic tapes. An additional layer with holes was laminated on top of one of the porous layers to provide mechanical strength and rigidity.

Experimental

The YSZ components of the fuel cells were fabricated using YSZ green tapes prepared by tape casting. The YSZ powder (8 mol% Y₂O₃, TZ-8Y, Tosoh) used in the tapes was initially ball milled for 20 h with water and a dispersant (Darvan C, R.T. Vanderbilt Company,

Inc.) to break up agglomerates. Emulsion-type binder solutions (Duramax HA-12 and B-1000, Rohm and Haas) were added to the slurry and mixed by stirring for 24 h before casting. Pyrolyzable pore formers such as graphite (325 mesh, Alfa Aesee) and polystyrene-divinylbenzene (200-400 mesh, Alfa Aeser) were added together with the YSZ powder to the tapes used in the electrodes in order to introduce porosity.

An SOFC was prepared by lamination of various green tapes using a uniaxial hydraulic press equipped with heating platens (Carver Inc.). To improve the mechanical strength of the cell a relatively thick YSZ support layer was used. This support layer was in turn laminated together with the layers that would make up the cathode, electrolyte, and anode, as shown schematically in Fig. 1. The thicknesses of the anode, cathode, and electrolyte layers after firing were 100 μm, 60 μm, and 25 μm, respectively. The anode layers contained a mixture of graphite and polystyrene-divinylbenzene pore formers, while the cathode layer contained only graphite. After lamination, the tapes were fired at 1823 K for 4 h. The anode and cathode composites were fabricated using impregnation of the porous YSZ matrices with aqueous solutions. The final composition of the tested cell was 15 wt% CeO₂, 21 wt% Cu, 9 wt% Co for the anode and 40 wt% La_{0.6}Sr_{0.4}CoO₃ for the cathode.

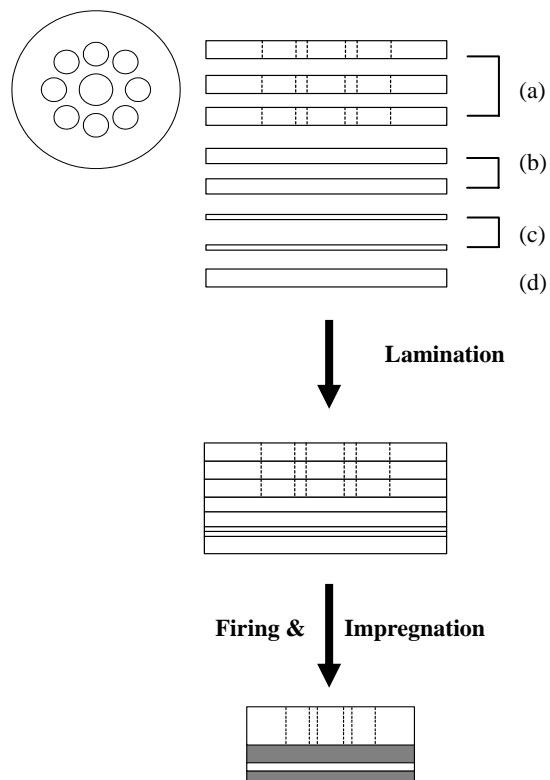


Figure 1. Schematic of the fabrication procedure for the laminated cells. (a) support layer, (b) YSZ + graphite + polystyrene divinylbenzene, (c) dense YSZ, (d) YSZ + graphite

Results and Discussion

Figure 2 shows an SEM image of a cross section near the electrolyte interface of the cell that was prepared by the lamination process shown in Figure 1, prior to the impregnation of the anode and cathode materials. Only small pores in the range of 1 to 2 μm in diameter were present in the cathode layer, while the anode layer had large pores with a size of about 20 μm in addition to the small pores. The small and large pores in the electrodes were introduced by graphite and polystyrene-divinylbenzene pore formers, respectively. The porosities of the anode and cathode porous layers were 65 % and 70%, respectively. The cell consists of three support layers, two anode layers, two electrolyte layers and a cathode layer. The micrograph demonstrates that there was good contact between the electrolyte layer and the porous YSZ electrode layers, with no evidence for cavities between layers. This result shows the microstructure of the electrodes can be engineered by laminating several layers having different microstructures. Furthermore, the dense support layer was found to provide mechanical strength to the cell so that thin electrolytes and electrodes can be used. This indicates some of the issues encountered in electrolyte or electrode supported cells can be avoided by using support layers [8].

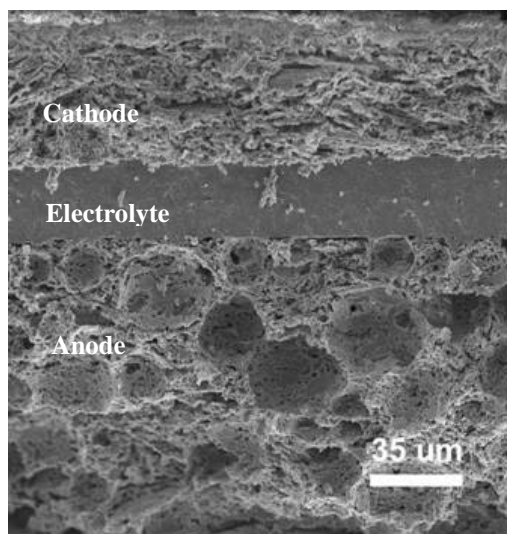


Figure 2. SEM image of the YSZ structure used for making the cell in this study

In previous work, it was shown that $\text{Cu}_{0.7}\text{Co}_{0.3}$ bimetallic mixtures are stable towards carbon fiber formation in the presence of hydrocarbon fuels, even though Cu and Co do not form an alloy [9]. It appears that Cu coats the surface of the Co crystallites, suppressing carbon formation. However, the presence of the Co within the anode still enhances the electrochemical performance. The performance of the $\text{Cu}_{0.7}\text{Co}_{0.3}\text{-CeO}_2\text{-YSZ|YSZ|LSCo-YSZ}$ cell in H_2 and n-butane at 1023 K is shown in Figure 3. For operation using H_2 with 3 vol% H_2O , the open-circuit voltages (OCV) were close to the theoretical, Nernst potential of 1.1 V. A maximum power density of 770 mW/cm^2

was achieved at 1023 K. For n-butane, the OCV was slightly lower than predicted by the Nernst potentials, ~ 1.12 V. The maximum power density was 490 mW/cm^2 at 1023 K, lower than that with H_2 , showing that the chemical oxidation reaction must partially limit performance.

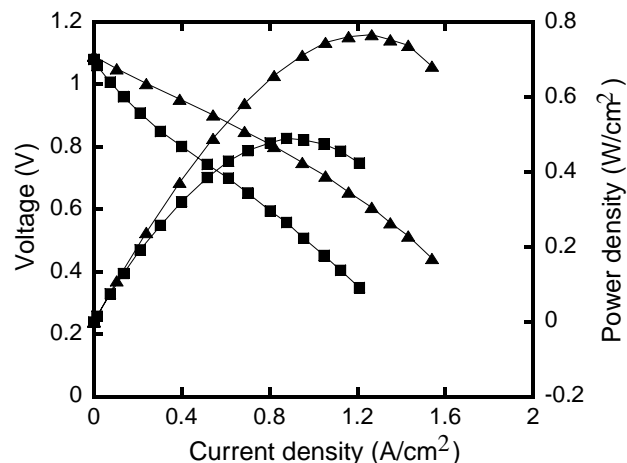


Figure 3. Cell performance curves at 1023 K in (\blacktriangle) H_2 and (\blacksquare) n-butane

Conclusions

We have demonstrated a new fabrication method for SOFCs for direct utilization of hydrocarbon fuels. The method involved lamination of ceramic tapes prepared by tape casting with or without pore formers and a single step firing, followed by impregnation of nitrate solutions. Utilization of perforated support layers allowed SOFCs consisting of thin electrolytes and thin electrodes to be fabricated, providing flexibility in designing cell structure.

Acknowledgements. This work was funded by DARPA, through the Palm Power Program.

References

1. W. Galvita, V. D. Belyaev, A. V. Frumin, A. K. Demin, P. E. Tsiakaras, and V. A. Sobyenin, *Solid State Ionics*, **2002**, 152, 551
2. X. Zhang, S. Ohara, T. Chen, and T. Fukui, *Fuel*, **2002**, 81(8), 989
3. S. Park, J. M. Vohs, and R. J. Gorte, *Nature*, **2000**, 404, 265.
4. E. P. Murray, T. sai, and S. A. Barnett, *Nature*, **1999**, 400, 649.
5. B. C. H. Steele, I. Kelly, H. Middleton, and R. Rudkin, *Solid State Ionics*, **1988**, 28, 1547.
6. R. J. Gorte, S. Park, J. M. Vohs, and C. Wang, *Adv. Mater.*, **2000**, 12, 1465.
7. H. He, Y. Huang, J. Regal, M. Boaro, J. M. Vohs, and R. J. Gorte, *J. Am. Ceram. Soc.*, **2004**, 87, 331.
8. EG&G Technical Services Inc. and Science Applications International Corporation, *Fuel Cell Handbook*, 6th Edition, Ch.8, pp. 11-23, US Department of Energy, Morgantown, WV (**2002**).
9. S.-I. Lee, J. M. Vohs, and R. J. Gorte, *J. Electrochem. Soc.*, In press.

ANALYTICAL AND EXPERIMENTAL STUDY OF OXYGEN REDUCTION MECHANISM ON OXYGEN ELECTRODES OF SOFCs: Case study on $\text{La}_{(1-x)}\text{Sr}_x\text{MnO}_3$

Bilge Yildiz, Gerardo Jose la O', Yang Shao-Horn

Electrochemical Energy Laboratory
Massachusetts Institute of Technology,
77 Massachusetts Ave., Cambridge, MA02139

Introduction

The power of a solid oxide fuel cell (SOFC) is limited by the current associated with oxygen reduction at the cathode under a given operating voltage. The current can in general be treated as the combination of charge transfer in the cathode from two pathways, as shown in Figure 1. The first is the adsorption and reduction of oxygen at the cathode surface followed by bulk diffusion of the ions that yield the charge transfer at electrode/electrolyte interface at the 2PB (Figure 1a). The second is the surface- adsorption and transport of oxygen that leads to the reduction of oxygen and charge transfer at the 3PB region (Figure 1b). A theoretical model that takes into account the defined combined current behavior to simulate physically the cell I-V characteristics is necessary to understand the electrochemical behavior of the SOFC cathode under different operating conditions and for optimizing the properties of cathode materials.

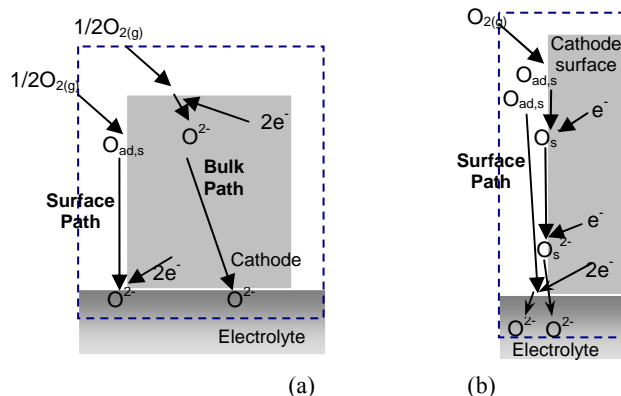


Figure 1. (a) Bulk and surface as the main charge transfer pathways on an SOFC cathode. (b) Parallel charge transfer schemes for the surface pathway of an SOFC cathode.

Although this two-pathway charge transfer behavior and modeling of SOFC cathodes has been studied in literature, a comprehensive physical model that takes into account the effect of both pathways has not been developed. A theoretical model for understanding the I-V characteristic of SOFC electrodes has initially been developed by Adler et al. [1] and this work provides important insights for charge transfer characteristics in SOFC electrodes. However, the model considers only the bulk process followed by 2PB vacancy exchange and it is limited to mixed ionic and electronic conducting electrodes with bulk ionic transfer much faster than surface charge transfer. Although there have been few recent studies that model both bulk and surface pathways [1-4], both pathways are not treated in a single coupled consistent model. For example, the overpotential have been treated as an independent variable rather than being coupled to the oxygen reaction on cathode [2,3].

To further complicate our understanding of oxygen reduction at the cathode, there is lack of consistent experimental evidence to explain the surface reaction characteristics, even for the most commonly used cathode $\text{La}_{(1-x)}\text{Sr}_x\text{MnO}_{3+\delta}$ (LSM) system [5,6]. While the surface path typically dominates the cell current for porous LSM electronic conductor electrode, the oxygen ion diffusion along the bulk path of LSM is shown to control the current in dense thin film LSM

electrodes. In addition, under high cathodic polarization (typically $< -200\text{mV}$) the LSM system becomes a mixed electronic and ionic conductor [7] and allows the bulk path of charge transfer in LSM to be a major contributor to cell current. Therefore, it is essential to develop a physical model to analyze the charge transfer characteristics of SOFC cathodes from both surface and bulk pathways under different operating conditions and electrode configurations.

In our study, we plan to develop a two dimensional continuum model that handles the surface and bulk charge transfer pathways in a coupled and consistent way for SOFC cathodes. We first model the surface charge transfer characteristics - the rate determining pathway and the rate determining steps (rds), of LSM cathode as our initial case study. This paper presents the analytical and experimental study of oxygen reduction on LSM under different temperature and voltage conditions. The reaction pathway on the surface and rate limiting step revealed in this study will be used to determine the oxygen reduction rate along the surface path required in the coupled continuum model.

Theoretical Analysis

The overall oxygen reduction reaction can be represented as



where V_O^y and O_0^y refer to vacancies and oxygen ions in the electrolyte YSZ lattice, respectively. This reaction consists of multiple consecutive steps, one or more of which may be rate determining. Two surface dominated schemes for oxygen reduction on LSM are first considered in this work, as presented in Table 1. Both pathways can occur in parallel to contribute to the cathode current. Other surface models that include 2 electron charge transfer at one step or the transport of totally reduced oxygen (O^{2-}) on the LSM surface away from the 3PB are not considered in this preliminary study.

The rate equations of the proposed reaction steps in each model are written as a function of rate constants and concentrations of species for each step. We assume that the steps that are not rds occur much faster than the rds and thus the net rate of these steps is taken as zero provided that they are in equilibrium. This approach allows the determination of the overall rate of oxygen reduction, r , without computing intermediate species concentrations, and the final rate expression consists of the following parameters: P_{O_2} , temperature, overpotential, and a combination of rate constants that can be correlated with the exchange current density for the cathode.

Table 1. Selected Reaction Models for Oxygen Reduction on LSM

STEPS	EQUATION	PROCESS / LOCATION
Model 1		
1	$\text{O}_{2(g)} \Leftrightarrow 2\text{O}_{ad,s}$	Dissociative adsorption on LSM surface
2	$\text{O}_{ad,s} + e^- \Leftrightarrow \text{O}_s^-$	Partial reduction of $\text{O}_{ad,s}$ on the surface or the extended 3PB
3	$\text{O}_s^- \Leftrightarrow \text{O}_{3PB}^-$	Diffusion of intermediate oxygen species O_s^- along the surface to 3PB
4	$\text{O}_{3PB}^- + e^- \Leftrightarrow \text{O}_{3PB}^{2-}$	Complete reduction of intermediate oxygen species at 3PB
5	$\text{O}_{3PB}^{2-} + V_O^y \Leftrightarrow \text{O}_0^y$	Transfer of O^{2-} at 3PB into YSZ lattice
Model 2		
1	$\text{O}_{2(g)} \Leftrightarrow 2\text{O}_{ad,s}$	Dissociative adsorption on LSM surface
2	$\text{O}_{ad,s} \Leftrightarrow \text{O}_{3PB}$	Diffusion of $\text{O}_{ad,s}$ to 3PB along the surface
3	$\text{O}_{3PB} + e^- \Leftrightarrow \text{O}_{3PB}^-$	Partial reduction of O_{3PB} at 3PB or extended 3PB
4	$\text{O}_{3PB}^- + e^- \Leftrightarrow \text{O}_{3PB}^{2-}$	Complete reduction of intermediate oxygen species O_{3PB}^- at 3PB
5	$\text{O}_{3PB}^{2-} + V_O^y \Leftrightarrow \text{O}_0^y$	Transfer of O^{2-} at 3PB into YSZ lattice

The current from each pathway is then expressed as follows:

$$i_m = -n_e F r_m \quad [2]$$

$$\text{and } i_m = i_{m,a} - i_{m,c} \quad [3]$$

where

$$i_{m-a} = 1 / \sum_j (1/i_{m-a,j}) \quad \text{and} \quad i_{m-c} = 1 / \sum_j (1/i_{m-c,j}) \quad [4]$$

$$\text{Total current from each possible scheme: } i = \sum_m i_m \quad [5]$$

Eq.'s 2-5, the subscripts *a* and *c* represent anodic and cathodic reactions as shown in Table 1, respectively. The parameters *m* and *j* stand for each model and for each of the rds in the model, respectively. In this work, *m* stands for Model 1 and Model 2 in Table 1. Surface diffusion and oxygen ion transfer to YSZ are considered as the rate limiting steps in both models.

As the cathode current is expressed a function of overpotential or cell voltage, one can derive the impedance *Z* for the oxygen reduction process from:

$$Z(\omega) = \frac{FFT(\eta(\omega, t))}{FFT(I(\omega, t))} \quad [6]$$

where η , *I*, FFT, ω and *t* represent overpotential, cell current, fast Fourier transform, frequency and time respectively.

The exchange current density expressions for the surface transport of oxygen and the vacancy transfer at LSM/electrolyte interface were obtained from Chen et al [8]. Figure 2 shows the cell resistance calculated from Eq. 6 plotted against the reciprocal of temperature. The slope of the plot is then used to calculate the activation energy, E_a , of the rds, which is 1.55 eV in this case. This value suggests the rate determining [10-12] mechanisms of dissociative adsorption or surface diffusion on LSM.

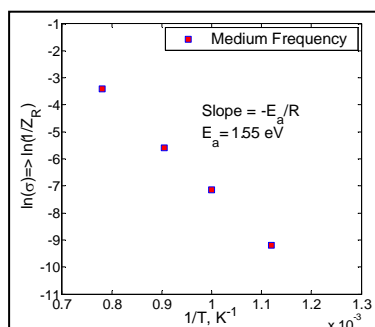


Figure 2. Calculated reciprocal resistances as a function of temperature at 1 atm based on theoretical evaluation (0.1 – 500 Hz)

Experimental Analysis

The $\text{La}_{(1-x)}\text{Sr}_x\text{MnO}_{3+\delta}$ with $x=0.2$ cathode and 8YSZ electrolyte samples were prepared by RF sputtering on a single crystal silicon wafer. AC impedance measurements were performed at 0V DC (OCV) with 20mV of amplitude using a Solartron 1260 frequency response analyzer in the frequency range of 0.01 to 10^7 Hz in the temperature range from 450°C to 550°C and at atmospheric pressure. Preliminary AC impedance data showed two semicircles, which became more distinct at lower temperatures, in Figure 3. The resistances in the AC impedance spectra at different temperatures were calculated and the dependence of the reciprocal of resistance was used to find the activation energy of the rate determining process(es), as shown in Figure 4.

The activation energy of 1.1eV was found for the high frequency arc, which is close to values reported for the transfer of oxide ions from LSM to YSZ lattice as $1\text{eV}^{[11]}$.

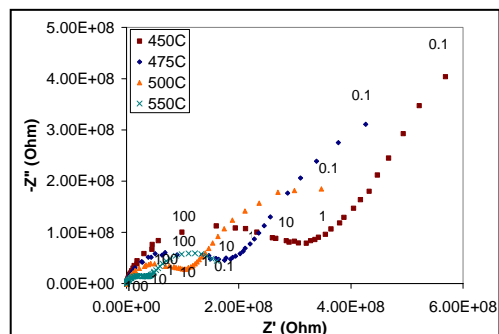


Figure 3. Impedance data obtained for LSM/YSZ at OCV

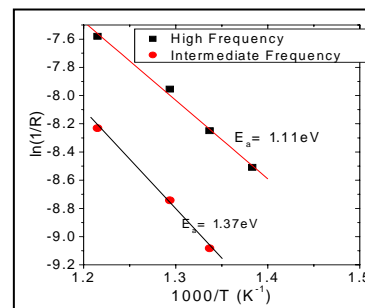


Figure 4. Calculated reciprocal resistances as a function of temperature at 1 atm based on impedance measurements.

The activation energy of 1.37eV was found for the intermediate frequency arc, which could be associated with the dissociative adsorption or the surface diffusion of oxygen species on LSM. The range of activation energy for these processes, although widely studied, greatly varies in the literature - the overall range of E_a for these processes reported falls from 1.5 to 2 eV [10-11]. It should be noted that, the 1.55 eV value for E_a obtained from theoretical impedance analysis having surface diffusion as one of the rds is similar to the E_a found experimentally for the intermediate frequency arc. This preliminary result suggests that the surface diffusion, not the dissociative adsorption, is one of the rds for the oxygen reduction in our experiments.

Additional experiments under changing P_{O_2} and temperature conditions and modeling work are underway to probe surface reaction mechanisms for LSM, which is essential to develop continuum models of the SOFC cathodes in two-dimensional geometry.

References

- (1) Adler, S.B., Lane, J.A., Steele, B.C.H., *J. Electrochem. Soc.* **1996** 143 (11): 3554-3564
- (2) Svensson, A.M., Sunde, S., Nisancioglu, K., *J. Electrochem. Soc.* **1998** 145 (4): 1390-1400
- (3) Coffey, G. *J. Electrochem. Soc.* **2003** 150 (8): A1139-A1151
- (4) Tanner, C.W., Fung, K.Z., Virkar, A.V., *J. Electrochem. Soc.* **1997** 144 (1): 21-30
- (5) Jorgensen, M.J., Mogensen, M., *J. Electrochem. Soc.* **2001** 148 (5): A433-A442
- (6) McIntosh, S., Adler, S.B., *Electrochem. Solid St.* **2004** 7(5): A:111-A114
- (7) Hammouche, A., Siebert, E., *J. Electrochem. Soc.* **1991** 138 (5): 1212-1216
- (8) Chen, X.J., Khon, K.A., Chan, S.H., *J. Power Sources* **2003** 123(1): 17-25
- (9) Juhl M., Primdahl, S., Manon C., Mogensen M., *J. Power Sources* **1996** 61 (1-2): 173-181
- (10) Murray, E.P., Barnett, S.A., *Solid State Ionics* **2001** 143: 265-273
- (11) Siebert, E., Hammouche, A., Kleitz, M., *Electrochim Acta* **1995** 40 (11): 1741-1753

Cerium L_{III}-edge EXAFS Investigation of the Structure of Crystalline and Amorphous Cerium Oxides

Ahmed M. Shahin¹ and Thomas P. Schuman¹, Fernande Grandjean^{1,2}, and Gary J. Long¹

¹Department of Chemistry, University of Missouri-Rolla, Rolla-MO 65409-0010, USA.

²Department of Physics, B5, University of Liège, B-4000 Sart, Belgium

Introduction

As a consequence of changing properties, e.g., mechanical, magnetic, or electrical, the nanocrystalline phase of rare earth metal oxides has become of immense interest.¹ Of these, cerium oxides have attracted considerable research interest due to a diversity of applications. For instance, the basicity function of cerium oxide when combined with the hydrogenation property of a metal such as Pt or Pd denotes cerium oxide as a promising conversion catalyst. Thus, cerium oxide can lead to selective hydrogenation catalysis of unsaturated compounds.² Of interest is the ability of the cerium oxide to store oxygen. The phenomenon is associated with a fast valence change in the solid, i.e., $\text{Ce}^{\text{IV}} \leftrightarrow \text{Ce}^{\text{III}}$, and also with anionic vacancies $\text{CeO}_2 \rightarrow \text{CeO}_{2-x} + (x/2)\text{O}_2$.³ In this study, we report the synthesis of cerium oxide using different precipitation conditions. We also investigated the valence state of cerium ions and covalence with oxide ligands by varying the reaction conditions.

Experimental section

A dilute aqueous ammonia solution (0.01M) was added dropwise to a mixture of 0.05 mol of an aqueous solution of cerium nitrate hexahydrate, $\text{Ce}(\text{NO}_3)_3 \cdot 6\text{H}_2\text{O}$, and hydrogen peroxide. Because the oxidation with H_2O_2 is slow in an acidic media, a few drops (10-20) of aqueous ammonia were added to accelerate the oxidation of Ce^{III} to Ce^{IV} . Cerium oxide was precipitated at two different hydrogen peroxide concentrations. The molar ratios of cerium to hydrogen peroxide were 1:0.8 (sample **I**) and 1:1.2 (sample **II**).

X-Ray Absorption Measurements. X-ray absorption measurements were carried out at the unfocused 4-3 beamline of Stanford Synchrotron Radiation Laboratory. The measurements were carried out in both transmission and fluorescence modes at room temperature.

Results and Discussion

XANES Spectral Results. X-ray diffraction (XRD) patterns of both hydrous CeO_2 and **I** revealed a fluorite structure with a particle size of ~6 nm derived from the line broadening.⁴ The particle size of anhydrous CeO_2 was larger than that of hydrous CeO_2 and sample **I**, whereas **II** was amorphous.⁴ The XANES spectra for anhydrous CeO_2 , hydrous CeO_2 , **I**, and **II** are depicted in Figure 1. Four peaks were fit in the XANES spectra, a high energy peak A, main peak B, low energy peak C, and pre-edge peak D. Peaks A and B were assigned as due to a mixture of the multielectron configurations $L4f^0 5d^1$ and $L4f^1 5d^1$, respectively, where L denotes the hole in the 2p shell, and $5d^1$ refers to the excited electron in the previously unoccupied 5d state.⁵ Integration of peak C at ~5723 eV displayed a different area for each of the samples. Based on this and other⁴ observations, the electronic transition that occurred at ~5723 eV was interpreted as arising from a combination of crystal field splitting and excitation of different amounts of a Ce^{III} contaminant present in all the samples. Unfortunately, the characteristic white line of a typical Ce^{III} compound, $\text{Ce}(\text{NO}_3)_3 \cdot 6\text{H}_2\text{O}$, is observed at the same energy as peak C.⁶ No significant change in the white line areas, as determined from the many-body configuration theory for a core transition to localized electronic states, was observed in all of the samples under

study. Furthermore, changing the hydrogen peroxide concentration during the precipitation of cerium oxide did not result in a significant change in the electronic cerium mixed-valence state.

Modeling of the XANES spectra, in terms of the one-electron band structure of the crystal for a core transition to delocalized electronic states, is a useful approach to determine the cerium valence state and to support the results obtained from the many-body configuration theory for a core transition to localized electronic states. The XANES features have been calculated using FEFF8.20 code, figure 2.⁷ The calculated valences obtained from the XANES spectra simulation using FEFF8.20 are in agreement with those obtained from the many-body configuration theory, Table 1.

EXAFS Spectral Results and Discussion. Results of the fitting of the EXAFS spectra are summarized in Table 2. The extracted k^2 -weighted EXAFS oscillations, the corresponding Fourier filtered data, and modeled EXAFS results for anhydrous CeO_2 , hydrous CeO_2 , **I**, and **II** are shown in Figure 3. The EXAFS spectrum of the amorphous precipitate (sample **II**) exhibited a different structure than that of either anhydrous CeO_2 , hydrous CeO_2 , or **I**. Above the spurious low-R feature, the major oxygen Fourier transformed peak appeared dampened and had practically non-existent outer-shell, Ce-Ce or Ce-O₂, features. The increase of Ce-O1 distance in **II** reflects a high- σ^2 value and the necessity of allowing an additional anharmonic correction term for the O1 path. Visual inspection of the hydrous CeO_2 and **I** spectra showed that the samples' near-neighbor structure deviated significantly from either anhydrous CeO_2 or **II**. The Ce-O1, the Ce-Ce, and the Ce-O2 neighbor coordinations in hydrous CeO_2 appeared more ordered with smaller σ^2 as compared with **I**, or **II**, but less ordered than the crystalline anhydrous CeO_2 . Analysis of EXAFS spectrum of **I** indicated comparable oscillation amplitudes to those of hydrous CeO_2 . The distance between cerium centers and oxygen neighbors in the first coordination shell are of similar magnitude, 2.360 and 2.364 Å for hydrous CeO_2 and **I**, respectively. However, larger deviations were observed in Ce-Ce and Ce-O2 distances between hydrous CeO_2 and **I** samples. Hydrogen peroxide thus induced changes in the coordination spheres around cerium, longer bond distances and fewer coordinated atoms. The parameters in the EXAFS analysis yielded higher N_{O1} values, higher σ^2 , and longer Ce-O bond distances for both hydrous CeO_2 , **I**, and especially **II** compared to anhydrous CeO_2 . Increasing the coordination number, N1, was attributed to incorporating H_2O molecules that resulted in decreasing the crystalline order. The evaluation of each parameter in going from anhydrous CeO_2 to **II** indicates a decrease in crystalline order. The Fourier transformed peak representing the Ce-Ce interaction of hydrous and **I** were more pronounced than in amorphous **II**, and less pronounced than in crystalline anhydrous CeO_2 . The enhanced Ce-Ce distance, and the decreased coordination number, N2, in both hydrous CeO_2 and **I** compared with anhydrous CeO_2 were attributed to a higher degree of defect sites in these nanocrystalline materials.

Conclusions

Different hydrogen peroxide concentrations were employed during the precipitations of cerium oxide. XANES analysis clearly showed a significant change in the intensity of the white line peaks of precipitated cerium oxide revealing a smaller particle size as compared to anhydrous CeO_2 . However, no significant change in cerium spectroscopic valence for precipitated cerium oxides was observed, regardless of peroxide concentration, in comparison to the anhydrous CeO_2 . Precipitation of cerium oxide utilizing H_2O_2 resulted in an increased bond distance, $R_{\text{Ce-O}}$, as well as coordination number of the first coordination shell Ce-O. A decrease in the coordination numbers of the second shell, Ce-Ce, and the third shell, Ce-O, were observed from the radial distribution function. Furthermore, the Debye-Waller factor for the three shells exhibited a

consistent trend as the value of the three coordination shells increased going from anhydrous CeO₂, hydrous CeO₂, sample I, to sample II. Based on these observations, the degree of disorder increased with increasing H₂O₂ concentration during precipitation of cerium oxide, consequently increasing the potential for cerium oxide precipitate to function as oxygen traps. Decreasing the particle size of cerium oxide precipitates, with probable increase in oxygen trapping capability offers additional insight into the enhancement of the fuel cells performance using cerium oxide precipitates.

Table 1. Cerium *L*_{III}-edge XANES Fits of the Two Characteristic Peaks.

Sample	Anhydrous CeO ₂	Hydrous CeO ₂	I	II
Peak (A) position	5735.1	5735.2	5734.3	5734.7
Peak (A) width	3.5	3.2	3.6	3.8
Peak (B) position	5727.6	5727.1	5726.5	5726.5
Peak (B) width	2.8	2.9	3.0	3.2
Valence-Least square fitting	3.45	3.51	3.47	3.48
FEFF-calculated valence	3.48	3.49	3.51	3.52

Table 2. Parameters Extracted from Least-Squares Fitting of the EXAFS Spectra

Sample	Crystallographic data	Anhydrous CeO ₂	Hydrous CeO ₂	I	II
Ce-O1 R(Å)	2.343	2.343*	2.360 (2)	2.364 (3)	2.420 (1)
Ce-O1 N1	8	8*	9.5 (1)	10 (1.5)	11.5(1.3)
Ce-O1 σ^2 (10^{-3}Å^2)	-	3.20(4)	6.45(5)	9.43(2)	10.22 (6)
Ce-Ce R(Å)	3.826	3.826*	3.847 (3)	4.122 (2)	3.814 (4)
Ce-Ce N1	12	12*	7.4 (1.1)	6.6 (1.6)	3.6 (1)
Ce-Ce σ^2 (10^{-3}Å^2)	-	1.50(2)	3.30(6)	4.20(1)	9.60(2)
Ce-O2 R(Å)	4.487	4.487*	4.210 (5)	4.127 (17)	-
Ce-O2 N1	24	24*	18.0 (1.6)	16.1 (1)	-
Ce-O2 σ^2 (10^{-3}Å^2)	-	2.40(1)	3.20(5)	4.80(5)	-

* Fixed parameters

Acknowledgement. Support for this project was provided through the Air Force Research Laboratory Materials and Manufacturing Directorate, project manager Steve Szaruga. Portions of this research were carried out at the Stanford Synchrotron Radiation Laboratory, a national user facility operated by Stanford University on behalf of the U.S. Department of Energy, Office of Basic Energy Sciences.

References

- (1) Winterer, M.; Nitsche, R.; Hahn, H., *J. Phys. IV France* **1997**, 7, C2-1211.
- (2) Fierro, J. L. G.; Soria, J.; Sanz, J.; Rojo, M. J., *J. Solid State Chem.* **1987**, 66, 154.
- (3) Sun, Y.; Sermon, P. A., *J. Mater. Chem.* **1996**, 6, 1025.
- (4) Schuman, T., "Cerium oxide pigments for anti-corrosion primer coatings," submitted.
- (5) Bianconi, A.; Marcelli, A.; Dexpert, H.; Karnatak, R.; Kotani, A.; Jo, T.; Petiau, J., *Phys. Rev. B* **1987**, 35, 806.
- (6) Wu, Z.; Benfield, R. E.; Guo, L.; Li, H.; Yang, q.; Grandjean, D.; Li, q.; Zhu, H., *J. Phys.: Condens. Matter* **1994**, 6, 8429.
- (7) Ankudinov, A. L.; Bouldin, C.; Rehr, J. J.; Sims, J.; Hung, H., *Phys. Rev. B* **2002**, 65, 104107.

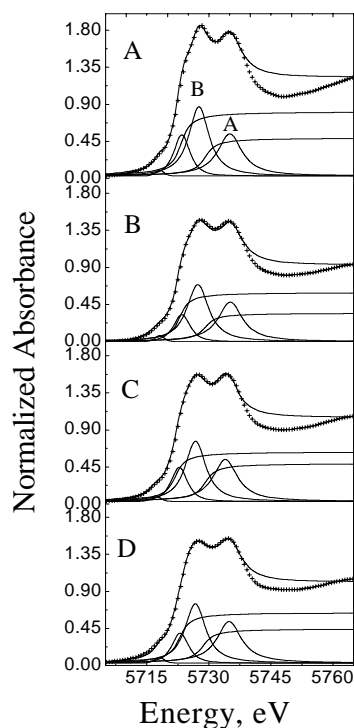


Figure 1. Ce *L*_{III}-edge XANES spectra with fits of (A) anhydrous CeO₂, (B) hydrous CeO₂, (C) Sample I, and (D) Sample II.

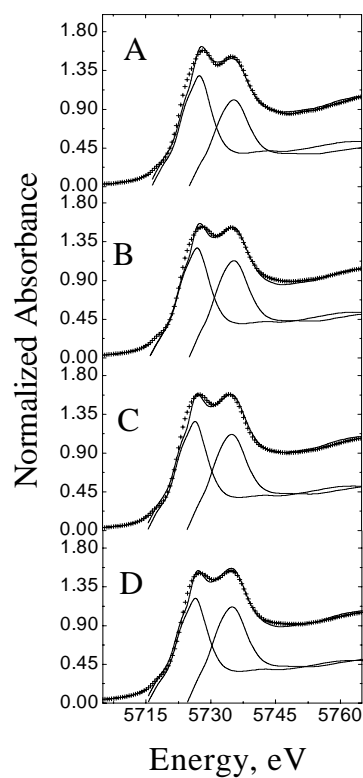


Figure 2. Ce L_{III} -edge XANES spectra with the calculated XANES spectra of (A) anhydrous CeO_2 , (B) hydrous CeO_2 , (C) Sample I, and (D) Sample II.

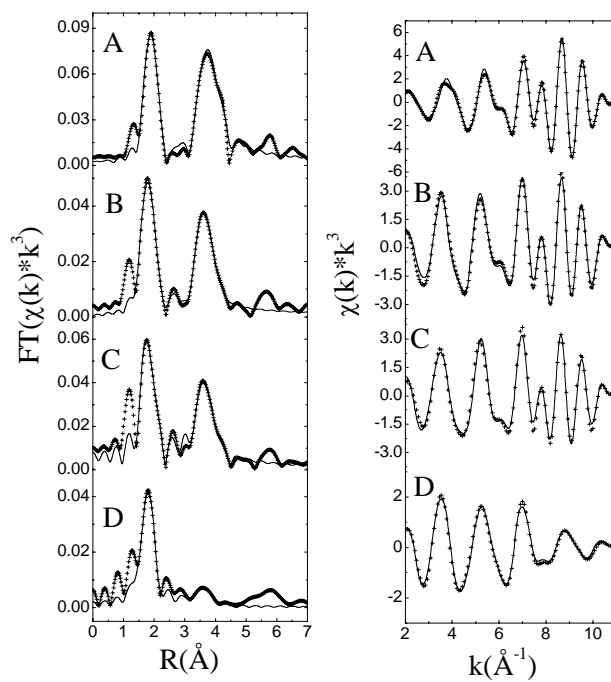


Figure 3. R-space fit result for (A) anhydrous CeO_2 , (B) hydrous CeO_2 , (C) Sample I, and (D) Sample II. Right Panel: Corresponding Fourier-filtered data back-transformed fit.

Deposit Formation within a Solid Oxide Fuel Cell (SOFC) Operating on Butane

Katie O'Gara, Chad Sheng and Anthony M. Dean

Chemical Engineering Department
Colorado School of Mines
Golden, CO 80401

Introduction

Fuel cell technology presents the possibility of increased energy efficiency with decreased detrimental environmental impact over conventional combustion. Solid-oxide fuel cells (SOFC), in particular, offer a very promising method for direct production of electrical energy from currently available fossil fuels, thus postponing the need to build a hydrogen delivery infrastructure. Hybrid SOFCs, coupled with a heat recovery system such as a gas turbine generator, have the potential for fuel-to-electricity efficiencies approaching 75–80%. However, the use of hydrocarbon fuels opens the possibility of deposit formation. The high operating temperatures of a SOFC can lead to fuel degradation and formation of carbonaceous deposits within the fuel channels and porous anode structures. SOFCs that run on H_2 as a fuel source often utilize nickel as the electrical conductor. However, nickel is known to react with hydrocarbons to form deposits. Several studies have reported on the use of different materials to minimize deposit formation, e.g. [1], as well as upstream conversion of hydrocarbon fuels to syngas (CO and H_2) as a way to avoid deposit formation, e.g. [2].

An important feature of SOFC operation is the electrochemical formation of H_2O and CO_2 on the anode side. These species form at the three-phase (fuel, anode, electrolyte) boundary and diffuse through the porous anode to the anode channel, thus diluting the fuel stream. While still in the anode, these species can participate in “internal reforming” reactions, performing the same function of converting hydrocarbon fuel to CO and H_2 that might be accomplished by the upstream reforming discussed earlier. Under these conditions it is likely that the water-gas shift reaction would also take place, converting $CO + H_2O$ to $H_2 + CO_2$. These reactions can further complicate the identity of the “fuel” that will participate in the electrochemical reactions. In addition, steam gasification, to remove any deposits already formed, might be catalyzed by the metal in the anode cermet.

A complete SOFC model is very complex, requiring descriptions of kinetics in multiple phases and coupling the kinetics to multiple transport processes. Chemical reactions within the SOFC occur in three regions: in the anode channel (gas-phase kinetics), on the surface of the porous anode (heterogeneous catalysis) and at the three-phase boundary (electrochemical catalysis). Thus the homogeneous and heterogeneous kinetics have the potential to substantially change the nature of the species that ultimately undergo electrochemical oxidation. It is essential to account for such kinetic modifications to properly characterize SOFC operation and predict the overall efficiency.

As a first step toward characterizing the complex kinetics, we need to make sure that we properly understand the gas-phase hydrocarbon chemistry. The effect of gas phase reactions of methane in SOFCs has been reported [3]. We have recently extended this approach to butane, which is significantly more reactive than methane and thus more representative of a range of hydrocarbon fuels [4]. We showed that we could capture the effect of temperature on both conversion and major product selectivity using a detailed chemical mechanism. In this work, we focus on the effects of the electrochemical production of H_2O and CO_2 on the gas-phase production rate of deposits. Earlier it was shown that the

electrochemical production of H_2O and CO_2 did indeed significantly impact the predictions regarding deposit formation from methane [3]. Here we discuss the effects of H_2O and CO_2 on deposits from butane, and we also explore the effects of upstream reforming and partial oxidation on deposit formation.

Reaction Mechanism. The reaction mechanism that was utilized in this study consists of 291 species and 2498 elementary reactions [4]. The mechanism includes pyrolysis and oxidation kinetics for C_6 and smaller species. It includes molecular weight growth chemistry to allow formation of PAH species up to C_{24} . Beyond formation of naphthalene, PAH growth is modeled using the approach proposed by Frenklach and Warnatz [5].

Deposit Formation from Butane Pyrolysis. In our experiments, qualitative observations of deposit formation were made by examining the quartz reactor after running a specific mixture containing butane through the reactor for 4 hours. We observed no apparent deposit formation within the reactor for any of the mixtures at $650^\circ C$ or lower temperatures. As the reactor temperature was increased to $700^\circ C$, an obvious deposit film was observed on the inner walls of the quartz reactor with the neat butane (100% nC_4) mixture. The deposit film was noticeably less dense for a 50/50 (by mole) nC_4/N_2 mixture, and barely evident for a 50/50 nC_4/H_2O mixture. The first inference from these qualitative observations is that dilution does play a role in minimizing deposit formation. This is to be expected, since the lower concentration of reactive species would be expected to decrease the rate of molecular weight growth leading to deposits. The marked difference in the nitrogen and steam mixtures suggests that the steam is either actively participating in inhibition of molecular weight growth or that it is participating in some type of gasification of the deposit. All three mixtures show significant deposit formation at $800^\circ C$.

To compare to the kinetic model, we considered all species in the model predictions above C_4 (denoted as C_5^+) as potential deposit precursors. The predicted C_5^+ mole fraction is a very strong function of temperature as illustrated in Fig. 1.

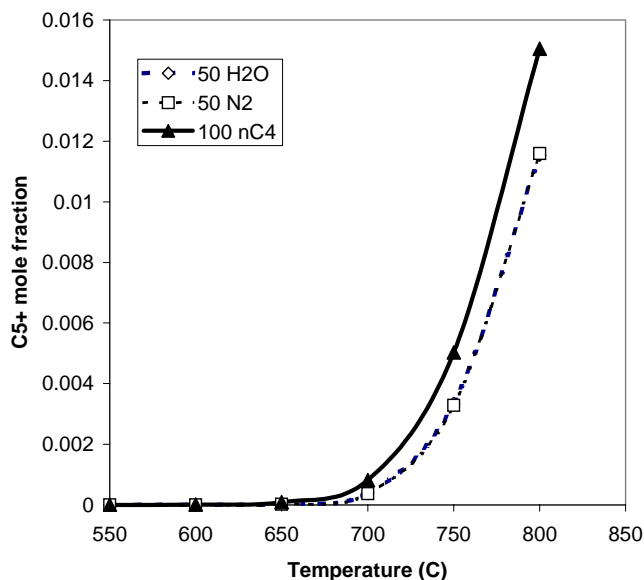


Figure 1. Predicted effect of temperature on the mole fraction of C_5^+ species.

It is encouraging to note that the predicted rapid increase in deposit precursors near $700^\circ C$ is consistent with the experimental observations. The predicted C_5^+ values for the steam and nitrogen dilution cases are virtually identical. This is consistent with our

observation that any gas-phase reactions of steam are very slow under these conditions, and thus steam is simply acting as a diluent, just like nitrogen. This is in contrast to the experimental observations that steam diminished deposit formation. This effect is probably due to heterogeneous reactions. The ratio of C_{5+} predicted for the neat butane case to that of the diluted mixtures decreases from approximately five at 550°C to only slightly greater than unity at 800°C. Thus at the higher temperatures, the predictions suggest that the inhibition of deposit formation by dilution is much less effective.

Effects of Electrochemistry on Deposit Formation. To account for electrochemical production of steam and carbon dioxide, we assume a current density of 0.5 amp/cm² and use the overall stoichiometry to determine the number of moles formed:



We then allow this electrochemical flux to enter uniformly along the anode channel as pictured below.

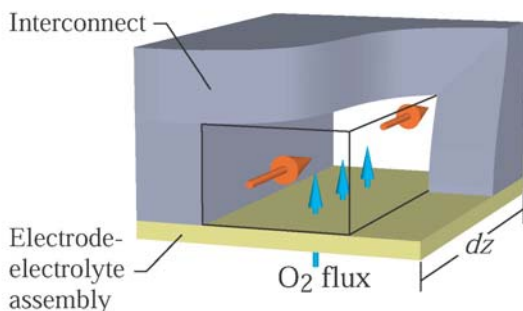
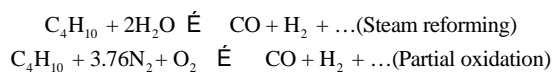


Fig. 2 illustrates the effect of this electrochemical flux on the temperature dependence of formation of C_{5+} . The predictions show that added dilution from the CO_2 and H_2O production allows operation at higher temperatures. By comparing to Fig. 1, note that the effect of the electrochemical production is larger than that due to 50/50 dilution by N_2 .

Effects of Partial Oxidation or Steam Reforming on Deposits. We also looked at the effect of pretreating the fuel by partial oxidation or steam reforming on the amount of C_{5+} species produced at various temperatures. The results of the fuel stream being split, 50% treated and 50% sent directly to the fuel cell, for both pretreatment options are also shown in Fig. 2. The fuel composition used in the model came from equilibrium calculations based on of the following stoichiometries:



As expected, upstream partial oxidation and reforming of the fuel further reduces the propensity to form deposits because it dilutes the stream and breaks the fuel down into lighter species that are less likely to form deposits. When the entire fuel stream was pretreated, we observed no signs of molecular weight growth at temperatures below 1000°C.

Conclusion

The kinetic model predicts a significant decrease in the amount of C_{5+} species formed when electrochemistry is accounted for and even less when there is upstream steam reforming or partial oxidation of the fuel, possibly allowing for a higher operation temperature of the SOFC. Because heterogeneous chemistry at the anode surface was not included in these predictions, the actual amount of deposit formation cannot be predicted from this model. Nevertheless, the fact

that certain metals can be added to the anode to promote internal reforming suggests this is an additional mechanism to avoid deposit formation.

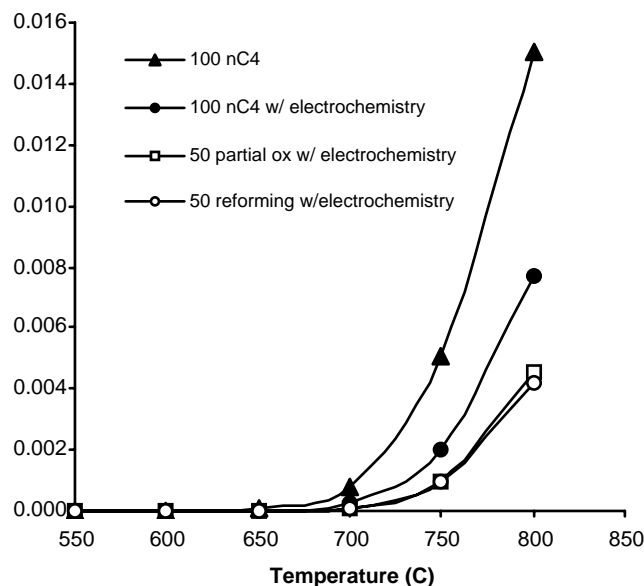


Figure 2. Predicted effect electrochemistry and pretreating the fuel on the mole fraction of C_{5+} species produced vs temperature.

Acknowledgements. This work was funded under DARPA Contract Number MDA972-01-C-0068 and a DoD Multidisciplinary University Research Initiative (MURI) program administered by the Office of Naval Research under Grant N00014-02-1-0665. The authors would like to thank ITN Energy Systems, Inc. for the use of their facilities where the experimental work was conducted. We also would like to thank Hans-Heinrich Carstensen and Chitral Naik for providing some of the elementary reaction rates used in the current model and Gaurav Gupta for performing some of the modeling calculations.

References

- Lu, C., et al., *SOFCs for Direct Oxidation of Hydrocarbon Fuels with Samaria-Doped Ceria Electrolyte*. Journal of The Electrochemical Society, 2003. **150**(3): p. A354-A358.
- Krummenacher, J.J., K.N. West, and L.D. Schmidt, *Catalytic partial oxidation of higher hydrocarbons at millisecond contact times: decane, hexadecane, and diesel fuel*. Journal of Catalysis, 2003. **215**: p. 332-343.
- Walters, K.M., et al., *Homogeneous kinetics and equilibrium predictions of coking propensity in the anode channels of direct oxidation solid-oxide fuel cells using dry natural gas*. Journal of Power Sources, 2003. **123**(2): p. 182-189.
- Sheng, C.Y. and A.M. Dean, *The importance of gas-phase kinetics within the anode channel of a solid-oxide fuel cell*. J. Phys. Chem A, asap.
- Frenklach, M. and J. Warnatz, *Detailed Modeling of PAH Profiles in a Sooting Low-Pressure Acetylene Flame*. Combustion Science and Technology, 1987. **51**: p. 265-283.